Trends in Mathematics
Research Perspectives CRM Barcelona Vol.8

Alessandro Colombo
Mike Jeffrey
J. Tomàs Lázaro
Josep M. Olm
Editors

Extended Abstracts Spring 2016

Nonsmooth Dynamics

CRM CENTRE DE RECERCA MATEMÀTICA

Birkhäuser

Trends in Mathematics

Research Perspectives CRM Barcelona

Volume 8

Series editors

Enric Ventura
Antoni Guillamon

Since 1984 the Centre de Recerca Matemàtica (CRM) has been organizing scientific events such as conferences or workshops which span a wide range of cutting-edge topics in mathematics and present outstanding new results. In the fall of 2012, the CRM decided to publish extended conference abstracts originating from scientific events hosted at the center. The aim of this initiative is to quickly communicate new achievements, contribute to a fluent update of the state of the art, and enhance the scientific benefit of the CRM meetings. The extended abstracts are published in the subseries Research Perspectives CRM Barcelona within the Trends in Mathematics series. Volumes in the subseries will include a collection of revised written versions of the communications, grouped by events.

More information about this series at http://www.springer.com/series/13332

Alessandro Colombo · Mike Jeffrey
J. Tomàs Lázaro · Josep M. Olm
Editors

Extended Abstracts Spring 2016

Nonsmooth Dynamics

Birkhäuser

Editors
Alessandro Colombo
Department of Electronics, Information and Bioengineering
Politecnico di Milano
Milano
Italy

Mike Jeffrey
Department of Engineering Mathematics
University of Bristol
Bristol
UK

J. Tomàs Lázaro
Departament de Matemàtiques
Universitat Politècnica de Catalunya
Barcelona
Spain

Josep M. Olm
Departament de Matemàtiques
Universitat Politècnica de Catalunya
Barcelona
Spain

ISSN 2297-0215 ISSN 2297-024X (electronic)
Trends in Mathematics
ISSN 2509-7407 ISSN 2509-7415 (electronic)
Research Perspectives CRM Barcelona
ISBN 978-3-319-55641-3 ISBN 978-3-319-55642-0 (eBook)
DOI 10.1007/978-3-319-55642-0

Library of Congress Control Number: 2017936891

Mathematics Subject Classification (2010): 34-02, 34H10, 34H20, 34F05, 34D05, 34D15, 34D10, 34D30, 34E05, 34E10, 34E15, 34C07, 34C15, 34C23, 34C29, 34C41, 34A36, 34A38, 34A60, 39-02, 93C30, 93C40, 93D09, 93D21

Printed on acid-free paper

This book is published under the trade name Birkhäuser
The registered company is Springer International Publishing AG
The registered company address is: Gewerbestrasse 11, 6330 Cham, Switzerland
(www.birkhauser-science.com)

Preface

It is traditional for these volumes to contain short articles from a conference held during a research program. Given the level of activity throughout the *CRM Intensive Research Program on Advances in Nonsmooth Dynamics*, from the outset we decided to focus this set of Extended Abstracts on the long-term program. So, here you will find a collection of Abstracts from the opening *Conference on Open Problems in Nonsmooth Dynamics*, held from February 1 to 5, 2016, the *Advanced Course on Piecewise Smooth Maps and Flows*, held from April 11 to 15, 2016, the *Climate Workshop*, held from March 29 to April 1, 2016, and many more short articles summarizing seminars or informal presentations, as well as discussions that arose over the course of the three-month program.

More than 120 researchers took part in the program, around 54 as researchers in residence, with others attending the workshops and events held every few weeks. Themed weeks also focussed on control electronics, life science applications including sleep–wake cycles and predator–prey models, contact mechanics including the Painlevé paradox and impacting chaos, genetic regulatory models and systems with many switches, friction models derived from slow-fast or rate-and-state systems, and methods of regularization. The actual list of theoretical and applied problems being discussed is much longer. Nonsmooth dynamics in 2016 is an incredibly active field of research and finds new applications every year. In the following pages, you will find a taster.

On the final day of the program, we met to review the open problems that remained or had arisen during the program. The certainly not exhaustive list of most prominent problems included external variable models of switching and the various alternatives for regularizing nonsmooth systems using probabilistic, fractal, or shadowing rules. We discussed the need for a better understanding of the link between different discontinuous solution concepts such as blow-up/sliding/layers and the applied models they represent (e.g., genetic regulatory models and climate models), particularly how stability/uniqueness/robustness in a discontinuous model relates to real switching in physical and biological models. We discussed the new methods that are still needed for studying n-dimensions (invariant measures, dimension of attractors, center/invariant manifolds). We discussed that a "less is

more" approach needs to be applied to developing new analytical methods and computational tools. We discussed the surprising results that had been found for how noise and other nonidealities affect switching, and the need to understand the effect of nonlinear terms on the many leading order expressions that are now important in local classifications.

We also made a list of the big problems that have been solved recently, including during the program. The major ones included recent results on pausing in nonsmooth systems, the understanding of convex combinations or canopies as an extension of Filippov's convex sets, progress made during the program concerning how various kinds of regularization (hysteresis/delay/noise/discretization) affect sliding along the intersections of systems (to be reported later), we reviewed progress on the twofold singularity, on understanding how additive white noise affects sliding modes (largely resolved, up to technical issues), and we were shown that piecewise linear systems can have infinitely many limit cycles (with a nonlinear or nonsmooth switching boundary).

Many, but not all, of these are captured in the following pages.

Milan, Italy — Alessandro Colombo
Bristol, UK — Mike Jeffrey
Barcelona, Spain — J. Tomàs Lázaro
Barcelona, Spain — Josep M. Olm
September 2016

Contents

On Degenerate Cycles in Planar Filippov Systems

Kamila da S. Andrade, R.M. Martins, and Marco Antonio Teixeira

Abstract The main objective of this paper is to study bifurcations of a vector field in a neighborhood of a cycle having a homoclinic-like connection at a saddle-regular point. In order to perform such a study it is necessary to analyze how the cycle can be broken, in this way the approach is to look separately at local bifurcations and at the structure of the first return map defined near the cycle.

1 Preliminary Concepts

Consider χ^r the set of all C^r-vector fields defined in $\mathbb{R}^2$ endowed with the C^r-topology. For $X, Y \in \chi^r$ define

$$Z(x, y) = \begin{cases} X(x, y), & h(x, y) \geq 0, \\ Y(x, y), & h(x, y) \leq 0, \end{cases}$$

where $h : \mathbb{R}^2 \to \mathbb{R}$ is a smooth function such that $\Sigma = h^{-1}(0) \subset \mathbb{R}^2$ is a codimension 1 embedded submanifold, called the switching manifold. Such a vector field Z, as defined above, is called a piecewise smooth vector field and it is usually denoted by $Z = (X, Y)$. We also denote $\Sigma^+ = \{(x, y) \in \mathbb{R}^2 : h(x, y) > 0\}$ and $\Sigma^- = \{(x, y) \in \mathbb{R}^2 : h(x, y) < 0\}$.

Let Ω^r be the set of all $Z = (X, Y)$ with $X,\ Y \in \chi^r$, then Ω^r can be identified with $\chi^r \times \chi^r$ and thus it is naturally endowed with the product topology. In the switching manifold three regions are distinguished (see Fig. 1): the *crossing region*,

K. da S. Andrade (✉)
Department of Mathematics, UFG, IME, Goiânia, GO 74690-900, Brazil
e-mail: ksandrade.mat@gmail.com

R.M. Martins · M.A. Teixeira
Department of Mathematics, Unicamp, IMECC, Campinas, SP 13083-970, Brazil
e-mail: rmiranda@ime.unicamp.br

M.A. Teixeira
e-mail: teixeira@ime.unicamp.br

A. Colombo et al. (eds.), *Extended Abstracts Spring 2016*,
Trends in Mathematics 8, DOI 10.1007/978-3-319-55642-0_1

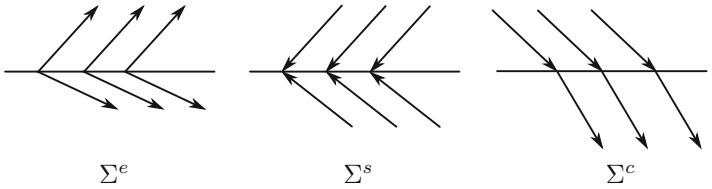

Fig. 1 Illustrations of the regions in Σ

$$\Sigma^c = \{p \in \Sigma : XhYh(p) > 0\},$$

the *sliding region*,

$$\Sigma^s = \{p \in \Sigma : Xh(p) < 0 \text{ and } Yh(p) > 0\},$$

and the *escaping region*,

$$\Sigma^e = \{p \in \Sigma : Xh(p) > 0 \text{ and } Yh(p) < 0\},$$

where $Xh(p) = \langle X, \nabla h\rangle(p)$ is the Lie derivative of h in relation to the vector field X, analogously $Yh(p) = \langle Y, \nabla h\rangle(p)$ is the Lie derivative of h in relation to Y.

The concept of solutions and trajectories follows Filippov's convention: it implies that multiple solutions through points in $\overline{\Sigma - \Sigma^c}$ are being considered; see [1, 2].

2 Statement of the Problem and Results

The main objective is to study bifurcations of a homoclinic-like connection through a saddle-regular point, then consider a piecewise smooth vector field $Z_0 = (X_0, Y_0)$. In order to conduct an analysis as simple as possible some generic conditions are stated:

(i) $BS(1)$: X_0 has a hyperbolic saddle $S_{X_0} \in \Sigma$, the unstable and stable manifold of S_{X_0}, $W^u(X_0, S_{X_0})$ and $W^s(X_0, S_{X_0})$, respectively, are transversal to Σ at S_{X_0};
(ii) $BS(2)$: Y_0 is transversal to Σ, $W^u(X_0, S_{X_0})$, and $W^s(X_0, S_{X_0})$ at S_{X_0};
(iii) $BS(3)$: the sliding vector field near the saddle point has S_{X_0} as a non-degenerate singularity;
(iv) $BSC(1)$: the unstable manifold of S_{X_0} which lies in Σ^+, $W^u_+(X_0, S_{X_0})$, is transversal to Σ at $P_{X_0} \neq S_{X_0}$;
(v) $BSC(2)$: Y_0 is transversal to Σ at P_{X_0} and there exists $t_0 > 0$ such that $\varphi_{Y_0}(t_0, P_{X_0}) = S_{X_0}$ with $\varphi_{Y_0}(t, P_{X_0}) \in \Sigma^-$ for all $0 \leq t \leq t_0$, where $\varphi_{Y_0}(s, p)$ denotes the flow of Y_0 through p;
(vi) $BSC(3)$: there exists a first return map defined inside the bounded region delimited by $W^u_+(X_0, S_{X_0})$ and $\varphi_{Y_0}(t, P_{X_0})$.

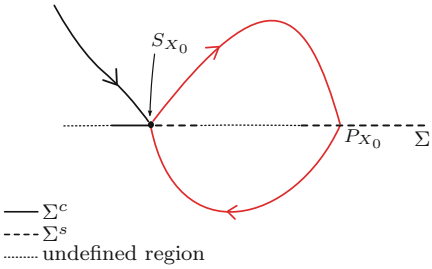

Fig. 2 A degenerate cycle through a saddle-regular point

Under these conditions, there exists a degenerate cycle through the saddle-regular point $S_{X_0} \in \Sigma$ which is a homoclinic-like connection, see Fig. 2.

In order to analyze all the bifurcations of this kind of degenerate cycle, observe that there are two structures to be broken, the boundary singularity and the connection; in what follows, we look carefully at these two structures. For the first one, the approach is to study the local bifurcation of the saddle-regular point, while for the second one, the approach is to study the structure of the first return map.

2.1 Bifurcations of a Saddle-Regular Point

As shown in Kuznetsov–Rinaldi–Gragnani [3], there are three different bifurcation cases: BS_1, BS_2, and BS_3. In BS_1 and BS_2 a pseudo-node merges when the saddle is a real singularity (i.e., a singularity of X in Σ^+) and the difference between them is the position of the pseudo-node. In BS_3 a pseudo-saddle merges when the saddle is a virtual singularity (i.e., a singularity of X in Σ^-).

2.2 Structure of the First Return Map

In order to conduct an analysis of the first return map, consider $\mathcal{V}_{X_0}$ a neighborhood of X_0 such that any $X \in \mathcal{V}_{X_0}$ has a unique singularity near S_{X_0} which is a hyperbolic saddle S_X. We assume that, locally around the saddle point S_X, the vector field X is given by the following normal form; see Roussarie [4].

Theorem 1 *Let X be a vector field sufficiently smooth having the origin as a hyperbolic saddle point and consider $r = -\lambda_1/\lambda_2$ the hyperbolicity ratio of the saddle point (where $\lambda_2 < 0 < \lambda_1$ are the eigenvalues of the saddle point). Then, there exists a map $N : \mathbb{N} \to \mathbb{N}$ such that, in some neighborhood of the saddle point, X is C^k-equivalent to the polynomial vector field*

$$x\frac{\partial}{\partial x}+\left(-r+\frac{1}{q}\sum_{i=1}^{N(k)}\alpha_{i+1}(x^p y^q)^i\right)y\frac{\partial}{\partial y},$$

if $r = p/q \in \mathbb{Q}$. *If* $r \notin \mathbb{Q}$, X *is* C^k*-equivalent to the linear vector field*

$$x\frac{\partial}{\partial x}-ry\frac{\partial}{\partial y}.$$

We restrict ourselves to the class of non-resonant vector fields, i.e., to the class of vector fields having irrational hyperbolicity ratio. Consider $Z = (X, Y) \in \mathcal{V}_{Z_0}$ where X has an irrational hyperbolicity ratio. The first return map is constructed in the following manner: let σ be a section in Σ^+ "above" the saddle point, let ρ_1 be the map given by the flow of X from Σ (near the saddle point) to σ, let ρ_2 be the map given by the flow of X from σ to Σ (near P_{X_0}), and let ρ_3 be the map given by the flow of Y from Σ (near P_{X_0}) to Σ (near the saddle point). Now, the first return map, which is defined in a half-open interval, is $\pi_Z(x) = \rho_3 \circ \rho_2 \circ \rho_3(x)$.

In each case of a real saddle, boundary saddle or virtual saddle, there is a different starting point to the first return map. Now, the strategy is to understand the graph of the first return map when we approximate the starting point. This analysis is performed by using the normal form given in Theorem 1 and the construction above. Then, it is shown that the graph of the first return map π_Z with starting point a_Z satisfies the following conditions:

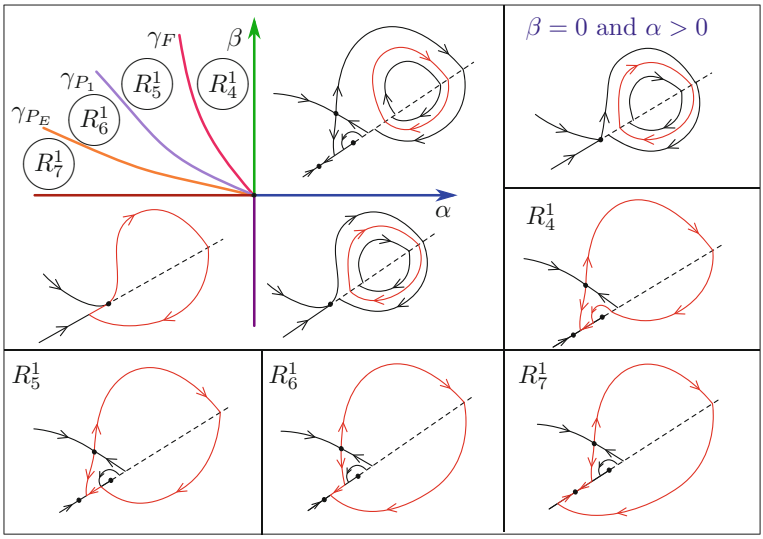

Fig. 3 Bifurcation diagram of $Z_{\alpha,\beta}$: case DSC_{11}

(i) if the saddle point is virtual, on the boundary or real with $r > 1$, the graph of π_Z tends to be tangent to the horizontal direction when we approximate to a_Z;
(ii) if the saddle point is real and $r < 1$, the graph of π_Z tends to be vertical when we approximate to a_Z.

Based on all these analyses, the bifurcation diagrams can be sketched. The case where we have a BS_1 local bifurcation for the saddle-regular point and $r > 1$ is illustrated in Fig. 3.

References

1. A.F. Filippov, *Differential Equations with Discontinuous Right-Hand Sides*, vol. 18, Mathematics and its Applications (Kluwer Academic Publishers Group, Dordrecht, 1988)
2. M. Guardia, T.M. Seara, M.A. Teixeira, Generic bifurcations of low codimension of planar Filippov systems. J. Differ. Equ. **250**, 1967–2023 (2011)
3. Y.A. Kuznetsov, S. Rinaldi, A. Gragnani, One-parameter bifurcations in planar Filippov systems. Int. J. Bifurc. Chaos Appl. Sci. Eng. **13**(8), 2157–2188 (2003)
4. R. Roussarie, *Bifurcation of Planar Vector Fields and Hilbert's Sixteenth Problem* (Birkhuser, Basel, 1998)

Sliding Dynamics on Codimension-2 Discontinuity Surfaces

Mate Antali and Gabor Stepan

Abstract In this paper, the properties of codimension–2 discontinuity sufaces of vector fields are presented which can arise from e.g., spatial Coulomb friction. Concepts of sliding region and sliding dynamics are defined for these systems.

1 Introduction

Switching surfaces of Filippov systems are codimension–1 manifolds in the phase space, where the vector field is discontinuous; see, e.g., di-Bernardo–Budd–Champneys–Kowalczyk [3]. Codimension–2 discontinuity manifolds can also exist, for example at the intersection of two switching surfaces; see Dieci–Difonzo [4] and Jeffrey [5]. However, *isolated* codimension-2 discontinuities can also come about, e.g., from the Coulomb friction between the surfaces of 3D bodies. In this paper, we investigate these systems analogously to the concepts of Filippov systems.

2 Isolated Codimension–2 Discontinuity Manifolds

2.1 Filippov Systems

Consider a bimodal Filippov system in the form

$$F(x) = \begin{cases} F_1(x) & \text{if} \quad H(x) > 0, \\ F_2(x) & \text{if} \quad H(x) < 0, \end{cases}$$

M. Antali (✉) · G. Stepan
Deparment of Applied Mechanics, Budapest University of Technology and Economics, Budapest, Hungary
e-mail: antali@mm.bme.hu

G. Stepan
e-mail: stepan@mm.bme.hu

A. Colombo et al. (eds.), *Extended Abstracts Spring 2016*,
Trends in Mathematics 8, DOI 10.1007/978-3-319-55642-0_2

where F_1 and F_2 are smooth vector fields on $\mathbb{R}^m$ and the smooth function $H : \mathbb{R}^m \to \mathbb{R}$ defines the switching manifold $\Sigma := \{x \in \mathbb{R}^m : H(x) = 0\}$. We can call Σ the codimension–1 discontinuity surface of F with uniform degree 1 of smoothness; see di-Bernardo–Budd–Champneys–Kowalczyk [3, p. 75].

At a given point $x_0 \in \Sigma$, let $n_1(x_0) := \nabla H(x_0)/ \parallel \nabla H(x_0) \parallel$ and $n_2(x_0) := -n_1(x_0)$ be the unit vectors orthogonal to Σ. The orthogonality and the norm $\parallel \cdot \parallel$ are defined by the usual scalar product $\langle \, , \, \rangle$ on $\mathbb{R}^m$. The uniform 1 degree of smoothness ensures that at any point $x_0 \in \Sigma$, the directional limits

$$\lim_{\epsilon \to 0^+} F\big(x_0 + \epsilon n_1(x_0)\big) = F_1(x_0), \qquad \lim_{\epsilon \to 0^+} F\big(x_0 + \epsilon n_2(x_0)\big) = F_2(x_0)$$

both exist and $F_1(x_0) \neq F_2(x_0)$. In the next subsection, codimension–2 discontinuity surfaces with similar properties are defined.

2.2 The Codimension-2 Case

Let Σ be a $m-2$ dimensional smooth manifold embedded in $\mathbb{R}^m$. At a point $x_0 \in \Sigma$ of the manifold, let $\mathcal{T}_{x_0}\Sigma$ denote the tangent space of the manifold and let $\mathcal{O}_{x_0}\Sigma$ denote the corresponding orthogonal complement. At each point $x_0 \in \Sigma$, let us choose two orthonormal basis vectors $n_I(x_0)$ and $n_{II}(x_0)$ of $\mathcal{O}_{x_0}\Sigma$, which depend smoothly on x_0. Then, the set of unit vectors of $\mathcal{O}_{x_0}\Sigma$ can be generated by

$$n(\phi)(x_0) = n_I(x_0)\cos\phi + n_{II}(x_0)\sin\phi,$$

$\phi \in [0, 2\pi)$; see Batlle [2]. At a point x_0 of the manifold, the function $n(\phi)$ gives the unit vector of $\mathcal{O}_{x_0}\Sigma$ corresponding to the direction described by the angle ϕ.

Let $F : \mathbb{R}^m \setminus \Sigma \to \mathbb{R}^m$ be a vector field. If the limit exists, let us define

$$F_*(\phi)(x_0) = \lim_{\epsilon \to 0^+} F\big(x_0 + \epsilon n(x_0)(\phi)\big).$$

Definition 1 (*Codimension–2 discontinuity surface*) Consider the vector field F on $\mathbb{R}^m$ and the $m-2$ dimensional smooth manifold Σ in $\mathbb{R}^m$. Suppose that: (i) F is smooth on $\mathbb{R}^m \setminus \Sigma$; (ii) $F_*(\phi)(x_0)$ exists for all $x_0 \in \Sigma$ and $\phi \in [0, 2\pi)$; (iii) $F_*(\phi)(x_0)$ depends smoothly on both variables; and (iv) for any given $x_0 \in \Sigma$, the function $F_*(\phi)$ is not constant. Then, Σ is the *isolated codimension–2 discontinuity surface* of F.

The system F with this type of discontinuity is *not* a Filippov system, and not even a piecewise smooth system. There is not switching between two types of smooth dynamics, but near the discontinuity set, we get infinitely many directional limits of the vector field.

3 Crossing and Sliding Regions

In case of Filippov systems, the crossing region $\vec{\Sigma}$, and the sliding region $\hat{\Sigma}$ are defined, respectively, by

$$\vec{\Sigma} := \{x_0 \in \Sigma : \langle F_1, n_1\rangle \cdot \langle F_2, n_2\rangle (x_0) < 0\},$$

$$\hat{\Sigma} := \{x_0 \in \Sigma : \langle F_1, n_1\rangle \cdot \langle F_2, n_2\rangle (x_0) > 0\}.$$

In case of crossing, trajectories reaching Σ also pass over Σ, while in case of sliding, trajectories are stuck into the discontinuity set either in forward or in reverse direction of time.

In case of a codimension–2 discontinuity surface, the crossing and sliding regions can be defined analogously:

Definition 2 The *crossing region* $\vec{\Sigma}$ of a codimension–2 discontinuity surface Σ is the set of points $x_0 \in \Sigma$ for that: (i) there exists $\phi_1 \in [0, 2\pi)$ such that $\langle F_*(\phi_1), n(\phi_1)\rangle (x_0) > 0$; and (ii) there exists $\phi_2 \in [0, 2\pi)$ such that $\langle F_*(\phi_2), n(\phi_2)\rangle (x_0) < 0$.

Definition 3 The *sliding region* $\hat{\Sigma}$ of a codimension–2 discontinuity surface Σ is the set of points $x_0 \in \Sigma$ for that: (i) $\langle F_*(\phi), n(\phi)\rangle (x_0) < 0$ for all $\phi \in [0, 2\pi)$; or (ii) $\langle F_*(\phi), n(\phi)\rangle (x_0) > 0$ for all $\phi \in [0, 2\pi)$.

That is, sliding region requires that the discontinuity manifold has to be either attracting or repelling from *all directions*. If there exists an attracting and a repelling direction, the trajectories cross the discontinuity set.

4 Sliding Dynamics

By using Filippov's convex method, the sliding vector of Filippov systems can be calculated in the form $F_s = \sum_{i=1}^{2} \alpha_i F_i$, with $\sum_{i=1}^{2} \alpha_i = 1$ and $\langle F_s, n_1\rangle = 0$, where the dependence on the chosen point $x_0 \in \Sigma$ is not denoted. The resulting system of linear equations determines the weights α_1, α_2 and the sliding vector F_s unambiguously. The *convex* combination also requires $\alpha_1, \alpha_2 \geq 0$, which is true exactly in the closure of the sliding region $\hat{\Sigma}$.

Analogously, the sliding vector in the codimension–2 case can be written as a convex combination of the limit vector field,

$$F_s = \int_0^{2\pi} \alpha(\phi) F_*(\alpha) \mathrm{d}\phi, \tag{1}$$

where we require

$$\int_0^{2\pi} \alpha(\phi)\mathrm{d}\phi = 1, \qquad \langle F_s, n_I \rangle = 0, \qquad \langle F_s, n_{II} \rangle = 0. \tag{2}$$

Instead of the discrete weights, now we have a weight function $\alpha(\phi)$ over $[0, 2\pi)$. Due to the *convex* combination, $\alpha(\phi)$ has to be non-negative for all $\phi \in [0, 2\pi)$. In general, the construction (1)–(2) does not provide an unambiguous sliding vector F_s. This problem occurs also in the case of codimension–2 discontinuity surfaces generated from intersections of codimension–1 surfaces; see Jeffrey [5].

However, the method determines the sliding vector completely in the special case when $F_*(\phi)$ can be written into the form

$$F_*(\phi) = F_0 + A_1 \cos\phi + B_1 \sin\phi. \tag{3}$$

The practical importance of this class is that it contains the case of discontinuity from spatial Coulomb friction. From the Fourier expansion of the unknown weight function $\alpha(\phi)$, the condition (2) leads to the sliding vector

$$F_s = F_0 + \pi a_1 A_1 + \pi b_1 B_1, \tag{4}$$

where the coefficients a_1 and b_1 are determined by

$$\begin{bmatrix} \langle A_1, n_I \rangle & \langle B_1, n_I \rangle \\ \langle A_1, n_{II} \rangle & \langle B_1, n_{II} \rangle \end{bmatrix} \cdot \begin{bmatrix} \pi a_1 \\ \pi b_1 \end{bmatrix} = - \begin{bmatrix} \langle F_0, n_I \rangle \\ \langle F_0, n_{II} \rangle \end{bmatrix}. \tag{5}$$

It is an open question whether there exists a natural choice of F_s if $F_*(\phi)$ has a more general form than (3).

5 Example: Mass Points on the Plane with Coulomb Friction

The results are demonstrated on a simple mechanical system. Consider two mass points on the plane connected by a rigid rod with negligible mass; see Fig. 1. The mass of both mass points is m and their distance is $2d$. Suppose that one of the mass points is subjected to Coulomb friction with constant C magnitude of the friction force, and a constant torque M also acts in orthogonal direction of the plane.

The state of the system can be described by $x = (u_1, u_2, \omega)$, where the velocity components u_1 and u_2 are measured in the co–rotating coordinate frame, and ω is the angular velocity of the system. Then, Newton's Second Law leads to

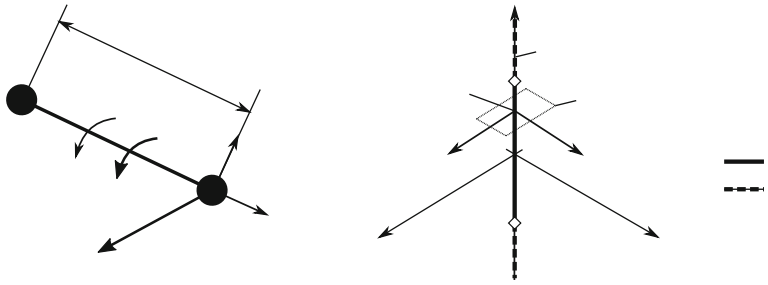

Fig. 1 Sketch of the mechanical system and its phase space

$$\dot{x} = F(x) = \\ = \left(-\frac{C}{2m}\frac{u_1}{\sqrt{u_1^2+u_2^2}} + \omega u_2 - \omega^2 d,\ -\frac{C}{m}\frac{u_2}{\sqrt{u_1^2+u_2^2}} - \omega u_1 + \frac{M}{2md},\ -\frac{C}{2md}\frac{u_2}{\sqrt{u_1^2+u_2^2}} + \frac{M}{2md^2} \right).$$

The codimension–2 discontinuity set is $\Sigma = \{(0, 0, \omega) : \omega \in \mathbb{R}\}$. Let $n_I = (1, 0, 0)$ and $n_{II} = (0, 1, 0)$, then, the limit vector field becomes

$$F_*(\phi) = \left(-\frac{C}{2m}\cos\phi - \omega^2 d,\ -\frac{C}{m}\sin\phi + \frac{M}{2md},\ -\frac{C}{2md}\sin\phi + \frac{M}{2md^2} \right). \tag{6}$$

As (6) has the form of (3), the formulae (4)–(5) can be applied, an we obtain $a_1 = -2md\omega^2/(C\pi)$, $b_1 = M/(2dC\pi)$, and $F_s = (0, 0, M/(4md^2))$. The sliding region can be calculated according to Definition 3 by finding $\langle F_*(\phi), n(\phi)\rangle\,(x_0) = 0$, and we get

$$\hat{\Sigma} = \left\{ (0, 0, \omega) : |\omega| < \hat{\omega} \right\}, \tag{7}$$

where $\hat{\omega}^2 = \sqrt{\left(\frac{C}{2md}\right)^2 - \left(\frac{M}{4md^2}\right)^2}$; see Fig. 1. In the case $M > 2dC$, there is no sliding region. These results are consistent with those calculated from the maximum admissible static friction force from the Coulomb model. Moreover, the presented method can be applied even if the static friction force cannot be determined; see Antali–Stepan [1].

Acknowledgements The research leading to these results has received funding from the European Research Council under the European Union's Seventh Framework Programme (FP/2007-2013)/ERC Advanced Grant Agreement n. 340889.

References

1. M. Antali, G. Stepan, Discontinuity-induced bifurcations of a dual-point contact ball. Nonlinear Dyn. **83**, 685–702 (2016)
2. J.A. Batlle, The sliding velocity flow of rough collisions in multibody systems. J. Appl. Mech. **63**(3), 804–809 (1996)

3. M. di Bernardo, C. Budd, A.R. Champneys, P. Kowalczyk, *Piecewise-Smooth Dynamical Systems* (Springer, London, 2008)
4. L. Dieci, F. Difonzo, The moments sliding vector field on the intersection of two manifolds. J. Dyn. Diff. Equat. (2015). doi:10.1007/s10884-015-9439-9
5. M.R. Jeffrey, Dynamics at a switching intersection. J. Appl. Dyn. Syst. **13**(3), 1082–1105 (2014)

Asynchronous Networks

Christian Bick and Mike J. Field

Abstract Asynchronous networks form a natural framework for many classes of dynamical networks encountered in technology, engineering and biology. Typically, nodes can evolve independently, be constrained, stop, and later restart, and interactions between components of the network may depend on time, state, and stochastic effects. We outline some of the main ideas, motivations and a basic result.

1 Asynchronous Networks: Motivation and Characteristics

Asynchronous networks are an approach to network dynamics that takes account of features encountered in networks from engineering and biology, especially neuroscience, and where techniques such as averaging or methods from statistical physics may miss essential structure (see Bick–Field [3, Sect. 1] for a careful discussion). Asynchronous networks may involve a mix of distributed and decentralized control, adaptivity, event driven dynamics, switching, varying network topology and hybrid dynamics. Network dynamics will generally only be piecewise smooth, nodes may stop and later restart, and there may be no intrinsic global time. Intended applications range from switching problems involving power grids and microgrids (see Dörfler–Chertkov–Bullo [6]), production and transport networks, and learning mechanisms from neuroscience such as Spike-Timing Dependent Plasticity (see Gerstner–Kempter–van-Hemmen–Wagner [8]). In these notes we sketch some of the main ideas and refer the reader to [3, 4] for more details and references. We summarize below some of the key features of asynchronous networks:

C. Bick (✉)
Department of Mathematics, Exeter University, Exeter EX4 4QF, UK
e-mail: c.bick@exeter.ac.uk

M.J. Field
Department of Mathematics, Imperial College, London SW7 2AZ, UK
e-mail: mikefield@gmail.com

A. Colombo et al. (eds.), *Extended Abstracts Spring 2016*,
Trends in Mathematics 8, DOI 10.1007/978-3-319-55642-0_3

(i) state dependent and/or stochastic variation in connection structure and dependencies between nodes;
(ii) synchronization events associated with stopping or waiting states of nodes;
(iii) order of events may depend on the initialization of the system;
(iv) dynamics is only piecewise smooth;
(v) aspects involving function, adaptation and control;
(vi) evolution only defined for forward time – systems are not time reversible.

1.1 Reductionism and Modularization of Dynamics

In nonlinear network dynamics and complex systems, generally, there is the question as to how far one can make use of reductionist techniques; see Ladyman–Lambert–Wiesner [10, 2.5]. For example, one approach, advanced by Kastan–Alon [9] in systems biology, has been the identification and description of *network motifs* (small network configurations that occur frequently in large biological networks). The underlying premise is that a modular, or engineering, approach to network dynamics is feasible: identify building blocks, connect together to form networks and then describe dynamical properties of the resulting network in terms of the dynamics of its components.

> *"Ideally, we would like to understand the dynamics of the entire network based on the dynamics of the individual building blocks." Alon* [1, p 27].

Such a reductionist approach works well in linear systems theory, where a superposition principle holds, or in the study of synchronization in weakly coupled nonlinear oscillators (for example, in Pecora–Carroll, [11]), but is usually unrealistic in the study of heterogenous networks modelled by a system of analytic nonlinear differential equations: network dynamics may bear little or no relationship to the intrinsic (uncoupled) dynamics of nodes.

If we emphasize function and allow for intermittent connection structure, then it may be possible to apply reductionist principles. In Fig. 1 we show schematics of a network with only intermittent connection between eight nodes.[1] Each node N_i will be given an initial state and started at time $T_i \geq 0$. Nodes interact depending on their state. For example, in the evolution depicted in Fig. 1, nodes N_1, N_2 will first interact during the event indicated by $\mathbf{E}^a$. Observe there is no global time defined for this system but there is a partially ordered temporal structure: event $\mathbf{E}^c$ always occurs after event $\mathbf{E}^a$ but may occur before or after event $\mathbf{E}^b$. This network has also a *function*: reaching the terminal states indicated on the right hand side of the figure. Observe the possibility of a (dynamical) deadlock: network function is not achieved.

[1] For example, view Fig. 1 as being part of a threaded computer program and $\mathbf{E}^a, \ldots, \mathbf{E}^h$ as being synchronization events – evolution of associated threads is stopped until each thread has finished its computation; variables are then synchronized across the threads.

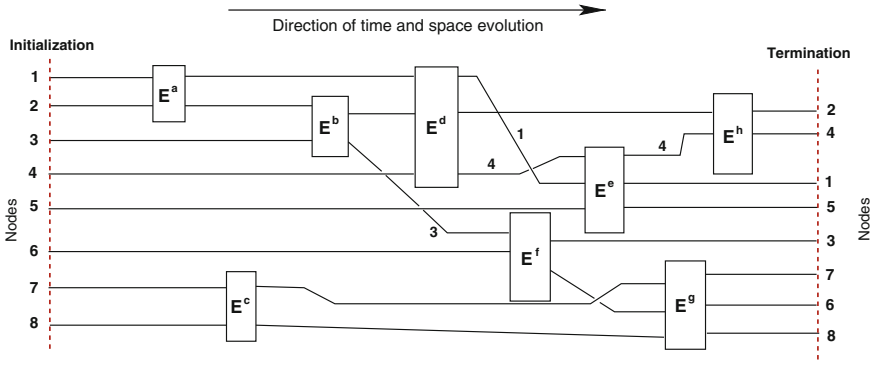

Fig. 1 A functional feedforward network with 8 nodes

Our main result is a *modularization of dynamics theorem*. Specifically, we give general conditions that enable us to describe the function of a large class of functional asynchronous networks in terms of the function of constituent subnetworks (as in Fig. 1; details are in Bick–Field [4]). The theorem allows for events depending on local times and for variation in the number of nodes (a dynamics version of a *Petri Net*; see David–Alla [5]). Nonsmoothness is a crucial ingredient needed for this result. In networks modelled by smooth dynamical systems, all nodes are effectively coupled to each other at all times and so information propagates instantly across the entire network. A spatiotemporal decomposition, such as is given by the modularization of dynamics theorem, is only possible if the network dynamics is nonsmooth and (subsets of) nodes are allowed to evolve independently of each other for periods of time. This allows us to construct discrete dynamical units (for example, Alon's motifs), each with its own function, that together make up the dynamics of the network. The result highlights what can get lost when averaging over a network: the averaging out of the functional units and their temporal relations that yield network function. A consequence is that, rather than asking how network dynamics can be understood in terms of the dynamics of constituents, one has to ask how network function can be understood in term of the function of constituents.

2 Abstraction

We give the formal setup for asynchronous networks in the simplest case, omitting most technical details (for these, see Bick–Field [3]), and conclude with an example of a transport network.

For $k \in \mathbb{N}$, define $\mathbf{k} = \{1, \ldots, k\}$ and $\mathbf{k}^\bullet = \mathbf{k} \cup \{0\}$, and assume a network with k nodes, $N_1, \ldots, N_k$. Let M_i denote the phase space of $N_i, i \in \mathbf{k}$, and set $\mathbf{M} = \prod_{i \in \mathbf{k}} M_i$, the network phase space. A vector field $\mathbf{f}$ on $\mathbf{M}$ is a *network vector field*.

Stopping, waiting, and synchronization are characteristic features of asynchronous networks. If the node of a network is stopped or partially stopped, then node dynamics will be constrained to a subset of the node phase space (a single point if the node is stopped). We codify this situation by introducing a *constraining node* N_0 that, when connected to N_i, implies that dynamics on N_i is constrained. Set $\mathcal{N} = \{N_0, \ldots, N_k\}$. We often abuse notation and refer to the *network* $\mathcal{N}$.

2.1 Connection Structures and Admissible Vector Fields

We represent interactions between distinct nodes in $\mathcal{N}$ by the network graph. Connections $N_j \to N_i$ encode *dependencies*, if $i, j \in \mathbf{k}$, and *constraints* if $j = 0$, $i \in \mathbf{k}$.

A *connection structure* α is a directed network graph on the nodes $\mathcal{N}$ such that for all $i \in \mathbf{k}$, $j \in \mathbf{k}^\bullet$, $i \neq j$, there is at most one directed connection $N_j \to N_i$. An α-admissible network vector field $\mathbf{f}$ has dependencies given by α (if $N_j \to N_i \notin \alpha$, $\mathbf{f}_i^\alpha$ will not depend on x_j and conversely). A *generalized connection structure* $\mathcal{A}$ is a set of connection structures on $\mathcal{N}$. An $\mathcal{A}$-*structure* $\mathcal{F}$ is a set $\mathcal{F} = \{\mathbf{f}^\alpha \mid \alpha \in \mathcal{A}\}$ of admissible vector fields.

2.2 The Event Map and Asynchronous Networks

Suppose a generalized connection structure $\mathcal{A}$ and an $\mathcal{A}$-structure $\mathcal{F}$ are given. Interactions between nodes in asynchronous networks may be state or time dependent. We consider state dependence and handle interactions and constraints using an *event map* $\mathcal{E} : \mathbf{M} \to \mathcal{A}$.

Given a generalized connection structure $\mathcal{A}$, $\mathcal{A}$-structure $\mathcal{F}$ and event map $\mathcal{E}$, the quadruple $(\mathcal{N}, \mathcal{A}, \mathcal{F}, \mathcal{E})$ defines an *asynchronous network*. Dynamics on $\mathcal{N}$ is given by the state dependent network vector field $\mathbf{F}$ defined by

$$\mathbf{F}(\mathbf{X}) = \mathbf{f}^{\mathcal{E}(\mathbf{X})}(\mathbf{X}), \quad \mathbf{X} \in \mathbf{M}. \tag{1}$$

Subject to quite simple regularity conditions (see Bick–Field [3]), the network vector field (1) will have a uniquely defined semi-flow (continuous in time but not necessarily in the initial state).

Although the integral curves of (1) are not always the same as those obtained using standard approaches to nonsmooth systems, there are relations between asynchronous networks and Filippov systems; see Filippov [7]. This is explored further in [2, 3].

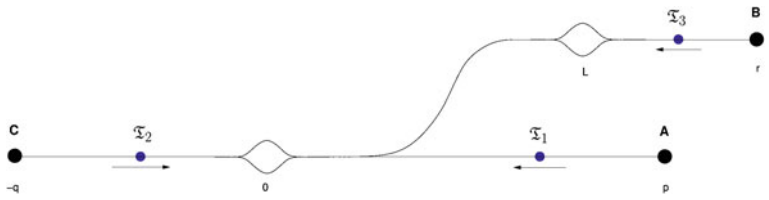

Fig. 2 Three trains going through passing loops at 0 and L

2.3 Example: Two Passing Loops on Single Track Lines

In Fig. 2, we show three trains that have to traverse two passing loops. Train $\mathfrak{T}_1$ starts at station A; train $\mathfrak{T}_2$ at C; train $\mathfrak{T}_3$ at B. Once train $\mathfrak{T}_2$ has traversed the first passing loop it will continue on the branch line towards the second passing loop and station B.

We model the transport network using our abstraction of an asynchronous network (see also Bick–Field [4]). Take $M_i = \mathbb{R}, \alpha_i = N_0 \to N_i, i \in \mathbf{3}$ (α_i corresponds to $\mathfrak{T}_i$ stopped). Take generalized connection structure $\mathcal{A} = \{\emptyset, \alpha_1, \alpha_2, \alpha_3, \alpha_1 \vee \alpha_3, \alpha_2 \vee \alpha_3\}$, where $\emptyset$ denotes the empty connection structure. Let $v_2 > 0 > v_1, v_3$ and define the $\mathcal{A}$-structure $\mathcal{F}$ by

$$\mathbf{f}^{\emptyset} = (v_1, v_2, v_3), \qquad \mathbf{f}^{\alpha_1} = (0, v_2, v_3), \qquad \mathbf{f}^{\alpha_2} = (v_1, 0, v_3),$$

$$\mathbf{f}^{\alpha_3} = (v_1, v_2, 0), \qquad \mathbf{f}^{\alpha_1 \vee \alpha_3} = (0, v_2, 0), \qquad \mathbf{f}^{\alpha_2 \vee \alpha_3} = (v_1, 0, 0).$$

Define the event map $\mathcal{E} : \mathbf{M} \to \mathcal{A}$ by

$$\mathcal{E}(x_1, x_2, x_3) = \begin{cases} \alpha_1 & \text{if } x_1 = 0, x_2 < 0, \\ \alpha_2 & \text{if } x_1 > 0, x_2 = 0 \text{ or } x_2 = L, x_3 > L, \\ \alpha_3 & \text{if } x_2 < L, x_3 = L, \\ \alpha_1 \vee \alpha_3 & \text{if } x_1 = 0, x_2 < 0, x_3 = L, \\ \alpha_2 \vee \alpha_3 & \text{if } x_1 < 0, x_2 = 0, x_3 = L, \\ \emptyset & \text{otherwise.} \end{cases}$$

This defines the asynchronous network $\mathfrak{N} = (\mathcal{N}, \mathcal{A}, \mathcal{F}, \mathcal{E})$ and gives the correct train dynamics. The modularization of dynamics theorem applies to $\mathfrak{N}$; see Bick–Field [4] for details.

Acknowledgements C. Bick is supported, in part, by NSF Grant DMS-1265253 and Marie Curie IEF Fellowship (project 626111). M.J. Field is supported, in part, by NSF Grant DMS-1265253 and Marie Curie IIF Fellowship (project 627590).

References

1. U. Alon, *An Introduction to Systems Biology. Design Principles of Biological Circuits* (Chapman & Hall/CRC, Boca Raton, 2007)
2. C. Bick, Local representation of asynchronous networks by Filippov systems (in preparation)
3. C. Bick, M.J. Field, Asynchronous networks and event driven dynamics (preprint)
4. C. Bick, M.J. Field, Asynchronous networks: modularization of dynamics theorem (preprint)
5. R. David, H. Alla, *Discrete, Continuous, and Hybrid Petri Nets* (Springer, Berlin, 2010)
6. F. Dörfler, M. Chertkov, F. Bullo, Synchronization in complex oscillator networks and smart grids. PNAS **110**(6), 2005–2010 (2013)
7. A.F. Filippov, *Differential Equations with Discontinuous Righthand Sides* (Kluwer Academic Publishers, 1988)
8. W. Gerstner, R. Kempter, L.J. van Hemmen, H. Wagner, A neuronal learning rule for submillisecond temporal coding. Nature **383**, 76–78 (1996)
9. N. Kashtan, U. Alon, Spontaneous evolution of modularity and network motifs. PNAS **102**(39), 13773–13778 (2005)
10. J. Ladyman, J. Lambert, K. Wiesner, What is a complex system? Eur. J. Philos. Sci. **3**(1), 33–67 (2013)
11. L.M. Pecora, T.L. Carroll, Master stability functions for synchronized coupled systems. Phys. Rev. Lett. **80**, 2109–2112 (1998)

Regularization by External Variables

**E. Bossolini, R. Edwards, P.A. Glendinning,
M.R. Jeffrey, and S. Webber**

Abstract Regularization was a big topic at the 2016 CRM Intensive Research Program on Advances in Nonsmooth Dynamics. There are many open questions concerning well known kinds of regularization (e.g., by smoothing or hysteresis). Here, we propose a framework for an alternative and important kind of regularization, by external variables that *shadow* either the state or the switch of the original system. The shadow systems are derived from and inspired by various applications in electronic control, predator-prey preference, time delay, and genetic regulation.

1 Shadowing in One Variable

Begin with a one-dimensional dynamical system

$$\dot{x} = -\lambda + xb(x;\lambda), \tag{1}$$

where $\lambda = \text{sign}(x)$ with the sign function being ± 1 for $x \gtrless 0$ and having the set value $(-1,+1)$ for $x = 0$. This has an attracting fixed point on the discontinuity, where $\dot{x} = -\lambda$. Define a *switch-shadowing* system

E. Bossolini (✉)
Department of Applied Mathematics and Computer Science,
Technical University of Denmark, 2800 Kongens Lyngby, Denmark
e-mail: ebos@dtu.dk

R. Edwards
Department of Mathematics and Statistics, University of Victoria, Victoria,
BC V8W 2Y2, Canada
e-mail: edwards@uvic.ca

P.A. Glendinning
School of Mathematics, University of Manchester, Oxford Road, Manchester M13 9PL, UK
e-mail: p.a.glendinning@manchester.ac.uk

M.R. Jeffrey · S. Webber
Department of Engineering Mathematics, University of Bristol, Bristol BS8 1UB, UK
e-mail: mike.jeffrey@bristol.ac.uk

A. Colombo et al. (eds.), *Extended Abstracts Spring 2016*,
Trends in Mathematics 8, DOI 10.1007/978-3-319-55642-0_4

$$\dot{x} = -\lambda + xb(x;\lambda), \qquad \dot{y} = (x-y)/\gamma,$$

where $\lambda = \text{sign}(y)$, or a *state-shadowing* system

$$\dot{x} = -\lambda + yb(y;\lambda), \qquad \dot{y} = (x-y)/\gamma,$$

where $\lambda = \text{sign}(x)$, $\gamma > 0$ is small, and y is an external variable representing some extra stage in the switching process, such that each shadow system relaxes to (1) as $y \to x$. So, y tends to x like $e^{-t/\gamma}$ (for small γ where we can treat x as slow varying), i.e., y shadows x.

We restrict attention to the neighbourhood of the equilibrium at $x = y = \lambda = 0$ in each system. In the switch-shadowing system, the switching surface becomes $y = 0$, and sliding no longer occurs because solutions all cross the surface (because the y component does not switch) – the surface is 'transparent' in some nomenclature. In the state-shadowing system the switching surface remains sliding.

We will analyze these using switching layer methods (see Glendinning–Jeffrey [2] and next section).

For the switch-shadowing system on $y = 0$ the switching layer system is

$$\dot{x} = -\lambda + xb(x;\lambda), \qquad \varepsilon\dot{\lambda} = x/\gamma,$$

for $\lambda \in (-1,+1)$, $\varepsilon \to 0$, and the Jacobian of the equilibrium is

$$\begin{pmatrix} \frac{\partial \dot{x}}{\partial x} & \frac{\partial \dot{x}}{\partial \varepsilon\lambda} \\ \frac{\partial \varepsilon\dot{\lambda}}{\partial x} & \frac{\partial \varepsilon\dot{\lambda}}{\partial \varepsilon\lambda} \end{pmatrix} = \begin{pmatrix} b & -1/\varepsilon \\ 1/\gamma & 0 \end{pmatrix}$$

with eigenvalues $(b(0,0) \pm i\sqrt{4-b^2\gamma\varepsilon})/2\sqrt{\gamma\varepsilon} \to \frac{1}{2}b(0,0) \pm i\infty$ as $\varepsilon \to 0$. Outside the switching surface the dynamics spirals in as a 'fused focus' towards $x = y = 0$, but once there, in the x-λ dynamics, the attractivity depends on the sign of $b(0,0)$. In particular, if $b(0,0) > 0$ then the sliding equilibrium will become unstable, and a limit cycle will be formed inside the switching layer $(x,\lambda) \in \mathbb{R} \times (-1,+1)$.

For the state-shadowing system on $x = 0$ the switching layer system is

$$\varepsilon\dot{\lambda} = -\lambda + yb(y;\lambda), \qquad \dot{y} = -y/\gamma,$$

where $\lambda \in (-1,+1)$, and the Jacobian of the equilibrium is

$$\frac{\partial(\varepsilon\dot{\lambda},\dot{y})}{\partial(\varepsilon\lambda,y)} = \begin{pmatrix} -1/\varepsilon & b(0;0) \\ 0 & -1/\gamma \end{pmatrix}$$

with eigenvalues $-1/\gamma$ and $-1/\varepsilon \to -\infty$. In this case the equilibrium of the shadow system remains an attractor; see Fig.1.

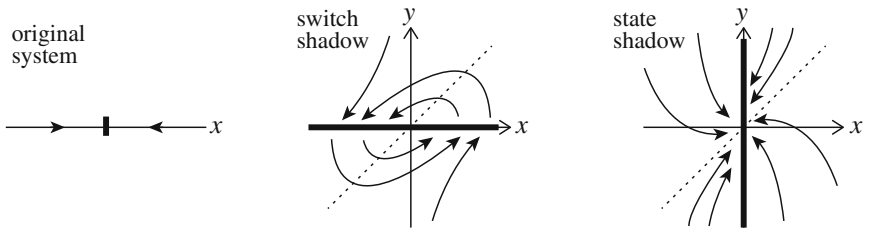

Fig. 1 The original system and its two shadow regularizations

2 Shadowing in *n* Variables

Now take a multivariable state $\mathbf{x} = (x_1, \ldots, x_n)$, and assume there is one switch for every coordinate (this can be generalized later). So we have switching functions $h_1, \ldots h_n$, and switching multipliers $\boldsymbol{\lambda} = (\lambda_1, \ldots, \lambda_n)$ where $\lambda_i \in [-1, +1]$, such that $\lambda_i = \text{sign } h_i$ for $h_i \neq 0$ and $\lambda_i \in (-1, +1)$ for $h_i = 0$. Letting $\mathbf{f}$ be a smooth function of $\mathbf{x}$ and $\boldsymbol{\lambda}$, the system

$$\dot{\mathbf{x}} = \mathbf{f}(\mathbf{x}; \boldsymbol{\lambda}), \tag{2}$$

where $\lambda_i = \text{sign } h_i$, is smooth except at the thresholds $\Sigma_i = \{\mathbf{x} \in \mathbb{R}^n : h_i = 0\}$.

In the piecewise smooth setting we assume each h_i is a regular function of $\mathbf{x}$, some $h_i = h_i(\mathbf{x})$. When $h_i = 0$ for some i, we blow up the switching surface $h_i = 0$ into a switching layer $\lambda_i \in (-1, +1)$, with dynamics given by $\varepsilon_i \dot{\lambda}_i = \mathbf{f}(\mathbf{x}; \boldsymbol{\lambda}) \cdot \nabla h_i$ for $\varepsilon_i \to 0$.

Take coordinates in which $h_i = x_i$ for $i = 1, \ldots, n$. When $\mathbf{x}$ lies on the intersection of all n switching thresholds, $x_1 = x_2 = \cdots = x_n = 0$, we study the dynamics in the codimension n switching layer $(\lambda_1, \ldots, \lambda_n) \in (-1, +1)^n$ given by

$$\underline{\underline{\varepsilon}}.\dot{\boldsymbol{\lambda}} = \mathbf{f}(\mathbf{0}; \boldsymbol{\lambda}), \qquad |\underline{\underline{\varepsilon}}| \to 0,$$

where $\underline{\underline{\varepsilon}}$ denotes the diagonal matrix with entries $\varepsilon_1, \ldots, \varepsilon_n$ or, in components, $\varepsilon_i \dot{\lambda}_i = f_i(\mathbf{0}; \lambda_1, \ldots, \lambda_n)$ for $i = 1, \ldots, n$. Sliding modes are equilibria of the fast system. We assume these lie at $\mathbf{x} = \boldsymbol{\lambda} = 0$, and are stable, which means that

$$\frac{\partial \underline{\underline{\varepsilon}}.\dot{\boldsymbol{\lambda}}}{\partial \underline{\underline{\varepsilon}}.\boldsymbol{\lambda}} = \underline{\underline{\varepsilon}}^{-1}.\frac{\partial \mathbf{f}}{\partial \boldsymbol{\lambda}} \tag{3}$$

has eigenvalues with negative real part at $(\mathbf{0}; \mathbf{0})$.

Define a switch-shadowing system

$$\dot{\mathbf{x}} = \mathbf{f}(\mathbf{x}; \boldsymbol{\lambda}), \qquad \dot{\mathbf{y}} = (\mathbf{x} - \mathbf{y})/\gamma,$$

where $\lambda_i = \text{sign}(y_i)$, or a state-shadowing system

$$\dot{\mathbf{x}} = \mathbf{f}(\mathbf{y}; \boldsymbol{\lambda}), \qquad \dot{\mathbf{y}} = (\mathbf{x} - \mathbf{y})/\gamma,$$

where $\lambda_i = \text{sign}(x_i), \gamma > 0$ is small (we could choose different γ_i for each component of $\mathbf{y}$), and $\mathbf{y}$ is an n-dimensional external variable. As before, both tend to (2) as $\mathbf{y}$ shadows $\mathbf{x}$. Each has an equilibrium at $\mathbf{x} = \mathbf{y} = \boldsymbol{\lambda} = 0$. For the switch-shadowing system on $\mathbf{y} = 0$ the switching layer system is

$$\dot{\mathbf{x}} = \mathbf{f}(\mathbf{x}; \boldsymbol{\lambda}), \qquad \varepsilon\dot{\boldsymbol{\lambda}} = \mathbf{x}/\gamma,$$

for $\boldsymbol{\lambda} \in (-1, +1)^n$, and the Jacobian of the equilibrium is

$$\begin{pmatrix} \frac{\partial \dot{\mathbf{x}}}{\partial \mathbf{x}} & \frac{\partial \dot{\mathbf{x}}}{\partial \underline{\underline{\varepsilon}}.\boldsymbol{\lambda}} \\ \frac{\partial \underline{\underline{\varepsilon}}.\dot{\boldsymbol{\lambda}}}{\partial \mathbf{x}} & \frac{\partial \underline{\underline{\varepsilon}}.\dot{\boldsymbol{\lambda}}}{\partial \underline{\underline{\varepsilon}}.\boldsymbol{\lambda}} \end{pmatrix} = \begin{pmatrix} \frac{\partial \mathbf{f}(0;0)}{\partial \mathbf{x}} & \underline{\underline{\varepsilon}}^{-1}.\frac{\partial \mathbf{f}(0;0)}{\partial \boldsymbol{\lambda}} \\ \underline{\underline{1}}/\gamma & 0 \end{pmatrix},$$

where $\underline{\underline{1}}$ is the $n \times n$ identity matrix. The stability of the term $\underline{\underline{\varepsilon}}^{-1}.\frac{\partial \mathbf{f}}{\partial \boldsymbol{\lambda}}$ from (3) does not guarantee stability of the shadow equilibrium, which will depend crucially on $\frac{\partial \mathbf{f}(0;0)}{\partial \mathbf{x}}$.

For the state-shadowing system on $x = 0$ the switching layer system is

$$\varepsilon\dot{\boldsymbol{\lambda}} = \mathbf{f}(\mathbf{y}; \boldsymbol{\lambda}), \qquad \dot{\mathbf{y}} = -\mathbf{y}/\gamma,$$

where $\lambda \in (-1, +1)$, and the Jacobian of the equilibrium is

$$\frac{\partial(\underline{\underline{\varepsilon}}.\dot{\boldsymbol{\lambda}}, \dot{\mathbf{y}})}{\partial(\underline{\underline{\varepsilon}}.\boldsymbol{\lambda}, \mathbf{y})} = \begin{pmatrix} \underline{\underline{\varepsilon}}^{-1}.\frac{\partial \mathbf{f}(0;0)}{\partial \boldsymbol{\lambda}} & \frac{\partial \mathbf{f}(0;0)}{\partial \mathbf{y}} \\ 0 & -\underline{\underline{1}}/\gamma \end{pmatrix}.$$

In this case it seems likely that the equilibrium of the shadow system remains an attractor, the stability of the term $\underline{\underline{\varepsilon}}^{-1}.\frac{\partial \mathbf{f}}{\partial \boldsymbol{\lambda}}$ from (3) and the term $-\underline{\underline{1}}/\gamma$ playing the crucial role.

3 Examples

The following examples motivated the shadow regularizations proposed above.

Genetic Regulatory Networks. A typical gene network protein-only model gives the dynamics of the concentration x_i of the protein product of a gene i, for $i = 1, \ldots, n$, as

$$\dot{x}_i = B_i(Z_1, \ldots, Z_n) - \alpha_i x_i \ , \qquad Z_i = \text{step}(x_i - \theta_i) \ ,$$

where $\alpha_i, \theta_i > 0$. In Edwards–Machina–McGregor–van-den-Driessche [1], this is extended to include the intermediary role of mRNA. Instead, we make x_i the concentration of the i-th mRNA molecule, and y_i the protein product concentration for

gene i, then the proposed model is

$$\dot{x}_i = B_i(Z_1, \ldots, Z_n) - \alpha_i x_i, \quad \dot{y}_i = \kappa_i x_i - \beta_i y_i, \quad Z_i = \text{step}(y_i - \theta_i),$$

with $\alpha_i, \beta_i, \kappa_i, \theta_i > 0$.

Time delay. Assume a system modelled by $\dot{x} = f(x; \lambda)$ with $\lambda = \text{sign}(x)$ actually switches not exactly when a solution $x(t)$ lies at $x(t) = 0$, but when $x(t - \tau)$ with a time delay τ. We can define a delayed variable $y(t) = x(t - \tau)$, or let

$$\dot{x} = f(x; \lambda), \qquad \dot{y} = (x - y)/\tau,$$

where $\lambda = \text{sign}(y)$.

Plankton. A predator-prey system discussed in Piltz [4] for predator population x_3 and prey populations x_1, x_2, is

$$\left.\begin{aligned} \dot{x}_1 &= \{r_1 - x_3\mu\}\, x_1 \\ \dot{x}_2 &= \{r_2 - x_3(1-\mu)\}\, x_2 \\ \dot{x}_3 &= \{q_1 x_1 \mu + q_2 x_2 (1-\mu) - m\}\, x_3 \end{aligned}\right\},$$

where $\mu = \text{step}(x_1 - a x_2)$, in terms of constants r_1, r_2, q_1, q_2, m, a. This assumes the consumption of prey is proportional to their population x_1 or x_2. If, instead, consumption is proportional to a variable y_1 or y_2, which tends towards the population, we have

$$\left.\begin{aligned} \dot{x}_1 &= r_1 x_1 - x_3 y_1 \mu \\ \dot{x}_2 &= r_2 x_2 - x_3 y_2 (1-\mu) \\ \dot{x}_3 &= \{q_1 y_1 \mu + q_2 y_2 (1-\mu) - m\}\, x_3 \\ \dot{y}_1 &= (x_1 - y_1)/\gamma_1 \\ \dot{y}_2 &= (x_2 - y_2)/\gamma_2 \end{aligned}\right\},$$

where $\mu = \text{step}(x_1 - a x_2)$.

Electronic sensors. A typical form for a piecewise affine control system is

$$\dot{\mathbf{x}} = \underline{\underline{A}}\mathbf{x} + \mathbf{b}u,$$

where $u = \text{step}(x_1 - \theta)$, in terms of a constant matrix A and vector $\mathbf{b}$ describing electronic components. In Kafanas [3] it is noted that, although a control system implements control on the state $\mathbf{x}$, it does so by measuring not $\mathbf{x}$ itself, but a sensor value $\mathbf{y}$, hence a more faithful model is

$$\dot{\mathbf{x}} = \underline{\underline{A}}\mathbf{x} + \mathbf{b}u, \qquad \dot{\mathbf{y}} = (\mathbf{x} - \mathbf{y}).\underline{\underline{\kappa}},$$

where $u = \text{step}(y_1 - \theta)$, for some diagonal matrix $\underline{\underline{\kappa}}$.

4 A United Form

We can express both the switch and state shadow regularizations together by writing

$$\dot{\mathbf{x}} = \mathbf{f}\left(\mathbf{s}_\mu(\mathbf{x}, \mathbf{y}); \boldsymbol{\lambda}\right), \quad \dot{\mathbf{y}} = (\mathbf{x} - \mathbf{y})/\gamma,$$

where $\lambda_i = \text{sign}\left(S_\mu(x_i, y_i)\right)$ for vector and scalar shadow functions $\mathbf{s}_\mu(\mathbf{x}, \mathbf{y})$ and $S_\mu(x, y)$ which satisfy $\mathbf{s}_\mu(\mathbf{x}, \mathbf{x}) = \mathbf{x}$ and $S_\mu(x, x) = x$, for example $\mathbf{s}_\mu(\mathbf{x}, \mathbf{y}) = \mu\mathbf{x} + (1 - \mu)\mathbf{y}$ and $S_\mu(x, y) = \mu x + (1 - \mu)y$. The switch-shadowing and state-shadowing systems are obtained at the extremes for $\mu = 1$ and $\mu = 0$ respectively. In the most general case we could consider γ to be a (contracting) matrix, and/or a function of $\mathbf{x}$ and $\mathbf{y}$.

In the future, it will be interesting to study how the stability of equilibria is affected under such regularizations in general, and the implications this has for the structural stability of piecewise smooth systems.

A final but important note must be made if the switching layer expression $\varepsilon\dot{\lambda} = \cdots$ is derived as the approximation to a smooth system (as in, e.g., GRN models [1]). Then, the ε on the lefthand side of this expression is actually a function of λ, which makes the vanishing entries of the Jacobians from $\frac{\partial \varepsilon\dot{\lambda}}{\partial \varepsilon \lambda}$ become nonzero and, while we expect this not to qualitatively affect the result as $\varepsilon \to 0$, further study is required.

References

1. R. Edwards, A. Machina, G. McGregor, P. van den Driessche, A modelling framework for gene regulatory networks including transcription and translation. Bull. Math. Biol. **77**, 953–983 (2015)
2. P. Glendinning, M.R. Jeffrey, *An introduction to piecewise smooth dynamics*, Advanced Courses in Mathematics - CRM Barcelona (Springer, Berlin, 2016)
3. G. Kafanas, Sensor effects in sliding mode control of power conversion cells, this volume
4. S. Piltz, Smoothing a piecewise-smooth: An example from plankton population dynamics, this volume

Characterizing Tipping in a Stochastic Reduced Stommel-Type Model in Higher-Dimensions

Chris Budd, Paul Glendinning, Kaitlin Hill, and Rachel Kuske

Abstract During the workshop on Climate Modeling in Nonsmooth Systems, one of the major discussions involved investigating including more realistic elements, such as fluctuations and time variation, in nonsmooth models that undergo a sudden transition, with an emphasis on conceptual climate models. A number of models were discussed, including the Stommel 1961 model, the Paillard 1997 model, the Eisenman–Wettlaufer 2009 model, and the Hogg 2008 model.

1 Introduction

There has been significant recent interest in classifying the various ways in which a dynamical system may undergo a critical transition, where there is a sudden large change in the state of the system as a parameter is varied; see Kuehn [7]. Conceptual climate models may provide pertinent examples of systems which may undergo a critical transition: there is currently broad scientific and public interest in whether sudden transitions may occur in certain climate systems, including the "thermohaline" circulation in the Atlantic; see [1, 8].

C. Budd (✉)
Department of Mathematical Sciences, University of Bath, Bath, UK
e-mail: mascjb@bath.ac.uk

P. Glendinning
School of Mathematics, University of Manchester, Manchester, UK
e-mail: p.a.glendinning@manchester.ac.uk

K. Hill
Department of Engineering Sciences and Applied Mathematics,
Northwestern University, Evanston, IL 60208, USA
e-mail: k-hill@u.northwestern.edu

R. Kuske
Department of Mathematics, University of British Columbia,
Vancouver, BC, Canada
e-mail: rachel@math.ubc.ca

A. Colombo et al. (eds.), *Extended Abstracts Spring 2016*,
Trends in Mathematics 8, DOI 10.1007/978-3-319-55642-0_5

2 The Stommel 1961 Model

During the workshop one major discussion involved investigating how fluctuations influence tipping in nonsmooth models. For example, in the case of periodic fluctuations Zhu, Kuske, and Erneux studied how the frequency of additive periodic forcing affects the timing of tipping from a smooth saddle-node bifurcation in a canonical system with a slowly drifting bifurcation parameter; see [15].

Given the range of conceptual models that include non-smooth dynamics in climate dynamics [5, 6, 10, 14], one could also ask how different type of fluctuations and time dependence will influence their behaviour. Here, we give a description of the Stommel model, as an illustration of the appearance of nonsmooth dynamics in climate models; see details in [14]. The Stommel model is a conceptual model of the ocean's thermohaline circulation, which is a part of the global ocean circulation that drives global ocean currents via density gradients determined by salt and heat fluxes; see Rahmstorf [12] for a brief description of the thermohaline circulation, and Dijkstra [3] for an expository analysis of the dynamics of the Stommel model.

In Stommel's model the Northern Hemisphere is represented by two well-mixed ocean boxes connected on the surface by an overflow and at the bottom by a capillary tube [14]; see Fig. 1. The temperature and salinity in the polar region box are given by T_p and S_p, respectively. Likewise, the temperature and salinity in the equatorial box are given by T_e and S_e. The equations for the model can be expressed in dimensionless form, after rescaling Dijkstra [3], as

$$\frac{dT}{dt} = \eta_1 - T(1 + |T - S|),$$
$$\frac{dS}{dt} = \eta_2 - S(\eta_3 + |T - S|),$$

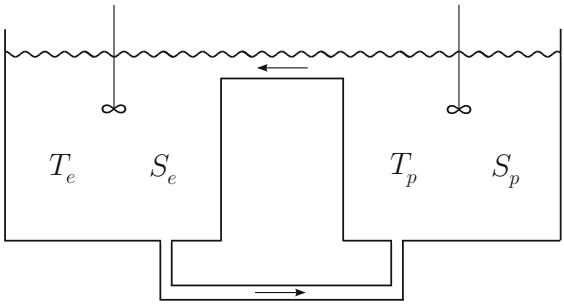

Fig. 1 Diagram of the two-box Stommel model, based on [14, Fig. 5]: (T_e, S_e) represent equatorial temperature and salinity, respectively, and (T_p, S_p) represent polar temperature and salinity. The boxes are connected on top by an overflow and on the bottom by a capillary tube. The flow rate between the two boxes is assumed to be equal and of opposite signs through the overflow and capillary tube

where $T \equiv T_e - T_p$ represents the temperature difference between the equatorial and polar boxes, $S \equiv S_e - S_p$ represents the corresponding salinity difference, and (η_1, η_2, η_3) are constants.

The Stommel model is of particular interest in the context of conceptual climate models due to the fact that the hysteresis observed in the model has consistently been observed in models with increased complexity as well, in certain parameter ranges in several intermediate-complexity models [13] and in some global circulation models [4, 9]. This consistency of results throughout the hierarchy of model complexity has lead to significant scientific consensus on the possibly that hysteresis is physically possible in the system [11].

Mathematically, the Stommel model is a nonsmooth system, with a switch wherever $T = S$. To simplify the location of the switch, one may define $V \equiv T - S$ so that the system becomes

$$\frac{dT}{dt} = \eta_1 - T(1 + |V|), \tag{1}$$

$$\frac{dV}{dt} = \eta_1 - \eta_2 + \eta_3(T - V) - T - V\,|V|\,. \tag{2}$$

There are two fold bifurcations in the (η_2, V) plane, one smooth and one nonsmooth; we are ultimately interested in determining which terms of the model are essential to this behavior and how one might embed similar bifurcation behavior in a higher-dimensional system. For the physically interesting values of the parameters, the Stommel model has either one or three fixed points. As the parameter η_2 varies, two of these experience a boundary equilibrium bifurcation (BEB) when $V = 0$ leading to a non-smooth fold bifurcation where both are annihilated/created [2]. The nature of this transition can be studied through normal form analysis, presented in [2, Chap. 5]. One of these fixed points coalesces with the third at a standard smooth saddle node bifurcation. For other values of the parameters η_1 and η_3, the BEB leads instead to a persistence of the fixed point, again in line with the normal form analysis in [2]. We are ultimately interested in determining which terms of the model are essential to this behavior and how one might embed similar bifurcation behavior in a higher-dimensional system. It is also of interest as to whether some of the more subtle dynamics associated with the nonsmooth bifurcation is realistic in a climate model. We can also explore whether similar behaviour is observed in more regular systems, for example, if the $|V|$ term is replaced by $\sqrt{\epsilon^2 + V^2}$, $\epsilon > 0$.

3 Workshop Discussion and Preliminary Steps

The discussion and ongoing study of the workshop participants centers on the idea of generating a reduced form of the Stommel model and determining possible behaviors of models with similar characteristics in higher dimensions. The goal of identifying an appropriate reduced model is to provide a well-understood basis upon which

more realistic fluctuations and time dependence can be built. In this section we outline the preliminary steps we have begun to take toward embedding the dynamics of the Stommel model in higher dimensions. Certainly the nonsmooth fold, and resulting hysteresis, observed in the Stommel model is generic to BEBs in many higher dimensional nonsmooth systems [2]. However, it is not clear at present whether the hysteretic behaviour identified by Dijkstra in experimental runs of global ocean circulation models, is due to a BEB as modelled in the Stommel system, or to the more usual mechanisms seen in smooth systems, associated with the existence of multiple saddle node bifurcations.

Our first step was to determine the reduced form of the Stommel model in one dimension,

$$\frac{dx}{dt} = -(\mu + 1) + 2\,|x| - H(x)x^2,$$

where $H(x)$ is the Heaviside function. This equation retains the Stommel model skeleton and has no attractors other than the stationary points. In two dimensions, the bifurcations in the original bifurcation diagram (one smooth fold and one nonsmooth fold) are preserved if the terms of the system (1), (2) are reduced to

$$\frac{dT}{dt} = \eta_1 - T(1 + |V|),$$
$$\frac{dV}{dt} = \eta_1 - \eta_2 - T,$$

which can be shown using the trace and determinant of the Jacobian.

At the workshop we also discussed possible behaviors of maps with similar forms. Going forward, we have begun working on classifying behavior which may occur in higher dimensional versions of the reduced Stommel model without changing the projected dynamics in the (η_2, V) plane. Future planned steps include investigating the influence of fluctuations and additional time variation.

References

1. P. Ashwin et al., Tipping points in open systems: bifurcation, noise-induced and rate-dependent examples in the climate system. Philos. Trans. R. Soc. A **370**, 1166–1184 (2012)
2. M. di Bernardo et al., *Piecewise-Smooth Dynamical Systems: Theory and Applications* (Springer, Berlin, 2009)
3. H. Dijkstra, *Nonlinear Climate Dynamics* (Cambridge University Press, New York, 2013)
4. S. Drijfhout et al., Catalogue of abrupt shifts in intergovernmental panel on climate change climate models. Proc. Natl. Acad. Sci. USA **112**, E5777–E5786 (2015)
5. I. Eisenman, J. Wettlaufer, Nonlinear threshold behavior during the loss of Arctic sea ice. Proc. Natl. Acad. Sci. USA **106**, 28–32 (2009)
6. A. Hogg, Glacial cycles and carbon dioxide: a conceptual model. Geophys. Res. Lett. **35**, L01701 (2008)
7. C. Kuehn, A mathematical framework for critical transitions: bifurcations, fast-slow systems and stochastic dynamics. Phys. D: Nonlinear Phenom. **240**, 1020–1035 (2011)

8. T. Lenton et al., Tipping elements in the Earths climate system. Proc. Nat. Acad. Sci. USA **105**, 1786–1793 (2008)
9. R. Marsh et al., Bistability of the thermohaline circulation identified through comprehensive 2-parameter sweeps of an efficient climate model. Clim. Dyn. **23**, 761–777 (2004)
10. D. Paillard, The timing of pleistocene glaciations from a simple multiple-state climate model. Nature **391**, 378–381 (1997)
11. S. Rahmstorf, The thermohaline ocean circulation: a system with dangerous thresholds? Clim. Chang. **46**, 247–256 (2000)
12. S. Rahmstorf, The concept of the thermohaline circulation. Nature **421**, 699 (2003)
13. S. Rahmstorf et al., Thermohaline circulation hysteresis: a model intercomparison. Geophys. Res. Lett. **32**, L23605 (2005)
14. H. Stommel, Thermohaline convection with two stable regimes of flow. Tellus **13**(2), 224–230 (1961)
15. J. Zhu, R. Kuske, T. Erneux, Tipping points near a delayed saddle node bifurcation with periodic forcing. SIAM J. Appl. Dyn. Syst. (to appear)

Global Bifurcations in a Class of Discontinuous Piecewise Linear Systems

Juan Castillo and Fernando Verduzco

Abstract In this work, we show some global bifurcations for a class of three-dimensional discontinuous piecewise linear (DPWL) systems having a unique two-fold point of visible-invisible type. We consider the simplest case of DPWL systems, with two vector fields separated by a switching plane with a unique equilibrium point in each half-space.

1 The DPWL Class Under Study

Consider the next family of three-dimensional DPWL system with two parameters separated by the switching plane $\Sigma = \{x \in \mathbb{R}^3 : x_1 = 0\}$,

$$\dot{x} = \begin{cases} F_1(x) = A_1 x + b_1, & \text{if } x_1 < 0, \\ F_2(x) = A_2 x + b_2, & \text{if } x_1 > 0, \end{cases} \tag{1}$$

where,

$$A_1 = \begin{pmatrix} 0 & 1 & 0 \\ 1 & 0 & 0 \\ 1 & 1 & -1 \end{pmatrix}, \quad A_2 = \begin{pmatrix} 0 & 0 & 1 \\ -1 & \mu & 0 \\ -1 & 1+\mu & -1 \end{pmatrix}, \quad b_1 = b_2 = \begin{pmatrix} 0 \\ 1 \\ 1+\delta \end{pmatrix},$$

with $\delta, \mu \in (-1, 1)$. This family has a unique two-fold point since $|M| = 1$, where $M = (e_1^T, e_1^T A_1, e_1^T A_2)^T$ (see [1, 5, 6]), with $e_1^T = (1, 0, 0)$, and this point is localized at the origin. In fact, the two-fold point is not a singularity of (1) since $F_1(0) = F_2(0)$ and the tangencies are visible-invisible at this point. On Σ we distinguish the following regions:

J. Castillo (✉) · F. Verduzco
Departamento de Matemáticas, Universidad de Sonora, Hermosillo, México
e-mail: juanc@mat.uson.mx

F. Verduzco
e-mail: verduzco@mat.uson.mx

A. Colombo et al. (eds.), *Extended Abstracts Spring 2016*,
Trends in Mathematics 8, DOI 10.1007/978-3-319-55642-0_6

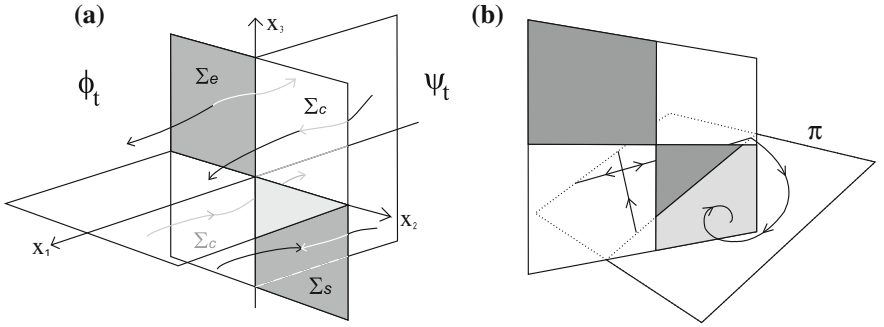

Fig. 1 (**a**) Flows and regions in normal form. We can see how the flows φ_t in $\{x_1 > 0\}$ and ψ_t in $\{x_1 < 0\}$ hit Σ_s, pull Σ_e or cross Σ_c, the switching plane Σ. (**b**) Dynamics on the invariant plane when there is a stable focus in $\{x_1 > 0\}$

$$\begin{aligned}\Sigma_s &= \{x \in \Sigma : x_2 > 0 \quad \text{and} \quad x_3 < 0\},\\ \Sigma_e &= \{x \in \Sigma : x_2 < 0 \quad \text{and} \quad x_3 > 0\},\\ \Sigma_c &= \{x \in \Sigma : x_2 x_3 > 0\};\end{aligned}$$

see Fig. 1a.

Lemma 1 *$w^T x = k$ is an invariant plane of the DPWL system (1) if and only if there exist real eigenvalues $\lambda \in \sigma(A_1)$ and $\gamma \in \sigma(A_2)$ such that*

$$\begin{cases} A_1^T w = \lambda w, \\ A_2^T w = \gamma w, \end{cases} \qquad \textit{and} \qquad \begin{cases} w^T b_1 + \lambda k = 0, \\ w^T b_2 + \gamma k = 0. \end{cases}$$

The equilibria of the vector fields $F_1(x)$ and $F_2(x)$ are $p_1 = (-1, 0, \delta)^T$ and $p_2 = (1 - \delta\mu, -\delta, 0)^T$, respectively. The spectrums of matrices A_1 and A_2 are, respectively, $\sigma(A_1) = \{-1, -1, 1\}$ and $\sigma(A_2) = \{-1, (\mu \pm i\sqrt{4 - \mu^2})/2\}$. Using Lemma 1, it is possible to prove that, for $\lambda = \gamma = -1$, the plane $\pi = \{x \in \mathbb{R}^3 : x_3 = x_2 + \delta\}$ is an attractive invariant plane for the DPWL system (1); see Fig. 1b.

Lemma 2 *The DPWL system (1) has the invariant plane π, on which the dynamics is given by the piecewise linear system*

$$\dot{y} = \begin{cases} (y_2, y_1 + 1)^T, & \textit{if} \quad y_1 < 0, \\ (y_2 + \delta, -y_1 + \mu y_2 + 1)^T, & \textit{if} \quad y_1 > 0. \end{cases}$$

Besides, since π is a global attractor, the bifurcations undergoing the family (1) happen at π.

Following Filippov's convex method (see Filippov [2]), we can define a sliding vector field in $\Sigma_s \cup \Sigma_e$ but, since the first component vanishes in this case, we define the planar sliding vector field

$$\dot{z} = F_s(z) = \frac{1}{x_2 - x_3}\begin{pmatrix} \mu x_2^2 + x_2 - x_3 \\ (1+\mu)x_2^2 - 2x_2x_3 + (1+\delta)(x_2 - x_3) + x_3^2 \end{pmatrix},$$

where $z = (x_2, x_3)^T$. Notice that $F_s(z)$ has no equilibria for the parameter values considered. Regardless of wether the equilibria exist, if we take an initial condition of the form $z_0 = (x_{20}, x_{20} + \delta)^T$, i.e., if we take $z_0 \in (\Sigma_s \cup \Sigma_e) \cap \pi$, then

$$F_s(z_0) = \begin{pmatrix} 1 - \frac{\mu}{\delta}x_{20}^2 \\ 1 - \frac{\mu}{\delta}x_{20}^2 \end{pmatrix}.$$

That is, the intersection of the invariant plane with the switching plane is also invariant under the sliding vector field.

2 Crossing Homoclinic Bifurcation: The Center-Saddle Case

If we make $\mu = 0$ and take δ as our bifurcation parameter in the DPWL system (1), this undergoes a bifurcation that is only possible in nonsmooth systems and it happens when δ varies from its nominal value $\delta = 0$.

Proposition 3 *Assuming $\mu = 0$ in the DPWL system (1), the following hold:*

(i) if $\delta = 0$, there exists a crossing homoclinic orbit connecting the saddle point p_1 to itself;

(ii) if $\delta < 0$ $(\delta > 0)$, there exists a stable (unstable) center-cycle, i.e., a bounded center configuration where its outermost periodic orbit (the tangent one to the boundary at the point $(0, -\delta, 0)^T$) is stable (unstable) from outside.

Remark 4 It is important to note that the sliding vector field in this case is linear, that is, $F_s(z) = (1, x_2 - x_3 + 1 + \delta)^T$. This is because the singularity at the origin is removed and moreover, when $\delta = 0$, it holds that $F_1(x) = F_2(x) = (x_2, 1, 1)^T$ for all $x \in \Sigma \cap \pi$. That is, the DPWL system (1) is continuous in π. The bifurcations considered in the next sections are obtained fixing δ and taking μ as the bifurcation parameter; see [3, 4, 7, 8].

3 The Focus-Center-Sliding Cycle Bifurcation

Proposition 5 *For the DPWL system (1) the following statements hold:*

(i) if $-1 < \delta < 0$ then there exists a stable focus for $\mu < 0$, a stable center-cycle for $\mu = 0$, and a stable sliding limit cycle for $\mu > 0$;

(ii) if $0 < \delta < 1$ then there exists an unstable sliding limit cycle for $\mu < 0$, an unstable center-cycle for $\mu = 0$, and an unstable focus for $\mu > 0$.

We exclude the case $\delta = 0$ since the DPWL system (1) does not satisfy the hypotheses given in Ponce–Ros–Vela [8].

4 Continuation of the Sliding Limit Cycle: Sliding Bifurcations

4.1 Buckling Bifurcation

Proposition 6 *For the DPWL system (1) the following statements hold:*

(i) if $-1 < \delta < 0$ *then there exists* $\mu_1 > 0$ *so that the standard piece of the stable sliding limit cycle returns to the sliding segment at the invisible fold point;*
(ii) if $0 < \delta < 1$ *then there exists* $\tilde{\mu}_1 < 0$ *so that the standard piece of the unstable sliding limit cycle returns to the sliding segment at the invisible fold point.*

4.2 Crossing Bifurcation

Proposition 7 *For the DPWL system (1) the following statements hold:*

(i) if $-1 < \delta < 0$ *then there exists* $\mu_2 > \mu_1$ *so that the stable sliding limit cycle becomes into a stable crossing limit cycle;*
(ii) if $0 < \delta < 1$ *then there exists* $\tilde{\mu}_2 < \tilde{\mu}_1$ *so that the unstable sliding limit cycle becomes into an unstable crossing limit cycle.*

5 Crossing Homoclinic Bifurcation: The Focus-Saddle Case

Proposition 8 *For the DPWL system (1) the following statements hold:*

(i) if $-1 < \delta < 0$ *then there exists a stable crossing limit cycle for* $\mu_2 \leq \mu < \mu_3$, *a crossing homoclinic orbit for* $\mu = \mu_3$, *and an unstable focus for* $\mu > \mu_3$;
(ii) if $0 < \delta < 1$ *then there exists an unstable crossing limit cycle for* $\tilde{\mu}_3 < \mu \leq \tilde{\mu}_2$, *a crossing homoclinic orbit for* $\mu = \tilde{\mu}_3$, *and a stable focus for* $\mu < \tilde{\mu}_3$.

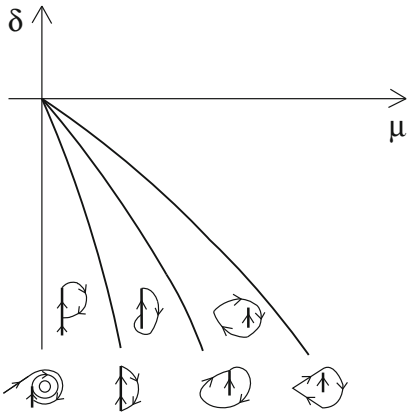

Fig. 2 Bifurcation diagram of the family (1) for the case $\mu \geq 0$ and $\delta < 0$

Figure 2 shows the bifurcation diagram of the family (1) for the case $\mu \geq 0$ and $\delta < 0$.

References

1. A. Colombo, M.R. Jeffrey, Nondeterministic chaos, and the two-fold singularity in piecewise smooth flows. SIAM J. Appl. Dyn. Syst. **10**, 423–451 (2011)
2. A.F. Filippov, *Differential Equations with Discontinuous Righthand Sides* (Kluwer Academic Publishers, Dordrecht, 1988)
3. E. Freire, E. Ponce, F. Torres, On the critical crossing cycle bifurcation in planar Filippov systems. J. Differ. Equ. **259**, 7086–7107 (2015)
4. M. Guardia, T.M. Seara, M.A. Teixeira, Generic bifurcations of low codimension of planar Filippov Systems. J. Differ. Equ. **250**, 1967–2023 (2011)
5. M.R. Jeffrey, A. Colombo, The two-fold singularity of discontinuous vector fields. SIAM J. Appl. Dyn. Syst. **8**, 624–640 (2009)
6. M.R. Jeffrey, S.J. Hogan, The geometry of generic sliding bifurcations. SIAM Rev. **53**, 505–525 (2011)
7. Yu.A. Kuznetsov, S. Rinaldi, A. Gragnani, One parameter bifurcations in planar Filippov systems. Int. J. Bifurc. Chaos **13**, 2157–2188 (2003)
8. E. Ponce, J. Ros, E. Vela, The focus-center-limit cycle bifurcation in discontinuous planar piecewise linear systems without sliding, in *Progress and Challenges in Dynamical Systems*, vol. 54, 335 Springer Proceedings in Mathematics and Statistics, ed. by S. Ibáñez, et al. (Springer, Berlin, 2013)

Single-Impact Orbits Near Grazing Periodic Orbits for an Impact Oscillator

D.R.J. Chillingworth

Abstract We describe a geometric approach to understand the mechanism of creation and annihilation of single-impact periodic orbits close to grazing for a general second-order one degree of freedom impact oscillator. Here, non-degenerate grazing (nonzero acceleration) is assumed, with approaches to degenerate grazing also outlined: this is work in progress. The method in principle extends to more degrees of freedom (coupled oscillators, for example) and to a variety of restitution rules such as soft impacts, delays or sticking.

1 Introduction

The local and global dynamics of a periodically forced damped linear oscillator with one degree of freedom with constant coefficients such as

$$\ddot{x} + d\dot{x} + kx = h \sin t, \quad x, t \in \mathbf{R}$$

are very well understood and can be found in almost any textbook on ordinary differential equations. The same cannot be said, however, if the variable x is constrained so that $x \geq c$ for a given constant c (the *clearance*) and a restitution law such as $\dot{x} \mapsto -r\dot{x}$ is applied whenever $x = c$. Many aspects of the behaviour are known and a wide range of results indicating tantalising geometrical structures evident in the global dynamics has been obtained, from the pioneering work of Whiston [16, 17] through the geometric, analytic and numerical investigations of Bishop [1], Budd et al., [5, 6], Chin–Ott–Nusse–Grebogi [10], Nordmark [13], Nordmark–Piiroinen [14], Zhao–Dankowicz [18] and many others to the very detailed numerical results due to Piiroinen [11]. Nevertheless, a full global picture is still lacking.

D.R.J. Chillingworth (✉)
Mathematical Sciences, University of Southampton, Southampton SO17 1BJ, UK
e-mail: drjc@soton.ac.uk

A. Colombo et al. (eds.), *Extended Abstracts Spring 2016*,
Trends in Mathematics 8, DOI 10.1007/978-3-319-55642-0_7

2 The Impact Surface

The purpose of this note is to advertise one particular application of an overall geometric approach to understanding the dynamics of an impact oscillator that was first introduced in Chillingworth [7], developed further in Chillingworth [8] and effectively exploited in applications, for example, by Mason–Humphries–Piiroinen [12]. Following Sotomayor–Teixeira [15], the key idea applied here to general nonlinear systems of the form

$$\ddot{x} + f(x, \dot{x}) = g(t), \quad x \in \mathbf{R} \tag{1}$$

is to 'straighten out' the flow of the system (1) regarded as an autonomous system in $(x, \dot{x}, t)$-space $\mathbf{R}^3$, whereupon the obstacle $x = c$ becomes a (non-planar) 2-manifold with some well-understood singular points and which is called here the *impact surface* V_c. Specifically

$$V_c := \{(v, \tau, t) \in \mathbf{R}^3 : x_c(v, \tau, t) = c\},$$

where we write $x_c(v, \tau, t) = x(c, v, \tau; \tau + t)$ denoting the solution of (1) with initial data $(x, \dot{x}) = (c, v)$ when $t = 0$. The sequence of impacts with $x = c$ for any orbit (although not the geometry of the orbit itself away from $x = c$) can be read off by starting at $(v, \tau, 0)$ in $\mathbf{R}^3$ with $v \geq 0$, proceeding along the positive t-axis until first meeting V_c, then applying a *re-set map* ϕ that takes the current data $(\dot{x}, \tau + t)$ as new initial data (v, τ), and finally applying the restitution map R that replaces $\dot{x}$ by $-r\dot{x}$ (or possibly something more general) before setting off again along the positive t-direction.

An elementary property of the impact surface is easily seen, namely, *grazing orbits*: the condition that an orbit with initial data (v, τ) should *graze* the obstacle (that is, $x = c$ and $\dot{x} = 0$) at $t = t_1$ is precisely the condition that the line parallel to the t-axis through $(v, \tau, 0)$ should be *tangent* to V_c at $t = t_1$.

3 Single-Impact Periodic Orbits

Suppose now that the forcing function $g(t)$ in (1) is periodic with period $T > 0$. Locating single-impact T-periodic orbits can be described geometrically as follows. Let

$$\gamma := \{(v, \tau, T) \in V_c \text{ and } (v, \tau, t) \notin V_c \text{ for } 0 < t < T\},$$

namely that part of the intersection of V_c with the plane $t = T$ that can be 'seen' in the positive t-direction from (v, τ) without obstruction by other parts of V_c. Let α be the projection of γ into the (v, τ)-plane (the points from which γ is 'seen') and let β be the image of γ under the re-set map ϕ. Then the points (if any) of $\alpha \cap R\beta$ (mod T in the τ-coordinate) are precisely the initial data points for single-impact T-periodic

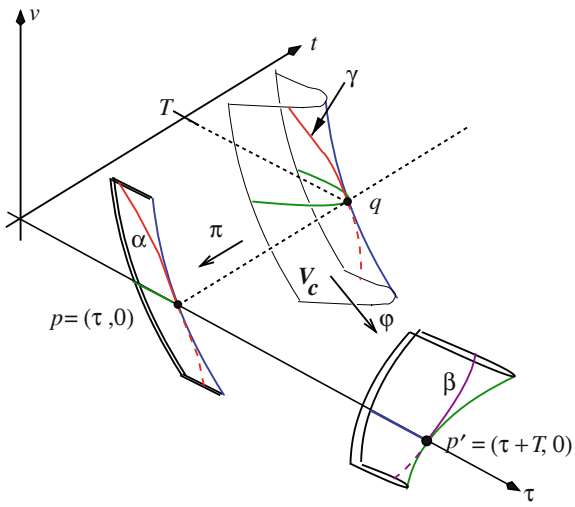

Fig. 1 The two curves $\alpha = \pi(\gamma)$ and $\beta = \phi(\gamma)$

orbits. From this point of view, therefore, the study of single-impact T-periodic orbits becomes the study of the intersections of α and $R\beta$.

Let π denote the restriction to $V_c \subset \mathbf{R}^3$ of the projection map $(v, \tau, t) \mapsto (v, \tau) \in \mathbf{R}^2$. The local geometry of the two maps $\pi, \phi\colon V_c \to \mathbf{R}^2$, as well as their perturbations, is governed by their singularity structure. The singular locus of the projection π is the *horizon curve* H_c, where V_c is tangent to the t-direction (that is, $\dot{x} = 0$). The singular locus of ϕ is, as shown in Chillingworth [7], the *zero curve* Z_c, where $v = 0$. The study of grazing single-impact T-periodic orbits and their bifurcations as c and/or other parameters are varied, therefore, becomes the study of the singularities of π and ϕ at points $q \in V_c$ where $v = 0$ and $\dot{x} = 0$, that is, at points of $H_c \cap Z_c$.

In the least degenerate case of a grazing single-impact T-periodic orbit the initial acceleration $a = a(\tau)$ is nonzero and so at the corresponding point q of γ the tangency of V_c with the t-direction is quadratic ($\ddot{x} = a \neq 0$). In this case (see Chillingworth [7]) each of π and ϕ has a *fold* singularity at q. The curve γ through q is in each case mapped to a curve tangent to the image of the fold curve; see Fig. 1.

Straightforward calculations show that the images of the fold curves for π and ϕ have tangent directions $(-x_v, x_\tau)$ and $(1, a)$ respectively, the subscripts denoting derivatives with respect to initial data, and so the curves $\alpha = \pi(\gamma)$ and $R\beta = R\phi(\gamma)$ cut transversely, provided $x_\tau - a r x_v \neq 0$, where for general $R(\dot{x}, \tau)$ we write $r = r(\tau) = -\partial R/\partial \dot{x}$ at $\dot{x} = 0$. With this generic assumption and in view of the stability of fold singularities, we immediately deduce the following result.

Proposition 1 *When $a(\tau) \neq 0$ the grazing single-impact T-periodic orbit is isolated (if v or τ varies there is no such nearby orbit). If μ is any perturbing parameter such that the intersections of α, $R\beta$ with the τ-axis pass through each other as μ passes through 0 then a single-impact (non-grazing) T-periodic orbit persists for one sign or the other of μ.*

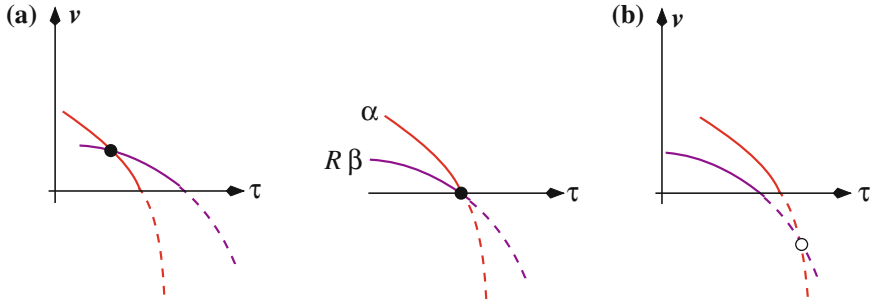

Fig. 2 Displacement of α and $R\beta$ after perturbation. In case (**a**) the single-impact periodic orbit is real ($v > 0$), while in case (**b**) it is unphysical ($v < 0$)

See Fig. 2 for a schematic illustration of this geometry. The case (a) shows a real impact with initial velocity $v > 0$, while case (b) shows a virtual impact ($v < 0$). Numerical continuation methods would of course detect both cases as it is only the physical interpretation of the model that causes (b) to be rejected. Note that if the grazing orbit at $\mu = 0$ is hyperbolic for the 'free' system (obstacle removed), then it persists as a non-impacting periodic orbit of the impact oscillator for one sign or the other of μ. When the impacting and non-impacting T-periodic orbits are present for the same sign of μ, the interaction is sometimes called a *nonsmooth fold* bifurcation.

The fold geometry just described was presented in Chillingworth–Nordmark [9], but the next challenge is to understand the more complicated singularity deformations that arise when a T-periodic orbit with degenerate graze (zero acceleration) is perturbed.

4 Degenerate Grazing

The singularity structure of the map $\pi\colon V_c \to \mathbf{R}^2$ plays a key role in understanding the geometry of impacting orbits close to a grazing orbit. The image in $\mathbf{R}^2$ of the singular set forms the so-called *apparent outline* or *apparent contour* of V_c viewed in the t-direction. The generic behaviour of apparent outlines and their deformations under perturbation is well understood as a sub-discipline of singularity theory; see, for example, [2–4]. The singularities of the re-set map $\phi\colon V_c \to \mathbf{R}^2$ play an equivalent role and, as shown above, it is the interaction of the singularities of π and ϕ that govern the existence of impacting T-periodic orbits.

For nondegenerate grazing as studied above the singularities are no worse than folds, which retain their geometry when perturbed. For degenerate grazing where $a(\tau) = 0$, however, the singularities are typically *swallowtail* and *beak-to-beak* singularities and break up or ('unfold') under perturbation, so that tracking the intersections of the arcs analogous to α and $R\beta$ above becomes a much more delicate task. In addition to this, the local geometry of V_c close to $(0, \tau)$ and for small $t > 0$

becomes significant: it controls complete and incomplete chatter arising from low-velocity impacts (see [5, 8, 14] for example) and alters the interpretation of $\alpha \cap R\beta$. There is much interesting geometry to elucidate here, and the investigation is work in progress.

5 Generalisations

The impact surface method extends in principle to higher dimensions, for example n coupled one degree of freedom oscillators with possible constraints $c_i \leq x_i \leq d_i$ for $i = 1, 2, \ldots, n$. The 'impact surface' becomes a union of $m \leq 2n$ objects, each typically a smooth manifold of codimension 1 in the space of initial data at impact together with time elapsed since impact, while the 'initial data' plane (to which data are re-set at each impact) becomes a union of m hyperplanes. Thus, there are m projection maps π_j and m re-set maps ϕ_j for $j = 1, \ldots, m$. The local analysis of singularities of these projection and reset maps continues to play a key role in governing the dynamical behaviour close to grazing, but of course the technical details become more complicated.

It is also straightforward to adapt the method to soft impacts (restitution with delay) or sticking: the impact surface and re-set map are unchanged, but the restitution map becomes heavily dependent on the phase τ.

These formalisms, hardly yet developed in applications, generate a wealth of open problems relating impact dynamics to geometry and singularity theory.

References

1. S.R. Bishop, Impact oscillators. Phil. Trans. Roy. Soc. London A **347**, 347–351 (1994)
2. J.W. Bruce, Seeing – the mathematical viewpoint. Math. Intell. **6**, 18–25 (1984)
3. J.W. Bruce, P.J. Giblin, *Curves and Singularities* (Cambridge University Press, Cambridge, 1984)
4. J.W. Bruce, P.J. Giblin, Outlines and their duals. Proc. London Math. Soc. **50**, 552–570 (1984)
5. C.J. Budd, F.J. Dux, Chattering and related behaviour in impact oscillators. Phil. Trans. Roy. Soc. London A **347**, 365–389 (1994)
6. C.J. Budd, F.J. Dux, A. Cliffe, The effect of frequency and clearance variations on single-degree-of-freedom impact oscillators. J. Sound Vib. **184**, 475–502 (1995)
7. D.R.J. Chillingworth, Discontinuity geometry for an impact oscillator. Dyn. Syst. **17**, 389–420 (2002)
8. D.R.J. Chillingworth, Dynamics of an impact oscillator near a degenerate graze. Nonlinearity **23**, 2723–2748 (2010)
9. D.R.J. Chillingworth, A.B. Nordmark, Periodic orbits close to grazing for an impact oscillator, in *Recent Trends in Dynamical Systems*, vol. 35, Springer Proceedings in Mathematics and Statistics, ed. by A. Johann, et al. (2013), pp. 25–37
10. W. Chin, E. Ott, H.E. Nusse, C. Grebogi, Grazing bifurcations in impact oscillators. Phys. Rev. E **50**, 4427–4444 (1994)
11. M. Di Bernardo et al., Bifurcations in nonsmooth dynamical systems. SIAM Rev. **50**, 629–701 (2008)

12. J.F. Mason, N. Humphries, P.T. Piiroinen, Numerical analysis of codimension-one, -two and -three bifurcations in a periodically-forced impact oscillator with two discontinuity surfaces. Math. Comput. Simul. **95**, 98–110 (2014)
13. A.B. Nordmark, Existence of periodic orbits in grazing bifurcations of impacting mechanical oscillators. Nonlinearity **14**, 1517–1542 (2001)
14. A.B. Nordmark, P.T. Piiroinen, Simulation and stability analysis of impacting systems with complete chattering. *Nonlinear Dyn.* **58**, 85–106 (2009)
15. J. Sotomayor, M.A. Teixeira, Vector fields near the boundary of a 3-manifold, *Dynamical Systems Valparaiso 1986*, vol. 1331, Lecture Notes in Math (Springer, Berlin, 1988), pp. 169–195
16. G.W. Whiston, Global dynamics of a vibro-impacting linear oscillator. J. Sound Vib. **118**, 395–429 (1987)
17. G.W. Whiston, Singularities in vibro-impact dynamics. J. Sound Vib. **152**, 427–460 (1992)
18. X. Zhao, H. Dankowicz, Unfolding degenerate grazing dynamics in impact actuators. Nonlinearity **19**, 399–418 (2006)

A Choice Between Smooth and Nonsmooth Models

Alessandro Colombo

Abstract Piecewise smooth systems are frequently used as an alternative representation of mena with multiple time scales. One would of course expect that the qualitative behaviour of a model be independent of the choice of a smooth or piecewise smooth representation. We address this issue by building on some classical results from piecewise smooth systems theory.

1 Smooth or Piecewise Smooth?

Piecewise smooth and slow-fast systems are frequently used as alternative mathematical representations of the same phenomenon. From an applied scientist's perspective, having a choice between two languages can be useful, for instance, to pick the most appropriate formalism for a given numerical analysis tool, as long as the differences in the results that can be expected are well understood. Unfortunately, the differences in the behaviour of a smooth and piecewise smooth system that were built to be 'close' are rarely well understood.

This problem was addressed many times in the literature, and a fruitful branch of research started from the work Sotomayor–Teixeira in [3] on the smoothing of a two-dimensional piecewise smooth system. What we propose here is a small extension of this branch, mostly built on classical results available in Filippov [1]. Our main results can be roughly stated as follows:

Statement 1 *The dynamics of a piecewise smooth system is a superset of the dynamics of the smooth system it represents (i.e., of its smoothing).*

Statement 2 *The bifurcation diagram of a piecewise smooth system contains all transitions in the bifurcation diagram of its smoothing, but some of these transitions can take place simultaneously.*

A. Colombo (✉)
DEIB, Politecnico di Milano, via Ponzio 34/5, Milan, Italy
e-mail: alessandro.colombo@polimi.it

A. Colombo et al. (eds.), *Extended Abstracts Spring 2016*,
Trends in Mathematics 8, DOI 10.1007/978-3-319-55642-0_8

These two statements are formalised in Theorems 10 and 12, respectively. With respect to existing results, they have the advantage of requiring no assumptions on dimensionality, the relative geometry of flow and discontinuity surfaces, or on structural stability. Furthermore, they are written assuming one smooth discontinuity boundary for the sake of simplicity, but nothing in the proof prevents their extension to arbitrarily many (possibly intersecting) boundaries.

The next section simply collects definitions and lemmas from Filippov [1], reported here for reference. Our original results are in Sect. 3.

2 Preliminary Results

Lemma 3 (Filippov [1, Lemma 1]) *If two nonempty closed sets A and B do not have common points and B is bounded, then there exists points $a \in A$ and $b \in B$ such that* $\inf_{x\in A,\, y\in B} |x - y| = |a - b| > 0$.

Definition 4 (*Upper semicontinuous*) The function $F(\mathbf{x})$ is *upper semicontinuous* at the point $\mathbf{x}$ if $\sup_{\dot{\mathbf{x}}'\in F(\mathbf{x}')} \inf_{\dot{\mathbf{x}}\in F(\mathbf{x})} \|\dot{\mathbf{x}}' - \dot{\mathbf{x}}\| \to 0$ as $\mathbf{x}' \to \mathbf{x}$, where $\|\cdot\|$ is the Euclidean norm.

Definition 5 (*Basic conditions*) A set-valued function $F(t, \mathbf{x})$ in a domain G satisfies the *basic conditions* if, for all $(t, \mathbf{x}) \in G$, the set $F(t, x)$ is nonempty, bounded, closed, convex, and the function F is upper semicontinuous in $t, \mathbf{x}$.

Lemma 6 (Filippov [1, Theorem 2]) *Let $F(t, \mathbf{x})$ satisfy the basic conditions in a closed bounded domain D. Then each solution of the inclusion $\dot{\mathbf{x}} \in F(t, \mathbf{x})$ lying within D can be continued on both sides up to the boundary of the domain.*

Definition 7 A vector function $\mathbf{y}(t)$ is a *δ-solution* of the inclusion $\dot{\mathbf{x}} \in F(\mathbf{x}, t)$ with F upper semicontinuous in $t, \mathbf{x}$ if, on a given interval, the function $\mathbf{y}(t)$ is absolutely continuous and almost everywhere $\dot{\mathbf{y}}(t) \in [\mathrm{co}F(t^\delta, \mathbf{y}^\delta)]^\delta$, where the superscript indicates a δ-neighbourhood of the superscripted set, and $\mathrm{co}(\cdot)$ is the convex hull of its argument.

Lemma 8 (Filippov [1, Lemma 1]) *Let $F(t, \mathbf{x})$ satisfy the basic conditions in the open domain G, and let $\{\mathbf{x}_i(t)\}$ be a sequence of δ_i-solutions of*

$$\dot{\mathbf{x}} \in F(t, \mathbf{x}) \tag{1}$$

lying for $a_i \le t \le b_i$ in a closed and bounded domain G, with $\delta_i \to 0$, $a_i \to a$, $b_i \to b$, $\mathbf{x}_i(a_i) \to \mathbf{x}_0$ and $\mathbf{x}_i(b_i) \to \mathbf{x}^*$. Then, from the sequence $\{\mathbf{x}_i(t)\}$, one can extract a subsequence which converges uniformly to the solution $\mathbf{x}(t)$ of (1) on each $[a', b'] \in (a, b)$, and $\mathbf{x}(a) = \mathbf{x}_0$, $\mathbf{x}(b) = \mathbf{x}^*$.

Lemma 9 (Filippov [1, Theorem 3]) *Let the function $F(t, \mathbf{x})$ satisfy the basic conditions in the domain G. Let all solutions of $\dot{\mathbf{x}} \in F(t, \mathbf{x})$ exist for $a \le t \le b$ and their graphs lie in G. Then the set H of the points lying on these graphs at $a \le t \le b$ is bounded and closed.*

3 Main Results

The following theorem proves that each orbit of the smoothing of a piecewise smooth system[1] uniformly converges to an orbit of the piecewise smooth system.

Theorem 10 *Consider two smooth vector fields f^+ and f^- defined over a common domain X, and take two smooth functions $h\colon X \to \mathbb{R}$ and $\phi\colon \mathbb{R} \to \mathbb{R}$, and three scalars $\lambda_l, \lambda_h \in \mathbb{R}$, $\epsilon \in \mathbb{R}_{\geq 0}$. Consider the system Σ_1 defined as*

$$\begin{aligned}
&\dot{\mathbf{x}} = F_1(t, \mathbf{x}) := f^+(\mathbf{x})\phi(h(\mathbf{x})/\epsilon) + f^-(\mathbf{x})(1 - \phi(h(\mathbf{x})/\epsilon))\\
&\phi(\cdot) \in [\lambda_l, \lambda_h],\\
&\phi(h(\mathbf{x})/\epsilon) = 1 \text{ when } h(\mathbf{x})/\epsilon \geq 1\\
&\phi(h(\mathbf{x})/\epsilon) = -1 \text{ when } h(\mathbf{x})/\epsilon \leq -1,
\end{aligned}$$

and the system Σ_2 defined as

$$\dot{\mathbf{x}} \in F_2(t, \mathbf{x}) := \begin{cases} f^+(\mathbf{x}), & h(\mathbf{x}) > 0\\ f^-(\mathbf{x}), & h(\mathbf{x}) < 0,\\ \text{co}\{\lambda_h f^+(\mathbf{x}), \lambda_l f^+(\mathbf{x}),\\ \quad (1-\lambda_h) f^-(\mathbf{x}), (1-\lambda_l) f^-(\mathbf{x})\}, & h(\mathbf{x}) = 0. \end{cases}$$

Solutions of Σ_2 are intended in the sense of Filippov. Assume that F_2 satisfies the basic conditions, and all its solutions exist for $a \leq t \leq b$ and have graph in an open domain G. Then, each orbit of Σ_1 uniformly converges to an orbit of Σ_2 in G for $\epsilon \to 0$.

Proof By Lemma 9, the set H of points $(t, \mathbf{x})$, $a \leq t \leq b$, belonging to the graph of solutions of Σ_2 is closed and bounded. By Lemma 3,

$$\inf_{\alpha \in H, \beta \in \partial G} |\alpha - \beta| = \rho_0 > 0. \tag{2}$$

Take a closed and bounded d-neighbourhood H^d of H, with $0 < 2d < \rho_0$, and take a sequence $\mathbf{x}_i(t)$ of solutions of $\Sigma_1(\epsilon_i)$, $i = 1, 2, \ldots$, with $|t_{0i} - t_0| \leq \epsilon_i$, $|\mathbf{x}_i(t_{0i}) - \mathbf{x}_0(t_0)| \leq \epsilon_i$.

By construction, we have that

$$F_1 \subset [\text{co} F_2(t^{\epsilon_i}, \mathbf{x}^{\epsilon_i})]^{\epsilon_i}, \tag{3}$$

where the superscript indicates an ϵ_i-neighbourhood of the superscripted set. By (2), H^d is contained in G so, by Lemma 6, each solution $\mathbf{x}_i(t)$ can be continued both sides

[1] In fact, of a slight generalization of the smoothing in [3], where the smoothing function ϕ is allowed to take values in an arbitrary interval $[\lambda_l, \lambda_h]$, as long as it goes to ± 1 out of an ϵ-neighbourhood of the discontinuity.

up to the boundary of H^d and, since H^d contains H, all $\mathbf{x}_i(t)$ exist for all $t \in [a, b]$. Also, observe that all solutions $\mathbf{x}_i(t)$ are absolutely continuous, being integrals of F_1, therefore by (3) they are ϵ_i-solutions of Σ_2. By Lemma 8, a subsequence of $\{\mathbf{x}_i(t)\}$ converges uniformly to a solution of Σ_2. □

Definition 11 (*see Kuznetsov* [2]) Two families of dynamical systems $\Sigma_{1,\epsilon}(p)$ and $\Sigma_{1,\epsilon'}(p')$ in the parameter p are *topologically equivalent* if

(i) there exists a homeomorphism of the parameter space $h_{\epsilon,\epsilon'}\colon \mathbb{R} \to \mathbb{R}$, $p' = h_{\epsilon,\epsilon'}(p)$,
(ii) and there exists a parameter dependent homeomorphism of the phase space, $h_{\epsilon,\epsilon',p}\colon \mathbb{R}^n \to \mathbb{R}^n$, mapping orbits of $\Sigma_{1,\epsilon}(p)$ at parameter p onto orbits of $\Sigma_{1,\epsilon'}(p')$ at parameter $p' = h_{\epsilon,\epsilon'}(p)$, and preserving the direction of time.

The following theorem states that the one-parameter bifurcation diagram of Σ_1 limits to the one-parameter bifurcation diagram of Σ_2 through a surjective but non-injective mapping, i.e., all transitions in the bifurcation diagram of Σ_1 are present in the bifurcation diagram of Σ_2, but some may take place simultaneously.

Theorem 12 *Consider the systems Σ_1 and Σ_2 from Theorem 10, and let p be a parameter of f^+ and f^-. Take two continuous functions $p_L(\epsilon)\colon [0, \epsilon_{\max}] \to \mathbb{R}$ and $p_H(\epsilon)\colon [0, \epsilon_{\max}] \to \mathbb{R}$, with $p_L(\epsilon) < p_H(\epsilon)$ for all $\epsilon \in [0, \epsilon_{\max}]$. Let the homeomorphism $h_{\epsilon,\epsilon'}$ of Definition 11 be surjective from $(p_L(\epsilon), p_H(\epsilon))$ to $(p_L(\epsilon'), p_H(\epsilon'))$ for all pairs $\{\epsilon, \epsilon'\}$. Assume that*

(1) for all $\epsilon, \epsilon' \in (0, \epsilon_{\max}]$, the families of systems $\Sigma_{1,\epsilon}(p)$, $p \in (p_L(\epsilon), p_H(\epsilon))$ and $\Sigma_{1,\epsilon'}(p)$, $p \in (p_L(\epsilon'), p_H(\epsilon'))$ are topologically equivalent;
(2) the homeomorphism $h_{\epsilon,\epsilon'}$ between the parameter spaces of $\Sigma_{1,\epsilon}$ and $\Sigma_{1,\epsilon'}$ is continuous in $|\epsilon - \epsilon'|$ and equal to the identity at $\epsilon = \epsilon'$;
(3) the homeomorphism $h_{\epsilon,\epsilon'}$ between the parameter spaces of $\Sigma_{1,\epsilon}$ and $\Sigma_{1,\epsilon'}$ is Lipschitz in p, with Lipschitz constant independent of ϵ.

Then, for any $\epsilon \in (0, \epsilon_{\max}]$,

(i) there exists a continuous but not necessarily invertible map $\mathcal{H}_\epsilon\colon [p_L(\epsilon), p_H(\epsilon)] \to [p_L(0), p_H(0)]$, $p' = \mathcal{H}_\epsilon(p)$, and
(ii) there exists a map $\mathcal{H}_{\epsilon,p}\colon \mathbb{R}^n \to \mathbb{R}^n$, not necessarily invertible in $\mathbf{x}$, mapping orbits of $\Sigma_{1,\epsilon}(p)$ at parameter p onto orbits of $\Sigma_2(p')$ at parameter $p' = \mathcal{H}_\epsilon(p)$.

Sketch of the proof Using Assumptions (1) and (2), for any $\Sigma_{1,\epsilon^*}(p)$ we can construct a path $p(\epsilon)\colon (0, \epsilon^*] \to \mathbb{R}$ such that all $\Sigma_{1,\epsilon}(p(\epsilon))$ are topologically equivalent systems. The map $\mathcal{H}_\epsilon(p)$ is the limit of $h_{\epsilon,\epsilon'}$ as $\epsilon' \to 0$, and is continuous being a limit of a sequence of Lipschitz maps (3). Then, by Theorem 10, each orbit of $\Sigma_{1,\epsilon}(p(\epsilon))$ uniformly converges to an orbit of $\Sigma_2(p(0))$ as $\epsilon \to 0$. The induced map is the map $\mathcal{H}_{\epsilon,p}$. □

References

1. A.F. Filippov, *Differential Equations with Discontinuous Righthand Sides* (Kluwer Academic Publishers, Dordrecht, 1988)
2. Yu.A. Kuznetsov, *Elements of Applied Bifurcation Theory*, 3rd edn. (Springer, Berlin, 2004)
3. J. Sotomayor, M.A. Teixeira, Regularization of discontinuous vector fields, in *Proceedings of the International Conference on Differential Equations* (Lisboa, 1996), pp. 207–223

Sliding Mode Control of Heterogeneous Systems

Manuel Domínguez-Pumar, Sergi Gorreta, Teresa Atienza, Elena Blokhina, and Joan Pons-Nin

Abstract This paper establishes a link between closed-loop controls for heterogeneous systems and sliding mode controls. We demonstrate that sliding mode analysis matches with experimental results from dielectric charge controllers. This approach provides a new way to analyze the behaviour of different heterogeneous systems.

1 Introduction

In heterogeneous systems some of the state variables are not part of electronic circuits or mechanical systems. In some cases these systems can be described by multiexponential models, on which different coexisting physical mechanisms generate different time responses, i.e., thermal response of devices, charge trapping in dielectrics, relaxation times in magnetic resonance imaging or even chemical sensing. The best performance is often obtained when working in closed-loop configurations, be it because the time response of the system is improved or because unwanted behaviour is avoided.

There is a link between sigma-delta modulators ($\Sigma\Delta$) and sliding mode controllers; see Sira-Ramírez [7]. This paper focuses on this connection in the case of heterogeneous systems described by multiexponential models. The study-case is a class of $\Sigma\Delta$ dielectric charge controllers for MEMS from [1, 6], shown in Fig. 1. We provide experimental results in which control bitstreams are analyzed and compared with sliding mode analysis. The effect of external disturbances due to ionizing radiation is also investigated.

M. Domínguez-Pumar (✉) · S. Gorreta · T. Atienza · J. Pons-Nin
Micro and Nano Technologies Group, Universitat Politècnica de Catalunya, Barcelona, Spain
e-mail: manuel.dominguez@upc.edu

E. Blokhina
School of Electrical, Electronic and Communications Engineering, University College Dublin, Dublin, Ireland

A. Colombo et al. (eds.), *Extended Abstracts Spring 2016*,
Trends in Mathematics 8, DOI 10.1007/978-3-319-55642-0_9

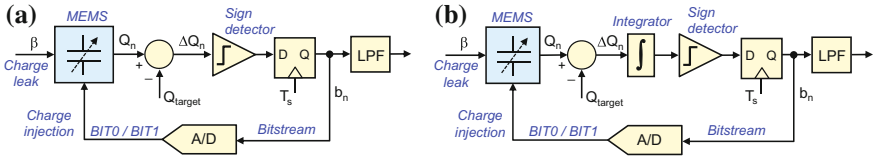

Fig. 1 ΣΔ controls of dielectric charging: (**a**) first order; (**b**) second order

2 ΣΔ Controls of Dielectric Charge and Average System

The control loops use two different waveforms, BIT0 and BIT1, both to actuate the MEMS and to indirectly sense the net charge stored in the dielectric; see Fig. 2. In the MEMS used, applying BIT0 increases such charge while BIT1 decreases it. In Fig. 1a the net charge is compared with a target value at sampling times nT_S and, depending on the result, either BIT0 or BIT1 is applied for the next cycle. The actuation provided is bipolar and the switching takes place at the surface of the state variables determined by *total charge constant and equal to target value*. This means that, under some conditions, a sliding movement takes place on this surface.

Let us first generate an 'equivalent average system' to take into account the predetermined voltage switching done within BIT0 and BIT1. For an arbitrary binary voltage signal $v(t) \in \{V^+, V^-\}$, we can describe the time-varying linear system as:

$$\dot{x}(t) = \begin{cases} A_1 x(t) + B_1, & v(t) = V^+, \\ A_0 x(t) + B_0, & v(t) = V^-, \end{cases}$$

where $A_i \in \mathbb{R}^{n\times n}$, $B_i \in \mathbb{R}^n$, $i = \{0, 1\}$. In our case, we may use the charging models obtained in Domínguez-Pumar–Gorreta–Pons-Nin–Blokhina–Giounanlis–Feely [2]. At the moment of switching between voltages, the state vector $x(t)$ is continuous. The output of the system is the net dielectric charge, $q(t) = c^T x(t)$, where $c = (1, \ldots, 1)^T \in \mathbb{R}^n$ and $q(t) \in \mathbb{R}$.

Now, considering the rapid deterministic switching related with BIT0 and BIT1 actuation signals, we have the following average control system, valid for $T_S \to 0$:

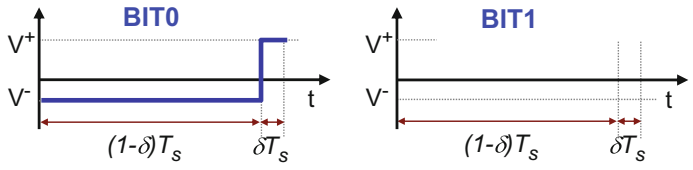

Fig. 2 Bipolar voltage waveforms used to actuate the MEMS

$$\dot{x} = \begin{cases} A_{b_1}x + B_{b_1}, & \sigma > 0, \\ A_{b_0}x + B_{b_0}, & \sigma < 0, \end{cases} \tag{1}$$

with $\sigma = c^T x(t) - Q_{\text{target}}$, being Q_{target} the desired-target amount of net charge, and

$$\begin{aligned} A_{b_1} &= (1-\delta)A_1 + \delta A_0, \quad B_{b_1} = (1-\delta)B_1 + \delta B_0, \\ A_{b_0} &= \delta A_1 + (1-\delta)A_0, \quad B_{b_0} = \delta B_1 + (1-\delta)B_0. \end{aligned}$$

3 Sliding within the Control Surface $\mathcal{S}$

To predict the conditions to have a sliding motion and the obtained behaviour of the bitstreams, let us now analyze the system using the average system obtained. Here, we apply the techniques used in relay feedback systems in [4, 5]. This will provide conditions guaranteeing the existence of a sliding region within the control surface $\mathcal{S}$.

We have that $\dot{\sigma} = c^T \dot{x}$. Assuming that the control law tends to compensate charge, i.e., we have $c^T B_{b_1} < 0$ and $c^T B_{b_0} > 0$, the following subset of the control surface

$$\Omega := \left\{x \in \mathbb{R}^n : c^T A_{b_1} x < -c^T B_{b_1}\right\} \cap \left\{x \in \mathbb{R}^n : c^T A_{b_0} x > -c^T B_{b_0}\right\} \cap \mathcal{S}$$

is attractive. This is due to the fact that, for any $x \in \mathbb{R}^n$ such that $\sigma(x) < 0$, we have $\dot{\sigma}(x) > 0$, whereas if $\sigma(x) > 0$ then we have $\dot{\sigma}(x) < 0$. Therefore, we have $\sigma\dot{\sigma} \leq 0$ in a neighbourhood of Ω, which means that $\Omega \subset \mathcal{S}$ is attractive.

Let us now assume that the conditions for an attractive control surface are fulfilled and that the control surface is reached, therefore $\sigma(x(t)) = c^T x(t) - Q_{\text{target}} = 0$. The average system, defined as the limit control for $T_S \to 0$, can be seen as a particular case of $\dot{x}(t) = f(\sigma(x))$, being $f(\sigma(x))$ a discontinuous function. Obtaining a solution in the sense of Filippov yields

$$f(\sigma(x))\Big|_{\sigma(x)=0} := \alpha(x) f(\sigma(\zeta))\Big|_{\zeta \to x, \sigma(\zeta)>0} + (1-\alpha(x))) f(\sigma(\zeta))\Big|_{\zeta \to x, \sigma(\zeta)<0,} \tag{2}$$

with $\alpha(x) \in [0, 1]$. In other words, the derivative will be tangent to the sliding surface, i.e., $f(\sigma(x))|_{\sigma(x)=0} \in T_{x(t)}\mathcal{S}$, being $\mathcal{S}$ the sliding manifold $\sigma(x) \equiv 0$. This implies that

$$\frac{d}{dt}(\sigma(x))\Big|_{\sigma(x)=0} = 0 = c^T \dot{x} = c^T f(\sigma(x))\Big|_{\sigma(x)=0,}$$

with $f(\sigma(x))|_{\sigma(x)=0}$ defined in (2), i.e., the system continues to slide on the surface $\sigma(x) = 0$. Taking this into account, $\alpha(x) \in [0, 1]$ must be such that

$$c^T \left[\alpha(x)\left(A_{b_1}x + B_{b_1}\right) + (1-\alpha(x))\left(A_{b_0}x + B_{b_0}\right)\right] = 0,$$

which means that

$$\alpha(x) = -\frac{c^T A_{b_0} x + c^T B_{b_0}}{c^T (A_{b_1} - A_{b_0}) x + c^T (B_{b_1} - B_{b_0})}. \tag{3}$$

In fact, $\alpha(x)$ is the average output of the $\Sigma\Delta$ modulator as a function of the instantaneous state vector $x(t)$. It may also be seen as the equivalent control necessary to keep the system in the sliding surface. From (3) we can find the non linear equation describing the time evolution of the system once it has reached the sliding surface

$$\dot{x} = \alpha(x) \left(A_{b_1} x + B_{b_1} \right) + (1 - \alpha(x)) \left(A_{b_0} x + B_{b_0} \right). \tag{4}$$

Expressions (3) and (4) describe the time evolution of the charge control once it is in the control surface $\sigma \equiv 0$. This represents the equivalent average system of the systems defined in (1) when the $\Sigma\Delta$ control is in the fast switching regime, the sliding region.

The average bitstream $\alpha(x)$ is obtained in real applications with a low pass filter; see Fig. 1. Although the spectrum properties of 1st and 2nd order $\Sigma\Delta$ modulators are clearly different, the average bitstream, i.e., the converted value of both controllers seen now as analog-to-digital converters, will be the same. The reason is that the average output will be the one necessary to keep the system on the control surface, i.e., $\mathrm{LPF}\{b_n\} = \alpha(x)$.

4 Experiments and Discussion

In the experiments, the charge is sensed through the voltage shift, an affine function of the net charge that can be easily obtained from measurements. Figure 3a reports a control experiment on which three different target voltage shifts (thus three values

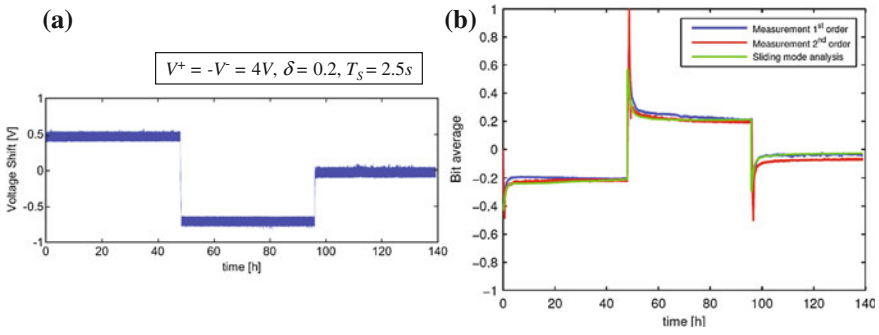

Fig. 3 (**a**) Voltage shift as a function of time when $\Sigma\Delta$ control is applied with three consecutive target voltage shifts, $+0.5V$, $-0.75V$, and $0V$; (**b**) sliding mode analysis compared with the actual measurements obtained with 1st and 2nd order $\Sigma\Delta$ controls

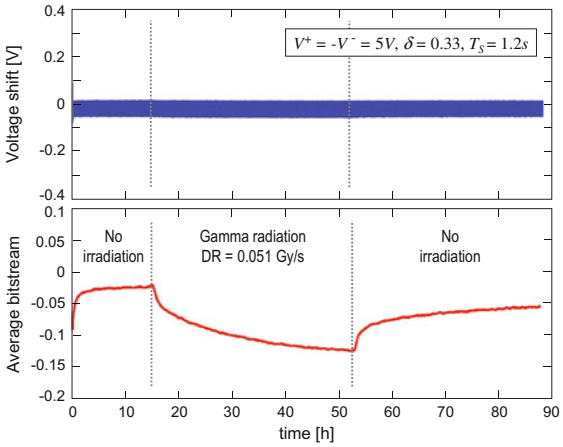

Fig. 4 Voltage shift and average bitstream when $\Sigma\Delta$ control is applied to set zero net charge, while the MEMS is under a sequence of radiation and no radiation steps

of Q_{target}) are successfully achieved. As stated above, no differences were found when using 1st or 2nd order $\Sigma\Delta$ controls. Figure 3b shows the excellent agreement between the experimental bitstreams obtained using $\Sigma\Delta$ controls and the sliding model analysis proposed here.

Figure 4 shows the results of an experiment in which ionizing Gamma radiation is applied to the MEMS while control is setting zero net charge. A clear correlation between the irradiation sequence and the average bitstream is observed. Specifically, from the moment on which irradiation starts there is a change in the bitstream, which is necessary to continue sliding on the control surface. This is compatible with a mismatched disturbance in the sliding mode controller due to the charge induced by radiation; see Domínguez-Pumar–Gorreta–Pons-Nin–Gómez-Rodríguez–González-Castaño [3].

References

1. E. Blokhina, S. Gorreta, D. López, D. Molinero, O. Feely, J. Pons, M. Domínguez-Pumar, Dielectric charge control in electrostatic MEMS positioners/varactors. IEEE JMEMS **21**, 559–573 (2012)
2. M. Domínguez-Pumar, S. Gorreta, J. Pons-Nin, E. Blokhina, P. Giounanlis, O. Feely, Real-time characterization of dielectric charging in contactless capacitive MEMS. Analog Integr. Circuits Signal Process **82**(3), 559–569 (2015)
3. M. Domínguez-Pumar, S. Gorreta, J. Pons-Nin, F. Gómez-Rodríguez, D.M. González-Castaño, Charge induced by ionizing radiation understood as a disturbance in a sliding mode control of dielectric charge. Microelectron. Reliab. **55**(9), 6–11 (2015)
4. J.M. Goncalves, A. Megretski, M.A. Dahleh, Global stability of relay feedback systems. IEEE Trans. Autom. Control **46**(4), 550–562 (2001)
5. J.M. Goncalves, A. Megretski, M.A. Dahleh, Global analysis of piecewise linear systems using impact maps and Lyapunov functions. IEEE Trans. Autom. Control **48**(12), 2089–2106 (2003)
6. S. Gorreta, J. Pons-Nin, E. Blokhina, O. Feely, M. Domínguez-Pumar, Delta-sigma control of dielectric charge for contactless capacitive MEMS. IEEE JMEMS **23**(4), 829–841 (2014)
7. H. Sira-Ramírez, *Sliding Mode Control: The Delta-Sigma Modulation Approach* (Birkhauser, Basel, 2015)

Limit Cycle Bifurcation from a Persistent Center at Infinity in 3D Piecewise Linear Systems with Two Zones

Emilio Freire, Manuel Ordóñez, and Enrique Ponce

Abstract We consider a specific family of three-dimensional differential systems whose vector field is continuous and piecewise linear, with two regions separated by a plane. After detecting a center configuration at infinity, we look for possible limit cycle bifurcation from such a center, by allowing parameter variations that do not destroy the center configuration.

1 Introduction

We study the mechanisms leading to the appearance of periodic orbits in a 3D PWL system with two linearity zones. The problem is motivated by a conjecture appearing in Ponce–Ros–Vela [3], regarding the bifurcation of a small limit cycle associated to a boundary equilibrium bifurcation. After some preparation work, which includes a blow-up, the bifurcation of the small limit cycle is associated to the existence of hyperbolic limit cycles in a differential system, namely

$$\begin{aligned} \dot{X} &= -Y, \\ \dot{Y} &= X - Z, \\ \dot{Z} &= 1, \end{aligned} \tag{1}$$

for $X < 0$, and

$$\begin{aligned} \dot{X} &= tX - Y, \\ \dot{Y} &= mX - Z, \\ \dot{Z} &= dX + 1, \end{aligned} \tag{2}$$

for $X > 0$. Here, the dot denotes derivative with respect a time τ, while t, m and d stand for the trace, the sum of second order minors and the determinant, respectively, of the matrix ruling the dynamics in the 'right' system.

E. Freire · M. Ordóñez · E. Ponce (✉)
Departamento de Matemática Aplicada II, Universidad de Sevilla, Sevilla, Spain
e-mail: eponcem@us.es

A. Colombo et al. (eds.), *Extended Abstracts Spring 2016*,
Trends in Mathematics 8, DOI 10.1007/978-3-319-55642-0_10

To investigate the existence of periodic orbits for system (1)–(2), we note first the following straightforward result.

Lemma 1 *If $d \leq 0$ then system (1)–(2) cannot have periodic orbits.*

It suffices to observe that, under hypothesis $d \leq 0$, the derivative $\dot{Z} > 0$ and so we cannot have closed orbits.

A first case where we can assure the existence of periodic orbits is when we are near a bifurcation of the type *focus-center-limit cycle*; see Carmona–Freire–Ponce–Ros–Torres [2, Theorem 1]. In such a case, an equilibrium point of node-focus type becomes a node-center leading to a bounded period annulus in the focal plane, with the biggest periodic orbit tangent to the plane $X = 0$. This critical situation appears when $m > 0$ and $mt - d = 0$ so that, if we consider t as being the bifurcation parameter then its critical value is $t_c = d/m$. Note that, according to Lemma 1, since $m > 0$ we must have $t_c < 0$.

By moving the bifurcation parameter t away from its critical value, a limit cycle can bifurcate from the mentioned periodic orbit tangent to the separation plane, under adequate hypotheses. In fact, by resorting to Carmona–Freire–Ponce–Ros–Torres [2, Theorem 1] for $d < 0$, we can state the following result.

Proposition 2 *System (1)–(2) with $0 < m \neq 1$ and $d < 0$ undergoes a focus-center-limit cycle bifurcation for $t = t_c$; that is, from the linear center configuration that exists for $X > 0$ when $t = t_c$, one limit cycle appears for $(1 - m)(t - t_c) > 0$ and $|t - t_c|$ sufficiently small.*

In particular, if $m < 1$ then the limit cycle bifurcates for $t > t_c$ and is orbitally asymptotically stable, while when $m > 1$ one unstable limit cycle bifurcates for $t < t_c$.

The limit cycle predicted by Proposition 2 will persist for some range of values of t until its possible disappearance in another bifurcation. Precisely, in this work we are interested in the characterization of another bifurcation allowing us to assure such disappearance (or its appearance, if we consider the opposite change in parameters) of the limit cycle. A pertinent remark in such approach is the following.

Remark 3 System (1) admits the first integral $H(X, Y) = (X - Z)^2 + (Y + 1)^2$, so that there exists the family of invariant cylinders $H(X, Y) = k$, which share as their common axis the straight line $X = Z$, $Y = -1$.

From Remark 3, we can surmise the existence of a center at infinity, generated by the above family of cylinders. Such a center, when considered in the corresponding Poincaré sphere, should be limited to the half-sphere corresponding to $X < 0$, so that from the outermost periodic orbit of the center another limit cycle bifurcation is possible.

We remark that, while in Proposition 2 the center configuration is lost after the bifurcation, here the change in parameters of the zone $X > 0$ does not alter the dynamics in the other zone at all, and so the center at infinity will persist after the possible bifurcation, to be just associated to a change in the stability of the outermost periodic orbit of the center.

2 Study of the Center at Infinity

Instead of considering the Poincaré compactification of the vector field (see Buzzi–Llibre–Medrado [1]) we can simply study the most interesting chart at infinity, by doing the change

$$X = \frac{u}{w}, \quad Y = \frac{v}{w}, \quad Z = -\frac{1}{w},$$

where we assume $w > 0$.

After this change of variables, we arrive to the differential system

$$\begin{aligned} \dot{u} &= -v + uw, \\ \dot{v} &= u + 1 + vw, \\ \dot{w} &= w^2, \end{aligned} \tag{3}$$

for $u < 0$, and

$$\begin{aligned} \dot{u} &= tu - v + u(d \cdot u + w), \\ \dot{v} &= mu + 1 + v(d \cdot u + w), \\ \dot{w} &= w(d \cdot u + w), \end{aligned}$$

for $u > 0$.

In the invariant plane $w = 0$ corresponding to the selected chart at infinity, it is easy to see now that for system (3) we have indeed a linear center at $(u, v, w) = (-1, 0, 0)$, which is responsible for a period annulus tangent to the straight-line $u = w = 0$ at the origin; see Fig. 1. This center is clearly a consequence of the invariant cylinders of system (1).

Following the method of closing equations, we first obtain approximations of high order both for the 'right' and the 'left' Poincaré maps in a neighborhood of the

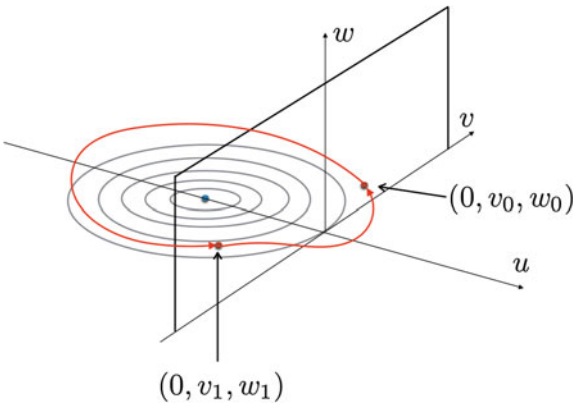

Fig. 1 In the choosen chart at infinity, the limit cycle bifurcates from a persistent center at the plane $w = 0$, located in the region $u < 0$

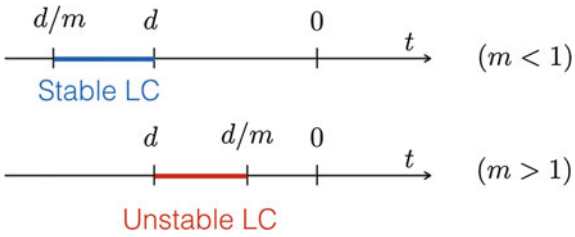

Fig. 2 The intervals of existence of the limit cycle according to Conjecture 5

origin at the plane $u = 0$. Thus, we compute $(v_1, w_1) = P_L(v_0, w_0)$ and $P_R(v_1, w_1)$, imposing the equality $(v_0, w_0) = P_R(v_1, w_1)$; see Fig. 1.

As we have an invisible tangency at the line $v = 0$ on such a plane, the 'right' map is an involution. Regarding Proposition 2, our main result is a kind of dual result, as follows.

Theorem 4 *System* (1)–(2) *with* $0 < m \neq 1$ *and* $d < 0$ *undergoes a limit cycle bifurcation from a center at infinity for* $t = d$*, so that one big limit cycle appears for* $(1 - m)(t - d) < 0$ *and* $|t - d|$ *sufficiently small.*

In particular, if $m < 1$ *then the limit cycle bifurcates for* $t < d$ *and is orbitally asymptotically stable, while when* $m > 1$ *one unstable limit cycle bifurcates for* $t > d$*.*

The proof of Theorem 4 requires a desingularization of the closing equations to arrive at the corresponding bifurcation equation; such long computations will be reported elsewhere.

Finally, it is natural to state the following conjecture; see Fig. 2.

Conjecture 5 System (1)–(2) with $0 < m \neq 1$ and $d < 0$ have at least one limit cycle for all the values of t between t_c and d. In particular, if $m < 1$ then for $t_c < t < d$ one limit cycle exists and it is orbitally asymptotically stable, while one unstable limit cycle exists for $d < t < t_c$ when $m > 1$.

References

1. C. Buzzi, J. Llibre, J.C. Medrado, Periodic orbits for reversible quadratic vector fields on $\mathbb{R}^3$. J. Math. Anal. Appl. **335**, 1335–1346 (2007)
2. V. Carmona, E. Freire, E. Ponce, J. Ros, F. Torres, Limit cycle bifurcation in 3D continuous piecewise linear systems with two zones. Application to Chua's circuit. Int. J. Bifurc. Chaos **15–10**, 3153–3164 (2005)
3. E. Ponce, J. Ros, E. Vela, Unfolding the fold-Hopf bifurcation in piecewise linear continuous differential systems with symmetry. Phys. D **250**, 3446 (2013)

Alternating Smooth and Nonsmooth Bifurcations in a Discontinuous Linear-Power Map

Laura Gardini, Roya Makrooni, and Iryna Sushko

Abstract We study the dynamics of a one dimensional discontinuous linear-power map. It has a vertical asymptote giving rise to new kinds of border collision bifurcations. We explain the peculiar periods of attracting cycles, appearing due to cascades of alternating smooth and nonsmooth bifurcations. Robust unbounded chaotic attractors are also described.

1 Introduction

The large number of applied models characterized by sharp switching between different states are ultimately described by nonsmooth systems. One of the efficient methods to investigate the dynamics of such systems is related to the construction of a first return map on some Poincaré section of the phase space, leading to piecewise smooth (PWS for short) maps, continuous or discontinuous. In particular, in engineering the well known Nordmark systems associated with grazing bifurcations (see [5, 6]) have been studied using PWS return maps with power function nonlinearities. The present study deals with a particular case of such a map. It is defined by two functions, $f_L(x)$ and $f_R(x)$, as follows:

L. Gardini (✉)
Dept. of Economics, Society, Politics (DESP), University of Urbino Carlo Bo,
Via A. Saffi n.42, 61029 Urbino, Italy
e-mail: laura.gardini@uniurb.it

R. Makrooni
Faculty of Mathematical Sciences, Shahid Beheshti University,
19839 Evin, Tehran, Iran
e-mail: r_makrooni@sbu.ac.ir

I. Sushko
Institute of Mathematics, National Academy of Sciences of Ukraine,
Tereshchenkivska st. 3, Kyiv 01601, Ukraine
e-mail: sushko@imath.kiev.ua

A. Colombo et al. (eds.), *Extended Abstracts Spring 2016*,
Trends in Mathematics 8, DOI 10.1007/978-3-319-55642-0_11

$$f : x \longmapsto f(x) = \begin{cases} f_L(x) = ax - 1 & if \quad x \le 0, \\ f_R(x) = bx^{-\gamma} - 1 & if \quad x > 0, \end{cases} \tag{1}$$

where a, b and γ are real parameters, $\gamma > 0$.

The PWS map (1) for $\gamma < 0$ corresponding to the continuous case, has been considered by many authors; see, e.g., di-Bernardo–Budd–Champneys–Kowalczyk [1]. One of the characteristic features of map (1) is the occurrence of border collision bifurcations (BCB for short). This term denotes the collision of an invariant set, typically a periodic point, with a border at which the system function changes its definition. In the study of one dimensional *continuous* PWS maps, the skew tent map is used as a border collision (BC) normal form, which is a powerful analytical tool to determine the effect of the BC of a cycle of any period; see Sushko–Avrutin–Gardini [7] for a survey.

Besides $\gamma < 0$, also the case $\gamma > 0$ in which map (1) is a *discontinuous* map with a vertical asymptote at $x = 0$, has been recently analyzed, mainly related to the case of free terms equal to $+1$; see [3, 4]. In the present work we consider the discontinuous map (1) and explain why peculiar cascades of alternating smooth and nonsmooth bifurcations are observed, leading to the appearance of attracting cycles of periods $p_{i+1} = 2p_i$ for odd i and $p_{i+1} = 2p_i - 1$ for even i, where $p_0 = n, n \ge 3$, is the period of an attracting cycle whose flip bifurcation (denoted *S-flip*) initiate the cascade. We show also that map (1) can possess unbounded chaotic attractors which are robust in some parameter regions and not robust in others. For all the proofs we refer to Gardini–Makrooni–Sushko [2].

A typical view of the bifurcation structure of the parameter space of f is presented in Fig. 1. In the following, after some preliminaries, we discuss first the parameter range $a < 0$, $b < 0$, associated with *invertible* map and, thus, with more simple

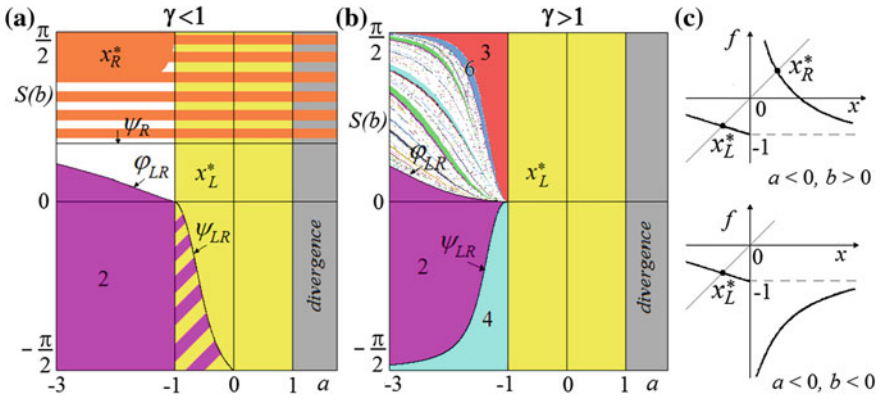

Fig. 1 2D bifurcation diagrams of f in the $(a, S(b))$-parameter plane, where $S(b) = \arctan(b)$, for $0 < \gamma < 1$ in (**a**) and $\gamma > 1$ in (**b**); stripped regions are related to coexistence, colored regions to attracting cycles of different periods, uncolored region to higher periodicity or chaotic attractors, *grey region* to divergence. In (**c**) examples of map f are shown

dynamics. Then we consider the range $a < 0, b > 0$, when f is *noninvertible*, which we split in two subcases, for $\gamma > 1$ and $0 < \gamma < 1$ related to quite different dynamics.

2 Preliminaries. Invertible Case: $b < 0$

The two partitions of the definition range of the map f are denoted as $I_L = (-\infty, 0]$ and $I_R = (0, +\infty)$. To denote an n-cycle $\{x_i\}_{i=0}^{n-1}$ of the map f, we use its symbolic representation, associating the symbol L with $x_i \in I_L$, and R with $x_i \in I_R$. The fixed points of f are denoted as $x = x_L^* = 1/(a-1) \in I_L$, and $x = x_R^* \in I_R$. The fixed point $x = x_L^*$ obviously exists for $a < 1$, being attracting for $|a| < 1$; at $a = -1$ it undergoes a degenerate flip bifurcation (DFB for short). The fixed point $x = x_R^*$ exists for $b > 0$; it is repelling for $\gamma \geq 1$, while for $0 < \gamma < 1$ it undergoes a subcritical flip bifurcation at

$$b = \frac{\gamma^\gamma}{(1-\gamma)^{\gamma+1}} =: \psi_R,$$

being repelling for $0 < b \leq \psi_R$ and attracting for $b > \psi_R$; see Fig. 1. The following propositions summarise the dynamics of f in the invertible case; see also Fig. 2.

Proposition 1 (Flip bifurcations of the 2-cycle LR) *Let $a < 0$, $b < 0$, and $\gamma > 0$. Then the map f given in (1) has a unique 2-cycle $\{x_0, x_1\}$ with $x_0 < 1/a < 0$, $x_1 > 0$, which undergoes a flip bifurcation at*

$$b = \frac{1}{a\gamma}\left(\gamma\frac{a+1}{1-\gamma}\right)^{\gamma+1} =: \psi_{LR}$$

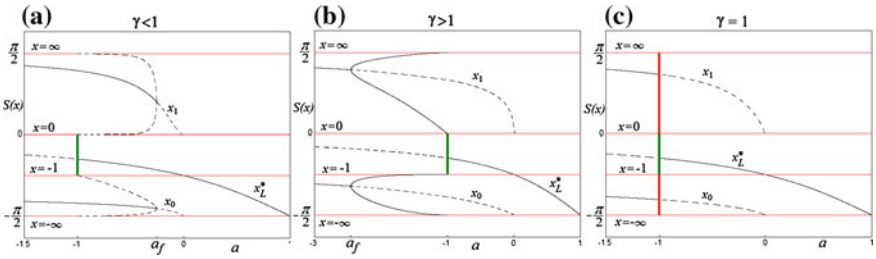

Fig. 2 Bifurcation diagram a vs $S(x)$ at $b = -5$, where $S(x) = \arctan(x)$. In (**a**) $\gamma = 0.5$, in (**b**) $\gamma = 2$ and in (**c**) $\gamma = 1$, associated with the subcritical, supercritical and degenerate flip bifurcations of the 2-cycle LR, respectively. For $a = 1$ related to DFB of x_L^* the interval $[-1, 0] \setminus x_L^*$ is filled by 2-periodic points; additionally, for $\gamma = 1$ intervals $(-\infty, -1] \setminus x_0$ and $[0, +\infty) \setminus x_1$ are filled by 4-periodic points, being associated with DFB of the 2-cycle. The value a_f is obtained by substituting $b = -5$ and the related value of γ to $b = \psi_{LR}$; see Proposition 1

for $\gamma \neq 1$, and $a = -1$ for $\gamma = 1$. This flip bifurcation is subcritical for $0 < \gamma < 1$ and the 2-cycle is attracting for $b < \psi_{LR}$; supercritical for $\gamma > 1$ and the 2-cycle is attracting for $b \geq \psi_{LR}$; degenerate for $\gamma = 1$, and the 2-cycle is attracting for $a < -1$. Moreover, as $a \to 0_-$, the repelling 2-cycle LR disappears by a nonregular BCB at $a = 0$: $\{x_0, x_1\}\,|_{a=0} = \{-\infty, 0\}$.

Proposition 2 (BCB of the 4-cycle) *Let $a < 0$, $b < 0$, and $\gamma > 0$. Then, for the map f given in (1) at $a = -1$, a nonregular BCB of a 4-cycle $(LR)^2$ occurs such that for $0 < \gamma < 1$ a repelling 4-cycle disappears as $a \to -1_+$; for $\gamma > 1$ an attracting 4-cycle disappears as $a \to -1_-$; the points of the 4-cycle $(LR)^2$ at $a = -1$ are $\{0, -\infty, +\infty, -1\}$.*

3 Noninvertible Case: $b > 0$, $\gamma > 1$ (Periodicity Regions)

Proposition 3 (map g) *Let $b > 0$ and $\gamma > 0$. Then the dynamics of the map f given in (1) are in one-to-one correspondence with the dynamics of the map g defined by three functions, $f_L(x)$, $f_M(x) = f_R^2(x)$ and $f_R(x)$, as follows:*

$$g\colon x \longmapsto g(x) = \begin{cases} f_L(x) = ax - 1 & \text{if} \quad x \leq 0, \\ f_M(x) = \frac{b}{(bx^{-\gamma}-1)^{\gamma}} - 1 & \text{if } 0 < x < f_R^{-1}(0) = b^{\frac{1}{\gamma}}, \\ f_R(x) = bx^{-\gamma} - 1 & \text{if } x \geq f_R^{-1}(0), \end{cases} \tag{2}$$

which is continuous at $x = 0$, with $g(0) = -1$, and discontinuous at $x = f_R^{-1}(0)$ with $\lim_{x \to f_R^{-1}(0)_-} g(x) = +\infty$ and $\lim_{x \to f_R^{-1}(0)_+} g(x) = 0$.

The auxiliary map g is of help to study the dynamics of f in the noninvertible case:

Proposition 4 *Let $b > 0$ and $\gamma > 1$ be fixed, and $a \in (a_R^h, -1)$, where $a = a_R^h$ satisfies the condition $b = -a(-a-1)^{\gamma}$ of the first homoclinic bifurcation of x_R^*. Then,*

(i) any fold bifurcation (either fold-BCB or S-fold) of the map g given in (2) is associated with the appearance of a pair of cycles for map f, one attracting and one repelling, whose periods differ by 1 (say n and $n-1$);

(ii) let $x = x^* > 0$ be a periodic point, closest to $x = 0$, of an attracting n-cycle of f with a negative eigenvalue, which attracts all points of the interval $(0, x^*)$, and let $R^2\sigma_0$ be the symbolic sequence of this cycle (here, σ_0 stands for the remaining symbolic sequence, necessarily starting with L). Then, decreasing a it is observed a cascade of alternating S-flip bifurcations and BCs leading to cycles whose symbolic sequences can be written as $R^2\sigma_k$, where $\sigma_k = \sigma_{k-1}T\sigma_{k-1}$, $k = 1, 2, \ldots$, with the alternating symbols $T = R^2$ and $T = L$. The symbol $T = R^2$ corresponds to an S-flip bifurcation, so that an attracting m-cycle in this cascade is followed by an attracting $2m$-cycle, while the symbol $T = L$ is

associated with a BC and the m-cycle is followed by an attracting $(2m-1)$*-cycle.*

For example, starting from an attracting 3-cycle, for decreasing a one observes a cascade of bifurcations leading to appearance of attracting cycles of periods 6, 11, 22, 43, …

4 Noninvertible Case: $b > 0, 0 < \gamma < 1$ (Dominant Chaos)

Proposition 5 (robust unbounded chaos) *Let* $0 < \gamma < 1$ *and* $0 < b \le \psi_R$. *Then,*

(i) for $a_L^h < a < -1$, *the map* f *has an unbounded chaotic attractor consisting of intervals* $[-1, f_R^2(-a-1)]$, $[f_L \circ f_R^2(-a-1), -a-1]$ *and* $[f_R(-a-1), +\infty)$; *here,* $a = a_L^h$ *satisfies the condition of the first homoclinic bifurcation of* x_L^* *defined by*

$$\frac{b}{(b(-a-1)^{-}\gamma - 1)^{\gamma}} = \frac{a}{a-1};$$

(ii) for $a_R^h < a \le a_L^h$ *the map* f *has an unbounded chaotic attractor consisting of intervals* $[-1, -a-1]$ *and* $[f_R(-a-1), +\infty)$;

(iii) for $a_{LR} < a \le a_R^h$, *depending on the value of b, the map* f *may have the attracting unbounded chaotic interval* $[-1, +\infty)$; *here,* $a = a_{LR}$ *satisfies the condition*

$$b = -\frac{1}{a\gamma}\left(-\gamma\frac{a+1}{\gamma+1}\right)^{\gamma+1}$$

of the fold bifurcation of the 2-cycle LR *(indicated in Fig. 1 as* ϕ_{LR}*);*

(iv) for $a < a_{LR}$ *almost all the trajectories converge to the attracting 2-cycle born crossing the curve* ϕ_{RL}, *and a chaotic repeller exists.*

Proposition 6 *Let* $0 < \gamma < 1$ *and* $b > \psi_R$. *Then,*

(i) for $a_L^h < a < -1$, *the attracting fixed point* x_R^* *of the map* f *coexists with a chaotic attractor in the unbounded invariant absorbing intervals*

$$[-1, f_R^2(-a-1)] \cup [f_L \circ f_R^2(-a-1), -a-1] \cup [f_R(-a-1), +\infty);$$

(ii) for $a_{RR}^h < a \le a_L^h$, *the attracting fixed point* x_R^* *of the map* f *coexists with a chaotic attractor in the unbounded invariant absorbing intervals* $[-1, -a-1] \cup [f_R(-a-1), +\infty)$; *here,* $a = a_{RR}^h$ *is related to the first homoclinic bifurcation of the repelling 2-cycle;*

(iii) for $a_{LR} < a \le a_{RR}^h$, *depending on the value of b, the fixed point* x_R^* *may be the unique attractor of the map* f, *and a chaotic repeller exists;*

(iv) for $a < a_{LR}$, *the attracting fixed point* x_R^* *coexists with an attracting 2-cycle born due to an S-fold crossing the curve* ϕ_{RL}, *and a chaotic repeller exists.*

Acknowledgements L. Gardini acknowledges the National Group of Mathematical Physics, INDAM Italian Research Group.

References

1. M. di Bernardo, C.J. Budd, A.R. Champneys, P. Kowalczyk, *Piecewise-Smooth Dynamical Systems: Theory and Applications*, vol. 163, Applied Mathematical Sciences (Springer, London, 2008)
2. L. Gardini, R. Makrooni, I. Sushko, Cascades of alternating smooth bifurcations and border collision bifurcations in a family of discontinuous linear-power maps, Geocomplexity Discussion Paper No.3/2016, ISSN:2409-7497, http://econpapers.repec.org/paper/cstwpaper/
3. R. Makrooni, F. Khellat, L. Gardini, Border collision and fold bifurcations in a family of piecesiwe smooth maps. Unbounded chaotic sets (2015)
4. R. Makrooni, F. Khellat, L. Gardini, Border collision and fold bifurcations in a family of piecesiwe smooth maps. Divergence but not only (2015)
5. A.B. Nordmark, Non-periodic motion caused by grazing incidence in an impact oscillator. J. Sound Vib. **145**, 279–297 (1991)
6. A.B. Nordmark, Universal limit mapping in grazing bifurcations. Phys. Rev. E **55**, 266–270 (1997)
7. I. Sushko, V. Avrutin, L. Gardini, Bifurcation structure in the skew tent map and its application as a border collision normal form. J. Diff. Equ. Appl. (2015)

Extending Slow Manifolds Near a Degenerate Transcritical Intersection in Three Dimensions

Christine Gavin, Philip J. Aston, and Gianne Derks

Abstract Motivated by a problem from pharmacology, we consider a general two parameter slow–fast system in which the critical set consists of a one dimensional manifold and a two dimensional manifold, intersecting transversally at the origin. Using geometric desingularisation, we show that for a subset of the parameter set there is an exchange of stabilities between the attracting components of the critical set and the direction of the continuation can be expressed in terms of the parameters.

1 Motivation

We consider the pharmacological model of dimerisation, where a receptor binds to two ligand molecules. The dimerisation model is an adaptation of the well studied target mediated drug disposition model (TMDD) in which the receptor binds to one ligand molecule; see Peletier–Gabrielsson [5] for more details. In both models, it is assumed that the binding is the fastest process. This gives a separation of time scales, which allows us to use geometric singular perturbation theory to analyse these models. For the TMDD model, the critical set reduces to two intersecting one dimensional manifolds. Using the results in Krupa–Szmolyan [3], it can be shown that the slow manifold connects the two attracting branches of the critical set. For the dimerisation model, the critical set reduces to an incoming one dimensional manifold and an outgoing two dimensional manifold that intersect. By analysing this type of intersection using geometric desingularisation, we will show the existence of a transfer to the two dimensional manifold and determine the direction of the orbit on this manifold away from the intersection, in terms of the model parameters.

C. Gavin (✉) · P.J. Aston · G. Derks
Department of Mathematics, University of Surrey, Guildford GU2 7XH, UK
e-mail: c.gavin@surrey.ac.uk

P.J. Aston
e-mail: p.aston@surrey.ac.uk

G. Derks
e-mail: g.derks@surrey.ac.uk

A. Colombo et al. (eds.), *Extended Abstracts Spring 2016*,
Trends in Mathematics 8, DOI 10.1007/978-3-319-55642-0_12

2 The General Problem

The canonical form for the problem of interest is given by

$$\begin{aligned}\dot{x}_1 &= (y + x_2)\, x_1 + \lambda_1 \varepsilon + \mathcal{O}\left([x_1 + x_2 + y + \varepsilon]\left[(x_1 + x_2 + y)^2 + \varepsilon\right]\right),\\ \dot{x}_2 &= (y + x_2)\,(x_1 - y + x_2) + \lambda_2 \varepsilon + \mathcal{O}\left([x_1 + x_2 + y + \varepsilon]\left[(x_1 + x_2 + y)^2 + \varepsilon\right]\right),\\ \dot{y} &= \varepsilon\,(1 + \mathcal{O}\,(x_1 + x_2 + y + \varepsilon))\,.\end{aligned} \tag{1}$$

The critical set is the union of the one dimensional manifold $\{x_2 = y, x_1 = 0 : y \in \mathbb{R}\}$ and the two dimensional manifold $\{x_2 = -y : x_1, y \in \mathbb{R}\}$. The incoming manifold $S_a^- = \{x_2 = y, x_1 = 0 : y < 0\}$ is attracting. Away from the intersection at the origin, Fenichel theory [1] tells us that the manifolds in the critical set persist for ε sufficiently small. We will investigate what happens to the incoming manifold, denoted by $S_{a,\varepsilon}^-$, as it passes by a neighbourhood of the origin, the extension of $S_{a,\varepsilon}^-$ is denoted by $\bar{S}_{a,\varepsilon}^-$. We do this using the blow up method and building on the work Krupa–Szmolyan [3].

3 Statement of the Main Result

For small fixed $\rho > 0$ and J a small open interval around 0 in $\mathbb{R}$, we define the following

$$\begin{aligned}\Delta^{\text{in}} &= \{\rho\,(0, -1, -1) + (x_1, 0, y) : x_1, y \in J\}\,,\\ \Delta_a^{\text{out}} &= \left\{\rho\left(\bar{x}_1^-, -1, 1\right) + (x_1, 0, y) : x_1, y \in J\right\},\\ \Delta_e^{\text{out}} &= \{\rho\,(0, 1, 0) + (x_1, 0, y) : x_1, y \in J\}\,,\end{aligned}$$

where $\bar{x}_1^- = \frac{1}{2}\left[1 + \lambda_1 - \lambda_2 - \sqrt{(\lambda_1 - \lambda_2 - 3)^2 - 8\,(\lambda_2 + 1)}\right]$.

Theorem 1 *For fixed (λ_1, λ_2), there exists $\varepsilon_0 > 0$ such that, for any $\varepsilon \in (0, \varepsilon_0]$,*

(i) if (λ_1, λ_2) is in the shaded region or along the black line in Fig. 1a, then the extension $\bar{S}_{a,\varepsilon}^-$ passes through Δ_e^{out} at $\left(h_x(\varepsilon), \rho, h_y(\varepsilon)\right)$, where $h_x(\varepsilon)$, $h_y(\varepsilon) = \mathcal{O}(\sqrt{\varepsilon})$;

(ii) if (λ_1, λ_2) is in the unshaded region in Fig. 1a, the extension $\bar{S}_{a,\varepsilon}^-$ passes through Δ_a^{out}.

The statement of this theorem is illustrated in Fig. 2.

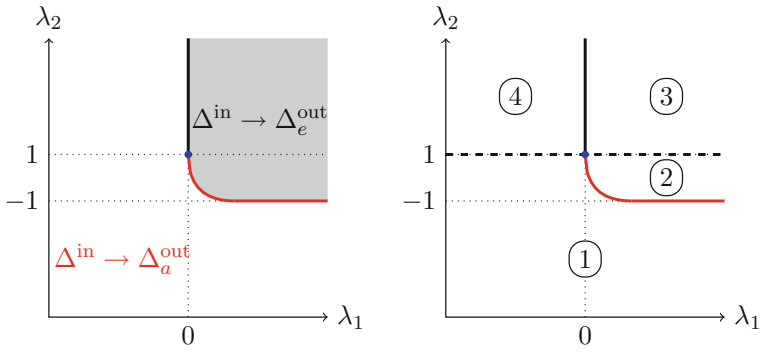

(a) Results of Theorem 1. **(b)** Four regions we consider.

Fig. 1 The curve shown in these two figures is the union of $\lambda_1 = 0$ for $\lambda_2 > 1$ (*black line*), $\lambda_2 = -1$ for $\lambda_1 > 2$ and $(\lambda_1 - \lambda_2 - 3)^2 - 8(\lambda_2 + 1) = 0$ for $0 < \lambda_1 \leq 2$ (*red curve*)

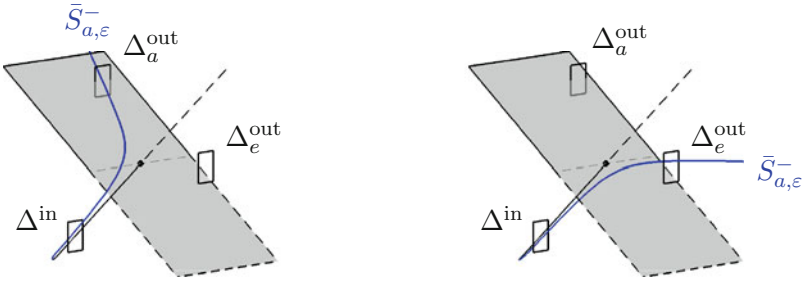

(a) Dynamics when there is a transition of stability. **(b)** Dynamics when there is a fast jump away from the origin.

Fig. 2 Summarises the results of Theorem 1. *Bold blue curve* gives the continuation of $S^-_{a,\varepsilon}$ in each case, denoted by $\bar{S}^-_{a,\varepsilon}$

4 Sketch of the Proof of the Main Result

We add the trivial equation $\dot{\varepsilon} = 0$ to system (1) and define a blow up of the region near the origin as $x_1 = r\bar{x}_1$, $x_2 = r\bar{x}_2$, $y = r\bar{y}$, $\varepsilon = r^2\bar{\varepsilon}$. Apart from the polar blow up with $\bar{x}_1^2 + \bar{x}_2^2 + \bar{y}^2 + \bar{\varepsilon}^2 = 1$, we will use five directional charts. The K_1 and K_3 charts are obtained by taking $\bar{x}_2 = -1$ and $\bar{x}_2 = 1$, respectively. The K_4 and K_5 charts are obtained by taking $\bar{x}_1 = -1$ and $\bar{x}_1 = 1$, respectively. We also have the K_2 chart which is obtained by taking $\bar{\varepsilon} = 1$. Figure 3 gives the dynamics in each of the directional charts that are used in this section; see Kuehn [4] and references therein for more details about the blow up technique.

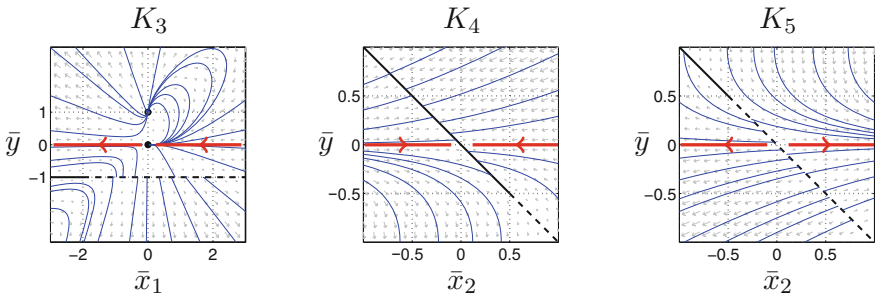

Fig. 3 Dynamics in the directional charts in the invariant plane $\bar{\varepsilon} = 0$. *Dashed lines* and *open circles* indicate that the point is unstable *while solid lines* and *closed circles* indicate that it is stable. The *red arrows* highlight the direction of the flow on the invariant line

In the polar blow up the sphere $\bar{\varepsilon} = 0$ has two steady states corresponding to the one dimensional critical manifold, denoted by P_a^- and P_r^+, where P_a^- corresponds to S_a^-. There is a continuous curve of steady states corresponding to the two dimensional critical manifold denoted by C. Furthermore, there are two steady states corresponding to the critical fibre which we call q_{in} and q_{out}. All isolated steady states have a one dimensional centre manifold and the curve C has a two dimensional centre manifold in the invariant hyperplane $r = 0$.

4.1 Dynamics in the K_2 Chart

The initial continuation of $S_{a,\varepsilon}^-$ is best described in the K_2 chart.

Lemma 2 *When $\lambda_1 = 0$, the plane $\bar{x}_1 = 0$ is invariant in the K_2 chart and the continuation of the centre manifold of P_a^- stays in this plane. When $\lambda_1 \neq 0$, the sign of $\bar{x}_1$ in the continuation is given by the sign of λ_1.*

Lemma 3 *If $\lambda_2 < 1$ then the centre manifold of P_a^- connects to the attracting part of the centre manifold of C and if $\lambda_2 > 1$ then the centre manifold of P_a^- connects to the centre manifold of q_{out}.*

Next, the further continuation on the centre manifolds is considered. If $\lambda_2 < 1$ then the K_1 chart is used and if $\lambda_2 > 1$ it is the K_3 chart. We divide the parameter space into four regions, shown in Fig. 1b, where we observe different types of continuations.

4.2 Dynamics on the Centre Manifold of C

The dynamics on the attractive part of the centre manifold of the curve C can be desingularised such that this part of the curve C has at most two fixed points, one

of which is $\bar{x}_1^-$ if it is real. Note that these two steady states are found by solving a quadratic equation so they are only real for a subset of (λ_1, λ_2) values.

(i) *Region one*: it can be shown that $\bar{x}_1^-$ is real and stable and the dynamics on the centre manifold are attracted to this point.
(ii) *Region two*: the solutions of the quadratic are complex or the fixed points on the attractive part of C have positive $\bar{x}_2$ hence they are not in K_1. It can be shown that the dynamics on the centre manifold moves the continuation in K_1 to the repelling part of the centre manifold of C. We then hand over to the K_5 chart as $\bar{x}_1 > 0$. The dynamics highlighted by the red arrow in Fig. 3c indicate that the continuation in K_5 has $\bar{x}_2 \to \infty$ and $\bar{y} \to 0$. Finally, we hand over to the K_3 chart where the fact that $\bar{x}_1 > 0$ and the dynamics highlighted by the red arrow in Fig. 3a indicate that the trajectory goes to q_{out}.

4.3 Dynamics on the Centre Manifold of q_{out}

The dynamics on the centre manifold of q_{out} (indicated by the red arrows in Fig. 3a) tell us that if the continuation approaches the K_3 chart with $\bar{x}_1 \geq 0$ then it is attracted to q_{out}, whereas if $\bar{x}_1 < 0$ it moves away from q_{out}.

(iii) *Region three:* by Lemma 2, we approach the K_3 chart with $\bar{x}_1 \geq 0$. Hence, the continuation goes to q_{out}.
(iv) *Region four:* the continuation approaches the K_3 chart with $\bar{x}_1 < 0$, hence it is repelled. We now hand over to the K_4 chart where the continuation is attracted by the centre manifold of C (indicated by the red arrow in Fig. 3b). The desingularised dynamics on the centre manifold directs the continuation towards the stable point $\bar{x}_1^-$.

The four possible types of continuations are shown in Fig. 4.

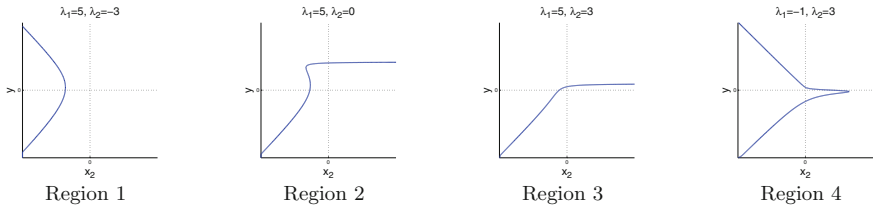

Fig. 4 A typical continuation from each region projected into the $x_2 - y$ plane. The x_1 evolution is not shown

5 Conclusion and Discussion

We have described the fate of the incoming attracting slow manifold. This gives the parameter values for which the slow manifold connects the two attracting manifolds of the critical set. The parameter values for the dimerisation model always lie in this set. Furthermore, we have determined a point $\bar{x}_1^-$ which gives the outgoing direction on the two dimensional manifold along which the continuation moves away from the intersection at the origin. Full details will be given in a forthcoming paper Gavin–Aston–Derks [2], which will also include results for continuations on the red line in Fig. 1a and on the size of the contraction of the transition map which transfers Δ^{in} to the appropriate Δ^{out} section.

Acknowledgements CG was supported in this work by the EPSRC Doctoral Training Grant 1363360. GD thanks the Centre de Recerca Matemàtica for the opportunity to discuss the work with other participants in the Intensive Research Program on Advances in Nonsmooth Dynamics.

References

1. N. Fenichel, Geometric singular perturbation theory for ordinary differential equations. J. Diff. Equ. **31**(1), 53–98 (1979)
2. C. Gavin, P.J. Aston, G. Derks, Extending slow manifolds near degenerate transcritical intersections in three dimensions (in preparation)
3. M. Krupa, P. Szmolyan, Extending slow manifolds near transcritical and pitchfork singularities. Nonlinearity **14**(6), 1473–1491 (2001)
4. C. Kuehn, *Multiple Time Scale Dynamics*. Applied Mathematical Society, vol. 191 (Springer, Berlin, 2015)
5. L.A. Peletier, J. Gabrielsson, Dynamics of target-mediated drug disposition. Eur. J. Pharm. Sci. **38**(5), 445–464 (2009)

Less Is More I: A Pessimistic View of Piecewise Smooth Bifurcation Theory

Paul Glendinning

Abstract The analysis of piecewise smooth bifurcations reveals an alarming proliferation of cases as the dimension of phase space increases. This suggests that a different approach needs to be taken when trying to describe bifurcations. In particular, it may not be helpful to analyze particular bifurcations at the level of detail that is standard for smooth systems.

1 Introduction

> *"Can you do addition?" the White Queen asked. "What's one and one and one and one and one and one and one and one and one and one?" "I don't know," said Alice. "I lost count."* [2, Chap. 9].

With the analysis of more bifurcations of piecewise smooth (PWS) systems it is becoming clear that there is a proliferation of cases as the dimension of the ambient phase space increases. In smooth dynamical systems, the centre manifold theorem implies that the range of typical local bifurcations is severely restricted and independent from the phase space dimension. Indeed, only the saddle-node bifurcation and Hopf bifurcation are generic, though the addition of symmetry or other special features can add complications. The global bifurcations of typical smooth systems are also constrained, although features such as Shilnikov's Theorems for homoclinic orbits, and the possibility of bifurcations being dense in parameter space mean that it may be impossible to give a complete description. Nonetheless, there are robust features common to all these bifurcations that can be described sensibly.

The situation for PWS systems appears significantly harder to deal with. Whereas typical smooth systems have a manageable number of fundamental bifurcations, the number of cases for PWS systems increases with the dimension of the phase space in such a way that a complete classification would require the enumeration of an

P. Glendinning (✉)
School of Mathematics, University of Manchester,
Oxford Road, Manchester M13 9PL, UK
e-mail: p.a.glendinning@manchester.ac.uk

A. Colombo et al. (eds.), *Extended Abstracts Spring 2016*,
Trends in Mathematics 8, DOI 10.1007/978-3-319-55642-0_13

infinite set of possibilities. This may be good for the production of academic papers, but it does not necessarily help us to understand potential applications.

These observations suggest that the attitude to bifurcations of PWS systems needs to be somewhat different from that applied to smooth systems. In particular, it may be more useful to develop weaker results which apply quite generally rather than to give a complete picture of the bifurcations that can occur (a list that might take forever). Such results might provide a rather less detailed description of possibilities, or the development of techniques that would allow a more detailed description if the occasion (i.e., the application) arose, but would not attempt to apply these methods to *all* possible situations without further motivation. This is the 'Less is More' philosophy of the title, described in greater detail in Glendinning [11].

In the remainder of this note we give examples of the proliferation described above.

2 Transitions to Chaos in PWS Maps

For smooth maps of the interval, for example the quadratic map, the transition to chaos is very easy to characterize. Let $\mathcal{P}$ be the set of periods for the map, i.e., if the map is f then $p \in \mathcal{P}$ if and only if f has a periodic orbit of least period p. It follows from the proof of Sharkovskii's Theorem that, for any *continuous* non-chaotic map of the interval,

$$\mathcal{P} = \{2^n \mid 0 \le n \le N\}$$

for some $N \in \{0, 1, 2, \dots\} \cup \{\infty\}$. To some extent this explains why period-doubling cascades are so ubiquitous, though it also holds for Nordmark's continuous square root map where the *stable* periodic orbits form a period-adding sequence; see Nordmark [14].

For PWS maps with discontinuities the situation is more complicated. If we consider maps with a single discontinuity and with two increasing continuous branches, then Gambaudo–Procaccia–Thomae–Tresser [6] shows that the only *infinite* sets of periods that can occur on the boundary of chaos are arbitrary period multiplying

$$\mathcal{P} = \{p_n \mid p_{n+1} = a_n p_n \;\; a_n \in \mathbb{N}, \; a_n \ge 2\}, \tag{1}$$

though these correspond to points on a one-parameter boundary of chaos in a two-parameter space; typically, the transition to chaos occurs after a finite number of periods are created. This is a good example of the early theory of PWS maps developed in the context of the bifurcations of smooth flows.

In the more general case of PWS maps with a single discontinuity and two continuous monotonic branches at least one of which is decreasing, there is a new robust route to chaos involving creation of infinitely many periodic orbits: the anharmonic route [7]. In the case of one increasing and one decreasing branch this generates fixed points and periods

$$\mathcal{P} = \{p_n \mid p_{n+1} = 2p_n + (-1)^n,\ p_1 = 2\},$$

and more general forms are also possible involving higher iterates of the map or maps with two decreasing branches.

Furthermore, if we consider all possible sets of periodic orbits for non-chaotic maps then the set of infinite possible periods on the boundary of chaos, ignoring the multiplying of (1), is given by a subshift of finite type corresponding to different sequences of renormalizations or induced maps; see Glendinning [8].

These results show that, even though the continuous case is constrained, what can happen in the discontinuous case is complicated by a proliferation from essentially one to uncountably many possibilities. Moreover, whilst these can be characterized, it is not clear which are relevant for the examples arising in PWS dynamics (which possibilities occur in expanding maps, or in piecewise linear maps?). The theory making this analysis possible was developed in the late 1970s (see Milnor–Thurston [13]) and these ideas are worth revisiting.

3 The Border Collision Normal Form

Now, consider continuous PWS maps in dimension greater than one. Suppose that phase space is divided into two regions by a switching surface and smooth maps are defined on each side of the surface, and the PWS map is continuous but not differentiable across the surface. Suppose a fixed point exists at some parameter value in one region, and as parameters vary it moves to intersect the switching surface. What happens?

Nusse–Yorke [15] shows that, given some genericity conditions, the bifurcation is described locally by the border collision normal form, with leading order terms

$$z_{n+1} = F(z_n) = \begin{cases} A_0 z_n + m & \text{if } x_1 < 0, \\ A_1 z_n + m & \text{if } x_1 > 0, \end{cases}$$

where $A_0 = \begin{pmatrix} t_0 & 1 \\ -d_0 & 0 \end{pmatrix}$, $A_1 = \begin{pmatrix} t_1 & 1 \\ -d_1 & 0 \end{pmatrix}$ and $m = \mu(1, 0)^T$.

This can be generalized to $\mathbb{R}^n$, where the map takes the same form and, provided some simple genericity conditions hold, the matrices A_i can be written in observer canonical form, where the first column is arbitrary and the remainder has ones on the upper off-diagonal and zeroes everywhere else, and $m = \mu(1, 0, \ldots, 0)^T$; see di Bernardo [3].

Using some beautiful technical results of Buzzi [1] and Tsujii [16], it is possible to prove bifurcations from fixed points to n-dimensional attractors in these maps.

Theorem 1 (Glendinning [9, 10]) *Consider the border collision normal form in $\mathbb{R}^n$ ($n = 2, \ldots$). There exist open regions of the parameter space B_n such that, for each parameter in B_n, if $\mu < 0$ then the border collision normal form has a stable fixed*

point; whilst if $\mu > 0$ then the border collision normal form has at least one attractor with an invariant measure absolutely continuous with respect to the n-dimensional Lebesgue measure. If $n = 2$, then the attractor has topological dimension 2; and if $n > 2$, then the attractor has Hausdorff dimension equal to n and generically has topological dimension n.

What about other transitions: can we go from attractors of any given Hausdorff dimension to any other Hausdorff dimension? If so, is this the right way of looking at the problem? If not, how much is the dynamics constrained and how should this be described?

4 Boundary Equilibrium Bifurcations

Boundary equilibrium bifurcations (BEBs) occur if a stationary point of a PWS system intersects the boundary of one of the regions on which the smooth components of the system are defined; see di-Bernardo–Budd–Champneys–Kowalczyk [4]. Even in planar flows there are twelve cases that need to be considered; see Filippov [5]. The example below of a flow in $\mathbb{R}^3$ shows just how complicated the bifurcation can become in higher dimensions. This example has a Shilnikov homoclinic orbit with a sliding section immediately after the bifurcation, and hence all the levels of complexity of this three-dimensional flow; see Glendinning [12].

The example uses two differential equations with switching surface $z = 0$, so F^+ defines the flow if $z > 0$ and F^- defines the flow if $z < 0$, where

$$F^+(\mathbf{x}, \nu) = \begin{pmatrix} -\rho & a & -\omega \\ 0 & \lambda & 0 \\ \omega & b & -\rho \end{pmatrix} \begin{pmatrix} x \\ y \\ z - \nu \end{pmatrix}, \quad F^-(\mathbf{x}, \nu) = (U_1, U_2, U_3)^T,$$

with $U_3 > 0$ and $U_k \neq 0$, $k = 1, 2$. The upper flow F^+ has a stationary point at $(0, 0, \nu)$ so there is a BEB if $\nu = 0$. Suppose that the remaining constants have been fixed, except ω which will be used to explore the sensitivity of the bifurcation to changes in the other parameters. Consider the case $\nu > 0$. By scaling, we may set $\nu = 1$ and then the final parameter ω can be used to determine the different dynamics that can occur.

The stationary point $(0, 0, 1)$ has eigenvalues λ and $-\rho \pm i\omega$ which may be chosen so that $\rho/\lambda < 1$. Thus, if there is a homoclinic orbit, i.e., an orbit approaching $(0, 0, 1)$ in both forwards and backwards time, the classic results of Shilnikov proving the existence of chaos hold with minor technological modifications to take the sliding section into account; see Glendinning [12]. Numerical simulations show that ω can be chosen so that the flow includes just such a homoclinic orbit and hence that the dynamics in $\nu > 0$ of this BEB is determined by a family of differential equations (as the other parameters vary) which has complicated bifurcation structure itself.

5 Conclusion

A subject comes of age when the extent and scope of the discipline is generally accepted. Whilst many of the issues described above have analogues in smooth bifurcation theory (for example, analysis of the fine structure of smooth Shilnikov bifurcations shows that there are infinitely many cases) there are still tensions for piecewise smooth bifurcation theory. What features should define a *useful* bifurcation theory in piecewise smooth dynamics? An attempt to answer this question is made in Glendinning [11]—here we have simply shown that a complete classification can lead to very long lists. Of course there are many other complications (e.g., noise and nonlinearity) not mentioned here, but the fundamental problem is: how do we select methods and results to avoid endless lists?

Acknowledgements I am grateful to Mike Jeffrey and Rachel Kuske for conversations that helped crystallize these ideas, and to the Simons Foundation for support at the CRM, Barcelona.

References

1. J. Buzzi, Absolutely continuous invariant measures for generic multi-dimensional piecewise affine expanding maps. Int. J. Bifurc. Chaos **9**, 1743–1750 (1999)
2. L. Carroll, *Through the Looking-Glass, and What Alice Found There* (Macmillan, London, 1871)
3. M. di Bernardo, Normal forms of border collision in high dimensional non-smooth maps. Proc. IEEE ISCAS **2003**(3), 76–79 (2003)
4. M. di Bernardo, C. Budd, A.R. Champneys, P. Kowalczyk, *Piecewise-Smooth Dynamical Systems: Theory and Applications*. Applied Mathematical Sciences, vol. 163 (Springer, London, 2008)
5. A.F. Filippov, *Differential Equations with Discontinuous Right Hand Sides* (Kluwer, Netherlands, 1988)
6. J.M. Gambaudo, I. Procaccia, S. Thomae, C. Tresser, New universal scenarios for the onset of chaos in Lorenz type flows. Phys. Rev. Lett. **57**, 925–928 (1986)
7. P. Glendinning, The anharmonic route to chaos: kneading theory. Nonlinearity **6**, 349–367 (1993)
8. P. Glendinning, Renormalization for the boundary of chaos in piecewise monotonic maps with a single discontinuity. Nonlinearity **27**, R143–R162 (2014)
9. P. Glendinning, Bifurcation from stable fixed point to N-dimensional attractor in the border collision normal form. Nonlinearity **28**, 3457–3464 (2015)
10. P. Glendinning, Bifurcation from stable fixed point to two-dimensional attractor in the border collision normal form, IMA J. Appl. Math. (2016). doi:10.1093/imamat/hxw001
11. P. Glendinning, Less is More II: An Optimistic View of Piecewise Smooth Bifurcation Theory, this volume (2017)
12. P. Glendinning, Shilnikov Chaos, Filippov Sliding and Boundary Equilibrium Bifurcations (in preparation)
13. J. Milnor, W. Thurston, On iterated maps of the interval, *Dynamical Systems LNM*, vol. 1342 (Springer, Berlin, 1988), pp. 465–563
14. A.B. Nordmark, Universal limit mapping in grazing bifurcations. Phys. Rev. E. **55**, 266–270 (1997)
15. H.E. Nusse, J.A. Yorke, Border collision bifurcations including period two to period three bifurcation for piecewise smooth systems. Phys. D **57**, 39–57 (1992)
16. M. Tsujii, Absolutely continuous invariant measures for expanding piecewise linear maps. Invent. Math. **143**, 349–373 (2001)

Less Is More II: An Optimistic View of Piecewise Smooth Bifurcation Theory

Paul Glendinning

Abstract The analysis of piecewise smooth bifurcations reveals an alarming proliferation of cases as the dimension of phase space increases. Rather than attempt the derivation of exhaustive lists of possibilities, we describe ways of giving less detailed, but possibly more useful, results.

1 Introduction

"Take some more tea", the March Hare said to Alice, very earnestly.

"I've had nothing yet", Alice replied in an offended tone, "so I can't take more".

"You mean you can't take less," said the Hatter: "it's very easy to take more than nothing."
[2, ch. 7].

Mathematicians often aim to produce classification theorems and, normally, these attempt to be as complete as possible. However, as argued in Glendinning [4], the number of bifurcations in piecewise smooth (PWS) systems increases alarmingly with the dimension of the ambient phase space or the complexity of the system, and this may mean that complete descriptions, in the same spirit as would be given for smooth systems, become infeasible and certainly become unwieldy. This creates a problem for mathematicians with a background in smooth bifurcation theory: there are many potentially beautiful problems such as the existence of Shilnikov homoclinic bifurcations with sliding segments in local bifurcations of stationary points of PWS systems (see Glendinning [4]), but if the general result is that for the boundary equilibrium bifurcation in $\mathbb{R}^n$ then the local dynamics can contain analogues of *any* bifurcation of smooth systems in $\mathbb{R}^n$, as may well be the case, then it is unclear how to proceed.

This dilemma suggests that mathematicians should find coarser, but generally useful, statements about the local bifurcation structure of PWS system and provide a

P. Glendinning (✉)
School of Mathematics, University of Manchester,
Oxford Road, Manchester M13 9PL, UK
e-mail: p.a.glendinning@manchester.ac.uk

A. Colombo et al. (eds.), *Extended Abstracts Spring 2016*,
Trends in Mathematics 8, DOI 10.1007/978-3-319-55642-0_14

general framework or set of techniques which researchers interested in applications can use on particular examples. Thus the theoretician might need to rein in his or her natural inclination towards a detailed classification and provide, instead, descriptions that are less complete but easier to follow and interpret. Or again describe some things that *cannot* happen (as so much can). In this paper we give some examples of results that fit into this 'less is more' way of seeing the dynamics of PWS systems.

2 PWS Maps of the Interval

There are a number of results describing the dynamics of PWS maps based on the ideas of Milnor–Thurston [6], which was circulating in preprint form from 1977. However, these results depend on a knowledge of kneading theory, an algebraic version of symbolic dynamics, and this means the proofs may seem abstruse, and a great deal of information is implicit in an algebraic invariant (the kneading invariant) which characterizes the *non-wandering set* of a map. (A point x is wandering if there exists an open neighbourhood U of x such that $f^n(U) \cap U = \emptyset$ for all $n > 0$, and a point is non-wandering if it is not wandering.) A weaker version of their theorems can be proved without recourse to new formalism. This simplified version is an example of the 'less is more' approach: the result is general, but for any example more work would be needed to add greater precision to statements. As is standard in the theory of maps of the interval, there is an issue about the existence of homtervals. These are open intervals J on which $f^n|J$ is a homeomorphism for all $n = 0, 1, 2, \ldots$

Whilst I do not know of a detailed proof of the conjecture below, it seems reasonable that it will follow by a similar argument to that used for Lemma 2 below, but with modifications to take homtervals into account (cf. [5, 6]). The dynamics is described in terms of Markov partitions and Markov graphs. A Markov partition is a union of closed sets that are permuted by the map and hence the images of elements in their complement, (L_i), are either disjoint, $f(L_i) \cap L_j = \emptyset$, or $L_j \subseteq f(L_i)$. This means that a Markov graph can be defined with vertices labelling the connected elements of the complement and a directed edge from i to j if $L_j \subseteq f(L_i)$. Given any (finite or infinite) path allowed by this graph, there exists a point passing through the sets in the order described by the path.

Conjecture 1 *Suppose that $f : I \to I$ is a PWS map with two continuous monotonic branches and a single critical point or point of discontinuity. Then, there exists $0 \le n \le \infty$ such that the nonwandering set can be written as a union $A_n \cup \left(\cup_0^{n-1} T_k\right)$ (disjoint except possibly T_{n-1} and A_n), where dynamics in T_k is determined by a finite Markov graph (possibly zero entropy) and A_n is (up to homtervals) a union of periodic orbits or a union of intervals if $n < \infty$ or a Cantor set if $n = \infty$.*

We will sketch a proof in the case that the map is differentiable and expanding away from the critical point or the point of discontinuity, which will be denoted by c. This is Lemma 2 below. The proof relies on the idea of induced maps and renormalization. If $c \in J$ write $J = J_0 \cup \{c\} \cup J_1$ where $J_0 = J \cap \{x < c\}$ and $J_1 = J \cap \{x > c\}$.

A map f is *renormalizable* if there exists J with $c \in J$ and positive n_0 and n_1 with $n_0 + n_1 > 2$ such that $f^{n_k}|J_k$, $k = 0, 1$, is a homeomorphism and

$$f^{n_0}(J_0) \cup f^{n_1}(J_1) \subseteq J.$$

If f is renormalizable, then the induced map $F : J \to J$ defined by $F(x) = f^{n_k}(x)$ if $x \in J_k$, $k = 0, 1$, is again a map with a single discontinuity or critical point.

Finally, $f : I \to I$ is *transitive* if for all open $J \in I$ there exists n such that $I = \cup_0^n c\ell(f^k(J))$.

Lemma 2 *If $f : I \to I$ with I smallest such interval and $|f'(x)| \geq a > 1$ if $x \neq c$, then either f is renormalizable or f is transitive.*

Where does this get us? If f is transitive then the non-wandering set is I. If f is renormalizable then the components of the set

$$K = \left(\bigcup_{k=0}^{n_0-1} f^k(J_0) \right) \cup \left(\bigcup_{r=0}^{n_1-1} f^r(J_1) \right)$$

are permuted by the map so the complement $I \backslash K$ is a union of closed intervals (possibly trivial or even empty) L_k such that either $f(L_i) \cap L_j = \emptyset$ or $L_j \subseteq f(L_i)$, the condition for a Markov graph. So, the dynamics is divided into the dynamics in the sets L_k which is determined by a finite Markov graph and the dynamics induced by the renormalized map (again a two monotonic branch map) in K.

Sketch of the proof of Lemma 2 Intervals expand under iteration so images of any open interval V must eventually intersect c. Call this image V_0. Then V_0 is divided into two by c and each component will also return for the first time. Either these returns are inside V_0 (so f is renormalizable) or define V_1 to be the union of V_0 and its first returns. Repeat and note that each return is after the same or a shorter number of iterations and hence either f is renormalizable or a larger interval V_2 can be constructed from V_1 and its returns. If f is not renormalizable then, for every interval, the process never stops, the return times tend to a limit, and the sets tend to a limit, V_∞. If the sum of the limiting return times is greater than one then f is renormalizable on V_∞ (a contradiction), otherwise return times are 1 (and this is achieved in finite time) and since I was minimal, $V_\infty = I$ and the map is transitive. □

This is a simple way of describing the dynamics of *all* piecewise monotonic maps with a single discontinuity. It has some detail (finite Markov graphs) but leaves a lot unsaid, so it does not require sophisticated arguments: *less is more*.

3 The Border Collision Normal Form: Young's Theorem

Let $\mathbf{x} = (x_1, x_2)^T$, then the border collision normal form

$$\mathbf{x}_{n+1} = \begin{cases} A_0\mathbf{x}_n + \mathbf{m} & \text{if } (x_1)_n \le 0 \\ A_1\mathbf{x}_n + \mathbf{m} & \text{if } (x_1)_n \ge 0 \end{cases}, \quad \text{with} \quad A_k = \begin{pmatrix} t_k & 1 \\ -d_k & 0 \end{pmatrix}, \quad k = 0, 1,$$

is a piecewise affine map of the plane, and $\mathbf{m} = \mu(1, 0)^T$.

The parameter μ is considered to be the bifurcation parameter and some results for these maps are described in Glendinning [4]. Banerjee–Yorke–Grebogi [1] show that the border collision normal form has parameters with a trapping region, and transverse intersections of stable and unstable manifolds and hence quasi-one-dimensional attractors: this has been called *robust chaos*. Young [7] provided the tools to make these statements more precise. Let $R = [0, 1] \times [0, 1]$ and let $S = \{a_1, \ldots, a_k\} \times [0, 1]$ be a set of vertical switching surfaces with $0 < a_1 < \cdots < a_k < 1$. Then, $f : R \to R$ is a Young map if f is continuous, f and its inverse are C^2 on $R \backslash S$, and $f = (f_1, f_2)^T$ satisfies the following expansion properties (H1)–(H3) on $R \backslash S$:

$$\inf \left\{ \left(\left| \frac{\partial f_1}{\partial x} \right| - \left| \frac{\partial f_1}{\partial y} \right| \right) - \left(\left| \frac{\partial f_2}{\partial x} \right| - \left| \frac{\partial f_2}{\partial y} \right| \right) \right\} \ge 0, \tag{H1}$$

$$\inf \left(\left| \frac{\partial f_1}{\partial x} \right| - \left| \frac{\partial f_1}{\partial y} \right| \right) = u > 1, \tag{H2}$$

$$\sup \left\{ \left(\left| \frac{\partial f_1}{\partial y} \right| + \left| \frac{\partial f_2}{\partial y} \right| \right) \left(\left| \frac{\partial f_1}{\partial x} \right| - \left| \frac{\partial f_1}{\partial y} \right| \right)^{-2} \right\} < 1. \tag{H3}$$

Let $Jac(f)$ denote the Jacobian matrix of f and recall that u is defined in (H2).

Theorem 3 (Young [7]) *If f is a Young map, $|Jac(f)| < 1$ for $x \in R \backslash S$, and there exists $N \ge 1$ s.t. $u^N > 2$ and if $N > 1$ then $f^k(S) \cap S = \emptyset$, $1 \le k < N$, then f has an invariant probability measure that has 'absolutely continuous conditional measures on unstable manifolds'.*

The technical conclusion in quotation marks means that the invariant measure projects nicely onto one-dimensional horizontal lines.

Remark 4 The theorem holds for C^2 functions so, provided perturbations of the normal form are C^2 in phase space and C^1 close in parameters, then conditions for the theorem will still hold (if they hold in the first place) and so behaviour is robust.

Remark 5 The theorem, as actually stated in Young [7], has $u^N > 2$ and $f^k(S) \cap S = \emptyset$, $1 \le k \le N$. However, no extra conditions on images of S are required if $N = 1$ and if $N > 1$ then the requirement is that f^N has similar geometry on vertical strips,

which only requires non-intersection up to the $(N-1)$-th iterate, so we are confident that Theorem 3 is what was intended in Glendinning [3].

The criteria for the theorem to hold are easy to verify numerically making it possible to determine regions on which Young's Theorem holds and compare these with theoretical bounds in Banerjee–Yorke–Grebogi [1]; see Glendinning [3] for details. The point about this result is that one could be tempted to provide further details such as the Hausdorff dimension of the support of the measure (the attractor), but that the statement that there is an attractor with an invariant measure having a nice one-dimensional projection gives the essential picture without overcomplicating the story: *less is more*.

4 Conclusion

The two results described here meet what I consider to be the 'less is more' criterion. They hold for a good range of models, they are informative, but there is much extra detail that they do not provide and they do not attempt a complete topological classifications. Given the hazards created by the proliferation of bifurcations in PWS systems outlined in Glendinning [4], we consider the existence of these results a cause for optimism, and they provide a template for the expression of further descriptions of PWS dynamics.

Acknowledgements I am grateful to Mike Jeffrey, Rachel Kuske and David Simpson for conversations that helped crystallize these ideas, and to the Simons Foundation for support at the CRM, Barcelona.

References

1. S. Banerjee, J.A. Yorke, C. Grebogi, Robust chaos. Phys. Rev. Lett. **80**, 3049–3052 (1998)
2. L. Carroll, *Alice's Adventures in Wonderland* (Macmillan, New York, 1865)
3. P. Glendinning, Invariant measures of the border collision normal form, preprint (2011)
4. P. Glendinning, Less is more I: a pessimistic view of piecewise smooth bifurcation theory, this volume (2016)
5. L. Jonker, D.A. Rand, Bifurcations in one-dimension. I. The non-wandering set. Invent. Math. **62**, 347–365 (1981)
6. J. Milnor, W. Thurston, On iterated maps of the interval, *Dynamical Systems*, vol. 1342, LNM (Springer, Berlin, 1988), pp. 465–563
7. L.S. Young, Bowen-ruelle measures for certain piecewise hyperbolic maps. Trans. AMS **287**, 41–48 (1985)

On Semi-local Structural Stability of Filippov Systems

Otávio M.L. Gomide, Marco A. Teixeira, and Ricardo M. Martins

Abstract We introduce the notion of semi-local structural stability which detects if a nonsmooth system is structurally stable around the switching manifold. More specifically, we characterize the semi-local structurally stable systems in a class of Filippov systems on a compact 3-manifold which has a simply connected switching manifold.

1 Basic Concepts

Let M be a compact oriented 3-manifold and let $f: M \to \mathbb{R}$ be a smooth function having 0 as a regular value, therefore $\Sigma = f^{-1}(0)$ is an embedded codimension 1 submanifold of M. Assume that Σ is connected and simply connected.

Consider $M^+ = f^{-1}([0, +\infty))$ and $M^- = f^{-1}((-\infty, 0])$. We define a *nonsmooth vector field* $Z = (X, Y)$ by:

$$Z(p) = \begin{cases} X(p), & \text{if } p \in M^+, \\ Y(p), & \text{if } p \in M^-, \end{cases} \tag{1}$$

where X and Y are vector fields of class $\mathcal{C}^r$ defined on $\overline{M^+}$ and $\overline{M^-}$, respectively. Denote by $\Omega^r(M)$ (or simply Ω^r) the set of nonsmooth vector fields with discontinuity manifold Σ.

O.M.L. Gomide (✉) · M.A. Teixeira · R.M. Martins
Department of Mathematics, IMECC, Unicamp, Campinas, SP 13083-970, Brazil
e-mail: otaviomleandro@hotmail.com

M.A. Teixeira
e-mail: teixeira@ime.unicamp.br

R.M. Martins
e-mail: rmiranda@ime.unicamp.br

A. Colombo et al. (eds.), *Extended Abstracts Spring 2016*,
Trends in Mathematics 8, DOI 10.1007/978-3-319-55642-0_15

If $\chi^r(M) = \chi^r$ is the set of smooth vector fields on M equipped with the $\mathcal{C}^r$-topology, then we consider $\Omega^r = \chi^r \times \chi^r$ endowed with the product topology.

Definition 1 The *Lie derivative* of f in the direction of the vector field $X \in \chi^r$ at $p \in \Sigma$ is defined as $Xf(p) = X(p) \cdot \nabla f(p)$, and the successive Lie derivatives are given by $X^n f(p) = X(p) \cdot \nabla X^{n-1} f(p)$. The *tangency set* of X with Σ is given by $S_X = \{p \in \Sigma;\ Xf(p) = 0 \text{ and } X(p) \neq 0\}$; and a point $p \in S_X$ is said to be a *tangential singularity*. Denote $S_Z = S_X \cup S_Y$.

Filippov's convention is used to define a local solution of $Z = (X, Y)$ (see Guardia–Seara–Teixeira [1]) and we denote $\Sigma_F = \Sigma^s \cup \Sigma^e$. We recall that the dynamics of Z in Σ_F is given by the *sliding vector field*

$$F_Z(p) = \frac{1}{Yf(p) - Xf(p)} \left(Yf(p)X(p) - Xf(p)Y(p)\right). \tag{2}$$

Now some essential types of tangential singularities are presented.

Definition 2 A point $p \in \Sigma$ is said to be a *fold* point of $X \in \chi^r(\overline{M^+})$ if $Xf(p) = 0$ and $X^2 f(p) \neq 0$. If $X^2 f(p) > 0$ (resp., $X^2 f(p) < 0$), then p is a *visible fold* (resp., *invisible fold*).

Remark 3 If $X \in \chi^r(\overline{M^-})$, the visibility condition is switched.

Definition 4 A point $p \in \Sigma$ is said to be a *stable cusp*, or simply a cusp, of X if $Xf(p) = X^2 f(p) = 0$, $X^3 f(p) \neq 0$ and $\{df(p),\ dXf(p),\ dX^2 f(p)\}$ is a linearly independent set.

Remark 5 The cusp points are isolated points located at the extremes of the curves of fold points. By compactness, it follows that S_X has at most a finite number of cusps.

2 Typical Tangency Sets

In this section, the generic form of the tangency set S_Z of a nonsmooth vector field $Z = (X, Y)$ is established.

Definition 6 A point $p \in S_Z$ is said to be a tangential singularity of type:

(i) *fold-regular* if either p is a fold point of X and regular of Y or p is a fold point of Y and regular of X;
(ii) *cusp-regular* if either p is a stable cusp point of X and regular of Y or p is a stable cusp point of Y and regular of X;
(iii) *two-fold* (or *fold-fold*) if $Xf(p) = Yf(p) = 0$ and $X^2 f(p) \neq 0 \neq Y^2 f(p)$.

Definition 7 A vector field $X \in \chi^r$ is said to be *simple* if either $S_X = \emptyset$ or S_X is composed by fold points of X with at most a finite number of cusp points. If $Z = (X, Y) \in \Omega^r$ is such that X and Y are simple and $S_X \cap S_Y = \emptyset$, then Z is said to be *simple*. Denote the set of simple nonsmooth vector fields by Ω^r_S.

Notice that S_Z is composed by fold-regular and cusp-regular points when Z is simple.

Proposition 8 *If $X \in \chi^r(M)$ is simple and $S_X \neq \emptyset$, then there exists $n \in \mathbb{N}$ such that $S_X = \sqcup_{i=1}^n S_X^i$, where each S_X^i is diffeomorphic to the unit circle $\mathbb{S}^1$.*

This result follows from the fact that 0 is a regular value of the Lie derivative $Xf : \Sigma \to \mathbb{R}$, under its hypotheses.

Proposition 9 *Let $X \in \chi^r(M)$ be a simple vector field such that $S_X \neq \emptyset$, and let C be a connected component of S_X. Then, there exist neighborhoods $\mathcal{V}$ of X in χ^r and V of C in Σ such that, for each $Y \in \mathcal{V}$, S_Y has a unique connected component in V.*

Proposition 10 *Let $X \in \chi^r(M)$ be a simple vector field such that $S_X \neq \emptyset$, then there exists a neighborhood $\mathcal{V}$ of X in $\chi^r(M)$ such that, for every $Y \in \mathcal{V}$, $S_Y \neq \emptyset$ has the same number of connected components of S_X.*

Corollary 11 *Ω^r_S is an open set in Ω^r.*

Remark 12 Ω^r_S is not dense in Ω^r since a two-fold point p, where $S_X \pitchfork S_Y$ at p, is an open property.

Definition 13 A nonsmooth vector field $Z_0 = (X_0, Y_0) \in \Omega^r$ is said to be *S-persistent* if there exists a neighborhood $\mathcal{V}$ of Z_0 in Ω^r such that, for every $Z \in \mathcal{V}$, there exists a homeomorphism $\varphi : S_{Z_0} \to S_Z$ preserving the topological type of tangential singularities. Denote by Ω^r_P the set of S-persistent nonsmooth vector fields.

It follows from the definition and the above results that $\Omega^r_S \subset \Omega^r_P$.

Proposition 14 *$Z = (X, Y) \in \Omega^r_P$ if and only if both X and Y are simple, and every $p \in S_X \cap S_Y$ is a two-fold point and $S_X \pitchfork S_Y$ at p.*

Theorem 15 *Ω^r_P is a residual set in Ω^r, i.e., it is the complement of a countable union of sets with empty interior closure.*

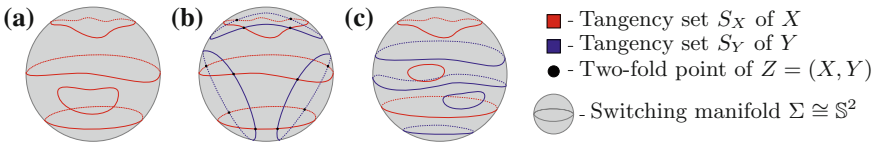

Fig. 1 (**a**) The general form of the tangency set of a simple vector field $X \in \chi^r$; (**b**) a typical tangency set of $Z \in \Omega^r_P$; (**c**) the general form of a typical tangency set for a simple nonsmooth vector field $Z \in \Omega^r_S$

Sketch of the proof It follows from Proposition 14, and Vishik [4, Theorem 2].

Finally, the definition of typical tangency set is established; see Fig. 1.

Definition 16 A nonsmooth vector field $Z \in \Omega^r$ has a *typical tangency set* if $Z \in \Omega^r_P$.

3 Semi-local Structural Stability

Now, the previous set Ω^r_P has to be (generically) restricted in order to get the persistence of the phase portrait of the vector field around the whole switching manifold.

3.1 Σ*-Block Stability*

Now, a formal language to deal with the problem it is introduced.

Definition 17 A subset $U \neq \emptyset$ of Σ is said to be a Σ*-block* of $Z \in \Omega^r$ if U is a connected component of $\Sigma^s \cup \Sigma^e$. The empty set $U = \emptyset$ is said to be a *(trivial)* Σ*-block* if $\Sigma^c = \Sigma$.

Now, a concept of structural stability for Σ-blocks is established. We remark that the term semi-local is used to refer a phenomenon occurring in a neighborhood of a compact set. It is similar to the concept of local behavior, by using a compact set instead of a point.

Definition 18 Let $Z_0 = (X_0, Y_0) \in \Omega^r$ and assume that it has a Σ-block U_0. If $U_0 \neq \emptyset$, then Z_0 is U_0*-stable* if there exists a neighborhood V of $\overline{U_0}$ (the closure of U_0 in Σ) in Σ and a neighborhood $\mathcal{V}$ of Z_0 in Ω^r such that, for every $Z \in \mathcal{V}$,

(i) Z has a Σ-block U such that $\overline{U} \subset V$;
(ii) V is minimal, i.e., there is a unique Σ-block in V;
(iii) there exist neighborhoods V_{Z_0} and W_{Z_0} of $\overline{U_0}$ and $\overline{U}$ in M, respectively, and a Σ-invariant order-preserving homeomorphism $h\colon V_{Z_0} \to W_{Z_0}$ which carries orbits of Z_0 onto orbits of Z.

If $U_0 = \emptyset$, then Z is U_0-stable if there exist neighborhoods V_{Z_0} and W_{Z_0} of Σ in M, and a Σ-invariant order-preserving homeomorphism $h\colon V_{Z_0} \to W_{Z_0}$ which carries orbits of Z_0 onto orbits of Z.

Remark 19 Notice that the concept of U_0-stability regards a small neighborhood of U_0 in M (not in Σ). Hence, it comprehends the sliding dynamics of $Z_0 = (X_0, Y_0)$ on U_0 and the orbits of X_0 and Y_0 which are sufficiently close of U_0.

Definition 20 We say that $Z \in \Omega^r$ is Σ-*stable* (or *semi-local structurally stable*) if every Σ-block U of Z is U-stable.

Notice that, if Z is Σ-stable then $Z \in \Omega^r_P$. The converse is not true, since two-fold points are not generically locally structurally stable (see Teixeira [3]).

3.2 The Σ-Stable Simple Nonsmooth Vector Fields

Now, Σ-stable nonsmooth vector fields in Ω^r_S are characterized.

Definition 21 Define $\Omega^r_0(S) \subset \Omega^r$ as the set of nonsmooth vector fields Z such that:

(i) Z is simple;
(ii) $F_Z|_{\overline{\Sigma_F}}$ has a finite number of hyperbolic pseudo-equilibria, which are contained in $\text{int}(\overline{\Sigma_F})$;
(iii) $F_Z|_{\overline{\Sigma_F}}$ has a finite number of hyperbolic pseudo-periodic orbits, which are contained in $\text{int}(\overline{\Sigma_F})$;
(iv) F_Z does not present any saddle connection;
(v) every orbit of F_Z has at most a unique tangency point with S_Z;
(vi) each saddle separatrix of F_Z is transversal to S_Z.

Theorem 22 *Assume Z is simple. Then, $Z \in \Omega^r_0(S)$ if and only if Z is Σ-stable.*

Sketch of the proof If some condition of $\Omega^r_0(S)$ is not satisfied then Z is not Σ-stable since a perturbation which changes the behavior of Z can be considered.

The main idea to prove the converse is to construct a neighborhood $\mathcal{V}$ of Z using the tools developed in the previous sections. Then, Peixoto's Theorem is used to provide homeomorphisms between the Σ-blocks in Σ; see Peixoto–Peixoto [2].

Finally, we can extend each homeomorphism into a neighborhood of the Σ-block in M (around the Σ-block). Therefore, each Σ-block is stable, which means that Z is Σ-stable.

The following result follows directly from Peixoto–Peixoto [2] and the characterization of $\Omega^r_0(S)$.

Theorem 23 *The set $\Omega^r_0(S)$ is an open dense set in Ω^r_S.*

References

1. M. Guardia, T.M. Seara, M.A. Teixeira, Generic bifurcations of low codimension of planar Filippov systems. J. Differ. Equ. **250**, 1967–2023 (2011)
2. M.C. Peixoto, M.M. Peixoto, Structural stability in the plane with enlarged boundary conditions. An. Acad. Bras. Ciencias **31** (1959)
3. M.A. Teixeira, Stability conditions for discontinuous vector fields. J. Differ. Equ. **88**(1), 15–29 (1990)
4. S.M. Vishik, Vector fields near the boundary of a manifold. Vestnik Moskovskogo Universiteta Mathematika **27**(1), 21–28 (1972)

Nonlinear Estimation of Synaptic Conductances via Piecewise Linear Systems

Antoni Guillamon, Rafel Prohens, Antonio E. Teruel, and Catalina Vich

Abstract We use the piecewise linear McKean model to present a proof-of-concept to address the estimation of synaptic conductances when a neuron is spiking. Using standard techniques of non-smooth dynamical systems, we obtain an approximation of the period in terms of the parameters of the system which allows to estimate the steady synaptic conductance of the spiking neuron. The method gives also fairly good estimations when the synaptic conductances vary slowly in time.

1 Introduction

The problem addressed in this manuscript is framed into the challenge of unveiling the functional connectivity in the brain; that is, to obtain information about strength and timing of the input currents (mediated by *synapses*) that a single neuron (the *post-synaptic* cell) receives from others (the *pre-synaptic* ones). In particular, we aim at disentangling the arrangement of excitation versus inhibition impinging on the cell. We will focus on the estimation of the conductances of these currents, a quantity which is not directly measurable but needs to be extracted from experimentally

A. Guillamon (✉)
Departament de Matemàtiques-EPSEB, Universitat Politècnica de Catalunya, Barcelona, Spain
e-mail: antoni.guillamon@upc.edu

R. Prohens · A.E. Teruel · C. Vich
Departament de Matemàtiques i Informàtica, Universitat de les Illes Balears, Palma, Spain
e-mail: rafel.prohens@uib.cat

A.E. Teruel
e-mail: antonioe.teruel@uib.es

C. Vich
e-mail: catalina.vich@uib.es

A. Colombo et al. (eds.), *Extended Abstracts Spring 2016*,
Trends in Mathematics 8, DOI 10.1007/978-3-319-55642-0_16

accessible data like the membrane potential of the neuron. For a review of the relevant concepts in neuroscience, we refer the reader to the book Ermentrout–Terman [4], and the introduction in Vich–Guillamon [8] for a quick survey on the problem of estimation of conductances. A major hindrance in this problem is the estimation when ionic currents are active, specially in spiking regimes, where ionic conductances are much higher than synaptic ones; see Guillamon–McLaughlin–Rinzel [6]. No methods are yet known to estimate synaptic conductances in this paradigm. From a mathematical point of view, this is indeed an inverse problem consisting of estimating some parameters from time courses of one variable of the associated dynamical system. In this work, we aim at giving a theoretical proof-of-concept by considering a simplified model of neuronal activity, namely a non-smooth caricature of the FitzHugh–Nagumo model (see Coombes–Thul–Wedgwood [3]), which allows a very sharp approximation of the nonlinear $f - I$ curve thanks to special properties of piecewise linear systems. Moreover, the same idea could be applied to smooth systems with approximate expressions of the corresponding $f - I$ curves. The model we consider is a version of the McKean model as described in Coombes [2], where the synaptic current, $I_{syn}(v)$, has been considered apart from the rest of external currents, I. That is, we consider the system

$$\begin{cases} C\dot{v} = f(v) - w - w_0 + I - I_{syn}(v), \\ \dot{w} = v - \gamma w - v_0, \end{cases} \tag{1}$$

where $I_{syn}(v) = g_{syn}(v - v_{syn})$ and $f(v)$ is defined in a continuous but non-differentiable way according to three zones of the phase space, left, middle and right: $f(v) = f_L(v) := -v$ if $v < a/2$, $f(v) = f_M(v) := v - a$ if $a/2 \leq v \leq (1 + a)/2$, and $f(v) = f_R(v) := 1 - v$ if $v > (1 + a)/2$. For the significance of the parameters involved in the model, see Coombes [2]. Here, we focus on the most relevant parameters for this work. We consider to have a single source of synaptic conductances, which is modeled by means of v_{syn}, the synaptic reversal potential, and $g_{syn} > 0$, the synaptic conductance. The ionic currents are modeled through the expression $f(v) - w - w_0$ in the first equation of (1), designed to mimic the qualitative behaviour of the N-shaped v-nullcline of more biophysically realistic models. Since C, the parameter related to cell membrane capacitance, is assumed to be small and bounded, $0 < C \ll 0.1$, system (1) is then a slow-fast dynamical system, where v is the fast variable and w is the slow one.

In Abbott [1] and Tonnelier–Gerstner [7], the authors show the existence of two values $I_1 < I_2$ for the applied current for which system (1) with $I_{syn}(v) = 0$ exhibits a periodic orbit, which is unique, if and only if $I_1 < I < I_2$. In Coombes [2], approximations of the period T were obtained, mainly based on the slow-fast nature of the system. More recently, in Fernández-García–Desroches–Krupa–Clément [5], the authors provide an approximate expression for the period T by taking advantage of the slow invariant manifolds for $C \ll 1$. We show that the previous scenario persists for $I_{syn}(v) \neq 0$ and that the interval where periodic orbits exist depends also on g_{syn} as well as the period, $T = T(C, I, g_{syn})$. We present a new approximation of

$T, \hat{T}$, which includes this dependence on g_{syn} and, moreover, improves the existing approximations. The key points are two refinements: the consideration of the flight time in the central region, and a special projection on the slow manifold.

In the range of applied currents in which the neuron is spiking, we have found numerical evidence that the period of this oscillation has a nonlinear but monotonic dependence on g_{syn}. Hence, as a consequence of this monotonicity, by knowing $\hat{T}$ and the applied current I (i.e., knowing the so-called $f - I$ curve), we can compute g_{syn} by solving numerically a non-linear equation with a unique solution, and thus we are able to estimate the steady synaptic conductance of the neuron, which is the goal of this work.

2 Main Result

It is easy to check that the system (1) with $f(v) = f_L(v)$ for all v has a unique fixed point, p_L; similarly, considering $f(v) = f_M(v)$ and $f(v) = f_R(v)$ respectively, we define p_M and p_R. When a limit cycle exists, both p_L a p_R, which have the same Jacobian matrix, lie on the middle zone and so, they are only *virtual equilibria*; however, their eigenvalues have influence in the dynamics. We denote by $\lambda_{q/s,L/M}$ the eigenvalues of the equilibrium points p_L and p_M of system (1), where q and s stand for "fast" (eigenvalue with the biggest modulus) and "slow", respectively. To ensure the existence of a periodic orbit, we need to consider the next set of hypotheses:

$$g_{syn} > 1 - \gamma^{-1}, \qquad |g_{syn} + C\gamma| < 1, \qquad 0 < C \leq C^*, \quad \text{and} \quad I_1 < I < I_2, \quad \text{(H)}$$

where

$$I_1 = \left(\frac{a}{2} - v_{syn}\right) g_{syn} + \frac{(\gamma+1)a - 2v_0 + 2\gamma w_0}{2\gamma}, \quad I_2 = I_1 + \frac{1}{2} g_{syn} + \frac{1-\gamma}{2\gamma}. \tag{2}$$

With these definitions, we can state the following result.

Theorem 1 *Given system* (1) *under hypothesis (H), for a sufficiently small* $C > 0$*, the period of the unique periodic orbit of the system can be written as* $T = \hat{T} + O(C)$*, with*

$$\hat{T} = \sum_{j=1}^{2} \frac{1}{\lambda_{s,L}} \ln\left(\left|\frac{\gamma(I - I_j)B_l}{\gamma(I - I_j)B_l + (-1)^j K_l}\right|\right) + \frac{1}{\lambda_{q,M}} \ln\left(\left|\frac{\gamma(I - I_j)B_m + K_m}{\gamma(I - I_j)B_m + K_{m,j}}\right|\right),$$

where

$$B_m = (\gamma + \lambda_{q,M})\left((G_{syn}+1)(\lambda_{s,L}-\lambda_{s,M}) - \gamma(\lambda_{s,L}+\lambda_{s,M}) - 2\lambda_{s,L}\lambda_{s,M}\right),$$
$$B_l = \lambda_{q,L} - \lambda_{s,L},$$
$$K_l = \frac{1}{2}(\gamma + \lambda_{q,L})(G_{syn} + \gamma + 2\lambda_{s,L} + 1),$$
$$K_m = \frac{1}{2}(\gamma + \lambda_{s,M})(G_{syn} - \gamma + 1)\left((G_{syn}+1)(\lambda_{s,L}-\lambda_{q,M}) - \gamma(\lambda_{s,L}+\lambda_{q,M}) - 2\lambda_{s,L}\lambda_{q,M}\right),$$
$$K_{m,1} = \frac{1}{2}(\gamma + \lambda_{q,M})(G_{syn} - \gamma + 1)\left((G_{syn}+1)(\lambda_{s,L}-\lambda_{s,M}) - \gamma(\lambda_{s,L}+\lambda_{s,M}) - 2\lambda_{s,L}\lambda_{s,M}\right),$$
$$K_{m,2} = \frac{1}{2}(\lambda_{q,M} - \lambda_{s,M})(\gamma + \lambda_{q,M})(G_{syn} - \gamma + 1)(G_{syn} + \gamma + 2\lambda_{s,L} + 1),$$
$$G_{syn} = g_{syn}\gamma.$$

Sketch of the proof The period is obtained through straightforward computations which are based on the local linearity of the vector field and the existence of two points, on the switching line, belonging to the periodic orbit. These two points are approximated as the intersection of the slow manifold with the switching line, since the periodic orbit is assumed to pass exponentially close of the slow manifold. □

3 Application to the Estimation of Conductances

All our numerical tests show evidences that $\hat{T}$ is monotonous with respect to g_{syn} in the spiking region $I \in (I_1, I_2)$; see (2). We have not been able to prove this property yet, but it works for practical purposes and allows us to compute good estimations of slowly-varying synaptic conductances in spiking regimes. It is quite obvious that forcing the system (1) with a steady conductance, the system will exhibit a periodic behaviour of period T and, therefore, solving the equation $\hat{T}(C, I, g_{syn}) = T$, we will recover the input synaptic conductance with high accuracy. The challenge, however, is to know whether the conductances can be well estimated when they fluctuate. To test it, we have forced the system (1) with prescribed conductance traces, $g_{syn}(t)$, and then proceed as follows:

(i) We extract the interspike intervals (distances from maxima) from the resulting voltage trace, thus obtaining a sequence of fluctuating periods $\{T_i\}_{i=1}^{N}$, where $N+1$ is the number of spikes in the simulation.
(ii) For each $i = 1, \ldots, N$, we have solved (numerically) the equation $\hat{T}(C, I, g_{syn}) = T_i$ and choose the positive solution $g_{syn,i}$ satisfying $I_1(g_{syn,i}) < I < I_2(g_{syn,i})$ to ensure that corresponds to a periodic orbit.

In Fig. 1, we show estimations obtained from three different prescribed inputs: a sinusoidal drive, an oscillatory drive with two frequencies, and a stereotypical synaptic input to a single cell in visual cortex (units scaled to match (1)). We observe fairly good estimations of synaptic conductances (see panels (**a**), (**b**), (**d**) and (**e**) in Fig. 1). Comparing panels (**a**) and (**b**), we observe that, including a higher frequency in the prescribed input, the estimations impoverish. In general, frequencies higher than the sampling frequency are difficult to estimate. However, the reconstructed voltage

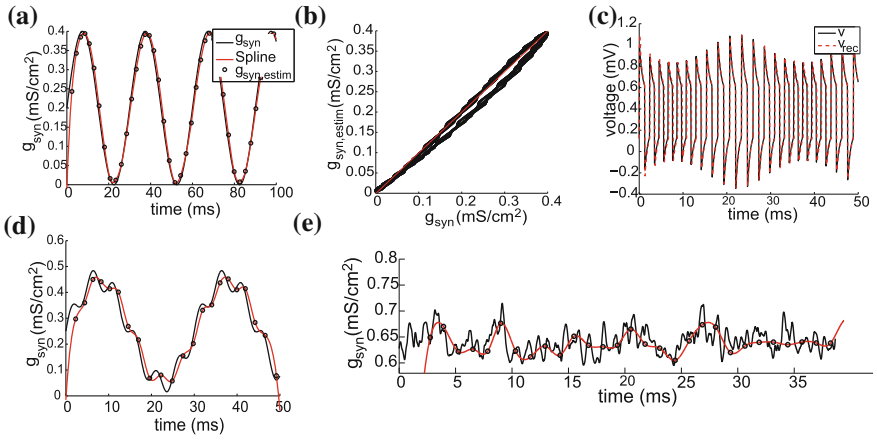

Fig. 1 Estimation of synaptic conductances for different inputs. (**a, d, e**) estimations of the time course of g_{syn} when the neuron's synaptic input is a sinusoidal drive, a two-frequency oscillatory drive and a conductance trace taken from a realistic model, respectively; the time courses of prescribed conductances appear in *black*, *open circles* indicate the estimates obtained with our algorithm and the spline interpolations of these estimates are plotted in *red*; (**b**) estimated values of g_{syn} against the prescribed values for the sinusoidal drive; (**c**) voltage trace using the prescribed conductances for the sinusoidal drive (*black*) compared to the voltage trace reconstructed using the estimated conductances (*red*)

using the estimated conductance (see panel (**c**)) exhibits a good agreement in both cases (only sinusoidal drive is shown). Notice that when the prescribed conductances are taken from a realistic model of V1 (see panel (**e**)), the estimation captures the overall conductance profile but does not match at a smaller scale. In realistic inputs, the conductances' time-scale is variable, being very short in some moments. Thus, we can only get a good estimation on average. A further improvement of our estimation method will consist of introducing more Poincaré sections to estimate flight times in shorter intervals (i.e., refining the sampling).

Acknowledgements This work is partially supported by the Spanish Ministry of Economy and Competitiveness through project MTM2015-71509-C2-2-R (AG), by the MCYT/FEDER grant number MTM2014-54275-P (RP, AT and CV) and by the Government of Catalonia under grant 2014-SGR–504 (AG).

References

1. L.F. Abbott, A network of oscillators. J. Phys. A: Math General **23**(16), 3835 (1990)
2. S. Coombes, Neuronal networks with gap junctions: a study of piecewise linear planar neuron models. SIAM J. Appl. Dyn. Syst. **7**(3), 1101–1129 (2008)
3. S. Coombes, R. Thul, K.C.A. Wedgwood, Nonsmooth dynamics in spiking neuron models. Phys. D **241**(22), 2042–2057 (2012)

4. G.B. Ermentrout, D.H. Terman, *Mathematical Foundations of Neuroscience* (Springer, New York, 2010)
5. S. Fernández-García, M. Desroches, M. Krupa, F. Clément, A multiple time scale coupling of piecewise linear oscillators. Application to a neuroendocrine system. SIAM J. Appl. Dyn. Syst. **14**, 643–673 (2015)
6. A. Guillamon, D.W. McLaughlin, J. Rinzel, Estimation of synaptic conductances. J. Physiol.-Paris **100**(1–3), 31–42 (2006)
7. A. Tonnelier, W. Gerstner, Piecewise linear differential equations and integrate-and-fire neurons: insights from two-dimensional membrane models. Phys. Rev. E **67**, 021908 (2003)
8. C. Vich, A. Guillamon, Dissecting estimation of conductances in subthreshold regimes. J. Comput. Neurosci. **39**(3), 271–287 (2015)

Integral Curves of a Vector Field with a Fractal Discontinuity

Jonathan Hahn and Mike R. Jeffrey

Abstract Nonsmooth systems are typically studied with smooth or piecewise-smooth boundaries between smooth vector fields, especially with linear or hyperplanar boundaries. What happens when there is a boundary that is not as simple, for example a fractal? Can a solution to such a system slide or "chatter" along this boundary? It turns out that the dynamics is rather fascinating, and yet contained within A.F. Filippov's theory (as promised in Utkin, Comments for the continuation method by A.F. Filippov for discontinuous systems, parts I and II, [2] from this volume).

As motivation, take a simple two-dimensional system with a discontinuity boundary formed of the Koch curve of height ε, for small ε. First consider the vector fields pointing horizontally above the surface and vertically below; see Fig. 1.

The boundary of the Koch curve has infinite length, and indeed between any two points on the curve the length is infinite. However, the time spend on smaller and smaller segments of the surface is ever decreasing. To find a solution to the problem

$$(\dot{x},\,\dot{y}) = \begin{cases} (\beta, 0) \text{ if } h > 0, \\ (0, 1) \text{ if } h < 0, \end{cases}$$

for some β from, say, an initial condition at the left extreme of the curve as shown, requires a recursive calculation.

The solution can only move up and to the right, via either vector field (with the vector field so oriented, sliding does not occur) along the curve. This implies that

J. Hahn (✉)
School of Mathematics, University of Minnesota, Minneapolis, MN 55455, USA
e-mail: hahnx240@math.umn.edu

M.R. Jeffrey
Department of Engineering Mathematics, University of Bristol,
Woodland Road, Bristol BS8 1UB, UK
e-mail: mike.jeffrey@bristol.ac.uk

A. Colombo et al. (eds.), *Extended Abstracts Spring 2016*,
Trends in Mathematics 8, DOI 10.1007/978-3-319-55642-0_17

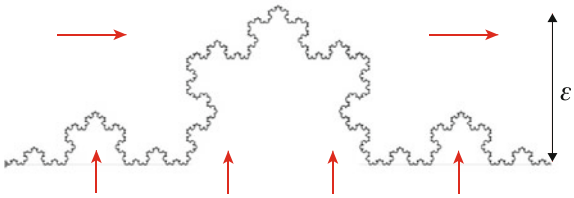

Fig. 1 The two vector fields separated by the Koch snowflake fractal boundary

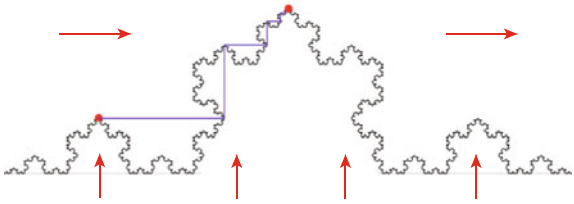

Fig. 2 The solution between the largest peak and second largest peak (*dotted*), iteratively moving *right* and *upward*

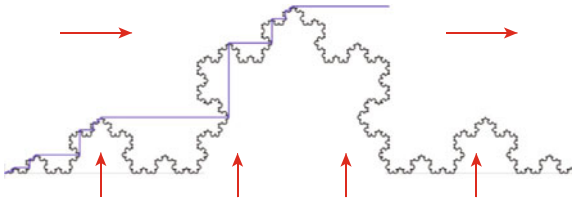

Fig. 3 The full solution with initial condition at the *left* extreme of the curve

the solution eventually reaches the highest peak of the switching surface. Having travelled only horizontally or vertically, the total distance travelled must be $1/2 + \sqrt{3}/3$. A similar argument can be made to show the solution must reach the smaller peak shown in Fig. 2. From that peak, the solution will move right until it reaches the fractal boundary again, and then upward until it again hits the fractal boundary shown below. From there, the fractal is a copy of the previous step, so we can recursively iterate this path, scaling by $1/3$ each time, until it reaches the largest peak.

The path through the first third of the path is a replica of the path we just drew, since the fractal contains a scaled copy of itself. Recursively filling in this path we can generate the full integral curve, with a total length of $1/2 + \sqrt{3}/3$. The integral curve is itself a fractal, but one of finite length; see Fig. 3.

What then happens if both vector fields impinge on the switching surface, e.g.,

$$(\dot{x}, \dot{y}) = \begin{cases} (\beta, -\beta) & \text{if } y > 0, \\ (0, 1) & \text{if } y < 0, \end{cases} \tag{1}$$

for $\beta > 0$? The motion is sketched approximately in Fig. 4.

Whatever form the motion takes, denoting the upper and lower vector fields as (f^+, g^+) and (f^-, g^-), the speed of travel along the x-direction must be

$$\dot{x} = \lambda f^+ + (1 - \lambda) f^-,$$

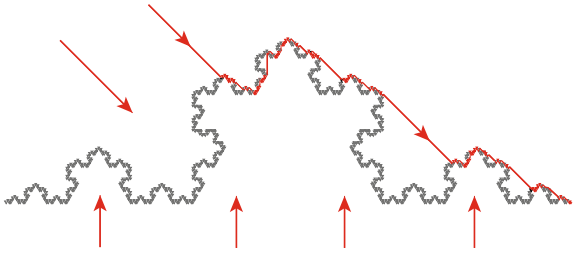

Fig. 4 Two vector field covering on a Koch curve switching surface, and an integral solution

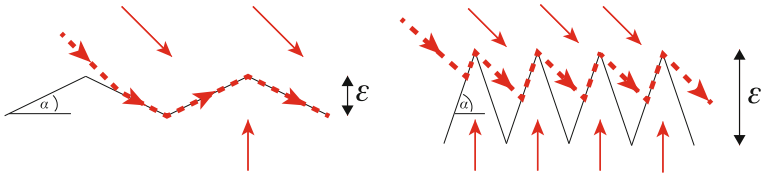

Fig. 5 Motion along a sawtooth switching surface if shallower (*left*) than the *upper* vector field, or steeper (*right*) so that stick-slip occurs

where the motion consists only of a proportion of time λ in f^+ and $1-\lambda$ in f^-. Even if the motion consists of a proportion of time $\mu^\pm$ in $f^\pm$, and the remaining proportion of time $1-\mu^+-\mu^-$ sliding along the surface with horizontal speed f^s, then

$$\dot{x} = \mu^+ f^+ + \mu^- f^- + (1-\mu^+-\mu^-) f^s$$

but, since $f^s = \lambda f^+ + (1-\lambda) f^-$ (by Filippov's method [1]),

$$\dot{x} = \mu^+ f^+ + \mu^- f^- + (1-\mu^+-\mu^-)\{\lambda f^+ + (1-\lambda) f^-\} = \nu f^+ + (1-\nu) f^-,$$

where $\nu = \mu^+ + (1-\mu^+-\mu^-)$. Solving for a value of ν that gives motion along the switching surface, approximating the average vertical motion as $\Delta y = \mathcal{O}(\varepsilon) \approx 0$, we find $\nu = g^-/(g^- - g^+)$ hence $\dot{x} = (g^- f^+ - g^+ f^-)/(g^- - g^+)$, in either case (i.e., with or without actual sliding along the surface), consistent with ideal Filippov sliding on $y = 0$.

A simple example will establish the principle behind this. Take (1), where $h = 0$ is some complex threshold. Let us consider first a basic piecewise linear surface, letting the switching surface be comprised of a sawtooth of angle α. As depicted in the Fig. 5, depending on whether $\alpha < \pi/4$ or $\alpha > \pi/4$, solutions slide along the sawtooth once they impact it, or slide and detach repeatedly.

For $\alpha < \pi/4$, the vector fields are always pointing into the surface, so sliding will occur everywhere. The sawtooth inclines have normal vectors $(\pm \sin\alpha, \cos\alpha)$, so the sliding condition for the vector fields above is

$$\begin{pmatrix} \pm\sin\alpha \\ \cos\alpha \end{pmatrix} \cdot \left\{ \lambda \begin{pmatrix} \beta \\ -\beta \end{pmatrix} + (1-\lambda) \begin{pmatrix} 0 \\ 1 \end{pmatrix} \right\} \quad \Longrightarrow \quad \lambda = \frac{\beta^{-1}}{1+\beta^{-1} \mp \tan\alpha},$$

and the average speed over the two inclines is

$$\langle \dot{x} \rangle = \frac{2}{\dot{x}_+^{-1} + \dot{x}_-^{-1}} = \frac{2}{2(1+\beta^{-1})} = \frac{1}{1+\beta^{-1}} \, .$$

For $\alpha > \pi/4$, firstly, if the distance between peaks is 1, and the distance travelled in the upper vector field before hitting the next incline is μ, then $\tan\alpha = \mu/(1-\mu)$, hence $\mu = 1/(1+\cot\alpha)$. Then the speed, averaging over motion through the upper vector field and sliding on the upward incline (using the sliding vector field above) is

$$\begin{aligned} \langle \dot{x} \rangle &= \frac{1}{\frac{\mu}{\dot{x}_+} + \frac{1-\mu}{\dot{x}_-}} = \frac{1}{\mu\beta^{-1} + (1-\mu)(1+\beta^{-1}+\tan\alpha)} \\ &= \frac{1+\tan\alpha}{\beta^{-1}\tan\alpha + 1 + \beta^{-1} + \tan\alpha} = \frac{1}{1+\beta^{-1}}. \end{aligned}$$

Let us compare these two results to the sliding vector field for a flat surface $y = 0$. Solving $\dot{y} = \lambda(-\beta) + (1-\lambda) = 0$ implies $\lambda = 1/(1+\beta)$ giving $\dot{x} = 1/(1+\beta^{-1})$. Hence, the form of the motion does not change the sliding vector field approximation – Filippov's method holds. These results are independent of the size of the sawtooth pattern. Likewise if we calculate the portions of motion through the upper vector field, lower vector field, and sliding vector field along the Koch curve, regardless of the fractal structure of the path, ultimately the distance travelled is finite and the speed of motion averages out to Filippov's sliding vector field.

The result extends, of course, to many other structures where motion entirely consists of motion through either the upper or lower vector field, or sliding according to the convex combination along the boundary between them. The switching surface might consist of a layer tiled with regions on which one or other vector field apply, with sliding and crossing regions on their edges, again perhaps of a fractal structure; see Fig. 6.

While an entertaining problem, this has the more serious aim of clarifying the nature of switching surfaces to which the sliding concept applies. Filippov's convex

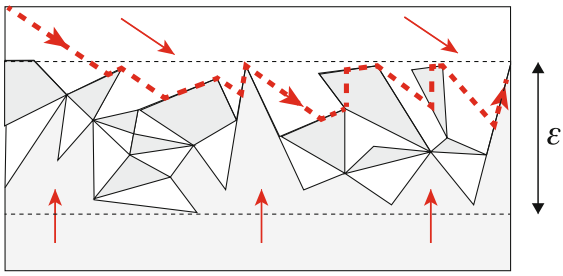

Fig. 6 Along a tiled switching surface of thickness $\varepsilon \to 0$, for the vector fields above, solutions will slide at a speed $\langle \dot{x} \rangle = 1/(1+\beta^{-1}) + \mathcal{O}(\varepsilon)$

combination methodology has very wide applications, and makes less assumptions about the nature of the switches surface than might be thought.

Finding the integral curves themselves is not a trivial problem, and although we have argued above that the sliding mode must be as in Filippov's theory, the explicit calculation above should be extended to demonstrate how the limit along a fractal surface tends to the convex combination result. It is possible that as yet unforeseen dynamical issues may arise with more interesting surfaces, for example in the case of two switches, a fractal surface can undoubtedly be expected to have less trivial consequences.

References

1. A.F. Filippov, *Differential Equations with Discontinuous Righthand Sides* (Kluwer Academic Publishers, Dordrecht, 1988)
2. V.I. Utkin, Comments for the continuation method by A.F. Filippov for discontinuous systems, parts I and II, this volume

Why Nonsmooth?

Mike R. Jeffrey

Abstract Perhaps we should wrap up this volume by asking why *nonsmooth dynamics* is the subject of a three month Intensive Research Program at the CRM (February to April 2016), why it was the subject of more than 2000 papers published in 2015 (and only 700 in the year 2000; data from Thomson Reuters Web of Science), and why it is a growing presence at international conferences involving mathematics and its applications. We briefly survey here why discontinuity is not only important in modeling real-world systems, but is also a fundamental property of many nonlinear systems.

Before we even encounter calculus, we are taught how to apply Newton's laws to collisions —the punctuation of smooth motion by violent changes of speed or direction. This is precisely the kind of thing that differential calculus usually avoids. So we dutifully keep calculus separate from the practical discontinuities we become increasingly familiar with: electronic switches, physical impacts, cellular mitosis, human decisions, physical properties changing across boundaries between media. But after many years in the wilderness, discontinuities are now also the subject of increasingly rich and sophisticated theory in the context of dynamics and differential equations.

Sometimes discontinuities afford a better representation of reality, other times they offer a computationally convenient caricature of nonlinearity. But in fact, and most fundamentally, they arise in the very calculus of 'smooth' *nonlinear* systems themselves. This is the idea set out below.

'Nonsmooth' is a casual form of the more precise term 'piecewise smooth', meaning smooth almost everywhere, except at certain isolated thresholds. So, almost everywhere, the systems in our purview submit to all of the theory pertaining of smooth dynamics, but at a discontinuity, as we are increasingly finding, all hell breaks loose. But we are also discovering how this can be tamed, and brought under the auspices of *piecewise smooth dynamical systems* theory.

M.R. Jeffrey (✉)
Department of Engineering Mathematics, University of Bristol,
Woodland Road, Bristol BS8 1UB, UK
e-mail: mike.jeffrey@bristol.ac.uk

A. Colombo et al. (eds.), *Extended Abstracts Spring 2016*,
Trends in Mathematics 8, DOI 10.1007/978-3-319-55642-0_18

1 Analytic Domains and Divergent Sums

Far from being a crude modeling tool, a discontinuity is actually a subtle phenomenon that arises in the series expansions of functions. We will first describe it for simple functions, then describe its application to things like WKBJ solutions of nonlinear differential equations, and to stationary phase or Laplace methods applied to integrals.

'What is your favourite sigmoid?' is a social opening line perhaps found only at workshops on nonsmooth dynamics, but its answer can be very revealing. A biologist may prefer a Hill function, the neural networkers a tanh function, the numericists an arctan. Look closely through all the complication of rate-and-state or hidden variables in earthquake models, and you'll often find the humble sign function of Coulomb friction.

A sigmoid function 'looks like an S', asymptoting to constants at its tails which we can scale to $+1$ and -1, and transitioning between the two in a smoothly differentiable fashion. How do you approximate such a transition? Take the example of the sigmoid

$$y(x) = \frac{x}{\sqrt{\varepsilon^2 + x^2}} \approx \text{sign}(x) \left\{1 - \tfrac{1}{2}(\varepsilon/x)^2 + \tfrac{3}{8}(\varepsilon/x)^4 - \tfrac{5}{16}(\varepsilon/x)^6 + \cdots\right\} \quad (1)$$

Here, we have not taken the usual Taylor approximation about some finite x value, e.g., $y = x/\varepsilon - x^3/2\varepsilon^3 + \cdots$ about $x = 0$, as such a polynomial approximation, to any order, cannot capture the asymptotic character of $y \to \pm 1$ as $x/\varepsilon \to \pm\infty$. That is instead given by approximating for large x/ε, about the 'point at infinity'. This is the approximation in (1), which captures the tails well, and even works quite well deep into the regions $|x| < \varepsilon$, only failing ultimately as x approaches zero. The leading order $\text{sign}(x)$ term signifies the transition, regulated as x/ε shrinks by the asymptotic terms in the tail.

As a series approximation, the behaviour of the righthand side of (1) is obvious. For $x/\varepsilon \gg 1$ the successive terms in $1 - \frac{1}{2}(\varepsilon/x)^2 + \frac{3}{8}(\varepsilon/x)^4 - \frac{5}{16}(\varepsilon/x)^6 + \cdots$ are ever shrinking, so the series converges. Moreover, because $|x/\varepsilon|$ is 'far from' the approximation's centre at infinity, the approximation is very accurate (of order $\mathsf{O}\left(\varepsilon^{p+2}/x^{p+2}\right)$ if we truncate (1) at the $(\varepsilon/x)^p$ term).

At $|x| = \varepsilon$ the trouble begins. The terms in the series are all of the same order (i.e., $|x|/\varepsilon = 1$), signalling that the series is no longer convergent, and no longer equates to the function on the lefthand side of (1). As x passes through the region $|x| < \varepsilon$ around zero this allows the series to change its analytic form from $1 - \frac{1}{2}(\varepsilon/x)^2 + \frac{3}{8}(\varepsilon/x)^4 - \frac{5}{16}(\varepsilon/x)^6 + \cdots$ to $-1 + \frac{1}{2}(\varepsilon/x)^2 - \frac{3}{8}(\varepsilon/x)^4 + \frac{5}{16}(\varepsilon/x)^6 - \cdots$. This creates the 'sign' function out the front.

When functions undergo a jump in their analytic series expansion like this, it need not be so simple, i.e., the forms for $x > 0$ and $x < 0$ could be entirely unrelated, say

$$y(x) = \begin{cases} y^+(x) \text{ if } x > +\varepsilon, \\ y^-(x) \text{ if } x < -\varepsilon, \end{cases}$$

for different analytic expressions $y^+(x)$ and $y^-(x)$. It turns out that any systems that jump in some way between different steady regimes of behaviour seem to do so in this way, controlled by such a *switching multiplier* y. The difficulty in engineering and natural sciences, in general, is that *we do not know* y. We do not even know what equations might govern y. In optics, y might be subject to a wave equation, in electromagnetism to Maxwell's laws, in a fluids problem to the Navier–Stokes equations, in quantum mechanics to Schrodinger's equation. In those contexts we can fill in the jump using asymptotic matching (see e.g., Bender–Orszag [1]). But what equations should the albedo of the Earth's surface obey in climate science? Or the immune response of species in an ecosystem? Or the interfacial contact force between rough irregular bodies? We know they jump, we know little of the process by which they do so. So, we admit our deficiency, model the parts we can model with confidence, and study the rest under the theory of *piecewise smooth* systems.

2 Coarse/Asymptotic Approx Where Precise Asymptotics Are Unknown

Take a variable $\mathbf{x} = (x_1, \ldots, x_n)$ whose dynamics depends on an external variable y, and assume y switches between values ± 1 as a function $\sigma(\mathbf{x})$ changes sign (generalizing from $\sigma = x$ above), as $\dot{\mathbf{x}} = \mathbf{f}(\mathbf{x}; y)$ and $\mathcal{D}y = p(y, \sigma, \varepsilon)$, where $\mathcal{D}$ is some differential or integral operator. Many classes of such equations lead to $y \sim \operatorname{sign}\sigma + \mathsf{O}(\varepsilon/\sigma)$. We already saw a trivial example above in (1), where y was taken to be a sigmoid. A number of models are given in Jeffrey [3], where $\mathcal{D}y = p$ is an ordinary differential equation, partial differential equation, or integral equation, for example:

(i) In the ordinary differential equation $\dot{\mathbf{x}} = \mathbf{f}(\mathbf{x}; y)$ and $\varepsilon\dot{y} = (1 - y^2)\sigma(\mathbf{x}) - \varepsilon y$, the variable y tends on the ε timescale to

$$y(\sigma) = \operatorname{sign}(\sigma) - \tfrac{\varepsilon}{2\sigma}\left\{1 - \tfrac{\varepsilon}{4|\sigma|} + \mathsf{O}\left((\varepsilon/|\sigma|)^3\right)\right\}.$$

(ii) In the partial differential equation $\dot{\mathbf{x}} = \mathbf{f}(\mathbf{x}; y)$ and $\varepsilon^2\dot{y} = \sigma(\mathbf{x})y_\sigma + \varepsilon y_{\sigma\sigma}$, the variable y relaxes on the ε timescale to

$$y(\sigma) = \operatorname{sign}(\sigma) - \tfrac{\sqrt{2\varepsilon/\pi}}{\sigma} e^{-\sigma^2/2\varepsilon}(1 - \sqrt{\varepsilon}/\sigma + \mathsf{O}\left(\varepsilon/\sigma^2\right)).$$

(iii) In summing over different oscillatory modes, or in using Laplace or Fourier methods, we often face an integral equation for y like

$$\dot{\mathbf{x}} = \mathbf{f}(\mathbf{x}; y) \qquad \text{and} \qquad y(\omega) = \int_{-\infty}^{\omega} dk\; a(k)\; e^{\psi(k)}.$$

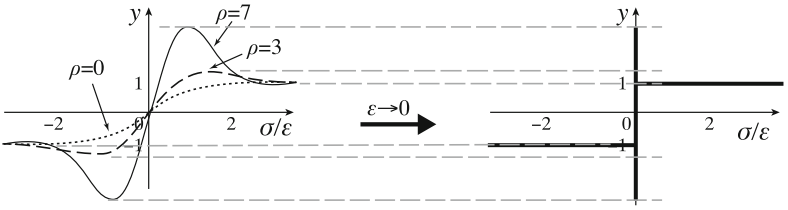

Fig. 1 The graphs of $y(\sigma)$ for different ρ, which all limit to a sign function as $\varepsilon \to 0$. For $\rho > 0$ the graph has peaks whose height is ε-independent, and therefore do not disappear as we shrink ε, but get squashed into the region $|\sigma| = \mathsf{O}(\varepsilon)$

If we take $a(k)$ to be slow (polynomially) varying, and $e^{\psi(k)}$ fast (exponentially) varying, its asymptotics consists of terms of the form

$$y(\sigma) \approx -\tfrac{a(\omega)e^{\psi(\omega)}}{\psi'(\omega)} + a(k_s)e^{\psi(k_s)}\sqrt{\tfrac{2\pi}{-\psi''(k_s)}}\tfrac{1+\text{sign}\,\sigma}{2} + \mathsf{O}(\varepsilon/\sigma)\,,$$

where $\sigma = \mathbb{I}\text{m}\,[\psi(0) - \psi(k_s)]$, and $\phi'(k_s) = 0$; see Jeffrey [3].

The point is that all of these take the form $y \sim \text{sign}\,\sigma + \mathsf{O}(\varepsilon/\sigma)$. In piecewise smooth dynamics we simply use $y = \text{sign}(\sigma)$ and appeal to Filippov [2] (or alternative) for the rest. But what if the $\mathsf{O}(\varepsilon/\sigma)$ tail is nontrivial? For example, consider

$$y(\sigma) = -(1-\rho)\frac{\varepsilon}{\sigma} + \text{sign}(\sigma)\frac{1+\frac{\varepsilon^2}{\sigma^2}}{\sqrt{1+(1-\rho)\frac{\varepsilon^2}{\sigma^2}}},$$

which is non-monotonic for $\rho \neq 0$ (and produces the ODE solution above for $\rho = 0$).[1] As Fig. 1 shows, this has ρ-dependent but ε-independent peaks, which retain their height in the limit $\varepsilon \to 0$. How should we distinguish models with different ρ in the limit $\varepsilon \to 0$? We need a way to preserve the nonlinearity of the function as $\varepsilon \to 0$ and $y \to \text{sign}(\sigma)$, i.e., to remove the ambiguity in $\text{sign}(\sigma)$ at $\sigma = 0$.

Placing y inside $\mathbf{f}(\mathbf{x}; y)$, we obtain an asymptotic expression for $\dot{\mathbf{x}}$, expressed very generally for some functions $\mathbf{p}_n(\mathbf{x})$ and $q(\sigma/\varepsilon)$, of the form

$$\dot{\mathbf{x}} = \mathbf{p}_0(\mathbf{x}) + \mathbf{p}_1(\mathbf{x})\,\text{sign}(\sigma) + q(\sigma/\varepsilon)\sum_{n=1}^{\infty}\mathbf{p}_{n+1}(\mathbf{x})(\varepsilon/\sigma)^n.$$

In Jeffrey [3] it is shown that this can be cast in an ε-independent form

$$\dot{\mathbf{x}} = \mathbf{f}(\mathbf{x}; y) = \frac{\mathbf{f}^+(\mathbf{x}) + \mathbf{f}^-(\mathbf{x})}{2} + \frac{\mathbf{f}^+(\mathbf{x}) - \mathbf{f}^-(\mathbf{x})}{2}y + \left(y^2 - 1\right)\mathbf{g}(\mathbf{x}; y). \qquad (2)$$

[1] For other examples try a Hill, tanh, or error function with complex argument $\sigma + i\rho$.

The first two terms will look familiar from Filippov's *convex combinations* of $\mathbf{f}^{\pm}$, if $y \in [-1, +1]$. The nonlinear term $\left(y^2 - 1\right)\mathbf{g}(\mathbf{x}; y)$ is described as *hidden* because, away from the switch where $y \sim \pm 1$, the term $y^2 - 1$ vanishes everywhere. Since (2) is ε-independent it remains valid as we take $\varepsilon \to 0$, so we may now treat y as simply a sign function, $y = \text{sign}(\sigma)$ for $\sigma \neq 0$ and $y \in [-1, +1]$ for $\sigma = 0$.

A by-product of this (see Jeffrey [3]) is a dynamical expression enabling us to resolve $y \in [-1, +1]$ for $\sigma = 0$,

$$\varepsilon \dot{y} = \mathbf{f}(\mathbf{x}; y) \cdot \nabla y(\mathbf{x})$$

as $\varepsilon \to 0$ on $\sigma = 0$. We call this the *switching layer* system, and refer to the region $y \in (-1, +1)$, $\mathbf{x}|_{\sigma=0} \in \mathbb{R}^{n-1}$, as the *switching layer* on $\sigma = 0$.

3 Purchase Your Zoo Guides Here

Whatever the process lying behind the discontinuity (above we have focussed on its occurrence as an asymptotic phenomenon), piecewise smooth dynamics allows us to identify the jump with a well-defined *switching surface*, a topological object with its own character (a manifold or variety), its own singularities (tangencies between it and the vector fields $\mathbf{f}(\mathbf{x}; \pm 1)$), and its own bifurcations (discontinuity-induced bifurcations).

Recent advances in nonsmooth dynamics have opened the flood doors to new discoveries, of new attractors and new forms of chaos, of bifurcations in systems with multiple switches, with symmetries, or with hidden dynamics. As discussed in Paul Glendinning's *Less Is More* articles in this volume, the endless classifications that are now possible create an exciting but ultimately self-serving exercise. There are bigger questions out there, about how we put these ideas to use in applications, and about what truly new phenomena there are to be found, such as bifurcations that violate the rules of smooth systems, singularities that break down determinism, and complex attractors that challenge our notions of dimension or codimension. Important too is to continue pushing forward our understanding of what it means to perturb a nonsmooth system, and what the effect is of modeling non-idealities like noise, hysteresis, and delay.

We *are* making real strides forward. You have hopefully found some solutions, and the beginnings of many ongoing discussions, in this volume.

References

1. C.M. Bender, S.A. Orszag, *Advanced Mathematical Methods for Scientists and Engineers I. Asymptotic Methods and Perturbation Theory* (Springer, New York, 1999)
2. A.F. Filippov, *Differential Equations with Discontinuous Righthand Sides* (Kluwer Academic Publishers, Dordrecht, 1988) (Russian 1985)
3. M.R. Jeffrey, The ghosts of departed quantities in switches and transitions, preprint (2015)

An Update on that Singularity

Mike R. Jeffrey

Abstract It took nearly 30 years from the translation of Filippov's seminal book to be able to say that the two-fold singularity is understood. We now know that its structural stability requires nonlinear switching or *hidden* terms, and that it comes in three main flavours, with numerous subclasses between which bifurcations can occur. We know that it is neither an attractor nor a repellor, but a bridge between attracting and repelling sliding and, in certain cases, is a source of determinacy-breaking.

1 A Bridge over Troubled Flows

Nothing epitomizes the intrigue of piecewise-smooth dynamics like the two-fold singularity. It is incredibly simple to describe —a point where a flow is tangent to a discontinuity threshold from both sides— yet intricate in its dynamics. Its understanding has pushed the boundaries of understanding in piecewise-smooth systems more than any other discontinuity-induced phenomenon.

It took nearly 30 years, from the translation of Filippov's seminal book introducing the two-fold to the english speaking world, to resolving its switching layer behaviour, before we could say that the two-fold singularity was understood. And it *is* now understood, in wonderful detail: its structural and asymptotic stability [8, 10], its bifurcations including its local form and the affect of higher orders [3, 4, 10], the winding numbers when a flow rotates around it [5], the determinacy or determinacy-breaking occurring when a flow passes through it [7], and even its extension to multiple switches [9].

We now know that the two-fold singularity's structural stability requires nonlinear switching or *hidden* terms, and that it comes in three main flavours, with numerous subclasses between which bifurcations can occur. We know that it is neither an attractor nor a repellor, but an organizing centre, a bi-directional bridge between attracting

M.R. Jeffrey (✉)
Department of Engineering Mathematics, University of Bristol, Woodland Road, Bristol BS8 1UB, UK
e-mail: mike.jeffrey@bristol.ac.uk

A. Colombo et al. (eds.), *Extended Abstracts Spring 2016*,
Trends in Mathematics 8, DOI 10.1007/978-3-319-55642-0_19

and repelling sliding on a switching surface, which can lead to the creation of a determinacy-breaking attractor (described as *non-deterministic chaos* in [1–3, 7]).

The developments towards understanding the two-fold singularity can be traced through the papers [3–6, 8–10, 15]. Attempts to look beyond nonsmooth theory into the effects of regularization, introducing a non-ideal switch that is smooth, noisy, delayed, or hysteretic, have begun in [11–13, 17]. Finally, while attempts to explore its applications in electronics or mechanics have so far been somewhat unsatisfactory, hints of a deeper role in phase randomization can be found in [14].

To summarize the story so far, we must begin, of course, with its definition.

Definition 1 A *two-fold* is a point $\mathbf{x}_p$ in a system

$$\dot{\mathbf{x}} = \left\{ \begin{array}{l} \mathbf{f}^+(\mathbf{x}) \text{ if } \sigma(\mathbf{x}) > 0 \\ \mathbf{f}^-(\mathbf{x}) \text{ if } \sigma(\mathbf{x}) < 0 \end{array} \right\}, \quad \text{where} \quad \left\{ \begin{array}{r} \sigma(\mathbf{x}_p) \\ \mathbf{f}^{\pm}(\mathbf{x}_p) \cdot \nabla\sigma(\mathbf{x}_p) \end{array} \right\} = 0$$

and, with certain non-degeneracy conditions satisfied at $\mathbf{x}_p$, namely $(\mathbf{f}^{\pm} \cdot \nabla)^2\sigma \neq 0$, $0 \notin \mathbf{f}^{\lambda} \cdot \nabla\mathbf{x}$ and, with transversality of the surfaces $\sigma = 0, \mathbf{f}^+ \cdot \nabla\sigma = 0, \mathbf{f}^- \cdot \nabla\sigma = 0$. We will introduce the combination $\mathbf{f}^{\lambda}$ below.

The local dynamics depends entirely on two parameters evaluated at $\mathbf{x}_p$,

$$\nu^+ = \frac{(\mathbf{f}^+\cdot\nabla)(\mathbf{f}^-\cdot\nabla)\sigma}{\sqrt{|(\mathbf{f}^+\cdot\nabla)^2\sigma.(\mathbf{f}^-\cdot\nabla)^2\sigma|}} \quad \text{and} \quad \nu^- = \frac{-\mathbf{f}^-\cdot\nabla\mathbf{f}^+\cdot\nabla\sigma}{\sqrt{|(\mathbf{f}^+\cdot\nabla)^2\sigma.(\mathbf{f}^-\cdot\nabla)^2\sigma|}},$$

characterizing the local curvature of the flow. The product $\nu^+\nu^-$ has a simple geometrical interpretation: it quantifies the jump in the vector field between $\mathbf{f}^{\pm}$ at the singularity. Measuring angles from to the '+' or '−' folds respectively, letting $s^{\pm} = \text{sign}(\mathbf{f}^{\pm} \cdot \nabla)^2\sigma$,

$$\nu^+\nu^- = -s^+s^-\frac{\cot\phi - \cot\theta_+^+}{\cot\phi - \cot\theta_+^-} = -s^+s^-\frac{\cot\phi + \cot\theta_-^-}{\cot\phi + \cot\theta_-^+},$$

where ϕ is the angle between the folds, and θ_j^i is the angle of $\mathbf{f}^i$ from the 'j' fold, measured in the plane spanned by $\mathbf{f}^+$ and $\mathbf{f}^-$, with i and j denoting the labels + or −.

The leading order expansion of the two-fold singularity (sometimes called the 'normal form' in a somewhat loose usage of the terminology) is given by

$$(\dot{x}_1, \dot{x}_2, \dot{x}_3) = \left\{ \begin{array}{l} (-x_2, -s^+, \nu^+) \text{ if } x_1 > 0 \\ (\ x_3\ ,\ \nu^-,\ s^-\ ) \text{ if } x_1 < 0 \end{array} \right\} + \left(\mathsf{O}\left(|\mathbf{x}|^2\right), \mathsf{O}\left(|\mathbf{x}|\right), \mathsf{O}\left(|\mathbf{x}|\right)\right), \quad (1)$$

where $s^{\pm} = \text{sign}\left[(\mathbf{f}^{\pm} \cdot \nabla)^2\sigma(\mathbf{x}_p)\right]$, and in higher dimensions by $\dot{x}_{i\geq 4} = \mathsf{O}\left(|\mathbf{x}|\right)$ for $i = 4, 5, \ldots$; see [4, 6].

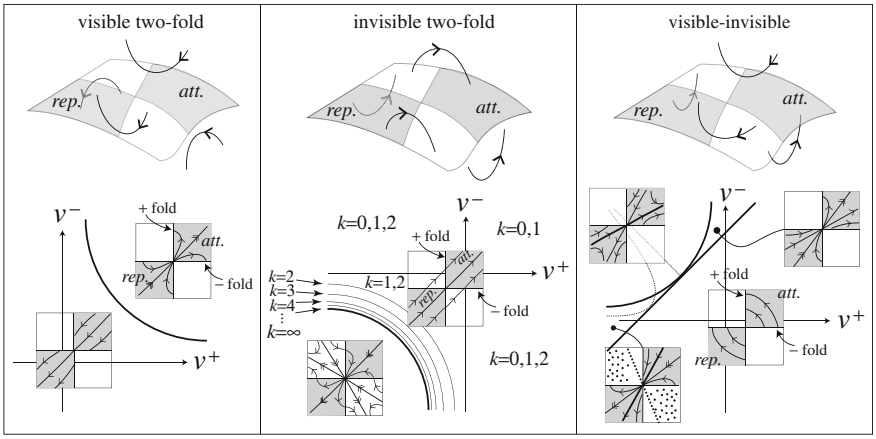

Fig. 1 Two-folds come in three flavours, formed by the different combinations of visible or invisible folds as determined by the signs of $s^{\pm}$. *Top* Regions of attracting sliding (*att.*, *shaded*), repelling sliding (*rep.*, *shaded*), and crossing (*unshaded*) all meet at the singularity. *Bottom* Their sliding and crossing topologies in the $\nu^{\pm}$ parameter plane are shown below; for the invisible two-fold, k is the number of windings between visits to the sliding regions, tending to infinity where $\nu^+\nu^- \geq 1$ in $\nu^{\pm} < 0$; see [4, 5] for details

2 Bifurcation Diagrams

Almost everything we understood until the year 2009 could already be found in Filippov's book [6], but much of it was presented in the form of unexplained diagrams whose original source is unknown (with their description emerging across [4, 5, 16]).

The wealth of information we have on the leading order dynamics (the truncation of (1)) is summarized in the Fig. 1 below; see [4, 5] for details.

The folds are: (i) both *visible* if $s^+ > 0$ and $s^- < 0$ at $\mathbf{x}_p$; (ii) both *invisible* if $s^+ < 0$ and $s^- > 0$ at $\mathbf{x}_p$; and (iii) one *visible* and one *invisible* if $s^+ s^- > 0$ at $\mathbf{x}_p$ (we sometimes refer to these as the *flavours* of two-fold).

3 Crossing Maps and Winding Numbers

The distinguishing feature of the invisible two-fold is that the flow can wind repeatedly around the singularity, making repeated visits to the crossing regions, possibly between entry/exit points to/from the attracting/repelling sliding regions.

Let $\mathbf{y} = (x_2, x_3)$ denote a point on the switching surface $x_1 = 0$, and $\mathbf{y}_i$ denote an iterate of the return map to the switching surface under the flow. A single return to the surface is given by

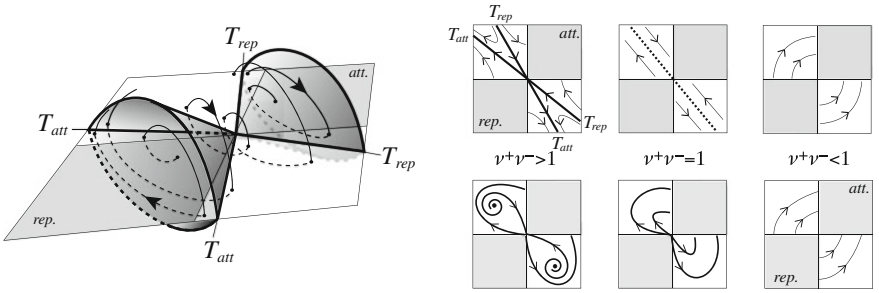

Fig. 2 The nonsmooth diabolo: invariant manifold (*left*) around an invisible two-fold. *Right top* shown in the switching plane, the manifold bifurcates and disappears at $\nu^+\nu^- = 1$; see Jeffrey–Colombo [10]. *Right bottom* the effect of higher order terms, showing a particular case leading to a determinacy-breaking attractor —as the flow exits the repelling sliding region, the crossing flow wraps it back around (via k windings) into the attracting sliding region, whereupon the sliding flow re-injects it back into the repelling region; when all local trajectories pass through the singularity, determinacy is broken; see Colombo–Jeffrey [3]

$$\mathbf{y}_{2m+1} = \underline{\underline{B}}^{\pm}\mathbf{y}_{2m}\,, \qquad \underline{\underline{B}}^{+} = \begin{pmatrix} -1 & 0 \\ -2\nu^+ & 1 \end{pmatrix} \quad \text{and} \quad \underline{\underline{B}}^{-} = \begin{pmatrix} 1 & -2\nu^- \\ 0 & -1 \end{pmatrix},$$

where $\underline{\underline{B}}^{+}$ and $\underline{\underline{B}}^{-}$ are applied in $x_2 < 0$ and $x_3 < 0$, respectively. Therefore, the second return map, on $x_2 < 0$ or $x_3 < 0$, is

$$\mathbf{y}_{2m+2} = \underline{\underline{A}}^{\pm}\mathbf{y}_{2m}\,, \qquad \underline{\underline{A}}^{\pm} = \underline{\underline{B}}^{\mp}\underline{\underline{B}}^{\pm}\,. \tag{2}$$

Since the maps are associated with folds, they are involutions so, $(\underline{\underline{B}}^{+})^2 = (\underline{\underline{B}}^{-})^2 = \underline{\underline{1}}$ and $\underline{\underline{A}}^{+} = (\underline{\underline{A}}^{-})^{-1}$. The solutions to the difference equation (2) are now obviously

$$\mathbf{y}_{2m} = (\underline{\underline{A}}^{+})^m\mathbf{y}_0 \qquad \text{or} \qquad \mathbf{y}_{2m} = (\underline{\underline{A}}^{-})^m\mathbf{y}_0\,,$$

and a little trigonometry using the substitution $\nu^+\nu^- = \cos^2\Theta$ provides

$$(\underline{\underline{A}}^{\pm})^m = \frac{\sin[2m\Theta]}{\sin 2\Theta}\underline{\underline{A}}^{\pm} - \frac{\sin[2(m-1)\Theta]}{\sin 2\Theta}\underline{\underline{1}}\,.$$

This is also the source of the crossing numbers k in the previous figure. The main dynamical features revealed by the map are shown in Fig. 2.

4 Sliding Dynamics and Hidden Instability

To derive sliding dynamics, we need to define a *combination* of $\mathbf{f}^{\pm}$ on the switching surface. It turns out that Filippov's combination hides a structural instability, in

$$(\dot{x}_1, \dot{x}_2, \dot{x}_3) = \tfrac{1}{2}(1+\lambda)(-x_2, -s^+, \nu^+) + \tfrac{1}{2}(1-\lambda)(x_3, \nu^-, s^-),$$

essentially because the value $\lambda = (x_3 - x_2)/(x_3 + x_2)$ for which sliding occurs is singular at $x_2 = x_3 = 0$. It is shown in Jeffrey [8] that a structurally stable combination is

$$(\dot{x}_1, \dot{x}_2, \dot{x}_3) = \tfrac{1}{2}(1+\lambda)\left(-x_2, -s^+, \nu^+\right) + \tfrac{1}{2}(1-\lambda)\left(x_3, \nu^-, s^-\right) + (1-\lambda^2)(\alpha, 0, 0)$$

for small $\alpha \neq 0$. A well-defined manifold $\mathcal{M}$ of sliding solutions then exists,

$$\mathcal{M} = \left\{ (\lambda, x_2, x_3) \mid \tfrac{1}{2}(1-\lambda)\, x_3 - \tfrac{1}{2}(1+\lambda)\, x_2 + \alpha(1-\lambda^2) = 0 \right\},$$

inside the layer $(\lambda, x_2, x_3) \in (-1, +1) \times \mathbb{R}^2$, with $\mathcal{M}$ normally hyperbolic except on

$$\mathcal{L} = \left\{ (\lambda, x_2, x_3) \subset \mathcal{M} : \ \lambda = 2\frac{2\alpha + x_3 - x_2}{x_3 + x_2} = -\frac{x_3 + x_2}{4\alpha} \right\},$$

which corresponds to the two-fold magnified inside the switching layer $\lambda \in (-1, +1)$, $(x_2, x_3) \in \mathbb{R}^2$. The dynamics inside the layer is given by

$$(\varepsilon\dot{\lambda}, \dot{x}_2, \dot{x}_3) = \tfrac{1}{2}(1+\lambda)\left(-x_2, -s^+, \nu^+\right) + \tfrac{1}{2}(1-\lambda)\left(x_3, \nu^-, s^-\right) + (1-\lambda^2)(\alpha, 0, 0),$$

for $\varepsilon \to 0$, which can be transformed into the well-known singularity of folded slow-manifolds associated with canards in smooth slow-fast systems,

$$(\varepsilon\dot{x}, \dot{y}, \dot{z}) = (y + x^2, pz + qx, r) + (\mathsf{O}(\varepsilon x, \varepsilon z, xz), \mathsf{O}\left(z^2, xz\right), \mathsf{O}(z, x)),$$

provided $\alpha \neq 0$, where $p, q, r,$ are real constants, and provided the conditions $\frac{1}{2}(\nu^+ - \nu^-) \leq 1 = -s^+ = s^-$ or $\frac{1}{2}(\nu^+ - \nu^-) \geq -1 = -s^+ = s^-$ do not hold.

References

1. M. Buchanan, Differentiating the discontinuous. Nat. Phys. - Thesis **7**, 589 (2011)
2. M. Buchanan, Generating chaos in a new way. Phys. Rev. Focus **28**, 1 (2011)
3. A. Colombo, M.R. Jeffrey, Non-deterministic chaos, and the two-fold singularity in piecewise smooth flows. SIAM J. Appl. Dyn. Syst. **10**, 423–451 (2011)
4. A. Colombo, M.R. Jeffrey, The two-fold singularity: leading order dynamics in *n*-dimensions. Phys. D **263**, 1–10 (2013)
5. S. Fernández-Garcia, D. Angulo-Garcia, G. Olivar-Tost, M. di Bernardo, M.R. Jeffrey, Structural stability of the two-fold singularity. SIAM J. Appl. Dyn. Syst. **11**(4), 1215–1230 (2012)
6. A.F. Filippov, *Differential Equations with Discontinuous Righthand Sides* (Kluwer Academic Publishers, Dortrecht, 1988). (Russian 1985)
7. M.R. Jeffrey, Non-determinism in the limit of nonsmooth dynamics. PRL **106**(25), 254103 (2011)
8. M.R. Jeffrey, Hidden degeneracies in piecewise smooth dynamical systems. Int. J. Bifurcations Chaos **26**(5), 1–18 (2016)

9. M.R. Jeffrey, Exit from sliding in piecewise-smooth flows: deterministic vs. determinacy-breaking. Chaos **26**(3), 1–20 (2016)
10. M.R. Jeffrey, A. Colombo, The two-fold singularity of discontinuous vector fields. SIAM J. Appl. Dyn. Syst. **8**(2), 624–640 (2009)
11. K.U. Kristiansen, S.J. Hogan, Regularizations of two-fold bifurcations in planar piecewise smooth systems using blow up, Submitted (2015)
12. J. Llibre, P.R. da Silva, M.A. Teixeira, Sliding vector fields via slow-fast systems. Bull. Belg. Math. Soc. Simon Stevin **15**(5), 851–869 (2008)
13. D.J.W. Simpson, On resolving singularities of piecewise-smooth discontinuous vector fields via small perturbations, *Discrete Continuous Dyn. Syst.* (to appear)
14. D.J.W. Simpson, M.R. Jeffrey, Fast phase randomisation via two-folds, Submitted (2015)
15. M.A. Teixeira, Stability conditions for discontinuous vector fields. J. Differ. Equ. **88**, 15–29 (1990)
16. M.A. Teixeira, Generic bifurcation of sliding vector fields. J. Math. Anal. Appl. **176**, 436–457 (1993)
17. M.A. Teixeira, J. Llibre, P.R. da Silva, Regularization of discontinuous vector fields on R^3 via singular perturbation. J. Dyn. Differ. Equ. **19**(2), 309–331 (2007)

Sensor Effects in Sliding Mode Control of Power Conversion Cells

Georgios Kafanas

Abstract Sliding mode controllers are ideally modeled as responding to the state of a system when, in practice, only a measurement of the state is available, provided by non-ideal sensors. We provide an equivalent control model for a buck converter system that includes the dynamics of the sensors. The results demonstrate some limitations of the basic equivalent control method in determining the stability of systems with sensors.

1 Introduction

Power electronics provide a class of variable structure systems where sliding mode control has been applied extensively. The implementation of most sliding mode controllers requires the evaluation of a function of the system state called the switching function. The system state is measured using sensors, which can also be modeled as dynamic systems.

In most design approaches, the exact sensor dynamics are neglected. The controller is designed assuming ideal sensors. The resulting switching frequency is evaluated and used to determine a sensor cut-off frequency that ensures timescale separation between the sensor and converter dynamics.

In efforts to improve the power density of converters, the switching frequency increases such that the converter and the sensors operate in similar time scales. Thus the basic assumption in the derivation of sliding mode control, that non-ideal behavior disappears as the switching frequency increases, is no longer valid. In this report, we investigate how the sensor dynamics affect the equivalent control method as a design and analysis tool for power electronics.

G. Kafanas (✉)
Department of Electrical and Electronic Engineering, Merchant Venturers Building, Woodland Road, Bristol BS8 1UB, UK
e-mail: georgios.kafanas@bristol.ac.uk

A. Colombo et al. (eds.), *Extended Abstracts Spring 2016*,
Trends in Mathematics 8, DOI 10.1007/978-3-319-55642-0_20

2 Dynamics of Sensors

In our model, the state of the system is not directly available but all state variables are measured by senors whose state is directly observable. The dynamics of the buck converter is modeled by a first order ordinary differential equation

$$\frac{dx_{\text{sys}}}{dt} = f_{\text{sys}}(x_{\text{sys}}, u),$$

where

$$f_{\text{sys}}(x_{\text{sys}}, u) = \begin{pmatrix} 0 & -\frac{1}{L} \\ \frac{1}{C} & -\frac{1}{RC} \end{pmatrix} \cdot x_{\text{sys}} + u \begin{pmatrix} 0 & -\frac{1}{L} \\ \frac{1}{C} & -\frac{1}{RC} \end{pmatrix}. \tag{1}$$

The state $x_{\text{sys}} = (i_L, v_C)^T$ of the buck converter consists of the current of the inductor, i_L, and the voltage of the capacitor, v_C. The control input u is discontinuous, taking values 0 or 1. We denote the measurement of some variable z by $\hat{z}$. A first order integrator is a good model for a popular class of sensors, the voltage and current transducers, over a wide range of switching frequencies.

To describe the dynamics of the extended system including the sensors, we add the sensor dynamics in the dynamics of the converter. The state of the converter, x_{sys}, and the sensors, x_{sen}, are

$$x_{\text{sys}} = \begin{pmatrix} i_L \\ v_C \end{pmatrix}, \qquad x_{\text{sen}} = \begin{pmatrix} \hat{i}_L \\ \hat{v}_C \end{pmatrix}.$$

The dynamics in the extended system are

$$\frac{dx_{\text{sys}}}{dt} = f_{\text{sys}}(x_{\text{sys}}, u), \qquad \frac{dx_{sen}}{dt} = f_{\text{sen}}(x_{\text{sys}}, x_{\text{sen}}),$$

where $u \in \{0, 1\}$ is the control input, f_{sen} is as defined in (1), and

$$f_{\text{sen}}(x_{\text{sys}}, x_{\text{sen}}) = \begin{pmatrix} k_i & 0 \\ 0 & k_v \end{pmatrix} \cdot \left(x_{\text{sys}} - x_{\text{sen}}\right).$$

The extended system state is now the combination of the converter and sensor states

$$x = \begin{pmatrix} x_{\text{sys}} \\ x_{\text{sen}} \end{pmatrix}.$$

The extended system dynamics is then $\frac{dx}{dt} = f(x, u)$, where

$$f\left(\begin{pmatrix} x_{\text{sys}} \\ x_{\text{sen}} \end{pmatrix}, u\right) = \begin{pmatrix} f_{\text{sys}}(x_{\text{sys}}, u) \\ f_{\text{sen}}(x_{\text{sys}}, x_{\text{sen}}) \end{pmatrix}.$$

The converter dynamics is independent of the sensors. This is a reasonable assumption, as the sensors draw small amounts of power from the converter.

3 Sliding Surfaces with Sensors

The objective of the controller is to maintain the state of the system in some manifold given by an equation of the form $H(x) = 0$. In the model of the buck converter extended to included non-ideal sensors, only the converter state is limited to a manifold $H(x_{\text{sys}}) = 0$. We let

$$H(x_{\text{sys}}) = \left(\cos\phi \ \sin\phi\right) \cdot \left(x_{\text{sys}} - x^*_{\text{sys}}\right), \tag{2}$$

where $x^*_{\text{sys}} = (v^*_C/R, v^*_C)^T$ is the desired pseudo-equilibrium of the sliding mode, and ϕ is a design parameter. The condition for the manifold $H(x_{\text{sys}}) = 0$ to be attracting under a control input u is

$$H(x_{\text{sys}}) \neq 0 \Rightarrow H(x_{\text{sys}}) \cdot [\mathcal{L}_{f(x,u)} H](x) < 0, \tag{3}$$

where the operator $\mathcal{L}_{f(x,u)}$ is the Lie derivative along flows in the vector filed defined by $f(x, u)$.

In a control system with sensor dynamics only the state of the sensors, x_{sen}, is available to construct the control input. The switching surface will be determined by the equation

$$H(x_{\text{sen}}) = 0. \tag{4}$$

Any implementation of the sliding mode control will actually impose the invariant $H(x_{\text{sen}}) = 0$ rather that $H(x_{\text{sys}}) = 0$.

4 Constructing the Equivalent Control

The equivalent control method from Edwards–Spurgeon [1] allows us to determine the continuous feedback control ensuring that, after the state reaches the surface (4), the state remains there. The equivalent control u_{eq} is defined as the control input u solving

$$[\mathcal{L}_{f(x,u)} H](x) = 0$$

on $H(x_{\text{sen}}) = 0$. In our system a modification to the traditional equivalent control method is made. Computing $[\mathcal{L}_{f(x,u)}H](x)$, the result

$$\begin{aligned}[\mathcal{L}_{f(x,u)}H](x) &= \nabla_x H \cdot \frac{dx}{dt} = \nabla_x H \cdot f(x,u) \\ &= \nabla_{x_{\text{sys}}} H \cdot f_{\text{sys}}(x_{\text{sys}}, u) + \nabla_{x_{\text{sen}}} H \cdot f_{\text{sen}}(x_{\text{sys}}, x_{\text{sen}}) \\ &= \nabla_{x_{\text{sen}}} H \cdot f_{\text{sen}}(x_{\text{sys}}, x_{\text{sen}}) = (k_i x_1 - k_i x_3)\cos\phi + (k_v x_2 - k_v x_4)\sin\phi,\end{aligned}$$

is not a function of u. Instead, we use $[\mathcal{L}_{f(x,u)}H](x) = 0$ as the switching surface, and thus define the equivalent control as the solution of

$$[\mathcal{L}^2_{f(x,u)}H](x_{\text{sen}}) = 0$$

on $[\mathcal{L}_{f(x,u)}H](x) = 0$. The resulting control input exists and is given by a function of x denoted $u_{\text{eq}}(x)$.

The desired pseudo-equilibrium of the system is $x^* = (x^{*T}_{\text{sys}}, x^{*T}_{\text{sen}})^T$, where $x^*_{\text{sen}} = x^*_{\text{sys}}$ and x^*_{sys} is defined by (2). The surfaces $H(x_{\text{sys}}) = 0$ and $[\mathcal{L}_{f(x,u)}H](x) = 0$ intersect at x^*; if x^* is a stable pseudo-equilibrium for the sliding mode on $[\mathcal{L}_{f(x,u)}H](x) = 0$ the system is stabilized on x^*, the desired state on $H(x_{\text{sys}}) = 0$.

5 System Stability

The system is stable under the control input u_{eq} if it makes the manifold $H(x_{\text{sys}}) = 0$ attracting. We introduce for $x = (x^T_{\text{sys}}, x^T_{\text{sen}})^T$ the equation

$$L(x) = H(x_{\text{sys}}) \cdot [\mathcal{L}_{f(x,u_{\text{eq}}(x))}H](x).$$

According to (3), the manifold $H(x_{\text{sys}}) = 0$ will be attracting if $H(x_{\text{sys}}) \neq 0$ implies $L(x) < 0$. With the transformation T from $z = (y, \varepsilon_1, \delta, \varepsilon_2)^T$ to $x = (i_L, v_C, \hat{i}_L, \hat{v}_C)^T$,

$$T\begin{pmatrix} y \\ \varepsilon_1 \\ \delta \\ \varepsilon_2 \end{pmatrix} = \begin{pmatrix} \frac{v^*_C}{R} \\ v^*_C \\ \frac{v^*_C}{R} \\ v^*_C \end{pmatrix} + y\begin{pmatrix} -\sin\phi \\ \cos\phi \\ -\sin\phi \\ \cos\phi \end{pmatrix} + \varepsilon_1\begin{pmatrix} \cos\phi \\ \sin\phi \\ \cos\phi \\ \sin\phi \end{pmatrix} + \delta\begin{pmatrix} 0 \\ 0 \\ -\sin\phi \\ \cos\phi \end{pmatrix} + \varepsilon_2\begin{pmatrix} 0 \\ 0 \\ \cos\phi \\ \sin\phi \end{pmatrix},$$

the function L is expressed in terms of perturbations z from the pseudo-equilibrium, x^*, of the sliding mode, $[\mathcal{L}_{f(x,u)}H](x) = 0$, as a quadratic form $\Lambda(z) = L(T(z))$, where $\Lambda(z) = z^T Q z$ for some symmetric matrix Q.

The quadratic form Λ is always negative when Q is negative definite. This is equivalent to all the eigenvalues of Q being negative. There are three eigenvalues:

(i) $\lambda_1 = 0$, with a two dimensional eigenspace. The eigenspace can be decomposed in a subspace where $H(x_{\text{sys}}) = 0$ and a subspace where $H(x_{\text{sen}}) = 0$ and $H(x_{\text{sys}})$ is not identically zero. In the later case, $H(x_{\text{sys}}) \neq 0$ and $L(x) = 0$ so, the surface is not attracting.
(ii) $\lambda_2 < 0$, with an eigenspace where $H(x_{\text{sys}}) \cdot H(x_{\text{sen}}) > 0$.
(iii) $\lambda_3 > 0$, with an eigenspace where $H(x_{\text{sys}}) \cdot H(x_{\text{sen}}) < 0$.

The spectral analysis of Q indicates that the manifold $H(x_{\text{sys}}) = 0$ is not attracting in pseudo-equilibrium point x^* under the equivalent control. Practical experience and simulations reveal that a limit cycle appears in the system under a hysteric implementation of the sliding mode controller. Thus, under the equivalent control, a stable limit cycle is expected to appear around the pseudo-equilibrium.

6 Conclusions

A model for the equivalent control of the buck converter with sensors was derived and used to determine the local stability of the pseudo-equilibrium on the sliding mode. The sliding mode control with direct access to the system state converts the discontinuous system to a continuous system where a stable equilibrium point exists. When the sensor dynamics is modeled, the equilibrium point of the sliding mode control becomes unstable. A stable limit cycle is expected to exist around this unstable equilibrium point.

Acknowledgements The author would like to thank Dr Mike R. Jeffrey for his insightful discussion and comments.

Reference

1. C. Edwards, S.K. Spurgeon, *Sliding Mode Control: Theory and Applications* (CRC Press, Boca Raton, 1998)

Variational Time Stepping for Nonsmooth Analytical System Dynamics

Claude Lacoursière and Tomas Sjöström

Abstract The discrete time variational principle is applied to the Lagrangian formulation of multidomain nonsmooth dynamics to produce a stable time stepping scheme. Examples from electronics are used to demonstrate how to construct pseudo-potentials of nonsmooth devices such as transistors.

Analytical system dynamics provides a systematic framework to construct the equations of motion of multidomain models; see Layton [7]. Elements are describes with scalar functions representing kinetic or potential energy or "dissipative pseudo potentials". Boundary conditions are then enforced using kinematic constraints of various types. The equations of motion are then derived using the Fourier D'Alembert principle of stationary action, which can include inequality and impact conditions using different families of variations; see Leine–Aeberhard–Glocker [8]. Numerical methods for time integration can then be derived using the discrete time variational principle; see Marsden–West [9]. These generally have advantageous properties such as symplecticity for conservative systems, and are stable even at low order.

We add two things to this, namely, a regularization procedure based on Legendre–Frenet transforms which allows to take the uniformly convergent limits of arbitrarily strong potentials, as well as "ghost" variables which help with the derivation of the equations of motion and numerical time integration methods of dissipative systems. We illustrate this with Coulomb friction for rigid bodies as well as bipolar junction transistors for electronics. Models for op-amps and other types of transistors are currently under development.

Let q and $\dot{q}$ be generalized coordinates and velocities of the entire system. We write $T(q, \dot{q})$ and $U(q)$ for total kinetic and potential energy, and $\mathfrak{R}(q, \dot{q}) \geq 0$ for dissipation pseudo-potentials. The latter are assumed sub-differentiable and they

C. Lacoursière (✉) · T. Sjöström
HPC2N/UMIT, University of Umeå, Umeå, Sweden
e-mail: claude@hpc2n.umu.se

T. Sjöström
e-mail: tomas_sjostrom@hotmail.com

A. Colombo et al. (eds.), *Extended Abstracts Spring 2016*,
Trends in Mathematics 8, DOI 10.1007/978-3-319-55642-0_21

generate forces according to $f = -\partial\mathfrak{R}/\partial\dot{q}$ and dissipate energy at the rate $\dot{q} \cdot f$. Holonomic constraints are defined with differentiable functions $g(q)$ which restrict q to $g(q) \geq 0$, and introduce forces according to $f = G^T\lambda$, where $G = \partial g(q)/\partial q$, and λ is a Lagrange multiplier. We also have non-holonomic constraints defined via restrictions $a(q, \dot{q})\dot{q} \geqq 0$, and produce forces $f = A\dot{\beta}$, where $A = \partial a/\partial\dot{q}$ and $\dot{\beta}$ is a Lagrange multiplier. The time derivative is explained shortly.

Strong potentials of the form $U(q) = (1/(2\epsilon))g^2(q)$ and pseudo-potentials $\mathfrak{R}(q, \dot{q}) = (1/(2\gamma))a^2(q, \dot{q})$ are useful for modeling and constraint realization. To be able to take the limit $\epsilon \to 0$ and $\gamma \to 0$, we use half Legendre transforms

$$U(q) = -\frac{\epsilon}{2}\|\lambda\|^2 - \lambda \cdot g(q),$$

$$\mathfrak{R}(q, \dot{q}) = -\frac{\gamma}{2}\|\dot{\beta}\|^2 - \dot{\beta} \cdot a(q, \dot{q}),$$

with $0 \leq \lambda \perp g(q) \geq 0$. The new variables λ and β can now be incorporated in new generalized coordinates $\tilde{q} = (q, \lambda, \beta)$. Given that the quadratic terms for λ and β are *negative*, these are ghost variables with no kinetic energy; see De Felice [3]. The limit of $\epsilon \to 0$ is well defined if we introduce dissipation (see Bornemann [1]) and this is then done with

$$\mathfrak{R}(\tilde{q}, \dot{\tilde{q}}) = \frac{\tau}{2\epsilon}\|\dot{g}\|^2 = -\frac{\tau\epsilon}{2}\|\dot{\lambda}\|^2 - \tau\dot{\lambda} \cdot \dot{g}(q),$$

which reveals the significance of writing $\dot{\beta}$ for the Lagrange multipliers of pseudo-potentials' Legendre transforms. The pseudo-potentials are known to converge to nonholonomic constraints as $\gamma \to 0$; see Karapetian [4]. As the notation suggests, we now consider all constraints as limits of strong potentials with $\epsilon = \gamma = 0$ and therefore, the variables $\tilde{q}$ are constrained only by inequalities. The Lagrangian and pseudo-potentials then read

$$\mathcal{L}(\tilde{q}, \dot{\tilde{q}}) = T(q, \dot{q}) - \bar{U}(q) + \frac{\epsilon}{2}\|\lambda\|^2 + \lambda \cdot g(q),$$

$$\mathfrak{R} = \bar{\mathfrak{R}} - \frac{\gamma}{2}\|\dot{\beta}\|^2 - \dot{\beta} \cdot a(q, \dot{q}),$$

where $\bar{U}(q)$ and $\bar{\mathfrak{R}}(q, \dot{q})$ are "weak" potentials and pseudo-potentials. The Fourier–D'Alembert principle then reads

$$\delta \int_0^T \mathrm{d}s\mathcal{L}(\tilde{q}, \dot{\tilde{q}}) - \int_0^T \mathrm{d}s\delta\tilde{q}(s)\frac{\partial\mathfrak{R}(\tilde{q}, \dot{\tilde{q}})}{\partial\dot{\tilde{q}}} \geq 0, \tag{1}$$

and the complementarity conditions $0 \leq \lambda \perp g(q) \geq 0$ and $0 \leq \dot{\beta} \perp a(q, \dot{q}) \geq 0$, as follows from our definitions (and is well known; see Lanczos [6]). These conditions

imply that if a limit condition is reached, the forces push the system back into the feasible region.

We use the discrete to variational principle (see Marsden–West [9]) to construct a time-stepping scheme using the definitions

$$S[\tilde{q}] = \int_0^T \mathrm{d}s\mathcal{L}(\tilde{q}, \dot{\tilde{q}}) = \sum_{k=0}^{N} \int_{kh}^{(k+1)h} \mathrm{d}\tilde{q}\mathcal{L}(\tilde{q}, \dot{\tilde{q}}) = \sum_{k=0}^{N} \mathbb{L}_d(\tilde{q}_k, \tilde{q}_{k+1}),$$

and

$$\int_0^h \mathrm{d}sf \cdot \delta\tilde{q}(s) = f_d^{(+)}(\tilde{q}_0, \tilde{q}_1)\delta\tilde{q}_0 + f_d^{(-)}(\tilde{q}_0, \tilde{q}_1)\delta\tilde{q}_1,$$

where $h > 0$ is a fixed time step. Details of the discretization are found elsewhere (see, e.g., Lacoursière–Linde [5]), and the final form reads

$$\begin{bmatrix} \tilde{M} & -G_k^T & -A_k^T \\ G_k & \tilde{\epsilon} & 0 \\ \bar{A}_k & 0 & \tilde{\gamma} \end{bmatrix} \begin{bmatrix} \dot{q}_{k+1} \\ \lambda \\ \nu \end{bmatrix} = \begin{bmatrix} M\dot{q}_k + hf \\ \zeta \\ \rho \end{bmatrix}, \tag{2}$$

with $0 \leqq \lambda \perp \zeta \geqq 0$, $0 \leqq \nu \perp \rho \geqq 0$ and $q_{k+1} = q_k + h\dot{q}_{k+1}$. All quantities with $\tilde{(\cdot)}$ depend on the timestep. Stepping then requires the solution of Mixed Linear Complementarity Problems (MLCP)s. This is solvable for conservative systems if we have bisymmetry, i.e., $\bar{A}_k = A_k$. When then have a P problem if $\tilde{\epsilon} > 0$ and $\tilde{\gamma} > 0$, and a P_0 problem otherwise; see Cottle–Pang–Stone [2]. The parameters $\tilde{\epsilon}$, $\tilde{\gamma}$ protect against rank deficiency and yet have physical meaning.

We now consider three examples where $\tilde{A} \neq A$, and analyze the feasibility of the MLCP in Eq. (2) with Coulomb friction, simple diodes and the bipolar transistor.

For Coulomb friction we introduce a distance function $g(q)$ leading to standard $0 \leq g(q) \perp \nu \geq 0$, where ν is the magnitude of the contact force. Stiction is enforced by defining a tangential contact velocity $v = A(q)\dot{q}$ where A is the projection onto the plane tangent to $\nabla g(q)$ and so, for finite viscosity,

$$\mathfrak{R}_s = \frac{1}{2\gamma}\|a(q, \dot{q})\|^2 = -\frac{\gamma}{2}\|v\|^2 - \dot{\beta} \cdot v.$$

The Coulomb cone condition is then $\|\dot{\beta}\| \leq \mu\nu$, where $\mu > 0$ is a friction coefficient. The maximum dissipation principle then states that $v \cdot \dot{\beta} = -\|v\|\|\dot{\beta}\|$. This is done by putting dissipative pseudo-potentials on the magnitude of the ghost $\dot{\beta}$ with

$$\mathfrak{R}_c = -\frac{1}{2\gamma}(\mu\nu - \|\dot{\beta}\|)^2 = \frac{\gamma}{2}\dot{\sigma}^2 + \dot{\sigma}(\mu\nu - \|\dot{\beta}\|),$$

where $0 \leq \dot{\sigma} \perp \mu\nu - \|\dot{\beta}\| \geq 0$. The negative sign is important and follows from the fact that β is a ghost variable and therefore negative energy. Taking the limit $\epsilon = 0 = \gamma$, the variational principle then leads to the forces on the original q variables, $G^T\nu$ and $A^T\dot{\beta}$, as well as the following equations corresponding to ν, $\dot{\beta}$, and $\dot{\sigma}$ derivatives in Eq. (1): $0 \leq g(q) \perp \nu \geq 0$, $A\dot{q} + t\dot{\sigma} = 0$ with $t = \dot{\beta}/\|\dot{\beta}\|$, and $0 \leq \mu\nu - t \cdot \dot{\beta} \perp \dot{\sigma} \geq 0$, showing that $\tilde{A} \neq A$. One can linearize the norm operator (see Stewart–Trinkle [10]) and in doing so, the MLCP in Eq. (2) is *copositive* meaning that it is solvable, with some caveats.

The simple diode with thermal voltage $v^{(\theta)}$ and reverse bias current $\dot{q}^{(r)}$ has current $\dot{q}$, no potential and no kinetic energy, but the dissipation potential

$$\mathfrak{R}^{(d)} = v^{(\theta)}\dot{q}^{(r)}\left(\log\left(1 + \frac{\dot{q}}{q^{(r)}}\right) - \frac{\dot{q}}{\dot{q}^{(r)}}\right), \tag{3}$$

where $\dot{q} \geq -\dot{q}^{(r)}$. Conservation of charge leads to Kirchhoff's current law after differentiation, $G\dot{q} = 0 = \dot{g}$, and the potential differences across the components are then $\Delta v = G^T\lambda$, where the Lagrange multipliers λ are node voltages. The constitutive equations then lead to

$$0 \leq \Delta v = \frac{\partial \mathfrak{R}^{(d)}}{\partial \dot{q}} = v^{(\theta)} \log\left(1 + \frac{\dot{q}}{\dot{q}^{(r)}}\right) \perp \dot{q} - \dot{q}^{(r)} \geq 0$$

and this still has the correct symmetry. Suitable discretization in time gives a nonzero numerical impedance.

Using the Ebers–Moll's equations, the bipolar transistor can be represented in terms of two "natural diodes" with currents $\dot{\tilde{q}}^{(1)}$ and $\dot{\tilde{q}}^{(2)}$ related to the Common–Emitter and Base–Emitter currents $\dot{q}^{(ce)}$, $\dot{q}^{(be)}$ via

$$\begin{bmatrix} \dot{\tilde{q}}^{(1)} \\ \dot{\tilde{q}}^{(2)} \end{bmatrix} = \begin{bmatrix} Q_{11} & Q_{12} \\ Q_{12} & Q_{22} \end{bmatrix} \begin{bmatrix} \dot{q}^{(ce)} \\ \dot{q}^{(be)} \end{bmatrix},$$

where the matrix $Q = \begin{bmatrix} Q_{11} & Q_{12} \\ Q_{12} & Q_{22} \end{bmatrix}$ is symmetric and positive definite. Each new current $\dot{\tilde{q}}^{(i)}$, $i = 1, 2$, satisfies the diode law in Eq. (3). Changing variables leads to changing Kirchhoff's current law to read

$$G\dot{q} = GQ^{-1}\dot{\tilde{q}}, \tag{4}$$

but the dynamics is then

$$0 \leq \Delta v^{(ce)} = v^{(\theta)} \log\left(1 + \frac{\dot{q}^{(1)}}{\dot{q}^{(r)}}\right) \perp \dot{\tilde{q}}^{(1)} - \dot{q}^{(r)} \geq 0,$$

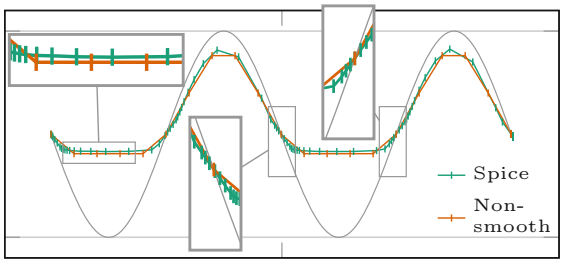

Fig. 1 Diode bridge simulations

$$0 \leq \Delta v^{(be)} = v^{(\theta)} \log\left(1 + \frac{\dot{q}^{(2)}}{\dot{q}^{(r)}}\right) \perp \dot{\tilde{q}}^{(2)} - \dot{q}^{(r)} \geq 0.$$

We now have an asymmetry in the system matrix in Eq. (2), which can be written as $H = H_0 \tilde{Q}$, where $\tilde{Q}$ is the block diagonal, symmetric and positive definite matrix representing the transformation in Eq. (4). If we assume that H_0 is a P_0 matrix, multiplicative properties of determinants lead to the conclusion that $H = H_0 \tilde{Q}$ is also P_0. But now that the bisymmetry is lost, H is no longer positive definite, and not copositive either. This brings questions regarding the solvability of the mixed system.

The plot in Fig. 1 is representative of numerical results which can be obtained with this method. The efficiency gain is obvious when counting the number of time steps required to simulate one period of a diode bridge. The order of the numerical method is low, but the efficiency gain is visible. We used large time steps here, one tenth of the period, to demonstrate how the nonsmooth stepping has good stability properties. Multidomain results are similar but would go beyond the scope here.

We have shown how non-smooth analytical systems dynamics can be formulated applied systematically to multidomain systems, and discretized to produce stable and efficient time-stepping schemes. Only natural boundary conditions for coupling different domains are used, and the technique allows for ideal, infinitely stiff couplings without artificial elasticity. There are open questions related to solvability, however, and the conversion of conventional models to this formulation is counter-intuitive.

References

1. F.A. Bornemann, *Homogenization in Time of Singularly Perturbed Mechanical Systems*, vol. 1687, Lecture Notes in Mathematics (Springer, Berlin, 1998)
2. R.W. Cottle, J.S. Pang, R.E. Stone, *The Linear Complementarity Problem*, Computer Science and Scientific Computing (Academic Press, New York, 1992)
3. A. De Felice, Are modified gravity models free of ghosts? J. Phys. A: Math. Theor. **40**(25), 7061 (2007)
4. A.V. Karapetian, On realizing nonholonomic constraints by viscous friction forces and Celtic stones stability. J. Appl. Math. Mech. **45**(1), 42–51 (1981)

5. C. Lacoursière, M. Linde, Spook: a variational time-stepping scheme for rigid multibody systems subject to dry frictional contacts. Technical report UMINF 11.09, Department of Computing Science, Umeà University (2011)
6. C. Lanczos, *The Variational Principles of Mechanics*, 4th edn. (Dover Publications, New York, 1986)
7. R.A. Layton, *Principles of Analytical System Dynamics*, Mechanical Engineering Series (Springer, Berlin, 1998)
8. R.I. Leine, U. Aeberhard, C. Glocker, Hamilton's principle as variational inequality for mechanical systems with impact. J. Nonlinear Sci. **19**(6), 633–664 (2009)
9. J.E. Marsden, M. West, Discrete mechanics and variational integrators. Acta Numer. **10**, 357–514 (2001)
10. D.E. Stewart, J.C. Trinkle, An implicit time-stepping scheme for rigid body dynamics with inelastic collisions and Coulomb friction. Int. J. Numer. Methods Eng. **39**, 2673–2691 (1996)

The Chaotic Behavior of Piecewise Smooth Dynamical Systems on Torus and Sphere

Ricardo M. Martins and Durval J. Tonon

Abstract In this work we discuss the appearance of minimal trajectories for the flow of piecewise smooth dynamical systems defined in the two dimensional torus and sphere in such a way that the switching manifold breaks the manifold into two connected components. We show that the number of pseudo-singularities of the sliding vector field is an invariant for the structural stability and study global bifurcations. Using a generic normal form, we prove that these systems can present chaotic behavior.

1 Introduction

In this paper we consider piecewise smooth dynamical systems of the form

$$\dot{\mathbf{x}} = \begin{cases} X(\mathbf{x}) & \text{if } \mathbf{x} \in \mathbb{M}^+, \\ Y(\mathbf{x}) & \text{if } \mathbf{x} \in \mathbb{M}^-, \end{cases} \tag{1}$$

where $\mathbb{M}$ is the sphere $\mathbb{S}^2$ or the torus $\mathbb{T}^2$ decomposed as $\mathbb{M} = \mathbb{M}^+ \cup \mathbb{M}^-$, with $\Sigma = \mathbb{M}^+ \cap \mathbb{M}^-$ a smooth curve breaking $\mathbb{M}$ into two connected components and X, Y are smooth vector fields on $\mathbb{M}$. The dynamics over Σ is defined to satisfy Filippov's convention; see Filippov [4]. A dynamical system like (1) will be denoted by (X, Y) and referred to as the vector field (1).

The theory of piecewise smooth vector fields has been developing very fast in the last years, mainly due to its strong relation with branches of applied science, such as mechanical, aerospace engineering, electrical and electronic engineering,

R.M. Martins (✉)
Institute of Mathematics, Statistics and Scientific Computing, University of Campinas, R. Sérgio Buarque de Holanda, 651, Campinas, São Paulo, Brazil
e-mail: rmiranda@ime.unicamp.br

D.J. Tonon
Institute of Mathematics and Statistics, Federal University of Goiás, Avenida Esperança s/n, Campus Samambaia, Goiânia, Goiás, Brazil
e-mail: djtonon@ufg.br

A. Colombo et al. (eds.), *Extended Abstracts Spring 2016*,
Trends in Mathematics 8, DOI 10.1007/978-3-319-55642-0_22

physics, economics, among others areas. Indeed, PSVF are in the boundary between mathematics, physics and engineering, see Makarenkov–Lamb [8] and Teixeira [10] for a recent survey on this subject, where models from control theory are discussed.

2 Main Results

Let $\mathbb{M}$ denote the two dimensional torus $\mathbb{T}^2$ or the sphere $\mathbb{S}^2$. In both cases, we will consider $\mathbb{M}$ obtained as the usual quotient of the square $I \times I = [0, 1] \times [0, 1]$.

Consider the switching manifold, denoted by Σ, as $\Sigma = \Sigma_1 \cup \Sigma_2 = \{(t, 0),\ t \in I\} \cup \{(t, \frac{1}{2}),\ t \in I\}$ for $\mathbb{M} = \mathbb{T}^2$, and $\Sigma = \{(t, \frac{1}{2}),\ t \in I\}$ for $\mathbb{M} = \mathbb{S}^2$. With the usual topologies on $I \times I$ generating $\mathbb{M}$, these choices of Σ break $\mathbb{M}$ into two connected components, $\mathbb{M}^+ = \mathbb{M} \cap (I \times [1/2, 1])$ and $\mathbb{M}^- = \mathbb{M} \cap (I \times [0, 1/2])$.

In this paper we study piecewise smooth vector fields $X = (X^+, X^-)$, where X^+ is defined on $\mathbb{M}^+$, and X^- is defined on $\mathbb{M}^-$. Over $\Sigma = \mathbb{M}^+ \cap \mathbb{M}^-$ we adopt Filippov's convention.

Our main goal is to describe the global dynamics of X in the cases where the singularities of X are generic or do not exist (regular case). The main techniques used are the theory of contact between a smooth vector field with the switching manifold and the dynamics of the first return map, which may be generalized to higher dimensions. We also employ a version of the Poincaré–Bendixson Theorem that was proved recently for PSVF on the plane; see Buzzi–de-Carvalho–Euzébio [1].

Local normal forms for the two dimensional case are exhibit in Guardia–Seara–Teixeira [5] and Kuznetsov–Rinaldi–Gragnani [7]. Therefore, we start the study of global dynamics on the two dimensional torus and sphere considering these families (only codimension zero). However, the normal forms of codimension zero for the three dimensional case (where the approach developed in this paper can be adapted) are exhibited in Carvalho–Tonon [3].

The main results are the following.

Theorem 1 *Let X be a PSVF defined on $\mathbb{M}$ with switching manifold Σ. Suppose that X is regular-transversal to Σ, without singularities or tangencies, taken in its normal form $X = (X^+, X^-)$, where $X^+(x, y) = (a, \sigma_1)$ and $X^-(x, y) = (b, \sigma_2)$, with $\sigma_i = \pm 1$, $i = 1, 2$.*

(i) If $\sigma_1\sigma_2 > 0$ and $\mathbb{M} = \mathbb{T}^2$ the trajectories of X are periodic if $a \pm b \in \mathbb{Q}$; otherwise, $\mathbb{M}$ is a non trivial wandering set.

(ii) If $\sigma_1\sigma_2 > 0$ and $\mathbb{M} = \mathbb{S}^2$ the trajectories of X connect the north and south poles of the sphere.

(iii) If $\sigma_1\sigma_2 < 0$ then the switching manifold presents a sliding motion that is a global attractor or repeller, according to the signs of σ_1 and σ_2.

Proof For proving (iii), note that if $\sigma_1\sigma_2 < 0$ then the system presents a sliding motion on one of components of the switching manifold, and the dynamics on the manifold is constant.

Now we prove (i) where $\mathbb{M} = \mathbb{T}^2$. Note that the existence of periodic orbits is equivalent to the existence of $n_0 \in \mathbb{N}$ such that $\varphi_X^{n_0}(p) = kp$, where $k \in \mathbb{N}$, $p \in \Sigma_1$ and φ_X is the flow of X. Given $p = (x, 0) \in \Sigma_1$ we get $\phi_{X^-}(p) = (a/2\sigma_1 + x, 1/2) = (x_2, 1/2)$ and $\phi_{X^+}(x_2, 1/2) = (a/2\sigma_1 + b/2\sigma_2 + x, 1) = (x_3, 1)$.

In this case, the global dynamics of X is given by the first return map and we can write explicity

$$\varphi_X^n(x, 0) = \overline{\left(\frac{n}{2}\left(\frac{a}{2\sigma_1} + \frac{b}{2\sigma_2}\right) + x, \frac{n}{2}\right)} \tag{2}$$

for $n \geq 2$, where overline denotes the representant of the class of equivalence (with respect to the equivalence relations $(x, 0) \sim (x, 1)$ and $(0, y) \sim (1, y)$ for defining the torus on $I \times I$).

Therefore, the necessary and sufficient condition to get periodic orbits, in this case, is $\overline{\varphi_X^{n_0}(x, 0)} = \overline{(x, 0)}$, for some $n_0 \in \mathbb{N}$. By (2), the last equation is satisfied if and only if

$$\frac{n_0}{4}\left(\frac{a\sigma_2 + b\sigma_1}{\sigma_1\sigma_2}\right) \in \mathbb{Z}$$

or, equivalently, $a \pm b \in \mathbb{Q}$. So, we conclude that there exist periodic orbits for X if and only if $a \pm b \in \mathbb{Q}$. Otherwise, if $a \pm b \notin \mathbb{Q}$, then the orbits of X are not periodic and X does not have singular points. Therefore, by applying the version of Poincaré–Bendixson Theorem for PSVF in Buzzi–de-Carvalho–Euzébio [1], we conclude that the orbits of X, in this case, are dense. This ends the proof of (i). The proof of (ii) is similar, but one has to recall that every trajectory connecting the top and bottom borders of the square are connecting the north and south poles of $\mathbb{S}^2$. □

Theorem 1 is a piecewise smooth version of the well know Kronecker–Weyl Equidistribution Theorem; see Hasselblatt–Katok [6, Proposition 4.2.1]. However, our approach is distinctly from that used in the proof of this theorem. In the present case, we analyse directly the dynamics of the first return map in the context of PSVF.

In the case where the PSVF present a finite number of fold singularities or a finite number of critical points of the sliding vector field, the topological behavior of X changes drastically when the number of these points changes. In particular, the presence of chaotic behavior is a generic property in the sense of Buzzi–de-Carvalho–Euzébio [2].

Theorem 2 *Let $X = (X^+, X^-)$ be a PSVF on $\mathbb{M}$, where X^+ is a linear flow transversal to Σ, and X^- is a vector field without singularities on $\mathbb{M}^-$ and with a finite and even number of visible tangencies. Then,*

(i) if $\mathbb{M} = \mathbb{T}^2$, generically X is chaotic on $\mathbb{T}^2$, that is, X is topologically transitive and present sensitive dependence on the initial conditions;

(ii) if $\mathbb{M} = \mathbb{S}^2$, generically $\mathbb{M} = \mathbb{M}_h \cup \mathbb{M}_c$, where $\mathbb{M}_h, \mathbb{M}_c$ are open invariant sets, $\mathbb{M}_h$ is foliated by homoclinic trajectories, and X restricted to $\mathbb{M}_c$ has a chaotic behavior (in the sense of [2]), with $\overline{\mathbb{M}}_h \cap \overline{\mathbb{M}}_c$ a homoclinic trajectory.

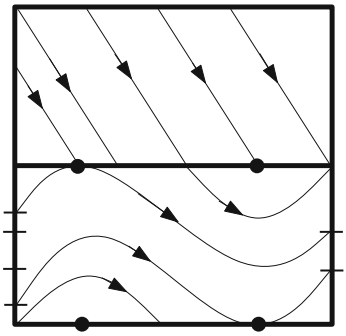

Fig. 1 Dynamics of $X = (X^+, X^-)$ on the hypotheses of Theorem 2

A proof of Theorem 2 can be found in Martins–Tonon [9], and Fig. 1 illustrates its dynamics.

Acknowledgements R.M. Martins is supported by FAPESP-Brazil project 2015/06903-8. D.J. Tonon is supported by grant#2012/10 26 7000 803, Goiás Research Foundation (FAPEG), PROCAD/CAPES grant 88881.0 68462/2014-01 and CNPq-Brazil grants 478230/2013-3 and 443302/-2014-6. This work was partially realized at UFG/Brazil as a part of project numbers 35796 and 040393 and also at CRM Barcelona, Spain. Part of this work was done during a visit of the first author to CRM Barcelona, Spain.

References

1. C. Buzzi, T. de Carvalho, R.D. Euzébio, On Poincaré–Bendixson theorem and non-trivial minimal sets in planar non smooth vector fields, arXiv:1307.6825
2. C.A. Buzzi, T. de Carvalho, R.D. Euzébio, Chaotic planar piecewise smooth vector fields with non trivial minimal sets. Ergod. Theory Dyn. Syst. (2014), http://journals.cambridge.org/abstract_S0143385714000674
3. T. de Carvalho, D.J. Tonon, Structural stability and normal forms of piecewise smooth vector fields on $\mathbb{R}^3$. Publ. Math. Debr. **86**, 1–20 (2015)
4. A.F. Filippov, *Differential Equations with Discontinuous Righthand Sides*, vol. 18, Mathematics and its Applications (Soviet Series) (Kluwer Academic Publishers Group, Dordrecht, 1988)
5. M. Guardia, T.M. Seara, M.A. Teixeira, Generic bifurcations of low codimension of planar Filippov systems. J. Differ. Equ. **250**, 1967–2023 (2011)
6. B. Hasselblatt, A. Katok, *Introduction to the Modern Theory of Dynamical Systems* (Cambridge University Press, Cambridge, 1995)
7. Yu.A. Kuznetsov, S. Rinaldi, A. Gragnani, One-parameter bifurcations in planar Filippov systems. Int. J. Bifurc. Chaos **13**(8), 2157–2188 (2003)
8. O. Makarenkov, J.S.W. Lamb, Dynamics and bifurcations of nonsmooth systems: a survey. Phys. D: Nonlinear Phenom. **241**, 1826–1844 (2012)
9. R.M. Martins, D.J. Tonon, Chaos in piecewise smooth vector fields on two dimensional torus and sphere, arXiv:1601.05670 [math.DS]
10. M.A. Teixeira, Perturbation theory for nonsmooth systems. Meyers: Encycl. Complex. Syst. Sci. **152** (2008)

Non-smooth Hopf-Type and Grazing Bifurcations Arising from Impact/Friction Contact Events

Karin Mora and Chris Budd

Abstract A new discontinuity-induced bifurcation, referred to as *nonsmooth Hopf-type bifurcation*, observed in a nonautonomous impacting hybrid systems in $\mathbb{R}^4$ is presented. The system studied models the bouncing motion, repeated instantaneous impacts with friction, in rotating machines with magnetic bearing support. At the nonsmooth Hopf-type bifurcation point a stable regular equilibrium and two unstable small amplitude 1-impact periodic orbits arise. The existence of this bifurcation scenario depends on a complex relationship between damping, the restitution, and the friction coefficient.

1 Introduction

Rotating machines with magnetic bearing support comprise a set of electromagnets which enable the levitation of a driven rotating beam. Their operation can be compromised, even result in destruction, through the interactions between the rotor and the touchdown bearing (TDB), which protects the rotor and other components. Assuming these interactions are instantaneous impacts, also referred to as bouncing, a hybrid system formalism can be adopted to study the dynamics and bifurcation structure.

The analysis of similar systems but without damping and/or stiffness has shown that these systems exhibit rich complex dynamics and *discontinuity-induced bifurcations* (DIB): Childs [1] showed that impact dynamics can give rise to parametric excitation in rotating machines; Li–Païdoussis [4] studied numerically the bifurcation structure of a simplified model without stiffness and damping; Lu–Li–Twizell [5] derive the existence condition for periodic orbits with one impact per period, referred to as 1-impact periodic orbits, in an undamped system, and Keogh–Cole [3] showed such orbits can also be observed in a system with damping and stiffness.

K. Mora (✉)
Department of Mathematics, University of Paderborn, Paderborn, Germany
e-mail: kmora@math.uni-paderborn.de

C. Budd
Department of Mathematics, University of Bath, Bath, UK

A. Colombo et al. (eds.), *Extended Abstracts Spring 2016*,
Trends in Mathematics 8, DOI 10.1007/978-3-319-55642-0_23

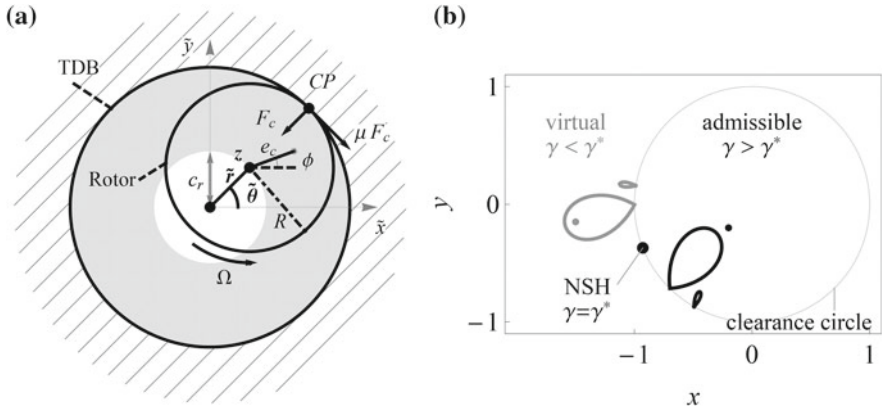

Fig. 1 (**a**) Schematic of a rotating machine with impact at the contact point CP. (**b**) Schematic of the nonsmooth Hopf-type bifurcation (NSH) at γ^* in phase space (x, y). As γ decreases towards γ^* the admissible equilibrium (*black dot*) and periodic orbits (*black loops*) bifurcate into virtual orbits (*grey*) at the NSH point. The amplitudes of the 1-impact periodic orbits (loops) vanish at the NSH point

In this work we adopt the latter spring-damper model, where Newton's law of restitution and Coulombs friction law account for the energy dissipation during impact; see Fig. 1a. We systematically analyse DIBs in impacting hybrid systems by studying 1-impact periodic orbits in the rotating frame. Due to the geometry of the problem, different coordinate systems are exploited to show how a seemingly degenerate bifurcation corresponds to a known one. We also show that one scenario, the *nonsmooth Hopf-type bifurcation*, is new. At this bifurcation point, a stable regular equilibrium and two unstable 1-impact periodic orbits arise; see Fig. 1b. The existence of this scenario depends on a complex relationship between damping, the restitution, and the friction coefficient. The majority of this extended abstract summarises the results reported in Mora–Budd–Glendinning–Keogh [6].

2 Magnetic Bearing System as an Impacting Hybrid System

2.1 Equation of Motion in Free Flight

We consider a simplified mechanical model of a rigid magnetic bearing system comprising a rotor spinning with constant speed $\Omega > 0$ within a clearance radius c_r to the fixed TDB; see Fig. 1a. The rotor has radius R and mass m. The system is under proportional-integral-derivative (PID) control and thus the effect of the magnetic bearing on the rotor's response can be modelled by a linear spring–damper system with stiffness k and damping c. In free flight, the complex equation of motion

of the rotor with centre $z \in \mathbb{C}$ is given by

$$m\ddot{z}(\tau) + c\dot{z}(\tau) + kz(\tau) = f_u\, e^{i\Omega\tau}, \qquad \text{if} \quad |z(\tau)| < c_r, \tag{1}$$

where the $(\dot{})$ denotes the derivative with respect to time τ, $f_u \in \mathbb{C}$ is the mass unbalance force with $f_u = m\, e_c\, \Omega^2 e^{i\phi}$ and depends on the unbalance eccentricity e_c, and unbalance phase ϕ. Below we alternate between Cartesian coordinates $z = \tilde{x} + i\,\tilde{y}$ and polar coordinates $z = \tilde{r}e^{i\tilde{\theta}}$ to better illustrate the system's properties.

2.2 Reset Law

The *reset* law describes the velocity change of the dynamical system (1) at the i-th impact, i.e., if $|z_i| = c_r$, at time τ_i with $i \in \{0, 1, 2, \ldots\}$. It maps the velocity immediately before impact $\dot{z}_{i,-} := \dot{z}(\tau_{i,-})$ to the corresponding velocity immediately after impact $\dot{z}_{i,+} := \dot{z}(\tau_{i,+})$, while the position z_i is unaffected by the impact, i.e., $z_{i,-} = z_{i,+} = z_i$.

We make three assumptions to obtain the reset law. Firstly, the TDB behaves like an infinitely stiff surface, which cannot be penetrated. Then, the finite contact forces are approximated by idealized impulsive normal and tangential forces, F_c and F_f, respectively. Secondly, the rotational speed $\Omega > 0$ is large and thus unaffected by the impact, and it remains fixed. Thirdly, both Ω and the radii ratio R/c_r are large, so that the relative velocity $v_{rel,i,\pm}$ at the contact point CP,

$$v_{rel,i,\pm} = R\Omega + c_r\dot{\tilde{\theta}}_{i,\pm}, \qquad \text{if} \quad |z_i| = c_r,$$

does not change sign and remains positive during an impact; see Fig. 1a. Then, the reset law is consistent with other restitution models such as the kinematic and energetic impact law; see Nordmark–Dankowicz–Champneys [7]. The reset law, derived by applying the law of momentum conservation as well as F_c and F_f, can be stated in polar coordinates

$$\dot{\tilde{r}}_{i,+} = -d\dot{\tilde{r}}_{i,-}, \quad \text{and} \quad \dot{\tilde{\theta}}_{i,+} = \dot{\tilde{\theta}}_{i,-} - \mu(1+d)\frac{\dot{\tilde{r}}_{i,-}}{c_r}, \qquad \text{if} \quad |z_i| = c_r, \tag{2}$$

where d is the restitution coefficient, and μ is the friction coefficient.

2.3 Scaling and the Rotating Frame

The hybrid dynamical system (1), (2) is simplified by introducing dimensionless time $t = \Omega\tau$, and radius $r = \tilde{r}/c_r$, and by observing the system in the rotating frame, i.e.,

we introduce the complex coordinate $U = x + iy = re^{i\theta}$ with $\theta = \tilde{\theta} - t$. Then the equation of motion (1) in the rotating frame can be expressed in terms of the complex vector $\boldsymbol{w}(t) = \left(U(t), \dot{U}(t)\right)^{\mathsf{T}}$,

$$\dot{\boldsymbol{w}}(t) = A\boldsymbol{w}(t) + \boldsymbol{b}, \quad \text{if} \quad |U| \leq 1, \tag{3}$$

where the matrix A and the vector $\boldsymbol{b}$ are constant,

$$A = \begin{pmatrix} 0 & 1 \\ 1 - \omega^2 - i\gamma & -\gamma - 2i \end{pmatrix} \quad \text{and} \quad \boldsymbol{b} = \begin{pmatrix} 0 \\ \rho e^{i\phi} \end{pmatrix},$$

and where $\gamma = c/(m\Omega)$ is the scaled damping, $\omega^2 = k/(m\Omega^2)$ is the scaled stiffness, and $\rho = e_c/c_r$ is the scaled eccentricity radius. Similarly, the reset law (2) takes the form

$$\boldsymbol{w}_{i,+} = \boldsymbol{w}_{i,-} - \begin{pmatrix} 0 \\ (1+d)(1+i\mu)\dot{r}_{i,-}\ U_i \end{pmatrix}, \quad \text{if} \quad |U| = 1. \tag{4}$$

The impact surface is $\Sigma := \{\boldsymbol{w} : |U| = 1\}$. Orbits which are physically realistic are referred to as *admissible*, and *virtual* otherwise. Periodic orbits with one impact per period in the rotating frame are referred to as *1-impact periodic orbits*.

3 1-Impact Periodic Orbit

To derive the global necessary existence and stability conditions of the 1-impact periodic orbit, the Poincaré map $P_I : \Sigma \to \Sigma$, $\boldsymbol{w}_{i+1,-} = P_I(\boldsymbol{w}_{i,-})$ is applied. This map is nonlinear in general, uniquely defined if $\dot{r}_{i,-} > 0$ and smooth, provided that $\dot{r}_{i+1,-} > 0$; see di-Bernardo–Budd–Champneys–Kowalczyk [2]. 1-impact periodic orbits are fixed points of P_I. A system of algebraic equations derived from the hybrid flow of (3), (4) determine the impact period $T = T(\gamma, \omega, d, \mu)$, which does not depend on the unbalance force, the impact angle $\theta_{i,-} = \theta_{i,-}(T, \dot{r}_{i,-})$, the normal velocity $\dot{r}_{i,-} = \dot{r}_{i,-}(T)$, and the tangential velocity $\dot{\theta}_{i,-} = \dot{\theta}_{i,-}(T, \dot{r}_{i,-})$.

The global analysis of 1-impact periodic orbits shows that the impact map P_I can have at most finitely many fixed points with pairs of orbits having the same period. For the bifurcation analysis below we only consider the four orbits with the smallest period T_a, T_b, T_c, and T_d. They are the most likely orbits to be admissible. The larger the impact period T the more likely it is that the trajectories cross the boundary between the Poincaré points; this sufficient condition has to be determined numerically. The numerical stability analysis has shown that only one of these orbits, with period T_d and large amplitude, is stable.

The trajectories of these four orbits in the fixed frame correspond to periodic orbits if the ratio of the impact period and the period of the rotating frame $T/(2\pi)$ is a rational number. Otherwise these trajectories are impacting quasi-periodic orbits.

4 Nonsmooth Hopf-Type and Other Discontinuity-Induced Bifurcations

In this section we give a brief overview of the DIBs observed in the system (3), (4), as the scaled damping parameter γ is varied. We also show that the coordinate frame is crucial for classifying DIB scenarios.

The hybrid system in the co-rotating frame (3) has a stable equilibrium solution $\boldsymbol{w} = \boldsymbol{w}^* := -A^{-1}\boldsymbol{b}$ when impacts are absent. When it crosses the boundary $|U| = 1$ it transitions from an admissible to a virtual equilibrium in a boundary equilibrium bifurcation (BEB) at the point $\boldsymbol{w} = -A^{-1}\boldsymbol{b}$, $\gamma = \gamma^* := \sqrt{\rho^2 - (1-\omega^2)^2}$. In the fixed frame, this equilibrium corresponds to a periodic orbit with period 2π, which undergoes a degenerate grazing bifurcation for $\gamma = \gamma^*$. We consider this bifurcation degenerate as the orbit lies tangential to the impact surface Σ along the entire boundary.

Four 1-impact periodic orbits are created in a smooth fold bifurcation at $\gamma = \gamma_{F,1}$. If $\gamma^* < \gamma_{F,1}$, then these four orbits are admissible and as γ decreases the two small amplitude orbits undergo a second bifurcation with the regular equilibrium $\boldsymbol{w} = \boldsymbol{w}^*$ at the point $\gamma = \gamma^*$; see Fig. 1b. At this point all admissible orbits become virtual. This is a new type of DIB and is termed *nonsmooth Hopf-type* bifurcation (NSH) due to its nature. In the fixed frame, this scenario corresponds to the bifurcation of one nonimpacting periodic orbit, with period 2π which grazes, and two periodic or quasi-periodic orbits, i.e., if $T/(2\pi) \in \mathbb{Q}$ or $T/(2\pi) \in \mathbb{R} \setminus \mathbb{Q}$, respectively. Thus, it does not correspond to the nonsmooth fold bifurcation scenario; see di-Bernardo–Budd–Champneys–Kowalczyk [2]. If $\gamma^* > \gamma_{F,1}$ then only two of the 1-impact periodic orbits are admissible and the nonsmooth Hopf-type bifurcation is not observed.

Numerically, we have observed that, setting the friction coefficient μ to zero, with the same system parameters that give rise to four admissible 1-impact periodic orbits, only orbits with very large period $T > 20$ exist. The trajectories of these orbits are very likely not admissible. Thus we conjecture that the friction coefficient is a critical parameter for the existence of 1-impact periodic orbits and for observing the NSH bifurcation.

References

1. D.W. Childs, Rub-induced parametric excitation in rotors. ASME J. Mech. Des. **101**, 640–644 (1979)
2. M. di Bernardo, C. Budd, A. Champneys, P. Kowalczyk, *Piecewise-smooth Dynamical Systems: Theory and Applications*. Applied Mathematical Sciences, vol. 163 (Springer, London, 2008)
3. P.S. Keogh, M.O.T. Cole, Rotor vibration with auxiliary bearing contact in magnetic bearing systems part 1: synchronous dynamics. Proc. Inst. Mech. Eng. C J. Mech. Eng. Sci. **217**, 377–392 (2003)
4. G.X. Li, M.P. Païdoussis, Impact phenomena of rotor-casing dynamical systems. Nonlinear Dyn. **5**, 53–70 (1994)

5. Q.S. Lu, Q.H. Li, E.H. Twizell, The existence of periodic motions in rub-impact rotor systems. J. Sound Vib. **264**, 1127–1137 (2003)
6. K. Mora, C. Budd, P. Glendinning, P. Keogh, Non-smooth Hopf-type bifurcations arising from impact-friction contact events in rotating machinery. Proc. R. Soc. A **470**, 2171 (2014)
7. A.B. Nordmark, H. Dankowicz, A.R. Champneys, Discontinuity-induced bifurcations in systems with impacts and friction: discontinuities in the impact law. Int. J. Nonlinear Mech. **44**, 1011–1023 (2009)

Number of Limit Cycles for Some Non-generic Classes of Piecewise Linear Differential Systems

Douglas D. Novaes

Abstract Recently, some upper bounds were found for the maximum number of limit cycles for some non-generic classes of planar piecewise linear differential systems with two zones separated by a straight line. However, many distinct cases were considered. Here the main properties of those classes are identified, this allows us to unify the approach and to extend the results. We also study a new class of differential systems.

1 Introduction and Statements of the Main Results

Let $F^{\pm}(x, y) = A^{\pm}(x, y)^T + (b_1^{\pm}, b_2^{\pm})$, $A^{\pm} = (a_{ij}^{\pm})_{2\times 2}$, be linear vector fields. This work is concerned about crossing limit cycles of piecewise linear differential systems having the form

$$\left(\dot{x}, \dot{y}\right)^T = Z(x, y) = \left(F^+, F^-\right)(x, y) = \begin{cases} F^+(x, y) & \text{if} \quad x \geq 0, \\ F^-(x, y) & \text{if} \quad x \leq 0. \end{cases} \tag{1}$$

Denote by $\Sigma = \{(x, y) : y = 0\}$ the set of discontinuity of (1). From now on, a crossing limit cycle will be called only by limit cycle.

It was conjectured in Han–Zhang [5] that a planar piecewise linear differential system with two zones separated by a straight line has at most two limit cycles. A negative answer for this conjecture was provided in Huan–Yang [6] via a numerical example having three limit cycles. Analytical proofs for the existence of these three limit cycles were given in [3, 7]. Finally, in Freire–Ponce–Torres [4] some general conditions were studied to obtain these three limit cycles. Recently, perturbative techniques (see [9, 10]) were used together with newly developed tools on Chebyshev systems (see Novaes–Torregrosa [12]) to obtain three limit cycles in such systems.

D.D. Novaes (✉)
Departamento de Matemática, Universidade Estadual de Campinas,
Rua Sérgio Baruque de Holanda 651, Cidade Universitária Zeferino Vaz,
Campinas, São Paulo 13083–859, Brazil
e-mail: ddnovaes@ime.unicamp.br

A. Colombo et al. (eds.), *Extended Abstracts Spring 2016*,
Trends in Mathematics 8, DOI 10.1007/978-3-319-55642-0_24

When a general curve of discontinuity is considered instead of a straight line, there is no upper bound for the maximum number of limit cycles that a differential system of this family can have. It is a consequence of a conjecture stated in Braga–Mello [1] and then proved in Novaes–Ponce [11].

It is easy to see that $a_{12}^{\pm} > 0$ is a necessary condition for the existence of crossing limit cycles (see Freire–Ponce–Torres [2]). So, define

$$\delta^{\pm} = \frac{a_{22}^{\pm}}{a_{12}^{\pm}} b_1^{\pm} - b_2^{\pm}.$$

Let $\det(\cdot)$ and $\mathrm{tr}(\cdot)$ denote the determinant and the trace of a matrix, respectively. When $\det(A^{\pm}) \neq 0$ the vector field $F^{\pm}$ vanishes at the point

$$\left(x^{\pm}, y^{\pm}\right) = \left(\frac{a_{12}^{\pm} b_2^{\pm} - a_{22}^{\pm} b_1^{\pm}}{\det(A^{\pm})}, \frac{a_{21}^{\pm} b_1^{\pm} - a_{11}^{\pm} b_2^{\pm}}{\det(A^{\pm})} \right).$$

Note that $x^{\pm} = -a_{12}^{\pm} \delta^{\pm} / \det(A^{\pm})$.

In Llibre–Novaes–Teixeira [8], tools and ideas to estimate bounds on the maximum number of limit cycles that the differential system (1) can have were introduced. The equality $\mathrm{tr}(A^+)\mathrm{tr}(A^-) = 0$ was assumed in some of the cases considered there. The ideas of [8] can be followed straightly to obtain the next result.

Theorem 1 *If $tr(A^+)tr(A^-) = 0$, then the differential system (1) admits at most two limit cycles and this maximum is reached.*

Among all the cases addressed in [8], assuming that the lateral differential systems are non–singular, the authors also proved that if one of the lateral differential systems, F^+ or F^-, has a singularity on the line of discontinuity Σ then the differential system (1) can have at most two limit cycles. This result can be generalized as follows.

Theorem 2 *If $\delta^+ \delta^- = 0$ then the differential system (1) admits at most two limit cycles and this maximum is reached.*

In the above case, the equality $\mathrm{tr}(A^+)\mathrm{tr}(A^-) = 0$ is not assumed. In this direction a third result is obtained.

Theorem 3 *If $tr(A^+) + tr(A^-) = 0$, $\det(A^+) - \det(A^-) = 0$, and $\delta^+ + \delta^- = 0$, then the differential system (1) does not admit limit cycles.*

Let $F(x, y)$ be a linear vector field, and let $R(x, y) = (-x, y)$ be an involution. Assume that $F^+(x, y) = F(x, y)$ and $F^-(x, y) = -R \circ F \circ R(x, y + k)$, $k \in \mathbb{R}$. It easy to see that $Z = (F^+, F^-)$ satisfies the hypotheses of Theorem 3. The proof of Theorem 3 follows by showing that differential systems for which their hypotheses hold are actually equivalent to a differential system $Z = (F^+, F^-)$ such that $F^-(x, y) = -R \circ F \circ R(x, y + k)$. In this case, if $k = 0$ then Z is R–reversible which implies the non–existence of limit cycles. The parameter k breaks the reversibility, however limit cycles cannot appear.

In Sect. 2 some preliminary results are introduced. In Sect. 3 the proofs of Theorems 1, 2, and 3 are discussed. The proof of Theorem 3 is treated with more detail.

2 Preliminar Results

As usual, the following open regions are distinguished on Σ: *Crossing Region:* $\Sigma^c = \{p \in \Sigma : F_1^+(p)F_1^-(p) > 0\}$; *Escaping Region:* $\Sigma^e = \{p \in \Sigma : F_1^+(p) > 0, F_1^-(p) < 0\}$; and *Sliding Region:* $\Sigma^s = \{p \in \Sigma : F_1^+(p) < 0, F_1^-(p) > 0\}$. Let $\Sigma^{c^+} \subset \Sigma^c$ denote the points $p \in \Sigma^c$ such that $F_1^+(p) > 0$ and $F_1^-(p) > 0$.

Denote by $\varphi^{\pm}(t, x, y) = \left(\varphi_1^{\pm}(t, x, y), \varphi_2^{\pm}(t, x, y)\right)$ the solutions of the lateral differential systems $(\dot{x}, \dot{y})^T = F^{\pm}(x, y)$ such that $\varphi^{\pm}(0, x, y) = (x, y)$. The existence of an interval domain $I \subset \Sigma^{c^+}$ and functions $t^{\pm} : I \to \mathbb{R}^{\pm}$, such that, for $y \in I$, $\varphi_1^{\pm}(t^{\pm}(y), 0, y) = 0$, $\varphi_1^+(t, 0, y) > 0$ for every $0 < t < t^+(y)$, and $\varphi_1^-(t, 0, y) < 0$ for every $t^-(y) < t < 0$ is a necessary condition for the existence of limit cycles. In this case, the differential system (1) admits a limit cycle passing through $(0, y^*)$, $y^* \in I$, if and only if y^* is a solution of the equation

$$f(y) \doteq \varphi_2^+(t^+(y), 0, y) - \varphi_2^-(t^-(y), 0, y) = 0. \tag{2}$$

In general the functions $t^{\pm}(y)$ cannot be obtained explicitly. However, their inverse $\xi^{\pm} : t^{\pm}(I) \to I$ may be explicitly computed.

Proposition 4 *Assume that there exist an interval domain $I \subset \Sigma^{c^+}$ and functions $t^{\pm} : I \to \mathbb{R}^{\pm}$, such that, for $y \in I$, $\varphi_1^{\pm}(t^{\pm}(y), 0, y) = 0$, $\varphi_1^+(t, 0, y) > 0$ for every $0 < t < t^+(y)$, and $\varphi_1^-(t, 0, y) < 0$ for every $t^-(y) < t < 0$. Then, $t^{\pm}(y)$ are invertible and their inverses $\xi^{\pm} : t^{\pm}(I) \to I$ satisfy $\varphi_1^{\pm}(t, 0, \xi^{\pm}(t)) = 0$ for every $t \in t^{\pm}(I)$.*

In Freire–Ponce–Torres [2], assuming $a_{12}^+ a_{12}^- > 0$, which is a necessary condition for the existence of limit cycles, the authors provided the following normal form for the differential system (1):

$$\left(\dot{\widetilde{x}}, \dot{\widetilde{y}}\right)^T = \begin{cases} \widetilde{F}^+(\widetilde{x}, \widetilde{y}) & \text{if } \widetilde{x} > 0, \\ \widetilde{F}^-(\widetilde{x}, \widetilde{y}) & \text{if } \widetilde{x} < 0, \end{cases} \tag{3}$$

$$\widetilde{F}^+(\widetilde{x}, \widetilde{y}) = \begin{pmatrix} T^+ & -1 \\ D^+ & 0 \end{pmatrix} \begin{pmatrix} \widetilde{x} \\ \widetilde{y} \end{pmatrix} - \begin{pmatrix} -k \\ a^+ \end{pmatrix},$$

$$\widetilde{F}^-(\widetilde{x}, \widetilde{y}) = \begin{pmatrix} T^- & -1 \\ D^- & 0 \end{pmatrix} \begin{pmatrix} \widetilde{x} \\ \widetilde{y} \end{pmatrix} - \begin{pmatrix} 0 \\ a^- \end{pmatrix},$$

with $T^{\pm} = \operatorname{tr}(A^{\pm})$, $D^{\pm} = \det(A^{\pm})$, and

$$a^- = a_{12}^- b_2^- - a_{22}^- b_1^-, \quad k = \frac{a_{12}^-}{a_{12}^+} b_1^+ - b_1^-, \quad a^+ = \frac{a_{12}^-}{a_{12}^+}\left(a_{12}^+ b_2^+ - a_{22}^+ b_1^+\right).$$

The homeomorphism h, which transforms the differential system (1) into the canonical form (3), leaves the line of discontinuity Σ invariant. The crossing and sliding sets, tangency points, and boundary equilibria of the original differential system (1) are transformed by h into sets and points of the same type by the differential system (3). Moreover, there is a topological equivalence between the differential systems (1) and (3) for all their orbits not having points in common with the sliding set.

3 Sketches of the Proofs of the Main Results

The proofs of Theorems 1 and 2 follow by finding explicitly at least one of times $t^+(y)$ or $t^-(y)$. It is assured by hypotheses. Without loss of generality, suppose that one is able to find $t^-(y)$. Using Proposition 4 to invert the function $t^+(y)$ (which from hypotheses can be found explicitly as $\xi^+(t)$) Eq. (2) becomes equivalent to

$$g(t) \doteq f(\xi^+(t)) = \varphi^+(t, 0, \xi^+(t)) - \varphi^-(t^-(\xi^+(t)), 0, \xi^+(t)) = 0,$$

for which the number of solutions can be estimated; see Llibre–Novaes–Teixeira [8].

To see Theorem 3, take $F^{\pm}(x, y) = A^{\pm}(x, y)^T + (b_1^{\pm}, b_2^{\pm})$, $A^{\pm} = (a_{ij}^{\pm})_{2\times 2}$, and assume that $\operatorname{tr}(A^+) + \operatorname{tr}(A^-) = 0$, $\det(A^+) - \det(A^-) = 0$, and $\delta^+ + \delta^- = 0$. Thus the differential system (1) is transformed into the canonical form (3), where

$$\widetilde{F}^+(\widetilde{x}, \widetilde{y}) = \begin{pmatrix} T & -1 \\ D & 0 \end{pmatrix}\begin{pmatrix} \widetilde{x} \\ \widetilde{y} \end{pmatrix} - \begin{pmatrix} -k \\ a \end{pmatrix},$$
$$\widetilde{F}^-(\widetilde{x}, \widetilde{y}) = \begin{pmatrix} -T & -1 \\ D & 0 \end{pmatrix}\begin{pmatrix} \widetilde{x} \\ \widetilde{y} \end{pmatrix} - \begin{pmatrix} 0 \\ -a \end{pmatrix},$$

T and D are the trace and the determinant of the matrix A^+, respectively, $a = a^+$, and $k = (a_{12}^-/a_{12}^+)b_1^+ - b_1^-$. Taking the involution $R(x, y) = (-x, y)$, the relation $\widetilde{F}^-(x, y) = -R \circ \widetilde{F}^+ \circ R(x, y + k)$ is obtained. From now on we shall drop the tildes. As before, $\varphi^{\pm}(t, x, y) = \left(\varphi_1^{\pm}(t, x, y), \varphi_2^{\pm}(t, x, y)\right)$ denote the solutions of the lateral differential systems $(\dot{x}, \dot{y})^T = F^{\pm}(x, y)$ such that $\varphi^{\pm}(0, x, y) = (x, y)$. It is easy to see that $\varphi_1^-(t, x, y) = -\varphi_1^+(-t, -x, y + k)$ and $\varphi_2^-(t, x, y) = \varphi_2^+(-t, -x, y + k) - k$.

As a necessary condition for the existence of periodic solutions, assume the existence of an interval domain $I \subset \Sigma^{c^+}$ and a function $t^+ = \tau \colon I \to \mathbb{R}^+$, such that, for $y \in I$, $\varphi_1^+(\tau(y), 0, y) = 0$ and $\varphi_1^+(t, 0, y) > 0$ for every $0 < t < \tau(y)$. Note

that, in this case, $t^-(y) = -\tau(y+k)$. Indeed $\varphi_1^-(-\tau(y+k), 0, y) = -\varphi_1^+(\tau(y+k), 0, y+k) = 0$, and $\varphi_1^-(t, 0, y) = -\varphi_1^+(-t, 0, y+k) < 0$ for every $-\tau(y+k) < t < 0$ and $y + k \in I$. Let $\varphi_i = \varphi_i^+$ so, Eq. (2) reads

$$\begin{aligned} f(y) &= \varphi_2^+(\tau(y), 0, y) - \varphi_2^-(-\tau(y+k), 0, y) \\ &= \varphi_2(\tau(y), 0, y) - \varphi_2(\tau(y+k), 0, y+k) + k = 0. \end{aligned}$$

From the above expression it follows that the equation $f(y) = 0$, for $k \neq 0$, does not have solution for $y \in I$. Indeed, without loss of generality, assume that $y > 0$; if $k > 0$ then the first return of y to Σ, $\varphi_2(\tau(y), 0, y)$, is strictly greater than the first return of $y + k$ to Σ, $\varphi_2(\tau(y+k), 0, y+k)$. Therefore, $\varphi_2(\tau(y), 0, y) - \varphi_2(\tau(y+k), 0, y+k) > 0$ and consequently $f(y) > 0$. Analogously, if $k < 0$ we would conclude that $f(y) < 0$.

Acknowledgements The author would like to thank the referee for her/his helpful comments and suggestions. He is supported by the FAPESP grants 2015/02517-6 and 2015/24841-0 and by the European Community grants FP7-PEOPLE-2012-IRSES-316338 and FP7-PEOPLE-2012-IRSES-318999.

References

1. D.C. Braga, L.F. Mello, More than three limit cycles in discontinuous piecewise linear differential systems with two zones in the plane. Int. J. Bifurc. Chaos **24**, 1450056 (2014). (10 pages)
2. E. Freire, E. Ponce, F. Torres, Canonical discontinuous planar piecewise linear systems. SIAM J. Appl. Dyn. Syst. **11**, 181–211 (2012)
3. E. Freire, E. Ponce, F. Torres, The discontinuous matching of two planar linear foci can have three nested crossing limit cycles. Publ. Mat. **Extra**, 221–253 (2014)
4. E. Freire, E. Ponce, F. Torres, A general mechanism to generate three limit cycles in planar Filippov systems with two zones. Nonlinear Dyn. **78**, 251–263 (2014)
5. M. Han, W. Zhang, On Hopf bifurcation in non-smooth planar systems. J. Differ. Equ. **248**, 2399–2416 (2010)
6. S.M. Huan, X.S. Yang, On the number of limit cycles in general planar piecewise linear systems. Discrete Contin. Dyn. Syst. A **32**, 2147–2164 (2012)
7. J. Llibre, E. Ponce, Three nested limit cycles in discontinuous piecewise linear differential systems with two zones. Dyn. Contin. Discrete Impuls. Syst. Ser. B **19**, 325–335 (2012)
8. J. Llibre, D.D. Novaes, M.A. Teixeira, Maximum number of limit cycles for certain piecewise linear dynamical systems. Nonlinear Dyn. **82**, 1159–1175 (2015)
9. J. Llibre, D.D. Novaes, M.A. Teixeira, On the birth of limit cycles for non-smooth dynamical systems. Bull. Sci. Math. **139**, 229–244 (2015)
10. J. Llibre, D.D. Novaes, M.A. Teixeira, Limit cycles bifurcating from the periodic orbits of a discontinuous piecewise linear differential center with two zones. Int. J. Bifurc. Chaos **25**, 1550144 (2015). (11 pages)
11. D.D. Novaes, H. Ponce, A simple solution to the Braga–Mello conjecture. Int. J. Bifurc. Chaos **25**, 1550009 (2015). (7 pages)
12. D.D. Novaes, J. Torregrosa, On the extended Chebyshev systems with positive accuracy. Departament de Matemàtiques (2015). Preprint no. 13

An Equivalent Formulation of the Averaged Functions via Bell Polynomials

Douglas D. Novaes

Abstract We use Bell polynomials to provide an alternative formula for the averaged functions. This new formula can make the computational implementation of the averaged functions easier.

1 Introduction and Statement of the Main Results

The averaging theory is one of the best analytical methods to study isolated periodic solutions of differential equations in the presence of a small parameter; see, for instance, Llibre–Moeckel–Simó [5] and the references therein. Usually, this theory deals with differential systems in the following standard form

$$x'(t) = \sum_{i=0}^{k} \varepsilon^i F_i(t, x) + \varepsilon^{k+1} R(t, x, \varepsilon), \quad (t, x) \in \mathbb{R} \times D, \tag{1}$$

where D is an open bounded subset of $\mathbb{R}^n$, $|\varepsilon| \neq 0$ is a small parameter, and the functions $F_i : \mathbb{R} \times D \to \mathbb{R}^n$ for $i = 1, 2, \ldots, k$, and $R : \mathbb{R} \times D \times (-\varepsilon_0, \varepsilon_0) \to \mathbb{R}^n$ are T–periodic in the first variable and Lipschitz in the second variable. As one of the main hypotheses, it is assumed that the solution $\varphi(t, z)$ of the *unperturbed differential system*, $x'(t) = F_0(t, x)$, is T–periodic in the variable t for every initial condition $\varphi(0, z) = z \in D$.

The averaging method consists in defining a collection of functions $f_i : D \to \mathbb{R}^n$, called *averaged function of order i*, for $i = 1, 2, \ldots, k$, which control (their simple zeros control), for $|\varepsilon| \neq 0$ sufficiently small, the isolated periodic solutions of the differential system (1). In Llibre–Novaes–Teixeira [6] it has been established that

D.D. Novaes (✉)
Departamento de Matemática, Universidade Estadual de Campinas,
Rua Sérgio Baruque de Holanda, 651, Cidade Universitária Zeferino Vaz,
Campinas, São Paulo 13083–859, Brazil
e-mail: ddnovaes@ime.unicamp.br

A. Colombo et al. (eds.), *Extended Abstracts Spring 2016*,
Trends in Mathematics 8, DOI 10.1007/978-3-319-55642-0_25

$$f_i(z) = \frac{y_i(T,z)}{i!}, \tag{2}$$

where $y_i : \mathbb{R} \times D \to \mathbb{R}^n$, for $i = 1, 2, \ldots, k$, are defined recurrently by the following integral equation

$$\begin{aligned} y_1(t,z) &= \int_0^t \Big(F_1(s,\varphi(s,z)) + \partial F_0(s,\varphi(s,z))\, y_1(s,z) \Big) ds, \\ y_i(t,z) &= i! \int_0^t \Bigg(F_i(s,\varphi(s,z)) \\ &\quad + \sum_{l=1}^{i} \sum_{S_l} \frac{1}{b_1!\, b_2! 2!^{b_2} \cdots b_l! l!^{b_l}} \partial^L F_{i-l}(s,\varphi(s,z)) \bigodot_{j=1}^{l} y_j(s,z)^{b_j} \Bigg) ds. \end{aligned} \tag{3}$$

In Eq. (3), S_l denotes the set of all l-tuples of non-negative integers $(b_1, b_2, \ldots, b_l)$ satisfying $b_1 + 2b_2 + \cdots + lb_l = l$, and $L = b_1 + b_2 + \cdots + b_l$. Here, $\partial^L F(t,x)$ denotes the Frechet's derivative with respect to the variable x. It is a L–multilinear map applied to a "product" of L vectors of $\mathbb{R}^n$, $\bigodot_{j=1}^{L} y_j \in \mathbb{R}^{nL}$, where $y_j = (y_{j1}, \ldots, y_{jn}) \in \mathbb{R}^n$. Formally,

$$\partial^L F(t,x) \bigodot_{j=1}^{L} y_j = \sum_{i_1,\ldots,i_L=1}^{n} \frac{\partial^L F(t,x)}{\partial x_{i_1} \cdots \partial x_{i_L}} y_{1i_1} \cdots y_{Li_L}.$$

In [6, 7] the averaging theory at any order was developed to study isolated periodic solutions of nonsmooth but continuous differential system. Recently, the averaging theory has also been extended to study isolated periodic solutions of discontinuous differential systems; see [2, 4, 8, 9]. The next theorem is proved in Llibre–Novaes–Teixeira [6].

Theorem 1 (Llibre–Novaes–Teixeira [6]). *Assume the following conditions:*

(i) for each $i = 0, 1, \ldots, k$ and $t \in \mathbb{R}$, the function $F_i(t,\cdot)$ is of class C^{k-i}, $\partial^{k-i} F_i$ is locally Lipschitz in the second variable, and R is a continuous function locally Lipschitz in the second variable;

(ii) for some $r \in \{1, 2, \ldots, k\}$, $f_i = 0$ for $i = 1, 2, \ldots, r-1$ and $f_r \neq 0$;

(iii) for some $a^* \in D$ with $f_r(a^*) = 0$, there exists a neighborhood $V \subset D$ of a^* such that $f_r(z) \neq 0$ for all $z \in \overline{V} \setminus \{a^*\}$, and that $d_B(f_r(z), V, 0) \neq 0$.

Then, for $|\varepsilon| > 0$ sufficiently small, there exists a T–periodic solution $x(\cdot,\varepsilon)$ of (1) such that $x(0,\varepsilon) \to a^*$ when $\varepsilon \to 0$.

The above symbol d_B denotes the Brouwer degree; see Brouwer [1] for a general definition. When f_r is a C^1 function and the Jacobian determinant of f_r at $z \in V$ is distinct from zero (we denote $J_{f_r}(z) \neq 0$) then the Brouwer degree of f_r at 0 is given by

$$d_B(f_r, V, 0) = \sum_{z \in \mathbf{Z}_{f_r}} \operatorname{sign}\left(J_{f_r}(z)\right),$$

where $\mathbf{Z}_{f_r} = \{z \in V : f_r(z) = 0\}$. In this case, $J_{f_r}(a^*) \neq 0$ implies $d_B(f_r(z), V, 0) \neq 0$.

In Itikawa–Llibre–Novaes [2], there can be found some examples where higher order averaged functions (2) are used to estimate lower bounds for the maximum number of limit cycles of some classes of smooth and nonsmooth differential systems.

In practical means, the evaluation of the recurrence (3) is a computational problem. Therefore, in this notes, we shall use the partial *Bell polynomials* to provide an alternative formula for the recurrence (3). Since the Bell polynomials are implemented in algebraic manipulators as Mathematica and Maple, this new formula can make easier the computational implementation of the averaged functions. In the sequel, for p and q positive integers, we recall the partial Bell polynomials:

$$B_{p,q}(x_1, \ldots, x_{p-q+1}) = \sum_{\widetilde{S}_{p,q}} \frac{p!}{b_1! b_2! \cdots b_{p-q+1}!} \prod_{j=1}^{p-q+1} \left(\frac{x_j}{j!}\right)^{b_j},$$

where now $\widetilde{S}_{p,q}$ is the set of all $(p-q+1)$-tuples of nonnegative integers $(b_1, b_2, \ldots, b_{p-q+1})$ satisfying $b_1 + 2b_2 + \cdots + (p-q+1)b_{p-q+1} = p$, and $b_1 + b_2 + \cdots + b_{p-q+1} = q$.

Theorem 2 *For $i = 1, 2, \ldots, k$ the recurrence (3) reads*

$$\begin{aligned}
y_1(t,z) &= Y(t,z) \int_0^t Y(s,z)^{-1} F_1(s, \varphi(s,z))\, ds,\\
y_i(t,z) &= Y(t,z) \int_0^t Y(s,z)^{-1} \Big(i! F_i(s, \varphi(s,z))\\
&\quad + \sum_{m=2}^{i} \partial^m F_0(s, \varphi(s,z))\, B_{i,m}\big(y_1(s,z), \ldots, y_{i-m+1}(s,z)\big)\\
&\quad + \sum_{l=1}^{i-1} \sum_{m=1}^{l} \frac{i!}{l!} \partial^m F_{i-l}(s, \varphi(s,z))\, B_{l,m}\big(y_1(s,z), \ldots, y_{l-m+1}(s,z)\big) \Big) ds,
\end{aligned} \tag{4}$$

where $Y(t,z)$ is the $n \times n$ fundamental matrix solution of the periodic linear differential system $u'(t) = \partial F_0(t, \varphi(t,z))\, u(t)$ such that $Y(0,z) = Id$ is the identity matrix.

Proof Firstly, recall two equivalent definitions of the Faá di Bruno's Formula about the l-th derivative of a composite function; see Johnson [3]. Let g and h be sufficiently smooth functions then

$$\frac{d^l}{d\alpha^l} g(h(\alpha)) = \sum_{S_l} \frac{l!}{b_1!\, b_2!2!^{b_2} \cdots b_l! l!^{b_l}} g^{(L)}(h(\alpha)) \bigodot_{j=1}^{l} \left(h^{(j)}(\alpha)\right)^{b_j}$$
$$= \sum_{m=1}^{l} g^{(m)}(h(\alpha)) B_{l,m}\left(h'(\alpha), h''(\alpha), \ldots, h^{(l-m+1)}(\alpha)\right),$$

where S_l is the set of all l-tuples of non-negative integers $(b_1, b_2, \ldots, b_l)$ satisfying $b_1 + 2b_2 + \cdots + lb_l = l$, and $L = b_1 + b_2 + \cdots + b_l$, and $B_{l,m}$ is the partial Bell polynomials.

Now define a function $h(\alpha)$ such that $h(0) = \varphi(s, z)$ and $h^{(i)}(0) = y_i(t, z)$, for $i = 1, 2, \ldots, k$. Therefore the sum over S_l in the expression (3) for y_i reads

$$\frac{1}{l!}\frac{d^l}{d\alpha^l}\left(F_{i-l}(s, h(\alpha))\right)\Big|_{\alpha=0} = \sum_{S_l} \frac{1}{b_1!\, b_2!2!^{b_2} \cdots b_l! l!^{b_l}} \partial^L F_{i-l}(s, \varphi(s, z)) \bigodot_{j=1}^{l} y_j(s, z)^{b_j}$$
$$= \frac{1}{l!} \sum_{m=1}^{l} \partial^m F_{i-l}(s, \varphi(s, z)) B_{l,m}\left(y_1(s, z), \ldots, y_{l-m+1}(s, z)\right).$$

Substituting the above expression in (3) we get

$$y_i(t, z) = i! \int_0^t \Bigg(F_i(s, \varphi(s, z)) + \sum_{l=1}^{i} \sum_{m=1}^{l} \frac{1}{l!} \partial^m F_{i-l}(s, \varphi(s, z)) B_{l,m}\left(y_1(s, z), \ldots, y_{l-m+1}(s, z)\right) \Bigg) ds, \tag{5}$$

which is still an integral equation. We note that the function $y_i(s, z)$ appears in the right hand side of Eq. (5) only when $l = i$ and $m = 1$. Since $B_{i,1}\left(y_1(s, z), \ldots, y_i(s, z)\right) = y_i(s, z)$ and $y_i(0, z) = 0$ the above integral equation satisfies the linear differential equation

$$\frac{\partial}{\partial t} y_i(t, z) = \partial F_0(t, \varphi(t, z)) y_i(t, z) + i! F_i(t, \varphi(t, z)) + \sum_{m=2}^{i} \partial^m F_0(t, \varphi(t, z)) B_{i,m}\left(y_1(t, z), \ldots, y_{i-m+1}(t, z)\right) + \sum_{l=1}^{i-1} \sum_{m=1}^{l} \frac{i!}{l!} \partial^m F_{i-l}(t, \varphi(t, z)) B_{l,m}\left(y_1(t, z), \ldots, y_{l-m+1}(t, z)\right). \tag{6}$$

Hence, proceeding as above, now for y_1 in the expression (3), and solving the differential equation (6) for $i = 1, 2, \ldots, k$, we obtain (4). □

Acknowledgements The author would like to thank the referees for their helpful comments and suggestions. He is supported by the FAPESP grants 2015/02517-6 and 2015/24841-0 and by the European Community grants FP7-PEOPLE-2012-IRSES-316338 and FP7-PEOPLE-2012-IRSES-318999.

References

1. F. Brouwder, Fixed point theory and nonlinear problems. Bull. Amer. Math. Soc. **9**, 1–39 (1983)
2. J. Itikawa, J. Llibre, D.D. Novaes, A new result on averaging theory for a classe of discontinuous planar differential systems with applications. Revista Matemática Iberoamericana (2016, to appear)
3. W.P. Johnson, The curious history of Faá di Bruno's formula. The Am. Math. Monthly **109**(3), 217–234 (2002)
4. J. Llibre, D.D. Novaes, On the continuation of periodic solutions in discontinuous dynamical systems (2015). Preprint, arXiv:1504.03008
5. J. Llibre, R. Moeckel, C. Simó, *Central Configurations, Periodic Orbits, and Hamiltonian Systems*. Advanced Courses in Mathematics-CRM Barcelona (Birkhäuser, Basel, 2015)
6. J. Llibre, D.D. Novaes, M.A. Teixeira, Higher order averaging theory for finding periodic solutions via Brouwer degree. Nonlinearity **27**, 563–583 (2014)
7. J. Llibre, D.D. Novaes, M.A. Teixeira, Corrigendum: higher order averaging theory for finding periodic solutions via Brouwer degree. Nonlinearity **27**, 2417 (2014)
8. J. Llibre, A.C. Mereu, D.D. Novaes, Averaging theory for discontinuous piecewise differential systems. J. Differ. Equ. **258**, 4007–4032 (2015)
9. J. Llibre, D.D. Novaes, M.A. Teixeira, On the birth of limit cycles for non-smooth dynamical systems. Bull. Sci. Math. **139**, 229–244 (2015)

Smoothing a Piecewise-Smooth: An Example from Plankton Population Dynamics

Sofia H. Piltz

Abstract In this work we discuss a piecewise-smooth dynamical system inspired by plankton observations and constructed for one predator switching its diet between two different types of prey. We then discuss two smooth formulations of the piecewise-smooth model obtained by using a hyperbolic tangent function and adding a dimension to the system. We compare model behaviour of the three systems and show an example case where the steepness of the switch is determined from a comparison with data on freshwater plankton.

1 Introduction

Here, we consider an existing piecewise-smooth model for a system of one predator and two prey, inspired by studies of plankton populations suggesting predator-prey interaction and adaptive feeding of a predator governing the dynamics observed in a freshwater lake in spring; see Müller–Schlegel [4] and Tirok–Gaedke [10]. While the piecewise-smooth system providing prey switching is a possible mechanistic explanation for the observed patterns of population oscillations (see Piltz–Porter–Maini [6]), it is not clear whether there exists such "discontinuous" predator feeding behaviour. Therefore, we discuss here two smooth analogs of the piecewise-smooth system and compare their dynamical behaviour. In addition, we compare model predictions to data to get more insight into the steepness of the transition function.

2 Methods

We consider the following piecewise-smooth system describing adaptive feeding of a predator z on its preferred and alternative prey, p_1 and p_2, respectively:

S.H. Piltz (✉)
Department of Applied Mathematics and Computer Science, Technical University of Denmark, Asmussens Allé, Bygning 303B, 2800 Kongens Lyngby, Denmark
e-mail: shpi@dtu.dk

A. Colombo et al. (eds.), *Extended Abstracts Spring 2016*,
Trends in Mathematics 8, DOI 10.1007/978-3-319-55642-0_26

$$\dot{\mathbf{x}} = \begin{bmatrix} \dot{p}_1 \\ \dot{p}_2 \\ \dot{z} \end{bmatrix} = \left\{ \begin{array}{ll} f_+ = \begin{bmatrix} (r_1 - z)p_1 \\ r_2 p_2 \\ (Eq_1 p_1 - m)z \end{bmatrix}, & \text{if} \quad h = p_1 - a_q p_2 > 0 \\ \\ f_- = \begin{bmatrix} r_1 p_1 \\ (r_2 - z)p_2 \\ (Eq_2 p_2 - m)z \end{bmatrix}, & \text{if} \quad h = p_1 - a_q p_2 < 0 \end{array} \right\}. \tag{1}$$

The parameters r_1 and r_2 (where $r_1 > r_2 > 0$) are the respective per capita growth rates of the preferred and alternative prey, $e > 0$ is the proportion of predation that goes into predator growth, q_1 and q_2 are nondimensional parameters representing the predator's desire to consume the preferred and alternative prey, respectively, and $m > 0$ is the predator per capita death rate per day.

As a_q (which corresponds mathematically to the slope of tilted switching manifold $h = p_1 - a_q p_2 = 0$, and biologically, to the slope of the assumed linear trade-off in the predator's preference for prey) is decreased below its critical value ($a_{q_{\text{crit}}} = q_2/q_1$), the piecewise-smooth system undergoes a centre to two-part-periodic orbit (C2PO) bifurcation, where the eigenvalues of the pseudoequilibrium of the system cross the imaginary axis, and the cusp for f_+ is aligned with the pseudoequilibrium. In the C2PO bifurcation, an attracting pseudoequilibrium becomes repelling and an adding-sliding periodic orbit arises from a family of centres; see Piltz–Porter–Maini [6]. The mechanism of the C2PO bifurcation can be illustrated by the nullclines of the sliding vector field of (1): For $a_q < a_{q_{\text{crit}}}$, the cusp lies at the intersection of the boundary between crossing and sliding regions and one branch of a hyperbola-nullcline; see Fig. 1a. At the bifurcation point, both the pseudoequilibrium and the cusp move and become located on the same line (see Fig. 1b), and for $a_q > a_{q_{\text{crit}}}$, the pseudoequilibrium and the cusp are no longer aligned; see Fig. 1c.

The piecewise-smooth system in (1) can be smoothed out by using hyperbolic tangent functions as follows:

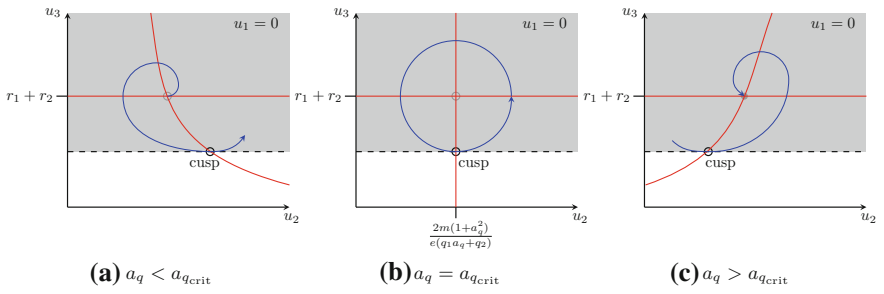

(a) $a_q < a_{q_{\text{crit}}}$ **(b)** $a_q = a_{q_{\text{crit}}}$ **(c)** $a_q > a_{q_{\text{crit}}}$

Fig. 1 The mechanism for the C2PO bifurcation in (1) represented after a coordinate change $u_1 = p_1 - a_q p_2$, $u_2 = a_q p_1 + p_2$, and $u_3 = z$ on the u_2-u_3-plane. We denote the repelling/attracting pseudoequilibrium with an open/filled grey circle, the cusp with an open *black circle*, nullclines in *red*, and an example trajectory in *blue*. We have shaded the sliding region

$$\begin{aligned}
\dot{p}_1 &= (r_1 - z)p_1\left(\tfrac{1+\tanh(k(p_1-a_q p_2))}{2}\right) + r_1 p_1\left(\tfrac{1-\tanh(k(p_1-a_q p_2))}{2}\right),\\
\dot{p}_2 &= r_2 p_2\left(\tfrac{1+\tanh(k(p_1-a_q p_2))}{2}\right) + (r_2 - z)p_2\left(\tfrac{1-\tanh(k(p_1-a_q p_2))}{2}\right),\\
\dot{z} &= (Eq_1 p_1 - m)z\left(\tfrac{1+\tanh(k(p_1-a_q p_2))}{2}\right) + (Eq_2 p_2 - m)z\left(\tfrac{1-\tanh(k(p_1-a_q p_2))}{2}\right),
\end{aligned} \tag{2}$$

where k determines the steepness of the hyperbolic tangent and of the predator's feeding behaviour. Alternatively, one can find a four-dimensional smooth analog for the system in (1) by constructing equations for a system variable q that changes in response to the prey abundance. Biologically, q can be considered as the predator's trait that undergoes contemporary (i.e., $\epsilon = 1$) or rapid ($\epsilon \ll 1$) evolution according to the fitness-gradient dynamics (see [1–3]):

$$\begin{aligned}
\tfrac{\mathrm{d}p_1}{\mathrm{d}t} &= \dot{p}_1 = g_1(p_1, p_2, z, q) = r_1 p_1 - q p_1 z,\\
\tfrac{\mathrm{d}p_2}{\mathrm{d}t} &= \dot{p}_2 = g_2(p_1, p_2, z, q) = r_2 p_2 - (1-q)p_2 z,\\
\tfrac{\mathrm{d}z}{\mathrm{d}t} &= \dot{z} = g_3(p_1, p_2, z, q) = eq p_1 z + e(1-q)q_2 p_2 z - mz,\\
\epsilon\tfrac{\mathrm{d}q}{\mathrm{d}t} &= \epsilon\dot{q} = f(p_1, p_2, q) = q(1-q)Ve(p_1 - a_q p_2),
\end{aligned} \tag{3}$$

where V is a nondimensional constant and constitutes the term for additive genetic variance, $q(1-q)V$.

3 Results

Using linear stability analyses, we find that the piecewise-smooth system (1) and its two smooth analogs, (2) and (3), all exhibit a steady state, where all three populations coexist at positive densities. In the case of the piecewise-smooth system, this steady state is a pseudoequilibrium located on the switching boundary and attracting for a large part of the parameter regime (i.e., when $a_q > q_2/q_1$); see Piltz–Porter–Maini [6]. Similarly, $a_q > q_2/q_1$ is a sufficient condition for stability of the same coexistence steady state in the smooth system (2), when k is large enough; see Piltz–Harhanen–Porter–Maini [5]. Moreover, there exists an interval of intermediate k values, $k_0 < k < k_1$, for which the coexistence state is stable also for $a_q < q_2/q_1$, [5]. However, the coexistence steady state in the four-dimensional smooth analog (3) (with $\epsilon = 1$) is stable only for $a_q = q_2/q_1$ and, otherwise, it is unstable; see Piltz–Harhanen–Porter–Maini [5]. For $\epsilon \ll 1$, there is a time scale difference between the fast dynamics of the added system variable q (i.e., evolutionary changes) and the slow population dynamics (i.e., demographic changes) in the smooth system (3). Thereby, singular perturbation theory can be used to show that there exist periodic orbits in the resulting 1 fast-3 slow system for $\epsilon = 0$ that persist for $\epsilon > 0$; see Piltz–Veerman–Porter–Maini [7].

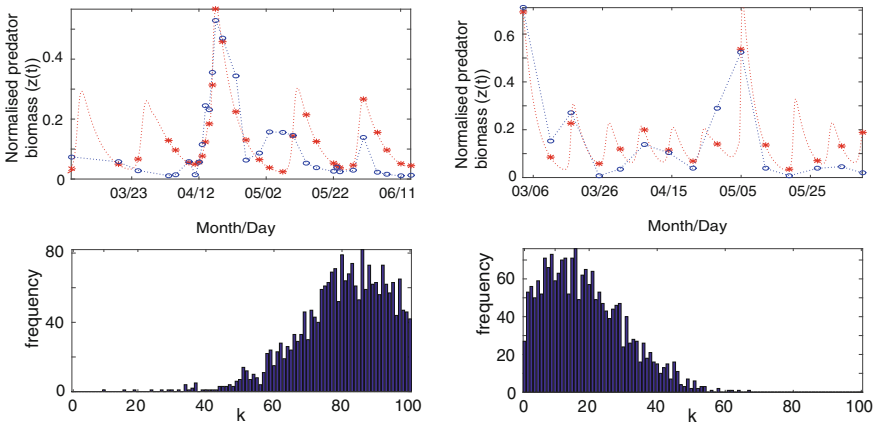

Fig. 2 Normalised predator abundance $z(t)$ for simulations of (2) [for parameter values $e = 0.25$, $q_1 = 1$, $q_2 = 0.5$, (*left*) $r_1 = 1.1$, $r_2 = 0.3$, $m = 0.2$, $a_q = 0.03$, $k = 86$, and (*right*) $r_1 = 2.3$, $r_2 = 0.5$, $m = 0.3$ $a_q = 0.03$, $k = 16$], (*circles*) normalised data, and frequency of k at the most strict tolerance level for (*left*, Tol = 0.008) selective predator *Rimostrombidum lacustris* in 1991 and (*right*, Tol = 0.02) unselective predator *Balanion planctonicum* in 1998 in Lake Constance; see [8, 9]

While it is not clear if the switch in the adaptive feeding of a predator on two prey is instantaneous as the piecewise-smooth system (1) assumes, it is not known which of the several possible smooth formulations best describe prey switching. To determine the steepness of a switch from z feeding on p_1 to p_2, and vice versa, we compare model predictions of (3) with data collected from *protist*-predators (i.e., single cell organisms that feed on phytoplankton). We simulate (3) numerically with several different parameter values — including the slope of the hyperbolic tangent k — calculate the distance to the data points, and either reject or accept k values that yield large or small least-square error between a simulation and the data. For the first iteration we choose k values from a uniform distribution between 1 and 100, and for the subsequent iterations we choose k from the accepted values of the previous iteration. Our parameter fitting suggests that large k values fit the data for a selective predator better than small, suggesting the use of a piecewise-smooth model as a good approximation for feeding behaviour; see Fig. 2.

4 Discussion

Although at the extremes (i.e., when $k \to \infty$ and when $q = 0$ and $q = 1$ for the smooth systems (2) and (3), respectively) the smooth analog agrees with the piecewise-smooth system (1), the dynamical behaviour of the two systems may not always be the same. For example, a smoothing with hyperbolic tangent function preserves the densities at, and stability of, the coexistence equilibrium when the transition is steep enough, whereas a smoothing that introduces an extra dimension

to the system changes the stability of the same equilibrium. In addition, where the smooth analog (2) exhibits convergence to an equilibrium for gradual transition, there is a periodic orbit in the piecewise-smooth system. These observations suggest that even though there is a parameter/variable regime where the piecewise-smooth system and its smooth analog overlap "on paper", their dynamical behaviour may be quite different.

One way to justify (or discard) the use of a piecewise-smooth model —either as a simplification of a steep transition or introduced by the physical or other properties of the application— is to construct several smooth analogs and let the data indicate which model best describes it. Data comparison can be used to get insight into the steepness of a discontinuous switch, as done here, or to choose between different competing models. The latter could be done with a heuristic method (e.g., model choice using approximate Bayesian computation with sequential Monte Carlo; see Toni–Welch–Strelkowa–Ipsen–Stumpf [11]) or using existing toolboxes for system identification (e.g., in MATLAB). As concerns analytical computations, the expressions for the equilibrium and its eigenvalues in the piecewise-smooth system (1) are much easier to analyse than those of its smooth analogs. However, despite the fact that the piecewise-smooth system has fewer parameters than its smooth analogs, numerical simulations of piecewise-smooth systems can result in long computation times because of more complex algorithms than those used to solve smooth systems. As a result, the advantage of fitting fewer parameters can be erased by longer computation times when several iterations are required for reliable parameter fitting.

References

1. P.A. Abrams, H. Matsuda, Y. Harada, Evolutionarily unstable fitness maxima and stable fitness minima of continuous traits. Evol. Ecol. **7**, 465–487 (1993)
2. M.H. Cortez, S.P. Ellner, Understanding rapid evolution in predator-prey interactions using the theory of fast-slow dynamical systems. The Am. Nat. **176**, E109–E127 (2010)
3. R. Lande, A quantitative genetic theory of life history evolution. Ecology **63**, 607–615 (1982)
4. H. Müller, A. Schlegel, Responses of three freshwater planktonic ciliates with different feeding modes to cryptophyte and diatom prey. Aquat. Microb. Ecol. **17**, 49–60 (1999)
5. S.H. Piltz, L. Harhanen, M.A. Porter, P.K. Maini, Two smooth analogs for a piecewise-smooth 1 predator-2 prey system (in preparation)
6. S.H. Piltz, M.A. Porter, P.K. Maini, Prey switching with a linear preference trade-off. SIAM J. Appl. Dyn. Syst. **13**, 658–682 (2014)
7. S.H. Piltz, F. Veerman, M.A. Porter, P.K. Maini, A predator-2 prey fast-slow dynamical system for rapid predator evolution. Preprint, arXiv: 1603.09076
8. K. Tirok, U. Gaedke, Spring weather determines the relative importance of ciliates, rotifers and crustaceans for the initiation of the clear-water phase in a large, deep lake. J. Plankton Res. **28**, 361–373 (2006)
9. K. Tirok, U. Gaedke, The effect of irradiance, vertical mixing and temperature on spring phytoplankton dynamics under climate change: long-term observations and model analysis. Oecologia **150**, 625–642 (2007)
10. K. Tirok, U. Gaedke, Internally driven alternation of functional traits in a multispecies predator-prey system. Ecology **91**, 1748–1762 (2010)
11. T. Toni, D. Welch, N. Strelkowa, A. Ipsen, M.P. Stumpf, Approximate Bayesian computation scheme for parameter inference and model selection in dynamical systems. J. R. Soc. Interface **6**, 187–202 (2009)

A Note on Frictional Slip Patterns

Thibaut Putelat

Abstract A possible origin of the frictional travelling waves usually occuring between sliding interfaces is discussed: various solutions, including propagating wavetrains, pulses and fronts, can appear under rate-and-state friction from homoclinic or heteroclinic bifurcations.

1 Introduction

The understanding of the spatio-temporal dynamics of frictional slip along extended solid interfaces is of great importance, both theoretically and in practice, across many industrial or natural contexts such as brake squeal or earthquake mechanics. Various regimes of stick-slip travelling waves are often observed numerically as for instance in the recent simulations of a brake pad [2], or experimentally as in the careful monitoring of friction rupture fronts controlling the onset of frictional slip [3]. The intricate nature and diversity of earthquakes recorded over the past decade ranging from aseismic events, episodic tremors, slow and fast earthquakes is also most startling; e.g., see [9, 11]. The emergence of such a variety of inhomogeneous frictional sliding modes, either in engineering or geophysical contexts, is a difficult problem due to its multiple scales nature caused by the complexity of the friction phenomenon, its modelling and its coupling with the elastic wave radiation. Even in the case of the idealised situation of a long thin elastic plate, a plethora of solution types, including propagating wavetrains, pulses and fronts, can appear under non-monotonic rate-and-state friction from homoclinic or heteroclinic bifurcations; see [12]. Here, we briefly sketch the analysis for visco-elastic rate-and-state friction models motivated by the experimental results reported in [7].

T. Putelat (✉)
Department of Engineering Mathematics, University of Bristol, Bristol, UK
e-mail: T.Putelat@bristol.ac.uk

A. Colombo et al. (eds.), *Extended Abstracts Spring 2016*,
Trends in Mathematics 8, DOI 10.1007/978-3-319-55642-0_27

2 Rate-and-State Friction

The phenomenological rate-and-state framework of friction [1, 13, 16] is a physically motivated smooth regularisation of Coulomb friction where three crucial experimental observations are incorporated, namely: the time dependence of static friction in quasi-stationary contact and the velocity dependence of dynamic friction, together with sliding memory effects via an interfacial state variable $\phi(t)$ quantifying the interface resistance to slip whose characteristic relaxation timescale is denoted t_*. Accordingly, classical rate-and-state models are usually defined by the pair of empirical equations

$$\tau = F(v, \phi; \sigma) \quad \text{and} \quad \dot{\phi} = -g(v, \phi; \sigma)/t_*, \tag{1}$$

where the interfacial shear stress τ depends on the interfacial slip rate v, state ϕ and normal stress σ, which is considered uniform here. A classical realisation is given by the Dieterich law defined by $F/\sigma := \mu_* + a\ln(v/V_*) + b\ln(\phi)$ and $g := \phi v/V_* - 1$; see [16]. Such friction models are remarkably *universal* across a wide variety of materials and can be microphysically justified from Eyring's theory of thermally activated rate processes (cf. [14]), which determine that the irreversible contribution to the interfacial slip rate is a nonlinear function $v_{\text{irr}} = f(\tau, \phi; \sigma)$. To extend the domain of validity of this framework into the moderate to high frequency domain, experimental observations [4, 6, 7] suggest to take into account the elastic deformation of the contact region from the introduction of an interfacial shear stiffness k. Hence, the total interfacial slip rate v results from the sum of these elastic and irreversible contributions, i.e., $v = \dot{\tau}/k + f(\tau, \phi; \sigma)$, or equivalently

$$\tau = F(v - \dot{\tau}/k, \phi; \sigma). \tag{2}$$

Classical rate-and-state friction models are formally recovered from (2) with $k \to \infty$.

3 Problem Formulation

Lying on a flat and rigid horizontal foundation, the sliding of a thin elastic plate of arbitrary wide extent driven by a constant shear stress $\bar{\tau} := \bar{\mu}\bar{\sigma}$ applied at its top and subjected to a uniform pressure $\bar{\sigma}$ is considered. The plate's thickness, density, Young's modulus and Poisson's ratio are respectively denoted h, ρ, E and ν. In the limit of large wavelength of the plate longitudinal wave ($\lambda \gg h$), the distribution of the longitudinal stress and displacement components can be assumed uniform across the plate's cross-section; see Kolsky [10]. The equation of motion of the plate then follows from considering the balance of forces applied to a cross-section of infinitesimal width. Coupled with rate-and-state friction $(1)_2$–(2), a dimensionless

'shallow layer' approximation to the three-dimensional elasto-dynamic equations is derived as, with abuse of notation,[1]

$$u_{,tt} - u_{,xx} + \tau = \bar{\tau}, \qquad \tau_{,t} = \kappa[u_{,t} - f(\zeta\tau, \phi)], \qquad \phi_{,t} = -rg(u_{,t}, \phi), \tag{3}$$

where $u(x,t)$ is the plate horizontal displacement. Denoting c_l the slab's longitudinal wavespeed defined by $c_l^2 = E/[\rho(1-\nu^2)]$, the key dimensionless parameters characterising the interplay between the elastic and frictional waves are $\zeta = (\rho c_l)/(\bar{\sigma}/V_*)$, $r = (h/c_l)/t_*$ and $\kappa = (kh)/(\rho c_l^2)$. Typically $r \ll 1$ represents the ratio of the perturbation propagation characteristic timescale over the characteristic interface rejuvenation timescale, whereas $\zeta \propto \bar{\sigma}^{-1} \ll 1$ is the ratio of the mechanical and interfacial impedances. Due to the large value of the interfacial stiffness ($> 10^{12}$ Pa/m), we expect $\kappa \gg 1$. We note however that such an interfacial stiffness could result from some interfacial gouge/wear instead of interfacial asperities, which could in turn reduce the order of magnitude of κ.

Within the travelling coordinate system $z := r(t + x/V)$ and denoting $v := rdu/dz$, the travelling-wave reduction of (3) leads to the multiple timescale dynamical system

$$\gamma dv/dz = \tau - \bar{\tau}, \quad d\tau/dz = (\kappa/r)[v - f(\zeta\tau, \phi)], \quad d\phi/dz = -g(v, \phi), \tag{4}$$

whose solution types and bifurcation structure are briefly described in what follows as the key parameters $\bar{\tau}$ and $\gamma := r(1 - V^2)/V^2$ are varied.

4 Stability of Uniform Sliding

The study of the stability of a uniform sliding state (v_0, ϕ_0) shows that the wavelength of linear waves is consistent with the long-wave approximation and that the interfacial stiffness is stabilising. The growth rate of an infinitesimal perturbation $\delta u := (u_{,t}, \phi) - (v_0, \phi_0) = (\hat{v}, \hat{\phi}) \exp[i(\omega t - kx)]$ is governed by the dispersion relation $k^2 - \omega^2 - i\omega\beta(\omega) = 0$, in which the ratio $\beta(\omega) = -\frac{rg_{,\phi}F'_{ss} + i\omega F_{,v}}{(rg_{,\phi} + i\omega)(1 + i\omega F_{,v}/\kappa)}$, represents the friction frequency response function defined and measured in Cabboi–Putelat–Woodhouse [7]. It can be shown (see also [15, 16]) that uniform and steady sliding is unstable for velocity-weakening friction ($F'_{ss} < 0$), through a Hopf bifurcation with critical angular frequency ω_c, to long wavelength perturbations whose wavenumbers satisfy $k < k_c$, where $k_c^2 = \omega_c^2\big\{1 + \big[rg_{,\phi}(F_{,v} - F'_{ss})\big]/\big[(rg_{,\phi})^2 + \omega_c^2\big]\big\}$ with $\omega_c^2 = -(rg_{,\phi})^2(F'_{ss}/F_{,v})/\big[1 + rg_{,\phi}(F_{,v} - F'_{ss})/\kappa\big]$. Along with examples of friction curves, Fig. 1a shows an example of domain of unstable wavelengths $\lambda > \lambda_c = 2\pi/k_c$. The interfacial stiffness increases λ_c which means its effect is stabilising.

[1] Note that all symbols are dimensionless quantities in what follows.

Besides, as the critical wavenumber for the Dieterich law reads $\bar{k}_c^2 = (r/\zeta)(b - a)(1 + r\zeta v^2/a)$ and bounds the instability domain, we can conclude that the long-wave approximation $\lambda_c \gg 1$ remains valid provided $r/\zeta \ll 4\pi^2/(b - a)$.

5 Variety of Solution Types

Varying the shear stress $\bar{\tau}$ between the local extrema of a spinodal friction model [13], we find the occurrence of travelling self-healing 'slip pulses', reminiscent of the pulses described by Heaton [8], arising from a homoclinic bifurcation of travelling periodic slip patterns born in a Hopf bifurcation promoted by velocity-weakening friction, see Fig. 1b, c. Such slip pulses are anchored at the equilibrium saddle point lying on the low-velocity-strengthening branch of the friction curve. Interestingly, the existence of a high velocity strengthening branch also allows the existence of 'stick pulse' which corresponds to a narrow travelling 'stick' zone. Along the bifurcated branch, travelling wave-trains of slip pulses develop from a canard explosion,

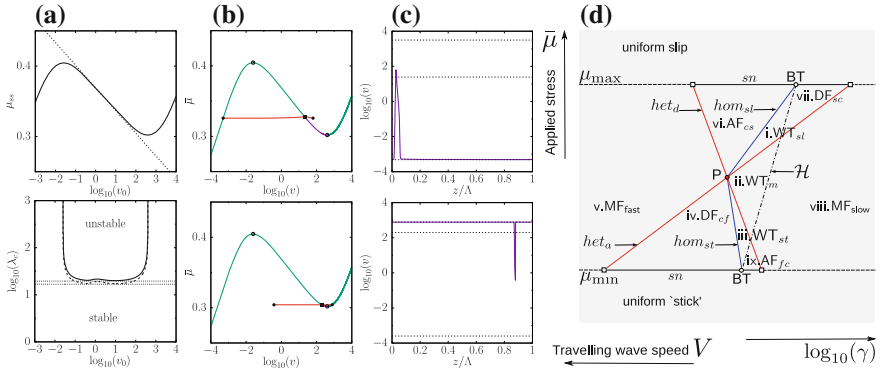

Fig. 1 (**a**) Steady-state friction characteristics and corresponding critical wavelengths λ_c ($r = 10^{-6}, \zeta = 10^{-7}$): $\kappa = 1$ (*solid line*), $\kappa \to \infty$ (*dashed line*). The domain of unstable wavelengths is limited to the domain of friction velocity weakening (*dotted lines*: monotonic friction). (**b**) Typical bifurcation diagrams for (4) under spinodal friction [13] leading to homoclinic connections (•) from the growth of wavetrains born at a Hopf bifurcation (■) (the *red lines* correspond to the maximum and minimum amplitude along the branch of periodic orbits): (*top*) slip pulse, (*bottom*) stick pulse. (**c**) Numerical approximations of slip pulse (*top*, $\gamma = 10^{-4}/\zeta$) and stick pulse (*bottom*, $\gamma = 10^{-6}/\zeta$) of period $\Lambda = 100$ for $\kappa = 100(r/\zeta)$ (the *dotted lines* delineate the three uniform sliding states). (**d**) Sketch of typical phase diagram of travelling wave patterns ($\kappa \to \infty$, see [12]): loci of slip pulses (hom_{sl}), stick pulses (hom_{st}), detachment fronts (het_d), attachment fronts (het_a) as saddle-saddle connections; Hopf bifurcation locus ($\mathcal{H}$); saddle-node bifurcation loci at the local extrema of friction (*sn*); Stick-slip wave-trains (WT). Generic detachment (DF), attachment (AF) and mixed (MF) fronts as saddle connections to the equilibrium point of the velocity weakening branch. Takens–Bogdanov points (BT). Uniform slab's slip rates solve $\mu_{ss}(v) \equiv \mu(v, \phi_{ss}(v)) = \bar{\mu}$ and $g(v, \phi_{ss}(v)) = 0$

which can lead either to wave-trains of slip or stick pulses. Heteroclinic connections corresponding to travelling 'detachment' (similar to [3, 5]) or 'attachment' fronts promoting the slab acceleration or deceleration are also possible. When the interfacial stiffness is neglected, these saddle-saddle connections exist on lines within a $(\gamma, \bar{\mu})$ phase diagram and delineate domains of generic travelling fronts and wavetrains of different types (see Fig. 1d and Putelat–et al. [12] for more details). The effect of κ on the topology of this phase diagram is under current investigation and will be published elsewhere. We note, however, that this bifurcation structure also strongly depends on the mathematical details of the friction model, in particular the state evolution equation. For instance, the classic monotonic Dieterich–Ruina friction models [16] only allows for wave trains of slip-pulse solutions in an exponentially narrow window of $\bar{\tau}$.

6 Conclusion

This work shows how introducing a smooth and non-monotonic rate-and-state interfacial friction model allows for the existence of different localised modes of frictional slippage as saddle-saddle connections with slip or stick pulses, detachment or attachment fronts along with travelling wavetrains, all in the same mathematical formulation of regional contact and within the well established theory of smooth dynamical system and global bifurcations. Careful consideration of the choice of the non-monotonic friction law and the type of interfacial state kinetics is necessary to capture the full richness of wave types. In such an idealised configuration of a thin elastic slab, this plethora of behaviours and the question of their physical selection may explain why friction experiments are difficult and associated with challenging repeatability issues [17]. This work may also shed new light on the complex and diverse dynamics of earthquake ruptures in particular with respect to the large variability of earthquake duration and frequency spectrum [9, 11]. Future work will explore the possibility of complex or irregular patterning from Shilnikov bifurcation or bursting dynamics scenarii that the three dimensional phase space and the slow-fast multiscale nature of system (4) may allow.

Acknowledgements The author acknowledges support by the UK EPSRC programme grant "Engineering Nonlinearity" (EP/K003836/1).

References

1. T. Baumberger, C. Caroli, Solid friction from stickslip down to pinning and aging. Adv. Phys. **55**(3–4), 279–348 (2006)
2. J. Behrendt, C. Weiss, N.P. Hoffmann, A numerical study on stickslip motion of a brake pad in steady sliding. J. Sound Vib. **330**(4), 636–651 (2011)

3. O. Ben-David, G. Cohen, J. Fineberg, The dynamics of the onset of frictional slip. Science **330**, 211–214 (2010)
4. P. Berthoud, T. Baumberger, Shear stiffness of a solid-solid multi-contact interface. Proc. Roy. Soc. Lon. A **454**, 1615–1634 (1998)
5. E. Bouchbinder, E.A. Brener, I. Barel, M. Urbakh, Slow cracklike dynamics at the onset of frictional sliding. Phys. Rev. Lett. **107**(23), 235501 (2011)
6. L. Bureau, T. Baumberger, C. Caroli, Shear response of a frictional interface to a normal load modulation. Phys. Rev. E **62**, 6810–6820 (2000)
7. A. Cabboi, T.A.F. Putelat, J. Woodhouse, The frequency response of dynamic friction: enhanced rate-and-state models. J. Mech. Phys. Solids **92**, 210–236 (2016)
8. T.H. Heaton, Evidence for and implication of self-healing pulses of slip in earthquake rupture. Phys. Earth Planet. Inter. **64**, 1–20 (1990)
9. S. Ide, Modeling fast and slow earthquakes at various scales. Proc. Jpn Acad. Ser. B Phys. Biol. Sci. **90**(8), 259–277 (2014)
10. H. Kolsky, *Stress Waves in Solids* (Oxford Clarendon Press, Oxford, 1953)
11. Z. Peng, J. Gomberg, An integrated perspective of the continuum between earthquakes and slow-slip phenomena. Nat. Geosci. **3**, 599–607 (2010)
12. T. Putelat et al. Phase plane analysis of localised frictional waves (submitted)
13. T. Putelat, J.H.P. Dawes, Steady and transient sliding under rate-and-state friction. J. Mech. Phys. Solids **78**, 70–93 (2015)
14. T. Putelat, J.H.P. Dawes, J.R. Willis, On the microphysical foundations of rate-and-state friction. J. Mech. Phys. Solids **59**(5), 1062–1075 (2011)
15. J.R. Rice, A.L. Ruina, Stability of steady frictional slipping. J. Appl. Mech. **50**(2), 343–349 (1983)
16. A.L. Ruina, Slip instability and state variable friction laws. J. Geophys. Res. **88**(B12), 10359–10370 (1983)
17. J. Woodhouse, T. Putelat, A. MacKay, Are there reliable models of friction? Philos. Trans. R. Soc. A **373**, 2051 (2015)

Climate in Barcelona Is Wonderful

Andrew Roberts

Abstract The Mathematics and Climate Research Network (MCRN) was invited to run an informal Climate Modeling Workshop as part of the Intensive Research Programme on Advances on Nonsmooth Dynamics hosted by the Centre de Recerca Matemàtica (CRM). The workshop was attended by a core group of about 10 participants with a nice mix of junior and senior researchers. A summary of the proceedings of the workshop is presented here.

1 Introduction

The Mathematics and Climate Research Network (MCRN) was invited to run an informal Climate Modeling Workshop as part of the Intensive Research Programme on Advances on Nonsmooth Dynamics hosted by the Centre de Recerca Matemàtica (CRM), in Barcelona. Kaitlin Hill, Julie Leifeld, and myself were happy to accept, and a workshop was organized with the help of programme organizer Mike Jeffrey. The workshop was attended by a core group of about 10 participants with a nice mix of junior and senior researchers, in addition to other attendees of the programme who selectively attended presentations of interest.

The number and lengths of presentations were limited in order to facilitate group discussions and collaboration. With the exception of the opening and concluding presentations given by myself and Chris Budd, respectively, the workshop's speakers were asked to highlight open problems involving conceptual climate models that contain (or may contain) nonsmooth dynamics. I was extremely happy with the quality of the discussions that arose throughout the workshop. Here, I will present a summary of the proceedings that were directly motivated from climate applications.

A. Roberts (✉)
Mathematics and Climate Research Network, Cornell University,
Ithaca, NY 14850, USA
e-mail: andrew.roberts@cornell.edu

A. Colombo et al. (eds.), *Extended Abstracts Spring 2016*,
Trends in Mathematics 8, DOI 10.1007/978-3-319-55642-0_28

2 Day 1: MCRN Organizers Present

I kicked off the workshop with an overview of conceptual climate models in order to make sure everyone had been exposed to the basics, beginning with foundational models such as Budyko's energy balance model [3], and Stommel's ocean circulation model [11]. Next, I highlighted some recent work from the MCRN and CliMathNet [1, 2, 8–10, 12]. Finally, I proposed that a rigorous treatment of a particular ocean circulation model by Colin de Verdiére [4] could motivate exploring possible dynamics when a singularly perturbed system contains a variable that is slow on one side of a switch an fast on the other.

Kaitlin Hill's presentation focused on the cryosphere, beginning with an overview of classical energy balance models and their connection to understanding a climate state known as Snowball Earth (where the entire planet is covered in ice). She continued to describe recent work done in the area by MCRN members [2], including an overview of her own work [5]. She also discussed her interest in developing and analyzing a conceptual model for fluid and salt convection through the mushy layer and nearby ocean. The mushy layer problem drew the attention of nearly all workshop attendees, leading to a large group discussion in the afternoon.

Rounding out the presentations on the first day was Julie Leifeld, who presented her research on Welander's model of convective mixing in the ocean [6, 7, 13]. Her presentation generated two interesting discussions throughout the week. The first consisted primarily of relationships between the blow-up method used in her analysis and regularization. The second was specific to her results, showing that a stable node border-collision bifurcation in the Welander model produces a continuum of homoclinic orbits at the bifurcation, and a large attracting periodic orbit after the bifurcation. It was pointed out that this behavior is reminiscent of a canard explosion, although the model has no time-scale separation. Thus, it is not clear what the analogs of the stable and unstable critical manifolds should be.

3 Day 2: CliMathNet Presentations

The second day featured presentations from the MCRN's partner network in the UK, CliMathNet. Paul Glendenning opened the day with a wonderful account of research that resulted from friendly conversations with his neighbour. He discussed a few variations on conceptual models of the first oxygenation event. The models he discussed were smooth, but contained rapid transitions that he proposed could be modeled with a switch.

Rachel Kuske then discussed relationships between nonsmooth dynamics and tipping points, particularly focusing tipping due to noise. Rachel's talk generated the most cohesive plan for a long-term research project involving at least four of the conference attendees. Motivated by Stommel's model [11], the group explored generalized nonsmooth saddle-node bifurcations. Part one of the research project will

involve determining if nonsmoothness can produce local behavior near a saddle-node bifurcation that leads to non-tipping behavior. Eventually, the group would like to see if the non-tipping persists under noise.

For the final presentation on the second day, Courtney Quinn presented on her research involving glacial cycles in the Quaternary period (2.6 million years ago until present). She explained that Milankovitch cycles explain some aspects of the oscillatory pattern, but the aspects that remain unexplained are likely due to internal processes. One particular example of an internal process is energy transport, and Courtney demonstrated the benefits of modeling energy transport using delay equations. A Boolean delay equation was introduced, incorporating a prevailing theme of the workshop, namely state switches.

4 Day 3: Summary and Discussion

Chris Budd opened the morning session of day three with a presentation tailored to integrating the many themes that had arisen in the presentations and discussions of the first two days. His talk served to organize the collective thoughts of the participants, often contextualizing the interesting questions in the broader areas of climate science and/or nonsmooth dynamics. Chris' talk was the perfect opening with the rest of the day, which was designed for discussion and collaboration. I would like to thank all of the presenters and participants for the insights and attitudes that made our deep discussions so enjoyable. I learned a lot as a result of the workshop, as I hope everyone did, and I anticipate the unresolved questions will lead to more insights in the future. One thing is certain, however: the climate in Barcelona is wonderful.

Acknowledgements I would like to thank the MCRN, funded through NSF grants DMS-0940363 and DMS-1239013, for their support. Additionally, I would like to thank the CRM and programme organizers for inviting us to participate.

References

1. P. Ashwin, P. Ditlevsen, The middle pleistocene transition as a generic bifurcation on a slow manifold. Clim. Dyn. **45**(9–10), 2683–2695 (2015)
2. A.M. Barry, R. McGehee, E. Widiasih, A Filippov framework for an extended Budyko model. Preprint, arXiv:1406.6028
3. M.I. Budyko, The effect of solar radiation variations on the climate of the earth. Tellus **21**(5), 39–692891 (1969)
4. A. Colin de Verdiére, The instability of the thermohaline circulation in a low-order model. J. Phys. Oceanogr. **40**, 757–773 (2010)
5. K. Hill, D.S. Abbot, M. Silber, Analysis of an arctic sea ice loss model in the limit of a discontinuous albedo. Preprint
6. J. Leifeld, Nonsmooth homoclinic bifurcation in a conceptual climate model. Preprint, arXiv:1601.07936

7. J. Leifeld, Perturbation of a nonsmooth supercritical Hopf bifurcation. Preprint, arXiv:1601.07930
8. A. Roberts, P. Glendinning, Canard-like phenomena in piecewise-smooth Van der Pol systems. Chaos **24**(2) (2014)
9. A. Roberts, R. Saha, Relaxation oscillations in an idealized ocean circulation model. Preprint
10. A. Roberts, E. Widiasih, M. Wechselberger, C. Jones, Mixed mode oscillations in a conceptual climate model. Phys. D **292–293**, 70–83 (2015)
11. H. Stommel, Thermohaline convection with two stable regimes of flow. Tellus **13**(2), 224–230 (1961)
12. J. Walsh, E. Widiasih, J. Hahn, R. McGehee, Periodic orbits for a discontinuous vector field arising from a conceptual model of glacial cycles. Preprint, arXiv:1511.01227
13. P. Welander, A simple heat-salt oscillator. Dyn. Atmos. Oceans **6**(4), 233–242 (1982)

Open Problems on Border-Collision Bifurcations

David J.W. Simpson

Abstract The collision of a fixed point with a switching manifold in a piecewise-smooth continuous map, known as a border-collision bifurcation, can give rise to a seemingly endless zoo of complicated dynamics. An understanding of these dynamics, which are described merely by piecewise-linear continuous maps, is one of the most fundamental problems in nonsmooth bifurcation theory. This extended abstract recalls some aspects of border-collision bifurcations and provides a list of pertinent open problems for future research.

A map on $\mathcal{D} \subset \mathbb{R}^N$ of the form

$$x \mapsto \begin{cases} f_1(x;\xi), & x \in \mathcal{D}_1, \\ \quad\vdots & \\ f_m(x;\xi), & x \in \mathcal{D}_m, \end{cases} \tag{1}$$

where each f_i is a smooth function of the state variable $x \in \mathcal{D}_i \subset \mathcal{D}$ and $\xi \in \mathbb{R}^M$ is a parameter, is said to be *piecewise-smooth*. As ξ is varied in a continuous fashion, collisions between invariant sets of (1) and its switching manifolds (the boundaries of the $\mathcal{D}_i$) give rise to *discontinuity-induced bifurcations*. Following [3, 11], we refer to the collision of a fixed point of (1) with a switching manifold as a *border-collision bifurcation* (BCB) if, in a neighbourhood of the bifurcation, the switching manifold is smooth, (1) is continuous, and derivatives $D_x f_i$ are bounded. Here, we briefly describe BCBs and list some open problems. For a more detailed review, refer the reader to Simpson [14].

D.J.W. Simpson (✉)
Institute of Fundamental Sciences, Massey University, Palmerston North, New Zealand
e-mail: d.j.w.simpson@massey.ac.nz

A. Colombo et al. (eds.), *Extended Abstracts Spring 2016*,
Trends in Mathematics 8, DOI 10.1007/978-3-319-55642-0_29

1 The Piecewise-Linear Approximation

In the neighbourhood of a BCB, (1) is piecewise-linear to leading order. To analyse a BCB it is helpful to study the piecewise-linear approximation to (1), because this approximation is relatively straightforward to study, and structurally stable dynamics of the approximation are exhibited by (1). Here, we write such piecewise-linear continuous maps as

$$x \mapsto \begin{cases} A_L x + b\mu\,, & x_1 \leq 0, \\ A_R x + b\mu\,, & x_1 \geq 0, \end{cases} \tag{2}$$

where $x = (x_1, \ldots, x_N)$ is the state variable, $\mu \in \mathbb{R}$ is a parameter governing the BCB, A_L and A_R are constant $N \times N$ matrices differing in only their first columns, and $b \in \mathbb{R}^N$ is a constant vector. The structure of the dynamics of (2) is independent to the magnitude of μ, so it suffices to describe the dynamics of (2) for each sign of μ (i.e. for $\mu < 0$ and $\mu > 0$) as the dynamics at $\mu = 0$ is typically unimportant.

2 Fixed Points and Period-Two Solutions

Here, we summarise the nature of the simplest invariant sets of (2) assuming that certain genericity conditions are satisfied (omitted for brevity). As noted in as early as in Brousin–Neimark–Feigin [1], the map (2) has two potential fixed points:

$$x_L = (I - A_L)^{-1} b\mu, \qquad x_R = (I - A_R)^{-1} b\mu.$$

These are admissible (i.e. valid fixed points of (2)) either for different signs of μ, or the same sign of μ. An LR-cycle (period-two solution involving one point with $x_1 \leq 0$ and one point with $x_1 \geq 0$) is admissible either for one sign of μ, or no sign of μ; see Feigin [4]. This suggests that there are five cases for the admissibility and coexistence of fixed points and period-two solutions of (2); see Feigin [5]. However, in [5] no example of the case that x_L and x_R exist for one sign of μ and an LR-cycle exists for the other sign of μ was given. Recently, linear algebra arguments were used to show that this case cannot occur; see Simpson [13]. Consequently, there are exactly four cases, and the results of [5] allow us to determine which case (2) belongs to by simply looking at the eigenvalues of A_L and A_R; see Table 1.

Table 1 The four cases for fixed points and period-two solutions of (2). For each $J = L, R$, the quantity σ_J^+ (resp. σ_J^-) denotes the number of eigenvalues of A_J greater than 1 (resp. less than -1).

		$\sigma_L^+ + \sigma_R^+$	
		Even	Odd
$\sigma_L^- + \sigma_R^-$	Even	x_L and x_R admissible for different signs of μ; LR-cycle virtual for all $\mu \neq 0$	x_L and x_R admissible for the same sign of μ; LR-cycle virtual for all $\mu \neq 0$
	Odd	x_L and x_R admissible for different signs of μ; LR-cycle admissible for one sign of μ	x_L, x_R and the LR-cycle admissible for the same sign of μ

3 Open Problems

Here we provide a list of open problems in no particular order.

(i) Mode-locking regions of (2) typically exhibit a distinctive chain structure with points of zero width called shrinking points. At a shrinking point, (2) has a periodic solution with two points on the switching manifold. The nature of mode-locking regions near shrinking points is explained by the unfolding theorems of [15, 16], but the overall structure and geometry of mode-locking regions is not understood. For instance what scaling laws govern the distribution of shrinking points and the width of the mode-locking regions?

(ii) With $N = 1$ (i.e. in one dimension) the only periodic solutions of (2) that can be attracting are those with symbolic itineraries involving either at most one L or at most one R; see [9, 10]. In higher dimensions, attracting periodic solutions are possible for a wider range of itineraries. It remains to classify such itineraries, even for $N = 2$.

(iii) Recently, it was shown that (2) can exhibit infinitely many attractors; see Simpson [12]. Grazing-sliding bifurcations of Filippov systems provide an important application for BCBs, and multiple attractors can be created in such bifurcations; see di-Bernardo–Kowalczyk–Nordmark [2]. As noted in Glendinning–Kowalczyk–Nordmark [7], it would be useful to know how many attractors can be created simultaneously in grazing-sliding bifurcations. It remains to show whether or not the mechanism for infinitely many attractors of [12] can be realised in grazing-sliding bifurcations.

(iv) In Glendinning [6] it was shown that (2) can exhibit attractors filling an N-dimensional region of the phase space. Moreover, such N-dimensional attractors are robust to small changes in the entries of A_L, A_R and b. Then, can (2) exhibit a k-dimensional attractor, for any $k = 1, \ldots, N$, that is robust in the same sense?

(v) Unlike local bifurcations of smooth maps, BCBs do not occur on centre manifolds. For this reason, dynamics near BCBs cannot be understood by the classical procedure of dimension reduction via a centre manifold. However, if the eigenvalues of A_L and A_R involve different orders of magnitude, an approximate dimension reduction may be possible in a manner akin to geometric singular perturbation theory.

(vi) Piecewise-linear discontinuous maps can be viewed as a natural generalisation of (2). The lack of continuity allows for more dynamical structures. These have been well studied in one dimension (see Granados–Alsedà–Krupa [8] for a recent review), but appear to be almost unexplored in higher dimensions.

References

1. V.A. Brousin, YuI Neimark, M.I. Feigin, On some cases of dependence of periodic motions of relay system upon parameters. Izv. Vyssh. Uch. Zav. Radiofizika **4**, 785–803 (1963). (in russian)
2. M. di Bernardo, P. Kowalczyk, A. Nordmark, Bifurcations of dynamical systems with sliding: derivation of normal-form mappings. Phys. D **170**, 175–205 (2002)
3. M. di Bernardo, C.J. Budd, A.R. Champneys, P. Kowalczyk, *Piecewise-Smooth Dynamical Systems. Theory and applications* (Springer, New York, 2008)
4. M.I. Feigin, Doubling of the oscillation period with C-bifurcations in piecewise continuous systems. J. Appl. Math. Mech. **34**(5), 822–830 (1970). Translation of Prikl. Mat. Mekh. **34**(5), 861–869 (1970)
5. M.I. Feigin, On the structure of C-bifurcation boundaries of piecewise-continuous systems. J. Appl. Math. Mech. **42**(5), 885–895 (1978). Translation of Prikl. Mat. Mekh. **42**(5), 820–829 (1978)
6. P. Glendinning, Bifurcation from stable fixed point to N-dimensional attractor in the border collision normal form. Nonlinearity **28**, 3457–3464 (2015)
7. P. Glendinning, P. Kowalczyk, A.B. Nordmark, Attractors near grazing-sliding bifurcations. Nonlinearity **25**, 1867–1885 (2012)
8. A. Granados, L. Alsedà, M. Krupa, The period adding and incrementing bifurcations: from rotation theory to applications. Preprint, http://arxiv.org/abs/1407.1895
9. S. Ito, S. Tanaka, H. Nakada, On unimodal linear transformations and chaos. Proc. Jpn. Acad. Ser. A **55**, 231–236 (1979)
10. Yu.L. Maistrenko, V.L. Maistrenko, L.O. Chua, Cycles of chaotic intervals in a time-delayed Chua's circuit. Int. J. Bifurc. Chaos **3**(6), 1557–1572 (1993)
11. H.E. Nusse, J.A. Yorke, Border-collision bifurcations including 'period two to period three' for piecewise smooth systems. Phys. D **57**, 39–57 (1992)
12. D.J.W. Simpson, Sequences of periodic solutions and infinitely many coexisting attractors in the border-collision normal form. Int. J. Bifurc. Chaos **24**(6), 1430018 (2014)
13. D.J.W. Simpson, On the relative coexistence of fixed points and period-two solutions near border-collision bifurcations. Appl. Math. Lett. **38**, 162–167 (2014)
14. D.J.W. Simpson, Border-collision bifurcations in $\mathbb{R}^n$. SIAM Rev. **58**(2), 177–226 (2016)
15. D.J.W. Simpson, J.D. Meiss, Shrinking point bifurcations of resonance tongues for piecewise-smooth, continuous maps. Nonlinearity **22**(5), 1123–1144 (2009)
16. D.J.W. Simpson, J.D. Meiss, Resonance near border-collision bifurcations in piecewise-smooth, continuous maps. Nonlinearity **23**(12), 3091–3118 (2010)

Nonsmooth Maps and the Fast-Slow Dynamics of Sleep-Wake Regulation: Part I

Anne C. Skeldon and Gianne Derks

Abstract Sleep-wake regulation is an example of a system with multiple timescales, with switching between sleep and wake states occurring in minutes but the states of wake or sleep usually existing for some hours. Here, we discuss some general features of models of sleep-wake regulation. We show that some typical models of sleep-wake regulation can be reduced to one-dimensional maps with discontinuities, and show that this reduction is useful in understanding some of the dynamical behaviour seen in sleep-wake models.

1 The Two-Process Model

Sleep is fundamental for the well-being and functioning of humans and animals [1, 2, 5], yet many features of sleep are not well understood. Mathematical models have played an important role in the investigation of proposed biological mechanisms, with the classic Two-Process (TP) model providing a successful and influential framework to describe key features of sleep-wake regulation; see Daan–Beersma–Borbély [3]. The TP model considers two interacting oscillating processes: a circadian process $C(t)$ and a homeostatic sleep process. The homeostatic sleep process takes the form of a relaxation oscillator that results in a sleep pressure, $H(t)$, which monotonically increases during wake and is dissipated during sleep. Switching from wake to sleep and from sleep to wake occurs at upper and lower threshold values of the sleep pressure, respectively. These threshold values are modulated by the periodic circadian process $C(t)$; see Fig. 1.

In its simplest form, the homeostatic sleep pressure, in normalized coordinates, is given by:

A.C. Skeldon (✉) · G. Derks
Department of Mathematics, University of Surrey, Surrey, Guildford GU2 7XH, UK
e-mail: a.skeldon@surrey.ac.uk

G. Derks
e-mail: g.derks@surrey.ac.uk

A. Colombo et al. (eds.), *Extended Abstracts Spring 2016*,
Trends in Mathematics 8, DOI 10.1007/978-3-319-55642-0_30

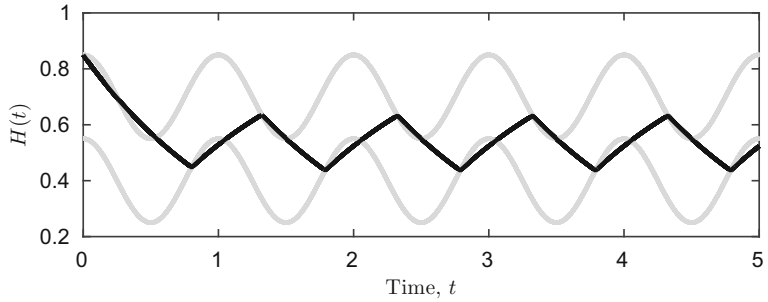

Fig. 1 Graphical illustration of the two process model showing the homeostatic sleep pressure, $H(t)$, increasing during wake and decreasing during sleep. Here, $a = 0.15$, $H_0^+ = 0.7$, $H_0^- = 0.4$, and $\chi^w = \chi^s = 1.25$

$$H(t) = \begin{cases} H_s(t) = H(t_0)\, e^{-(t-t_0)/\chi^s} & \text{(during sleep);} \\ H_w(t) = 1 + (H(t_0) - 1)\, e^{-(t-t_0)/\chi^w} & \text{(during wake).} \end{cases} \tag{1}$$

Switching from wake to sleep occurs when $H(t) = H^+(t) \equiv H_0^+ + aC(t)$, and from sleep to wake occurs when $H(t) = H^-(t) \equiv H_0^- + aC(t)$, where $C(t) = \cos(2\pi t)$ is the circadian oscillation and time has been scaled so that a period of one corresponds to a period of one day. The time constants χ^w and χ^s describe the rate of build-up and dissipation of the homeostatic sleep pressure during wake and sleep, respectively. The mean upper and lower thresholds are H_0^+ and H_0^-, respectively, and a is the amplitude of the circadian oscillation. The solution shown in Fig. 1 represents a sleep-wake pattern with one sleep episode per day. However, already in the first in-depth description of the model in Daan–Beersma–Borbély [3], it was recognised that, by varying the parameters, many different patterns of sleep could be obtained. One of our aims is to understand how these different patterns occur.

The TP model can be represented as a one-dimensional map by considering successive values of the sleep onset timing [6, 7], as illustrated in Fig. 2a and described as follows. Let the homeostatic sleep pressure $H(t)$ be on the upper threshold curve at time T_0^n, $H(T_0^n) = H^+(T_0^n)$, then run the TP model through one sleep/wake cycle to obtain the time T_0^{n+1} when $H(t)$ next reaches the upper threshold curve. Taking all values for $T_0^n \in [0, 1]$ and considering T_0^{n+1} mod 1 results in a map, as shown in Fig. 2c. Two features of the map that may be surprising at first sight are the following:

(i) The map has a gap with an infinite derivative to the left of the gap and a bounded derivative to the right of the gap;
(ii) The map is non-monotonic.

Both features are a consequence of points where $H(t)$ becomes tangent to one of the threshold curves. Specifically, the gap, and the nature of the derivatives local to the gap, are a consequence of a tangency of $H_s(t)$ with the lower threshold or $H_w(t)$ with the upper threshold. At such tangencies, neighbouring values of T_0^n are mapped to very different values of T_0^{n+1}, as shown in Fig. 2b.

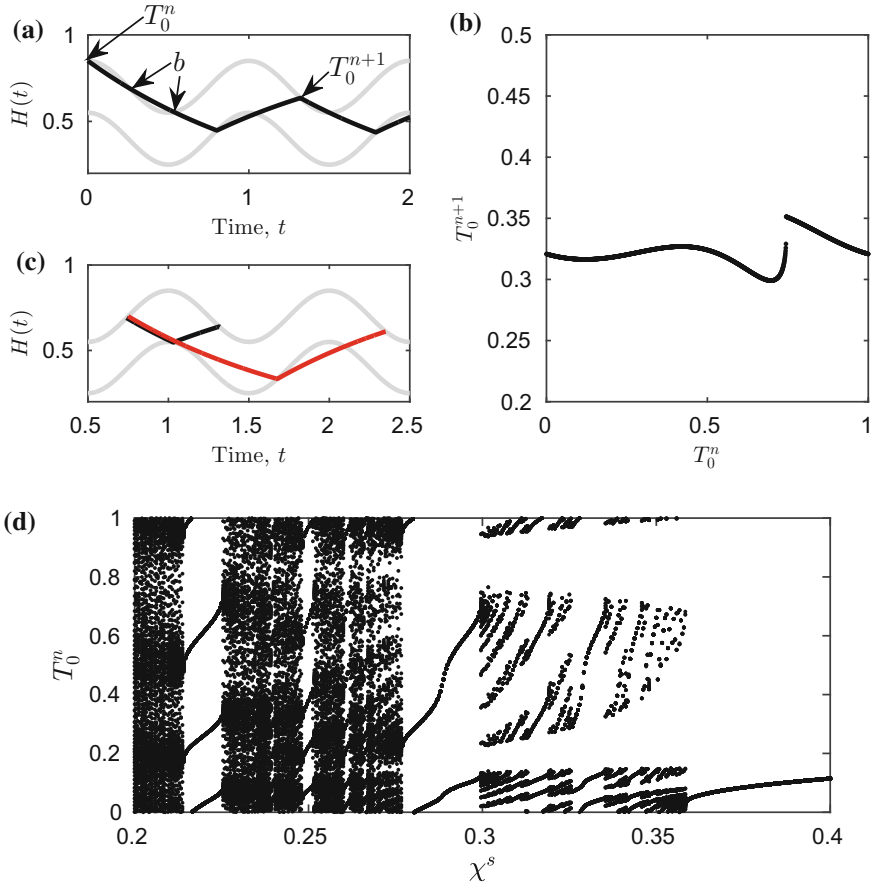

Fig. 2 (**a**) The two process model can be considered as a map giving a sequence of sleep onset times $T_0^n, T_0^{n+1}, \ldots$; here, $a = 0.15$, $H_0^+ = 0.7$, $H_0^- = 0.4$, and $\chi^w = \chi^s = 1.25$. A typical map generated by considering all $T_0^n \in [0, 1]$ is shown in (**c**). The discontinuity results from the trajectories which touch either the upper or lower thresholds at a tangency, as illustrated in (**b**). (**d**) Typical bifurcation diagram for varying χ^s, where $a = 0.15$, $H_0^+ = 0.7$, $H_0^- = 0.4$, and $\chi^w = \chi^s$

The non-monotonicity occurs as a consequence of tangencies of $H_s(t)$ with the upper threshold or $H_w(t)$ with the lower threshold. In Fig. 2a we show the consequences of tangencies of $H_s(t)$ with the upper threshold. The tangencies result in the map having three pre-images rather than one for some values of T_0^{n+1}. This can be seen in Fig. 2a, where the two points labelled 'b' and the point T_0^n all map to the same value T_0^{n+1}.

The presence of gaps and the non-monotonicity result in the map having a rich dynamical structure (see Granados–Alsedà–Krupa [4]) and explain the different types of solutions observed in Daan–Beersma–Borbély [3]. For example, border collisions leading to period-adding bifurcations can occur; see Fig. 2d. Such bifurcations have

physiological significance as they represent transitions between different numbers of sleep episodes in a day, suggestive of the changes in sleep patterns observed in babies and early childhood. The infinite gradient to the left of the discontinuity leads to saddle-node bifurcations and the non-monotonicity suggests that a period-doubling cascade leading to chaos may occur. These details are being investigated and will be published in future work.

This paper is the first of two papers on the dynamics of sleep. The second focusses on some more physiological models of sleep-wake regulation.

Acknowledgements The authors thank the Centre de Recerca Matemàtica for the opportunity to work with each other and other participants of the intensive programme on Advances in Nonsmooth Dynamics. ACS and GD are indebted to Prof. Derk-Jan Dijk of the Surrey Sleep Research Centre at the University of Surrey for introducing them to the area of mathematical modelling of sleep-wake regulation.

References

1. S.N. Archer, E.E. Laing, C.S. Möller-Levet, D.R. van der Veen, G. Bucca, A.S. Lazar, N. Santhi, A. Slak, R. Kabiljo, M. von Schantz, C.P. Smith, D.J. Dijk, Mistimed sleep disrupts circadian regulation of the human transcriptome. Proc. Natl. Acad. Sci. **111**, E682–E691 (2014)
2. F.P. Cappuccio, L. D'Elia, P. Strazzullo, M.A. Miller, Sleep duration and all-cause mortality: a systematic review and meta-analysis of prospective studies. Sleep **33**, 585–592 (2010)
3. S. Daan, D.G.M. Beersma, A.A. Borbély, Timing of human sleep: recovery process gated by a circadian pacemaker. Am. J. Physiol. **246**, R161–R178 (1984)
4. A. Granados, L. Alsedà, M. Krupa, The period adding and incrementing bifurcations: from rotation theory to applications. Preprint, arXiv:1407.1895
5. C.S. Möller-Levet, S.N. Archer, G. Bucca, E. Laing, A. Slak, R. Kabiljo, J. Lo, N. Santhi, M. von Schantz, C.P. Smitth, D.J. Dijk, Effects of insufficient sleep on circadian rhythmicity and expression amplitude of the human blood transcriptome. Proc. Natl. Acad. Sci. **110**, E1132–E1141 (2013)
6. M. Nakao, M. Yamamoto, Bifurcation properties of the two process model. Psychiatry Clin. Neurosci. **52**, 131–133 (1998)
7. A.C. Skeldon, D.J. Dijk, G. Derks, Mathematical models for sleep-wake dynamics: comparison of the two-process model and a mutual inhibition neuronal model. PLoS ONE **10**, e103877 (2014)

Nonsmooth Maps and the Fast-Slow Dynamics of Sleep-Wake Regulation: Part II

Anne C. Skeldon, Gianne Derks, and Victoria Booth

Abstract In part I, the Two-Process model for sleep-wake regulation was discussed and it was shown that it could usefully be represented as a one-dimensional map with discontinuities. Here, we discuss some recent, more physiological, models of sleep-wake dynamics. We describe how their fast-slow structure means that one can expect them to inherit many of the dynamical features of the Two-Process model.

1 Neuronal Models of Sleep-Wake Regulation

Recent experimental findings have led to the idea that sleep-wake regulation occurs by a 'flip-flop' switch between sleep and wake states generated through mutual inhibition between populations of sleep and wake promoting neurons; see Saper–Scammell–Lu [9]. This has led to several mathematical models extending the ideas of the Two-Process (TP) model to a more physiological setting: a recent review on this topic is given in Booth–Diniz-Behn [1]. These models consider the interactions between sleep- and wake-promoting neuronal populations that are modulated by the homeostatic sleep drive and the circadian rhythm of the TP model. They are described by systems of ordinary differential equations of the form

$$\tau_i \frac{d\mathbf{U}}{dt} + \mathbf{U} = \mathbf{G}(\mathbf{U}, H, C(t)), \qquad \mathbf{U} \in R^n, \tag{1}$$

$$\chi(\mathbf{U}) \frac{dH}{dt} + H = G_H(\mathbf{U}). \tag{2}$$

A.C. Skeldon (✉) · G. Derks
Department of Mathematics, University of Surrey, Guildford, Surrey GU2 7XH, UK
e-mail: a.skeldon@surrey.ac.uk

G. Derks
e-mail: g.derks@surrey.ac.uk

V. Booth
Departments of Mathematics and Anesthesiology, University of Michigan,
530 Church Street, Ann Arbor, MI 48109-1043, USA
e-mail: vbooth@umich.edu

A. Colombo et al. (eds.), *Extended Abstracts Spring 2016*,
Trends in Mathematics 8, DOI 10.1007/978-3-319-55642-0_31

Here, the elements of $\mathbf{U}$ represent activity levels of the neuronal populations either in terms of average firing rate or average membrane potential and, in some cases, the concentrations of key neurotransmitters. The variable H represents the homeostatic sleep pressure and $C(t)$ is a periodic circadian external drive. The vector-valued function $\mathbf{G}$ is sigmoidal in the population activity levels. The function G_H is sigmoidal with respect to the action of wake promoting neurons or is taken to be a hard switch between two threshold functions. The function $\chi(\mathbf{U})$ is either constant or takes one of two values dependent on the activity state of the wake population.

Two examples of models of this type are the Phillips and Robinson model (PR model) [6], and the Booth and Diniz-Behn model (BDB model) [3, 5]. The PR model includes two neuronal populations, one promoting sleep and one promoting wake. The BDB model distinguishes three neuronal groups, one for wake, one for rapid eye movement (REM) sleep and one for non-REM (nREM) sleep.

An essential common feature in these neuronal models is that, since τ_i is much smaller than both $\chi(\mathbf{U})$ and the period of $C(t)$, there is a separation of time scales between the neuronal dynamics and the dynamics of the homeostatic and circadian rhythms. Hence, there is a slow manifold $\mathbf{U}_0(H, C)$ that, to lowest order, is given by

$$\mathbf{U}_0 = \mathbf{G}(\mathbf{U}_0, H, C). \tag{3}$$

In the simplest setting, considering sleep as consisting of one state (nREM), the sigmoidal assumptions mean that Eq. (3) has one or three solutions parameterized by H and C. Consequently, the slow manifold takes the form of a folded surface with saddle-node bifurcations characterizing the position of the folds, as shown in Figs. 1a, b for the PR and the BDB models respectively; see [4, 10]. In these figures, in the fast dynamics, the 'upper' wake state and the 'lower' sleep states are stable, while the intermediate steady-states are unstable.

The slow dynamics of the homeostat H given by Eq. (2) result in H increasing (during wake) and decreasing (during sleep). Together with the periodic oscillation

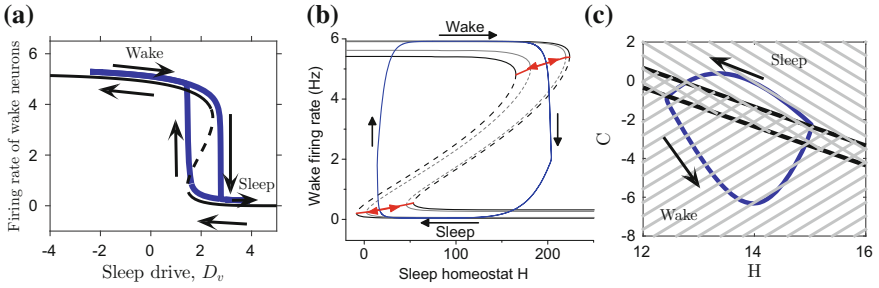

Fig. 1 (**a**) The slow manifold of the PR model along with a typical trajectory (the trajectory has been offset from the slow manifold for clarity); (**b**) the slow manifold and a trajectory for the BDB model; (**c**) the trajectory shown in (**a**) re-plotted in the (H, C)-plane: the saddle-node bifurcations where switching between wake and sleep occur are represented by the *thick black diagonal lines*

of the circadian C this leads to relaxation oscillations between wake and sleep states, shown by the blue curves in Figs. 1a and b. In the PR model, Fig. 1a, the dynamics of H and C are combined in a single 'sleep' drive parameter, $D_v = H(t) - C(t)$. In the BDB model, H and C are represented as separate inputs to the neuronal populations, resulting in the slow manifold being most apparent as a function of H, with C modulating the position of the slow manifold a function of time. An alternative illustration of these dynamics is to depict the slow manifold as a function of the two slow parameters, H and C, as shown in Fig. 1c, where the slow manifold of the PR model has been projected onto the (H, C)-plane.

2 Discussion

Although the neuronal models and the TP model are formulated in different ways, they share many common features: in Phillips–Robinson [7], it is shown how solutions of the PR model can be plotted in the form of the TP model, and in Skeldon–Dijk–Derks [10], it is shown that the slow dynamics of the PR model and the TP model can be formally identified in the limit that the soft switching functions in the PR model are replaced by hard switches. Consequently, essentially the same kind of patterns of sleep and wake can be expected in the PR model as are seen in the TP model. Furthermore, many of the different behaviours seen in simulations of the PR model, such as those explaining different mammalian sleep patterns in Phillips–Robinson–Kedziora–Abeysuriya [8], can then be understood as resulting from border collision bifurcations.

The common underlying structure described in Eqs. (1) and (2), suggests that not only the PR model but other neuronal models can be related to the TP model and to one-dimensional maps with discontinuities. This is indeed the case for the BDB model, in its simplest setting, as shown in Fig. 2. The sleep-wake switching behaviour of the BDB model can be plotted in the same spirit as the TP model; see Fig. 2a. Here, $H(t)$ switches between sleep and wake states and the position of the upper and lower saddle-node bifurcation points of the slow manifold are modulated by the circadian oscillation. The switch between sleep and wake states does not occur exactly when the trajectory reaches a threshold curve, as in the TP model, due to slow passage effects around the saddle-node points.

A one-dimensional map for successive sleep onset times can be computed for the BDB model (see Fig. 2b), where sleep onset timing is now specified relative to the phase of the circadian oscillation. This map is constructed by initialising the BDB model at a phase of the circadian cycle Φ_0^n at time $t = t_0^n$, with $C = C(t_0^n)$ and $H(t_0^n)$ such that $(H(t_0^n), C(t_0^n))$ and the firing rate and neurotransmitter variables $\mathbf{U}$ are set at their values at the upper saddle-node point in Fig. 1b. The system is then evolved through one sleep-wake cycle until an upper saddle-node point is reached again at time $t = t_0^{n+1}$ and circadian phase Φ_0^{n+1}. The map consists of all points Φ_0^{n+1} mod 1 such that $\Phi_0^n \in [0, 1]$. As in the TP model map, this map has gaps with infinite derivatives to the left of the gap and bounded derivatives to the right of the gap.

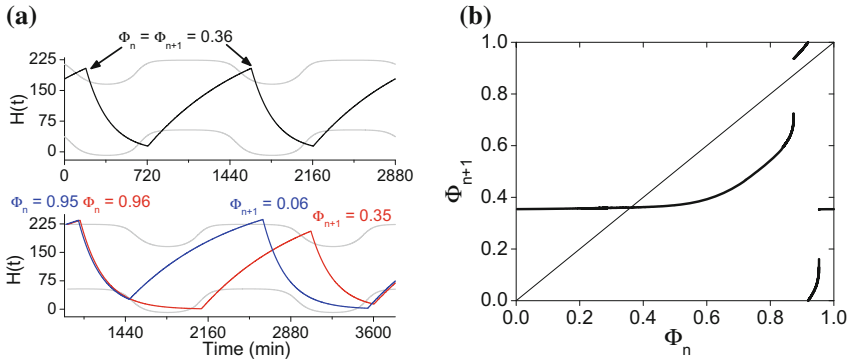

Fig. 2 (**a**) Sleep-wake switching in the BDB model: the homeostatic sleep drive $H(t)$ varies between threshold curves determined by the circadian modulation of the H values of the *upper* and *lower* saddle-node bifurcation points of the slow manifold (Fig. 1b); circadian phases of sleep onset times labeled for reference (colours match trajectory curves); (**b**) one-dimensional map of circadian phases of sleep onset Φ_{n+1} as a function of the previous sleep onset phase Φ_n computed from the BDB model when REM sleep is suppressed

These gaps occur due to model trajectories becoming tangent to the boundary curves defined by the saddle-node points of the slow manifold, as illustrated in terms of $H(t)$ in the lower panel of Fig. 2a. This reduction to a one-dimensional map is strongly suggestive that, like the PR model, border collisions are critical in understanding some of the dynamics of the BDB model.

Whereas the PR model only considers two neuronal populations and describes the two states of wake and sleep, the BDB model includes three neuronal groups and the three states of wake, nREM sleep and REM sleep. Humans normally oscillate between nREM and REM sleep during a typical night's sleep, with the longest interval of nREM sleep occurring at the beginning of sleep. By changing one of the parameters, the BDB model can capture the periodic switching between nREM and REM sleep. This transition occurs as a result of the steady-state of the lower branch of the slow manifold losing stability to be replaced by a stable periodic solution. The number of REM episodes during one night can be tuned, with Figs. 1b and 2 illustrating the particular case where there are no REM episodes. In the more complicated dynamical regimes, where oscillations between REM and nREM sleep exist, the model can still be reduced to a one-dimensional map, but each additional REM episode results in an additional discontinuity in the map. This intriguing structure is currently under investigation in Booth–Xique–Diniz-Behn [2].

There remain many unanswered questions and interesting dynamics to explore but a few points are clear. Sleep-wake regulation models are interesting and biologically relevant examples of systems. Recognising their non-smooth nature is important both in gaining an in-depth understanding of their dynamical behaviour and in understanding the extent to which different models have different dynamics.

Acknowledgements The authors thank the Centre de Recerca Matemàtica for the opportunity to work with each other and other participants of the intensive programme on Advances in Nonsmooth Dynamics. VB acknowledges her collaborator on this work Cecilia Diniz-Behn and support from the National Science Foundation DMS-1412119.

References

1. V. Booth, C.G. Diniz Behn, Physiologically-based modeling of sleep-wake regulatory networks. Math. Biosci. **250**, 54–68 (2014)
2. V. Booth, I. Xique, C.G. Diniz Behn, A one-dimensional map for the circadian modulation of sleep in a human sleep-wake regulatory network model. Centre de Recerca Matemàtica, Preprint #1223 (2016)
3. C. Diniz Behn, V. Booth, BoothSimulating microinjection experiments in a novel model of the rat sleep-wake regulatory network. J. Neurophysiol. **103**, 1937–1953 (2010)
4. B.D. Fulcher, A.J. Phillips, P.A. Robinson, Modeling the impact of impulsive stimuli on sleep-wake dynamics. Phys. Rev. E. Stat. Nonlin. Soft. Matter Phys. **78**, 051920 (2008)
5. R.D. Gleit, C. Diniz Behn, V. Booth, Modeling interindividual differences in spontaneous internal desynchrony patterns. J. Biol. Rhythm. **28**, 339–355 (2013)
6. A.J. Phillips, P.A. Robinson, A quantitative model of sleep-wake dynamics based on the physiology of the brainstem ascending arousal system. J. Biol. Rhythm. **22**, 167–179 (2007)
7. A.J. Phillips, P.A. Robinson, Sleep deprivation in a quantitative physiologically based model of the ascending arousal system. J. Theor. Biol. **255**, 413–423 (2008)
8. A.J. Phillips, P.A. Robinson, D.J. Kedziora, R.G. Abeysuriya, Mammalian sleep dynamics: how diverse features arise from a common physiological framework. PLoS Comput. Biol. **6**, e1000826 (2010)
9. C.B. Saper, T.E. Scammell, J. Lu, Hypothalamic regulation of sleep and circadian rhythms. Nature **437**, 1257–1263 (2005)
10. A.C. Skeldon, D.J. Dijk, G. Derks, Mathematical models for sleep-wake dynamics: comparison of the two-process model and a mutual inhibition neuronal model. PLoS ONE **10**, e103877 (2014)

Comments for the Continuation Method by A.F. Filippov for Discontinuous Systems, Part I

Vadim I. Utkin

Abstract The conventional existence-uniqueness theorems are not applicable for differential equations with right hand sides as discontinuous state functions. This is the case for the systems with discontinuous controls and sliding modes, when state trajectories belong to discontinuity surfaces. Many authors offered their methods of deriving sliding mode equations, or solution continuations on the discontinuity surfaces. Due to uncertainties of right hand sides, the proposed methods led to different solutions. These methods are compared, the reasons of ambiguity are discussed in the paper. It is assumed that any solution is under the umbrella of the method proposed by A.F. Filippov.

1 Introduction

The systems with control actions as discontinuous state functions are under discussion. Relay systems and variable structure systems belong to this class. Relay systems were employed actively at the first stage of the control theory history, because of their ease of implementation, and to help control reach its full potential. Voltage control of a DC generator, already described in the paper Kulebakin [3] from 1932, may serve as an example; see Fig. 1, top. Any comments are hardly needed for a modern reader. The principle operation mode, called "vibrational" in these papers, is nothing but sliding mode in the modern terminology. The term "sliding mode" can be found in the paper Nikolski [5] from 1934 about ship course control; see Fig. 1, bottom. The theoretical methods of analysis and design were summarized in the monographs Flugge-Lotz [2] and Tsypkin [6], published in the USA and USSR, respectively. Sliding modes on a switching line for relay control were studied in these monographs. The state plane of the system

$$\ddot{x} = u \tag{1}$$

with relay control

V.I. Utkin (✉)
The Ohio State University, Columbus, OH, USA
e-mail: utkin@ece.osu.edu

A. Colombo et al. (eds.), *Extended Abstracts Spring 2016*,
Trends in Mathematics 8, DOI 10.1007/978-3-319-55642-0_32

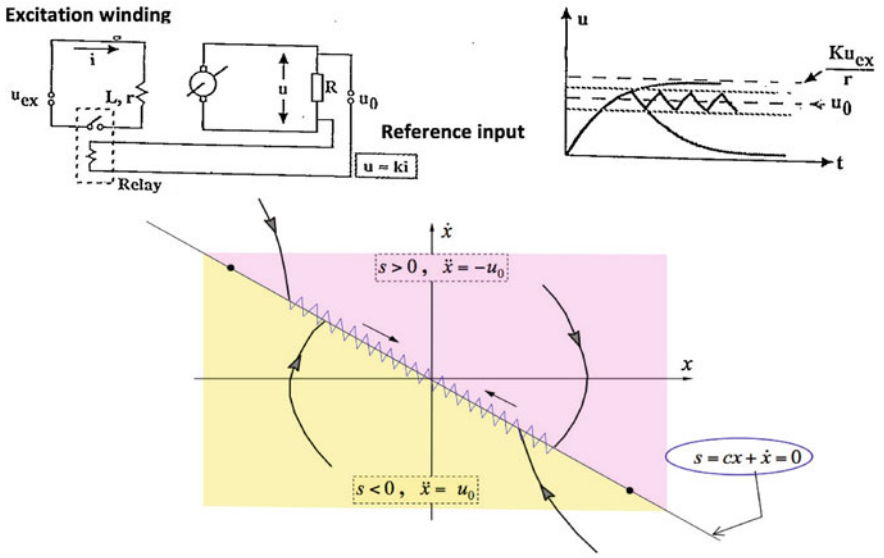

Fig. 1 Examples of sliding mode control

$$u = -u_0 \operatorname{sign}(s), \quad s = cx + \dot{x}, \quad u_0, c > 0. \tag{2}$$

The state vector $(x, \dot{x})$ reaches the line $s = 0$ after a finite time interval and then cannot leave it. This motion is called a sliding mode. The equation of switching line $cx + \dot{x} = 0$ is used as the motion equation. Its solution depends on the switching line equation and does not depend on properties of the plant to be controlled.

The property of invariance was utilized actively in the 1960's in variable structure systems, when the system behavior was studied in the space of an output variable and its time derivatives. In contrast to relay systems, the amplitude of the control signal u_0 depended on the state vector. All these facts are well-known for a long time, and mentioned in this paper to explain why development of new mathematical methods is needed for this class of systems. Formally the mathematical problem of describing sliding modes for the simplest second order systems (1) and (2) remains open. Indeed, a Lipshitz constant does not exist for discontinuous systems, and as a result the conventional uniqueness-existence theorems are not applicable. The above offered solution $x(t) = x_0 e^{-ct}$ to equation $cx + \dot{x} = 0$ looks doubtful: if this function is the solution, then it should turn the equation into an identity, but it is not clear what the function sign(s) = sign(0) is equal to.

A.F. Filippov offered a new method [1] of solution continuation on discontinuity surface for the systems with discontinuous right hand sides

$$\dot{x} = \begin{cases} f^+(x,t) \text{ if } s(x) > 0, \\ f^-(x,t) \text{ if } s(x) < 0, \end{cases} \quad x, f^+, f^- \in \mathbb{R}^n, \quad s \in \mathbb{R}. \tag{3}$$

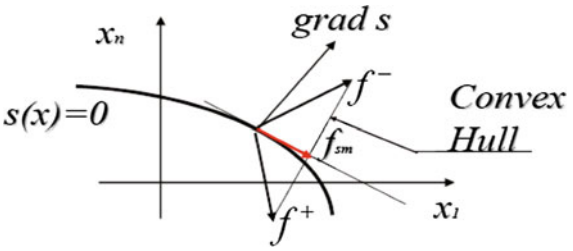

Fig. 2 Filippov method

For now, we confine ourselves to the simplified formulation of Filippov's method; see Fig. 2.

An equation $\dot{x} = f_{sm}$, with a vector field f_{sm}, describes a sliding mode on the surface $s(x) = 0$, found from the convex hull of vectors f^+ and f^-, which is a straight line connecting the ends of these vectors (Fig. 2), given by $f_{sm} = \mu f^+ + (1 - \mu) f^-$ for $0 \geq \mu \geq 1$. The vector f_{sm} lies in the intersection of the straight line with the tangential plane to the surface $s(x) = 0$, and the coefficient μ is found from equation $[\nabla(s)]^T f_{sm} = 0$. Actually, the method by Filippov postulates the sliding mode equation, but other methods of solution continuation on the discontinuity surface were offered in a set of publications. These methods are discussed and compared in this short paper.

2 Problem Statement

The motion of a finite-dimensional system with vector control is governed by the equation

$$\dot{x} = f(x, t, u), \qquad x, f \in \mathbb{R}^n, \quad u \in \mathbb{R}^m. \tag{4}$$

Similarly to the simple examples in the introduction, each component of the control is assumed to be a discontinuous state function

$$u_i = \begin{cases} u_i^+(x, t) \text{ if } s_i(x) > 0, \\ u_i^-(x, t) \text{ if } s_i(x) < 0, \end{cases} \quad i = 1, \ldots, m. \tag{5}$$

Scalar functions $s_i(x)$ are continuous-differentiable and any solution of (4) for any of the functions $u_i^{\pm}(x.t)$ exists and is unique. Sliding modes in (4) and (5) can occur at each of the surfaces $s_i(x) = 0$ and, on their intersection, $s(x) = 0, s^T = (s_1, \ldots, s_m)$; see Fig. 3. The set of problems of interest are then: how to find sliding mode equations, whether they are unique, and if not, how to substantiate a choice of motion equations for real processes.

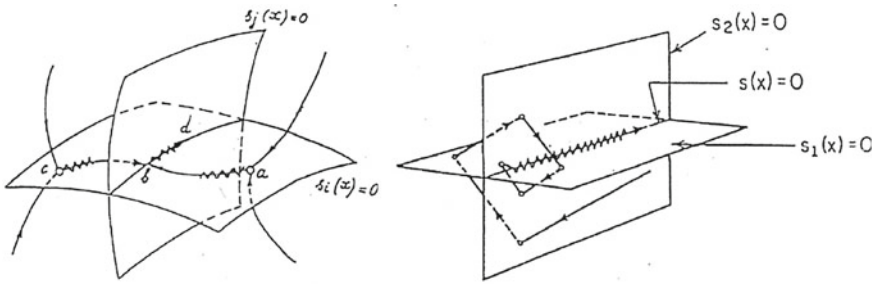

Fig. 3 Multidimensional sliding mode

3 Systems with Scalar Control

From the first view, system (4) and (5) with a scalar control $u \in \mathbb{R}$ is equivalent to system (3), studied by Filippov, with $f^+ = f(x,t,u^+)$, $f^- = f(x,t,u^-)$. However, dependence of the right hand side on the control gave birth to many methods of deriving sliding mode equations, dictated by natural engineering arguments. For example, relay control was replaced by a linear relation ks with k tending to infinity [6], since the input of the relay s is close to zero (the trajectory belongs to the surface $s(x) = 0$), while the output takes finite values. It was suggested to write down the solution in convolution form for linear systems, and to find a continuous control such that $s(t) = 0$; see Neimark [4]. Another method was based on the replacement of discontinuous control by a continuous one such that $s(t) = 0$; see Utkin [7]. These methods happened to result in different sliding motion equations and rather vivid discussions on what method was correct.

We start with the example which served as a reason for doubts in the correctness of Flippov's method,

$$\dot{x} = Ax + bu_1 + du_2, \quad u_1 = -M_1 \operatorname{sign}(s), \quad u_2 = -M_2 \operatorname{sign}(s). \tag{6}$$

Both components of control undergo discontinuities on the same plane $s(x) = cx = 0$ (A, b, d, M_1, M_2, c are constants). From the first view, the unique sliding equation can be derived by Flippov's method with $f^+ = Ax - bM_1 - dM_2$, $f^- = Ax + bM_1 + dM_2$. Let the control u_2 be implemented as a relay function with small hysteresis, and $M_1 \gg M_2$, then a sliding mode can be enforced for any value of $u_2 = M_2$ or $u_2 = -M_2$. Sliding mode equations can be derived following Flippov's method for $f^+ = Ax - bM_1 + du_2$, $f^- = Ax + bM_1 + du_2$. The control u_2 can take one of two possible values depending on initial conditions. This non-uniqueness was the reason of doubts. But these doubts can be easily eliminated if we use the exact recommendation of Filippov (in contrast to the simplified formulation in the introduction):

$$\dot{x} = f_{sm}, \quad f_{sm}(x,t) \in \lim_{\varepsilon \to 0} \operatorname{conv} f(x + \delta x, t, u + \delta x)) \backslash N,$$

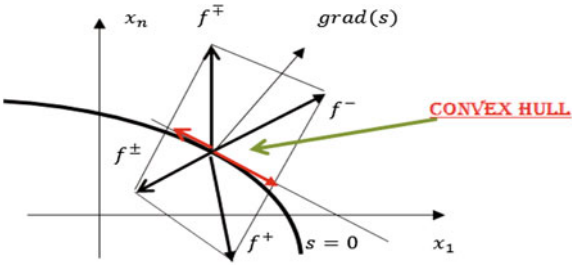

Fig. 4 Non-unique sliding mode equations

where conv $f(x + \delta x, t, u)$ means a minimal convex hull, corresponding to all values of control in the vicinity $||\delta x|| < \varepsilon$, and the symbol $\backslash N$ means that a set of zero measure can be excluded from this vicinity (or points of the discontinuity surface where the control is not defined). There are four possible vectors in the right hand side of the above example, corresponding to different combinations of u_1 and u_2. The minimal convex hull of the four vectors is the polygon depicted in Fig. 4, and its intersection with the tangential plane defines the set of all possible right hand sides in the sliding mode equations. This set includes two different motion equations in the above example, when control u_2 could take one of two possible values.

Filippov's method has a very simple interpretation in the time domain. Let the right hand side of (4) take one of k possible values $f_1, \ldots, f_k$ in the vicinity of some point in the state space, and let the time interval Δt consist of k subsets $\Delta t_1, \ldots, \Delta t_k$, $\Delta t = \sum_{i=1}^{k} \Delta t_i$ with values of right hand sides $f_1, \ldots, f_k$ correspondingly. Then

$$\dot{x} = \lim_{\Delta t 0} \rightarrow \frac{1}{\Delta t} \sum_{i=1}^{k} f_i \Delta t_i = \Sigma_{i=1}^{k} \mu_i f_i, \quad \mu_i = \frac{\Delta t_i}{\Delta t}, \quad \mu_i \geq 0, \quad \sum_{i=1}^{k} \mu_i = 1.$$

The right hand side is nothing but the convex hull of $f_1, \ldots, f_k$.

References

1. A.F. Filippov, *Differential Equations with Discontinuous Right Hand Side*. Math. set of papers, 99–128 (in Russian)
2. I. Flugge-Lotz, *Discontinuous Automatic Systems* (Princeton University Press, Princeton, 1953)
3. V.S. Kulebakin, On theory of automatic vibrational controllers for electric machines, in *Theoretical and Experimental Electronics*, vol. 4 (1932) (in Russian)
4. Yu.I. Neimark, On sliding modes in relay systems of automatic control. A&T **1** (1957) (in Russian)
5. G.N. Nikolski, On automatic stability of a ship on given course, in *Proceedings of Central Laboratory of Cable Communication*, vol. 1 (1934) (in Russian)
6. Ya.Z. Tsypkin, Theory of automatic regulation systems. Gostechizdat (1955) (in Russian)
7. V.I. Utkin, Sliding modes in optimization and control. Nauka (1981) (in Russian)

Comments for the Continuation Method by A.F. Filippov for Discontinuous Systems, Part II

Vadim I. Utkin

Abstract In the second part of this article, solution methods for scalar or vector control are considered.

1 Systems with Scalar Control (Continued)

As we can see in Part I of this paper, Filippov's method, offered as a postulate, represents a rather evident fact: if the velocity vector can take several values in a vicinity of some point in the state space then, due to switching, the right hand side of the equations of motion is their minimal convex hull and no other motions can appear. In this context it is interesting to compare Filippov's method with other approaches to describing sliding modes. The next example from the 1970s demonstrated the necessity of such comparison,

$$\dot{x}_1 = 0.3x_2 + ux_1, \quad \dot{x}_2 = -0.7x_1 + 4u^3x_1, \quad u = -\operatorname{sign}(x_1 s), \quad s = x_1 + x_2.$$

It is easy to show that functions s and $\dot{s}$ have opposite sign in the vicinity of the switching line $s = 0$, and sliding mode occurs on it. Two implementation versions of control were used for simulation: relay element with hysteresis, and a limiter (a high gain amplifier with bounded output); see Fig. 1.

The results of simulations seemed strange to us, at least at that time: motion in sliding mode proved to be stable in one case and unstable in the second case; see Fig. 2.

This effect was observed as the parameter a tended to zero. The sliding mode for relay with hysteresis was governed by the equation resulting from Filippov's method. The system with the limiter exhibited the sliding mode predicted by the so-called "Equivalent Control Method"; see Utkin [3]. The method implies the replacement of a discontinuous control by a continuous one u_{eq}, such that the time derivative $\dot{s} = (\nabla(s))^T f(x, t, u_{eq})$ is equal to zero identically. As can be seen from Fig. 3, left,

V.I. Utkin (✉)
The Ohio State University, Columbus, OH, USA
e-mail: utkin@ece.osu.edu

A. Colombo et al. (eds.), *Extended Abstracts Spring 2016*,
Trends in Mathematics 8, DOI 10.1007/978-3-319-55642-0_33

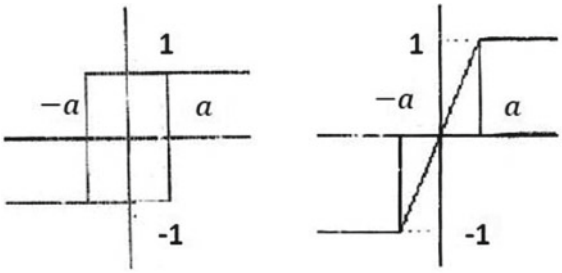

Fig. 1 Implementation of discontinuous control

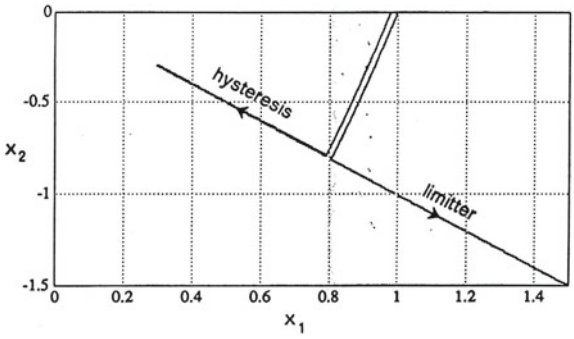

Fig. 2 State trajectories

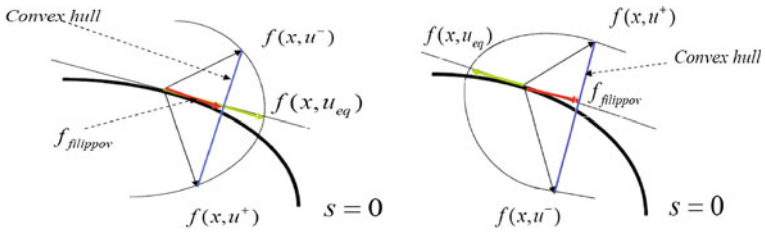

Fig. 3 Right-hand sides of sliding mode equations

the right hand parts of equations for these two methods, $f_{filippov}$ and $f(x, u_{eq})$, do not coincide.

Note that replacement of discontinuous control by a linear control with high gain, offered in Tsypkin [2], and replacement of it by a limiter in our example do coincide. Vectors $f_{filippov}$ and $f(x, u_{eq})$ in our example were located in opposite directions; see Fig. 3, right. This explains why one of the motions was stable and the other unstable.

The result seems a contradiction. However, it can be eliminated again if the motion equations are obtained following the exact recommendation of Filippov. For the first case, of relay with hysteresis, the control can take two values only, u^+ and u^-, and the

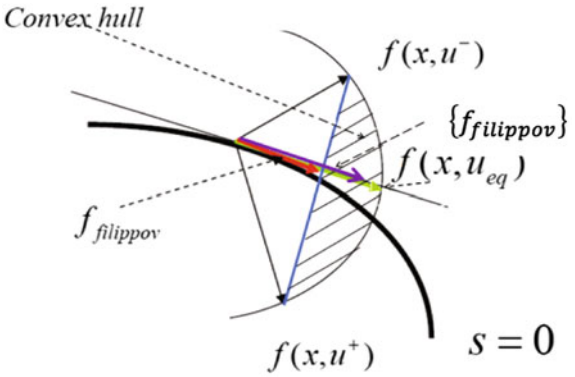

Fig. 4 Set of sliding mode equations in system with scalar control

convex hull is the straight line connecting the ends of vectors f^+ and f^-; see Fig. 4. The sliding mode equation is defined by the vector $f_{filippov}$ in the tangential plane. The case with a limiter control can take all values $u^- \geq u \geq u^+$, and the right hand side can be any vector on the arc connecting vectors f^+ and f^-; see Fig. 4. The convex hull for this case is the dashed sector. Its intersection with the tangential plane refines the set of all possible speed vectors $\{ccf_{filippov}\}$, or all possible sliding mode equations. The set includes both the motion resulting from the simplified form of Filippov method given in the introduction of Part I, and the motion defined by equivalent control method.

It makes sense to explain why a set of zero measure should be excluded in the solution continuation method (Part I, equation (6)). The speed vector (or control) on the discontinuity surface $s = 0$ can be found in the system context only. Attempts to assign it beyond this as a rule lead to contradiction. For example in the mechanical system

$$m\ddot{x} = F_{fr} - F(t),$$

Coulomb friction $F_{fr} = -F_0 \operatorname{sign}(\dot{x})$ undergoes discontinuities on the surface $\dot{x} = 0$, and a sliding mode occurs on this surface if $F_0 > |F(t)|$. It is evident that $F_0 > |F(t)|$ and this time function does not coincide with an arbitrary assigned (beyond the system context) value of F_{fr} on the switching surface.

The solution continuation method by Filippov enables all possible speed vectors to be obtained if all values of control in the vicinity $||\delta x|| < \varepsilon$ are known. The suggested method in Aizerman–Pyatnitskii [1] takes into account all values of control from a convex hull of their real values. The method can lead to a wider set, including values of speed vectors which can never appear (for example, if the control can take two values only).

2 Systems with Vector Control

Filippov's method is applicable to systems with vector control as well, when sliding modes occur in an intersection of several discontinuity surfaces; see Fig. 3 in Part I. First, the minimal convex hull of all possible speed vectors in the vicinity of the manifold $s(x) = 0$ should be found. The intersection of the set with the tangential manifold to $s(x) = 0$ defines all possible motions in the sliding mode. We will confine ourselves to one example only to demonstrate that, from the first view, contradiction between different methods of deriving sliding mode equations can be eliminated easily by "correct" application of Filippov's method.

The first two equations in the third order system

$$\begin{aligned} \dot{x}_1 &= u_1, \qquad u_1 = -\operatorname{sign}(x_1), \\ \dot{x}_2 &= u_2, \qquad u_2 = -\operatorname{sign}(x_2), \\ \dot{x}_3 &= u_1 u_2, \end{aligned} \tag{1}$$

are independent, and sliding mode exists in each of them with $x_1 = 0$, $x_2 = 0$. The function $x_1(t)$ is shown in Fig. 5.

Both equivalent controls are equal to zero and their substitution into the third equation means $x_3 = const$. However, in a real system, for example if both controls are implemented by a relay with hysteresis Δ (see Fig. 6), the average value of the product of the periodic functions u_1 and u_2 (see Fig. 7) is different from zero and can take any value from the interval $[1, -1]$, depending on phase shift ψ.

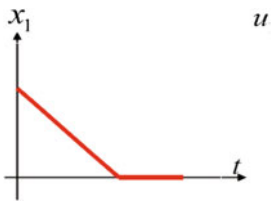

Fig. 5 Ideal sliding mode

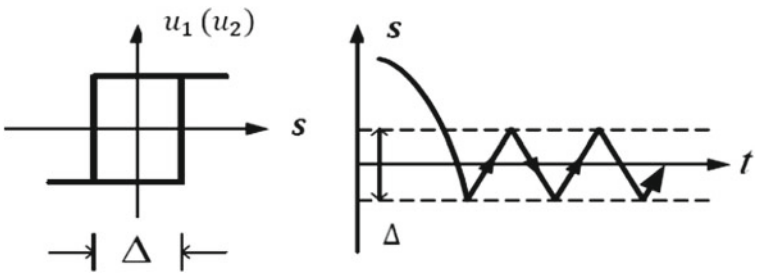

Fig. 6 System with hysteresis

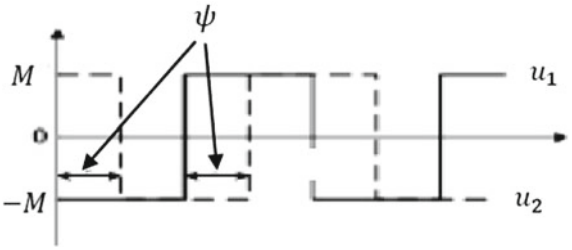

Fig. 7 Two components of control

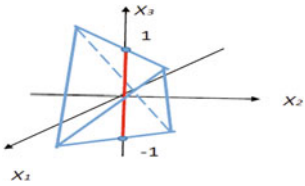

Fig. 8 Set of sliding mode equations in system with vector control

The high frequency component in the solution to the third equation is filtered out with Δ tending to zero, and x_3 is the solution to

$$\dot{x}_3 = A, \qquad -1 \leq A \leq 1, \qquad x_3 \neq const, \tag{2}$$

for a non-zero constant, as stated before. The same result follows from Filippov's method; see Fig. 8. Four possible state speed vectors correspond to four combinations of two control functions. Their convex hull is a tetrahedron, and its intersection with $x_1 = x_2 = 0$, or the x_3 axis on the interval $[-1, 1]$, defines the set of sliding mode equations.

3 Conclusion

The simple interpretation of Filippov's method, that coefficients of a convex hull are relative times of a finite or infinite numbers of continuous subsystems in the vicinity of a discontinuity manifold, enables us to state that any method of deriving sliding mode equations is in the framework of this method.

From the practical point of view it is important to answer the question of what the sliding mode equation is for this or that specific system. Generally speaking, equations beyond discontinuity surfaces do not let us find the equations of motion in these surfaces unambiguously. It can be done for affine systems only, if $m \times m$ matrix $\frac{\partial s}{\partial x} B$ in

$$\dot{x} = f(x, t) + B(x, t)u, \qquad B \in \mathbb{R}^{n \times m}$$

is nonsingular; see Utkin [3]. Otherwise, including our examples, we managed to derive the set of possible sliding mode equations based on Filippov's method. What is the sliding mode equation in a given real system? It depends on the implementation method, initial conditions, and the type of singularity of the matrix $\frac{\partial s}{\partial x} B$.

References

1. M.A. Aizerman, E.S. Pyatnitskii, Foundations of the theory of discontinuous systems. Autom. Remote Control **8**(P.2), 1242–1262 (1974)
2. Ya.Z. Tsypkin, Theory of automatic regulation systems, Gostechizdat (1955) (in Russian)
3. V.I. Utkin, Sliding modes in optimization and control. Nauka (1981) (in Russian)

Challenges from System Dynamics to Complexity and Piecewise-Deterministic Markov Processes: Market Modeling

Johnny Valencia and Gerard Olivar

Abstract This short paper proposes a general economics model for the supply and demand of a commodity in a domestic market, when investments are required for supporting it. Starting from System Dynamics, we recover a well-known model. Then, we improve the mathematical equations in order to be precise at the simulation level.

1 Introduction

The model is shown as a system of piecewise-smooth differential equations. Piecewise smooth and hybrid dynamical systems have been increasingly used in Engineering and Applied Sciences. More recently, these systems appeared also in Economics and Social Science, mainly in Sustainability Development, Bioeconomics and new knowledge areas. Theoretical work mainly deals with the problem of one surface dividing the state space into two different regions since, usually, a more complicated problem can be locally reduced to this situation. When two switching surfaces are taken into account, also the generic case is considered, where surfaces intersect transversally. Papers where more surfaces are considered do not abound in the literature since the number of different regions increases exponentially and the analysis becomes quite cumbersome. However, many applications lie on this multi-surface situation and one must mostly rely on the numerics, as in this paper.

Several nonsmooth bifurcations have been reported in the literature by the authors. They are the fingerprint of an intrinsic complex system. When several markets are connected, complex networks (in the dynamics and structure) naturally appear. Finally, stochasticity is introduced in the system in order to model the risk aversion of investment agents. This is done through Markov chains. This combination of

J. Valencia (✉)
Universidad Nacional de Colombia, Medellín, Colombia
e-mail: jovalenciacal@unal.edu.co

G. Olivar
Universidad Nacional de Colombia, Manizales, Colombia
e-mail: golivart@unal.edu.co

A. Colombo et al. (eds.), *Extended Abstracts Spring 2016*,
Trends in Mathematics 8, DOI 10.1007/978-3-319-55642-0_34

deterministic paths and stochasticity leads to the so-called Piecewise-Deterministic Markov Processes. Depending on the risk behavior, simulations show several decision patterns.

2 Modeling

2.1 Basic Model

The system of equations is as follows: the installed generation capacity is x_1, the generation capacity under construction is x_2, and the power demand is x_3. The system of differential equations is

$$\begin{cases} \dot{x}_1 = -rx_1 + qx_2 \\ \dot{x}_2 = -qx_2 + B \\ \dot{x}_3 = kAx_3 \end{cases}$$

(see Dyner [1] for how the model is stated and parameter values). Here, $B \equiv B(x_1, x_3)$ is given by the following non-smooth function

$$B(D_{inv}) = \begin{cases} 0 & \text{if} \quad D_{inv} \leq 0 \\ 500 & \text{if} \quad 0 < D_{inv} \leq 0.1 \\ 2500 & \text{if} \quad 0.1 < D_{inv}, \end{cases}$$

associated to the capacity building, where $A \equiv A(P)$ is the effect of price on demand and is calculated as

$$A(P) = \begin{cases} 1 & \text{if} \quad P = 0 \\ \left(\frac{P_{gen}}{P}\right)^{\varepsilon} & \text{if} \quad P \neq 0, \end{cases}$$

where P is the last price generation average, and the generation price $P_{gen} \equiv P_{gen}(MR)$ has a nonlinear expression

$$P_{gen}(MR) = \frac{a}{1 + e^{MR}} + b,$$

with reserve margin $MR \equiv MR(x_1, x_3)$, investment decision D_{inv}, and return over investment ROI, where

$$MR(x_1, x_3) = \begin{cases} \omega \text{ if } x_1 \leq x_3, \\ \frac{x_1 - x_3}{x_3} + \omega \text{ if } x_1 > x_3, \end{cases}$$

$$D_{inv} = \max(0, ROI),$$

$$ROI = \frac{P_{gen} - C_v + I}{C_{fv}}.$$

The reserve margin is a measure of system security. Hence, we include a parameter ω that takes into account a threshold (i.e., below this value, the system must invest and ensure minimum supply to avoid power outages).

A manuscript showing nonlinear and nonsmooth dynamics in this model have been submitted. Several non-smooth bifurcations appear leading to chaotic transitory behaviour; see Valencia–Olivar–Franco–Dyner [2].

2.2 Interconnection Model

If several countries are interconnected, as it is the case for example, in Panama, Venezuela, Colombia, and Peru, then we have a coupled system involving countries which generate energy for the other ones. For example, if we assume that a certain country (C1) is producing part of the energy for a certain country (C2) then we would have the following equations: for (C1)

$$\begin{cases} \dot{x}_1 = -r_1 x_1 + q_1 x_2 \\ \dot{x}_2 = -q_1 x_2 + B_1 \\ \dot{x}_3 = k_1 A_1 (x_3 + \theta_2 y_3), \end{cases}$$

and for (C2)

$$\begin{cases} \dot{y}_1 = -r_2 y_1 + q_2 y_2 \\ \dot{y}_2 = -q_2 y_2 + B_2 \\ \dot{y}_3 = k_2 A_2 (1 - \theta_2) y_3, \end{cases}$$

being $\theta_2 y_3$ the amount of demand in country (C2) which is produced in and sent from country (C1).

In the case of several countries, this can easily be generalized in a natural way to

$$\dot{x}_3 = k_1 A_1 (x_3 + \theta_2 y_3 + \theta_3 z_3 + \theta_4 w_3).$$

2.3 Multiple-Investments Model

Another interesting situation occurs when different energy investments are considered. For example, assume there are N investors $I_i, i = 1, \ldots, N$, each one investing B_i^1 for Hydro Power Stations and investing B_i^2 for Photovoltaic Power Stations. Then,

for the Hydro market, we will have

$$\begin{cases} \dot{x}_1 = -r_1 x_1 + q_1 x_2, \\ \dot{x}_2 = -q_1 x_2 + \sum_{i=1}^{N} B_i^1, \\ \dot{x}_3 = k_1 A_1 x_3, \end{cases}$$

and, for the Photovoltaic market,

$$\begin{cases} \dot{y}_1 = -r_2 y_1 + q_2 y_2, \\ \dot{y}_2 = -q_2 y_2 + \sum_{i=1}^{N} B_i^2, \\ \dot{y}_3 = k_2 A_1 y_3, \end{cases}$$

with different returns ROI^1 and ROI^2.

3 Non-Deterministic Model: PDMC

Finally, we consider the case when a decision on changing (or not) the investments, not only depends on the ROI but on a certain risk aversion of the investor. Thus we assume that, with probability $0 < p \leq 1$ the investor changes the investment when this is suggested by the ROI (for $p = 1$, we have the deterministic case studied before).

Then we have a Markov chain among the different investment states and the system has a deterministic part produced by the ODEs and a non-deterministic part produced by the decision rules (a Markov chain). This is called a PDMC (Piecewise-Deterministic Markov Chain). The matrix of probability transitions is

$$P = \begin{pmatrix} 1-p & p & 0 & 0 \\ 0 & 1-p & 0 & p \\ p & 0 & 1-p & 0 \\ 0 & 0 & p & 1-p \end{pmatrix}.$$

Several values for p lead to qualitatively different patterns.

4 Conclusion

Different models for electricity energy markets have been shown, starting from a well-known model in the literature; see Dyner [1]. Depending on several situations (country interconnection, investment diversification) systems of ODEs are coupled. Also, if risk aversion is introduced, non-deterministic models are obtained. Namely, the so-called Piecewise-Deterministic Markov Chains (PDMC).

Acknowledgements Johnny Valencia acknowledges support from the Colombian National Science Foundation COLCIENCIAS. Gerard Olivar also acknowledges support from CRM (Centre de Recerca Matemàtica) and the Faculty of Exact and Natural Sciences at Manizales, Universidad Nacional de Colombia.

References

1. I. Dyner, Energy modelling platforms for policy and strategy support. J. Oper. Res. Soc. **51**(2), 136–144 (2000)
2. J. Valencia, G. Olivar, C.J. Franco, I. Dyner, Nonsmooth dynamics in a model of energy market (preprint)